Carbon monoxide and Temperature in the upper atmosphere of Venus through the analysis of limb observations by VIRTIS/Venus Express

PhD Thesis by:

Gabriella Gilli

Granada 2012

INSTITUTO DE ASTROFÍSICA DE ANDALUCIA, CSIC

UNIVERSIDAD DE GRANADA

COVER IMAGE'S CREDITS:
Raúl Ruiz, "El niño de las pinturas"

UNIVERSIDAD de GRANADA
Departamento de Física Aplicada

INSTITUTO DE ASTROFÍSICA DE ANDALUCÍA

Carbon monoxide and temperature in the upper atmosphere of Venus through the analysis of limb observations by VIRTIS/Venus Express

Gabriella Gilli

Memoria de Tesis
presentada para optar al grado de
Doctor en Ciencias Físicas por la Universidad de Granada

Director de Tesis:

Dr. Miguel Angel López Valverde
Científico Titular del CSIC

Granada, 24 Febrero 2012

A mi Familia
y a mis Amigos

To the planet Venus

From "Whispers from Nature" (Part 10)

By Zoe Peterssen
Oxford, 1996

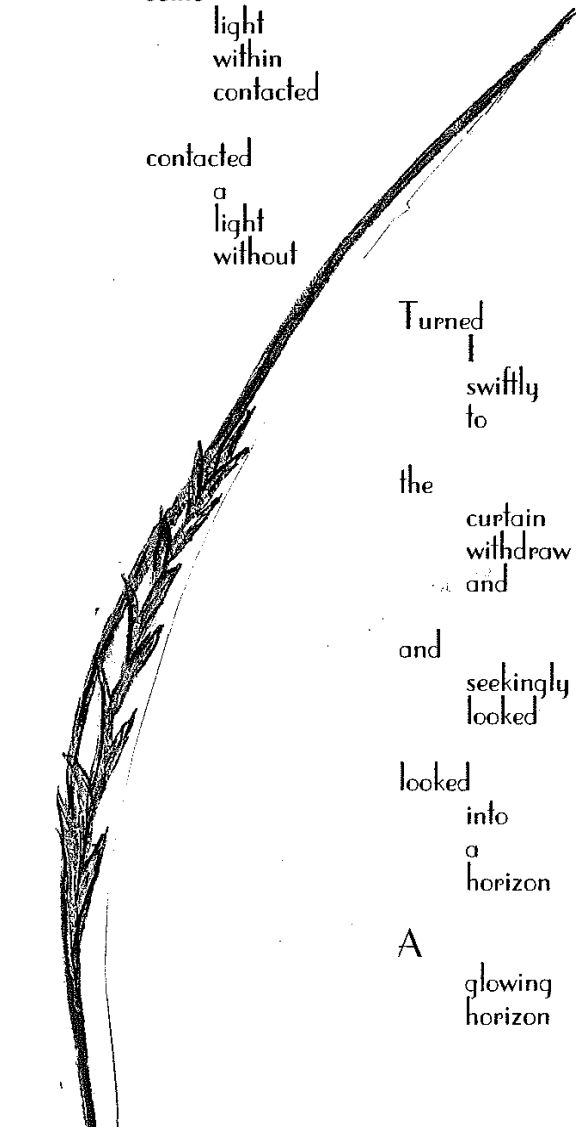

Cordiality

A
glow

some
light

some
light
within
contacted

contacted
a
light
without

Turned
I
swiftly
to

the
curtain
withdraw
and

and
seekingly
looked

looked
into
a
horizon

A
glowing
horizon

...

to
see

see
the
most
beautiful
morning
star

Hugged
her
I
did

Within
she

she
did
enter

and
speak

speak
in
a

a
very
soft
tune

Her
message
a

a
part
of
me
became

And
I

and
she

in
the
One
became

One

Agradecimientos

Estas paginas son para mi unas de las más importantes de esta memoria, porque aquí tengo la ocasión de expresar mi más sincera gratitud a todas las personas que han hecho posible la realización de esta Tesis.
En primer lugar quisiera agradecer a Miguel Angel, mi director de Tesis, por haberme abierto una puerta al fantástico mundo de la atmósfera venusina y marciana. Gracias por tu tiempo, tu paciencia y tu gran esfuerzo enfocado en mi formación científica. A pesar de las dificultades que todos solemos tener en estos años de doctorado, y las dudas que la carrera investigadora conlleva, nunca me he sentido sola en el camino, porque siempre he podido contar contigo. Eres el primer científico que conozco que se cayó en un "agujero negro" ¡y subió tan rápidamente!
También quisiera agradecer a los compañeros del grupo de atmósferas planetarias. Manuel y Bernd, por vuestros valiosos consejos y por darme ánimos en la fase final de la tesis. Gracias muy especialmente a Maya y Francisco: sois unas de las mejores personas que conozco, además de ser excelentes científicos. Siempre habéis tenido tiempo para mi, y buenas palabras cuando las he necesitado.

Thanks to all the VIRTIS/VEx Scientific Team, for their excellent and tireless work, and for giving me the chance to use the data of this instrument. In particular, I would like to thank Alex, Stéphane and the PIs Giuseppe and Pierre, to have always had a prompt response to all my doubts. Also, thanks to the people working at IFSI-INAF in Rome, and at AOPP in Oxford, which welcomed me warmly during my short-stays there.

El éxito de un trabajo se debe a una serie de factores, entre los cuales el entorno laboral y extra-laboral. Por esa razón debo de agradecer a muchos de mis compañeros del Instituto de Astrofísica de Andalucía (IAA-CSIC) y a mis Amigos/as (con "A" mayuscula) que me han apoyado muchísimo durante todos estos años, y a los cuales dedico esta tesis.
Begoña, tu sonrisa, tu presencia y tu actitud positiva, han sido para mi una gran inyección de optimismo. Y además, ¡no me he caido de la bici! Alberto y Vasiliki, ¡qué suerte que he tenido en compartir despacho con vosotros y pasar tantas horas juntos! Me ha encantado teneros a mi lado, y saber que estábais allí, aunque solo fuera para escucharme...Gracias por hacerme ver todo lo bueno de las cosas. Nieves, por ser tan buena conmigo, prestarme tu bici cuando me robaron la mía y tener siempre una infinidad de detalles. Gracias a ti tengo un compañero de piso único y muy especial: ¡mi Icaro! René, Olga y Julia, no solo he compartido con vosotros varias horas muy agradables y divertidas de almuerzos en la cafeteria del IAA, sino también me habéis apoyado y animado en los momentos mas difíciles. Lourdes, gracias por llevarme tantas veces de excursión contigo y por introducirme en la maravillosa Sierra Nevada. Carolina, por prepararme un riquísimo "p*ão* de queijo" y cantar conmigo en portugués. Mirjana, gracias por transmitirme paz y tranquilidad con tu presencia. Chandreyee, you know that you are my favorite cook, and one of my best confidant. Juande, !explícame como haces para tener siempre una respuesta a todo! Gracias por tu disponibilidad, y por ser tan Juande! Walter, por ofrecerme siempre tu ayuda, y por cederme la imagen 3D de Venus. Ginevra, por esas escapadas a la playa de fin de verano, y el paseo por el Albayzin soleado el día después de la entrega de la tesis. Javier P., por tu agradable compañía durante tu estancia en el IAA, y por compartir tu experiencia con IDL. Mirian, gracias por facilitarme el formato TeX para introducir los articulos en la tesis.

Al personal de seguridad del IAA, especialmente a Ana, por ser tan encantadora con todos nosotros y esos gazpachos de verano tan ricos, y a Juan por ese subidón de azúcar a las 3 de la mañana el día antes de entregar la tesis.

Y fuera del IAA, no puede faltar mi vecina y amiga Bec, por esos deliciosos desayunos en el Realejo, por cuidarme cuando estoy mala y ... ¡por subirte conmigo al Mulhacen! Manu, por tu alegría y esos ratos tan agradables y regeneradores de las ...vueltas por Granada. Y como no, Breezy: el dia que tú y yo brindamos en Canarias "¡A la beecaaaa!!" no sabíamos que nuestros destinos iban a cruzarse tantas veces. Anthony, por todos los buenos momentos que he compartido contigo y con tu música. La familia Ocaña, por todo el cariño que siempre me habéis transmitido.
Suru, siempre presente desde hace ya más de 10 años, casada o soltera, sabes que eres "la donna della mia vita". Gracias también a Alejo, por haberme sacado muchas veces de la rutina con esos viajes "super last-minute", y por sus buenos consejos para la tesis. Mis mas queridas amigas y compañeras de la "vuelta del mundo", Irene (la Lucertola) y Sarita, por el tiempo tan bueno que siempre he tenido con vosotras y por vuestra infinita paciencia en esperar y esperar, que algún día terminara la tesis. Ya nos vamos de viaje. ¿No?
Muchas gracias a Raúl, "El niño de las Pinturas", por realizar la portada mas bonita y original que haya podido tener nunca, y brindarme la oportunidad de hacer esta Tesis aun más especial. Y por dar vida y color a las calles de Granada.

En realidad debería seguir agradeciendo a muchisima más gente, porque aunque Granada sea por sí misma una ciudad maravillosa para vivir, estos años de tesis han sido tan entrañables e inolvidables gracias a todas las magnificas personas que he conocido. Gracias a mis compañeros senderistas, ciclistas y ecologistas varios... con los cuales he compartido tantos buenos ratos al aire libre, disfrutando de la naturaleza andaluza.

E finalmente, grazie infinite ai miei genitori, a mia sorella e a tutta la mia Famiglia. Vi ringrazio con tutto il cuore per avermi rispettato, compreso e appoggiato nelle mie scelte. So che per voi é molto difficile sapermi lontana. Per tutti gli sforzi che avete fatto in questi anni, e per tutte le volte che avete riunciato con generositá e con amore alla "vostra" felicitá per la "mia", questa tesis é sopratutto dedicata a vosotros.

Resumen

El planeta Venus, por su cercanía y dimensión parecida a la Tierra, ha sido uno de los objetos más atractivos para la ciencia planetaria, y uno de los más explorados desde satélite. Ya desde la primera era espacial (1960-1970), Venus reveló su cara más impredecible y desconocida, con temperaturas en superficie muy elevadas ($\sim 470^{o}$C) y una densa capa de nubes de acido sulfúrico. En las décadas de los 70-80, las técnicas de sondeo en el cercano IR permitieron penetrar en esa espesa capa de nubes y estudiar los fenómenos que ocurren en la baja atmósfera.
En cuanto a la alta atmósfera de Venus, que es el objeto de estudio de esta tesis, entre las misiones que más han contribuido a su conocimiento destacamos la sonda Pioneer Venus (Fimmel et al., 1983; Russell, 1992), y el sobrevuelo de la Cassini (Brown et al., 2004) en ruta hacia Saturno. Pioneer Venus proporcionó datos muy valiosos sobre la estructura vertical de la atmósfera de Venus, durante un ciclo solar completo, que permitieron el desarrollo del modelo semi-empirico VIRA (Venus International Reference Atmosphere) (Seiff et al., 1985; Hedin et al., 1983), muy usado hasta hoy en dia como atmósfera de referencia. Por su parte la sonda Cassini obtuvo medidas de las emisiones de "airglow" en el UV del O, N_2 y CO en la alta atmósfera del planeta. Todas estas medidas, junto a una serie extensa de observaciones desde tierra en diversos intervalos espectrales (Allen and Crawford, 1984; Clancy et al., 2012), han contribuido a nuestro conocimiento básico de las propiedades de la atmósfera de Venus, y al mismo tiempo han generado nuevas cuestiones sobre su composición detallada, su dinámica y evolución. Desde los años 80-90 hasta el 2006, cuando la misión Venus Express (VEx) llegó al planeta vecino (Titov et al., 2006), la mayoría de las misiones espaciales se dirigieron sobretodo al planeta Marte, dejando Venus prácticamente inexplorado durante casi 20 años.

Esta Tesis esta enfocada en el análisis de las recientes medidas de VIRTIS (Visible and Infrared Thermal Imaging Spectrometer), uno de los seis instrumentos a bordo de la Venus Express, que con una resolución espectral sin precedentes ha permitido sondear sistemáticamente la atmósfera de Venus desde el visible (0.3 -1 μm) hasta el cercano IR (1-5 μm). El principal objetivo de este estudio es explotar científicamente las medidas de VIRTIS en el limbo del planeta, para mejorar nuestro conocimiento de las capas más altas de la atmósfera de Venus. Dichas regiones son las menos exploradas de la atmósfera de Venus, y de los planetas en general, porque las bajas densidades que las caracterizan las hacen muy difíciles de observar. Además, estas capas presentan emisiones moleculares en el IR producidas bajo condiciones de no-equilibrio termodinámico local (no-ETL), por las transiciones vibro-rotacionales de las moléculas más activas radiativamente (Lopez-Puertas and Taylor, 2001). Las emisiones más intensas en la alta atmosfera de Venus son las producidas durante el dia por bandas moleculares del CO_2 en 4.3 μm y 2.7 μm, y del CO en 4.7 μm. El análisis y la interpretación de dichas emisiones requiere normalmente el uso de sofisticadas herramientas teóricas, como modelos de no-ETL específicos para las poblaciones vibracionales, rotacionales y de espín.
Los avances en las técnicas involucradas de sondeo remoto utilizadas por VIRTIS/VEx, nos han dado la oportunidad de observar la atmósfera de Venus con una elevada resolución espacial y espectral, y obtener información sobre su estructura térmica y composición. Sin embargo, las medidas de las alta atmósfera del planeta siguen siendo muy escasas, so-

bretodo durante el día y por encima de 100 km. La mayoría de las observaciones de VIRTIS se tomaron en geometría nadir, con el propósito de realizar mapas globales especialmente del hemisferio sur, una de las regiones menos exploradas por las misiones anteriores, y para permitir un sondeo optimo con VIRTIS, dada la geometría de la órbita de VEx. Sin embargo, precisamente debido a la forma tan elíptica de estas órbita, las medidas en geometría limbo desde la periapsis son mucho más limitadas. Aun así, estos datos constituyen una base imprescindible para derivar cuantitativamente los parametros geofísicos relevantes de la alta atmósfera de Venus.

Este estudio pretende realizar determinaciones de CO y de temperatura, entre 100 y 150 km, utilizando una selección de datos obtenidos con VIRTIS en el limbo y en el hemisferio diurno, entre el 2006 y el 2010. La memoria empieza con una breve introducción (capítulo 1) sobre la atmósfera de Venus y su estructura térmica, con particular hincapié en las capas más altas (90-170 km) y en el estado actual del conocimiento de la abundancia de CO y de temperatura de estas regiones atmosféricas. A continuación, los Capítulos 2 y 3 abordan el análisis de los datos y la validación dl modelo no-ETL utilizado en el mismo. Estos capítulos contienen un compendio de cuatro artículos, tres de ellos ya han sido publicados entre el 2009 y el 2011, y constituyen la parte principal de estos capítulos. El capítulo 4 contiene un manuscrito, todavía no publicado, con los resultados de la inversión de temperatura y CO. Cada uno de estos capítulos empieza con una pequeña descripción del trabajo desarrollado para los correspondientes artículos, y la discusión de los resultados principales. Asimismo, en ellos se detallan algunas tareas fundamentales para el desarrollo de esta tesis pero que no fueron incluidas en las publicaciones.

A continuación resumimos las tareas y las herramientas que se han utilizado en las tres fases principales de la tesis, que se describen en los capítulos centrales: análisis de las medidas IR de VIRTIS/VEx, validación del modelo no-ETL para Venus y la realización de los "retrievals" de la temperatura y de la abundancia de CO en la alta atmósfera venusina.

En primer lugar, el análisis de datos, se enfoca en las medidas infrarrojas (IR) de VIRTIS/VEx en la alta mesosfera/baja termosfera de Venus (90-170 km), durante el dia y en el limbo del planeta, donde estas emisiones son más intensas. En concreto, en el capítulo 2 analizamos todas las medidas de CO_2 en 4.3 μm y 2.7 μm y del CO en 4.7 μm, durante los primeros 4 meses de misión, y realizamos una serie de pruebas de consistencia interna, confección de mapas de radiancia y perfiles verticales de emisión, y corrección de algunos errores sistemáticos. Las principales características de estas emisiones, como su variación con el ángulo solar cenital (SZA) y con la altura fueron interpretadas con la ayuda de un modelo no-ETL para Venus, previamente desarrollado en el Instituto de Astrofísica de Andalucía (IAA) (Roldán et al., 2000; López-Valverde et al., 2007).

Aunque la tarea de validación de dicho modelo es parte integrante de todo el trabajo de tesis, el capítulo 3 esta especialmente centrado en este aspecto. En el se discute el comportamiento del modelo en la atmósfera de Venus y también en las de Marte y la Tierra. El trabajo consiste en analizar las más recientes observaciones desde satélite en 4.3 μm y 4.7 μm en las atmósferas de los tres planetas, con herramientas similares. Este estudio de planetología comparada resultó muy fructífero para ganar confianza en las principales predicciones del modelo, y para corregir algunos coeficientes colisionales que afectaban sobre todo a algunas bandas calientes del CO_2.

El cuarto capítulo describe una fase del trabajo que representa culminar el análisis

de los datos, al realizarse la inversión de las medidas, con un "retrieval" simultáneo de abundancias de CO y de temperaturas cinéticas en la alta atmósfera de Venus. Se discuten las características principales del método diseñado especialmente para el análisis de estos espectros de VIRTIS tomados en el limbo del planeta, se describe el conjunto de datos seleccionado, su preparación y promediado para la inversión, y un análisis de errores de los términos de mayor incertidumbre. Se ha prestado particular atención a las aproximaciones, limitaciones y ventajas del método de inversión, dado que el código desarrollado representa una herramienta nueva en el Departamento de Sistema Solar del IAA, con el potencial de su aplicación futura a observaciones en condiciones similares.

Los resultados concretos obtenidos se resumen en el capítulo de Conclusiones y Trabajo Futuro.

Contents

Chapter 1

Introduction

1.1 The planet Venus and its atmosphere

As the brightest of the planets, Venus has embellished the morning and evening skies of the Earth since the dawn of time and triggered scientific curiosity since the invention of the telescope. In 1610 observations by Galileo Galilei recorded for the first time the phases of Venus, similar to those of the Moon, although it seems that they had been observed before by sharp-eyed watchers of the sky. Also, Venus high reflectivity and most of its observational parameters, like its distance to the Earth and apparent diameter have been known from the early days of telescopic observations.

Among our neighbors in the solar system, Venus has been the planet most visited by man-made spacecrafts, partly because it is closer and easiest to reach from Earth than any other planet. Table 1.1 shows a list of the most relevant past mission to Venus before the arrival of Venus Express. The first successful space mission to Venus was the flyby performed by Mariner 2 in 1962, followed by Venera 4 in 1967 which was the first atmospheric probe to reach Venus: it carried out the first in situ measurements of its atmosphere. Over the following decades, Mariner 5 (1967) and 10 (1973) were sent to perform further flybys of Venus, while a long series of Venera 5-16 (1969-1983) orbiters and landers gave us, amongst other, first images from the surface and more in situ and remote atmospheric measurements. This first spatial era to Venus (1960s-1970s) revealed an exotic and unpredictable world, with a hot surface hidden below a thick and ubiquitous clouds layer, as well as inhospitable to water and to life.
The most ambitious mission exploring Venus was Pioneer Venus (Fimmel et al., 1983), consisting of an orbiter and a set of four atmospheric probes. The orbiter was operational from 1978-1992 and provided the scientific community with measurements of the atmosphere and the surface during a full solar cycle, as well as observations of the magnetic and plasma environment of Venus (Russell et al., 2006). In 1985 the two Vega balloons (Sagdeev, 1986) measured atmospheric winds and surface soil properties and the Magellan spacecraft (Plaut et al., 1992) in 1989 carried out the most detailed radar mapping of Venus' surface to date, and also gave some information about the density of the upper atmosphere during aerobracking maneuvers and obtained temperature and abundances by radio occultation down to 35 km, deeper than before.

During the 1990 flyby of the Galileo spacecraft in route to Jupiter, thanks to near-infrared measurements of clouds around 50 km altitude on the nightside, zonal and meridional winds, along with water vapor abundance profiles were derived (Carlson et al., 1992). Also, extreme-ultraviolet (EUV) dayglow spectra were taken by Cassini/Huygens in 1997 and in 1999 during its cruise to Saturn (Brown et al., 2004), which were recently used to calculate the intensity of O, N_2 and CO dayglow (Gérard et al., 2011).

List of the successful missions to Venus before Venus Express

Date	Mission	Type of mission	Experiment(s)
1962	Mariner 2	Flyby	Magnetometer
1967	Mariner 5	Flyby	Magnetometer Ultraviolet photometer Radio occultation
1967	Venera 4	Atmospheric probe	Magnetometer
1969	Venera 5 and 6	Atmospheric probes	Magnetometer
1970	Venera 7	Lander	
1972	Venera 8	Lander	
1974	Mariner 10	Flyby	Spectrophotometer
1975	Venera 9 and 10	2 orbiters and 2 landers	Radio occultation Magnetometer Visible airglow spectrometer
1978	Venera 11 and 12	Landers	Spectrophotometer
1978–1992	Pioneer Venus	1 orbiter, 1 bus and 4 atmospheric probes	Orbiter: • Radio occultation over a full solar cycle • Neutral mass spectrometer • Electron temperature probe • Ion mass spectrometer • Retarding potential analyzer • Ultraviolet and visible airglow observations • Magnetometer Bus: • Neutral mass spectrometer • Ion mass spectrometer
1981	Venera 13 and 14	Landers	
1983	Venera 15 and 16	Orbiters	Radio occultation
1985	Vega 1 and 2	Flyby + balloon + 1 lander	
1990–1994	Magellan	Orbiter	
1990	Galileo	Flyby	UV, fields and particles experiments
1998, 1999	Cassini	Flyby	UV spectrometer

Table 1.1: Successful missions to Venus, before Venus Express. After Witasse and Nagy (2006).

All those studies have given a basic knowledge of the properties of Venus, but at the same time they have generated new questions about its detailed atmospheric composition and dynamics, the interaction between surface and atmosphere, and its geological and atmospheric evolution. Demands of new data by the scientific community in the 90s, together with interesting and new ground based observations and with the availability of optimal instrumentation from other missions (Rosetta and Mars Express) paved the way for the European Space Agency (ESA) to take the initiative of promoting the Venus Express mission (VEx) in 2001 (Titov et al., 2002). It took less then 3 years from the approval to the launch of the mission to Venus which occurred in 2005. VEx is still in orbit since its arrival at Venus on 11th April 2006. With the new data from Venus Express, there is a picture emerging of Venus where the existing conditions and the ongoing processes are becoming clearer. The evolution of the planet and in particular the atmosphere and the climate are

topics of great interest, that also include aspects of comparative planetology. The comparison with the other terrestrial planets, the Earth in particular, is an important scientific objective and it is also one topic of this Thesis.
Venus is sometimes considered the twin planet of the Earth because of its size, distance to the Sun, mean density (see Table 1.1) and as far as we know approximately the same solid-body composition. The two planets also seem to have been quite similar in the epoch when they formed and cooled, probably with large inventories of CO_2 in Earth's atmosphere and liquid water oceans on the surface of Venus, but as a result of evolutionary processes, on Earth CO_2 is bound in carbonates in the crust whereas on Venus it exists mostly as gas (Faure and Mensing, 2007).
Despite the similarities, there are also remarkable differences between the two planets, like the absence of a natural satellite around Venus, the slow (243 Earth's days) retrograde rotation of its solid body and the absence of a measurable planetary venusian magnetic field. At a mean distance of 0.72 UA, Venus describes a quasi-circular orbit around the Sun in 224.70 days. Its small rotation axis obliquity (177 degree inclination), almost perpendicular to the ecliptic, ensures that seasonal effects are negligible. The conditions on Venus surface are also very extreme: high temperature and pressure, about 740 K and 92 bar, respectively, reign under a ver dense cloud layer of sulfuric acid droplets (Taylor, 2006).

	VENUS	EARTH	MARS
Distance from Sun (AU)	0.723	1	1.527
Min. distance from the Earth (10^6 km)	38.2	-	55.7
Max. distance from the Earth (10^6 km)	261.0	-	401.3
Min. apparent diameter from Earth (sec. of arc)	9.7	-	3.5
Max. apparent diameter from Earth (sec. of arc)	66.0	-	25.1
Orbit eccentricity	0.0067	0.0167	0.0935
Obliquity (deg)	177.36	23.45	25.19
Equatorial Radius (km)	6052	6378	3398
Mass (10^{24} kg)	4.87	5.98	0.642
Mean density (kg/m3)	5243	5515	3933
Length of the day (h)	2802	24	24.65
Albedo	0.59	0.39	0.15
Solar irradiance (W/m2)	2613.9	1367.6	589.2
Surface Temperature(K)	740	288	223
Surface pressure(bar)	92	1	0.006
Surface density (kg/m2)	6.58E+01	1.21E+00	1.42E-02
Main atmospheric composition	CO_2	N_2, O_2	CO_2

Table 1.2: Venus, Earth and Mars comparison of basic physical and orbital parameters. After Taylor (2006) and NASA website (http://nssdc.gsfc.nasa.gov/planetary).

Our current knowledge of the details of the Venus atmosphere and its climate system was mostly gathered by remote sounding with the Pioneer Venus Orbiter (PVO) in the IR and in-situ by the entry probe missions of the late 1970s and early 1980s (Russell, 1992;

Russell et al., 2006), and more recently from orbit by Venus Express (Titov et al., 2006, 2011). A description of the VEx mission, instruments on board and achievements will be given below in Section 1.2.1.

The dense atmosphere of Venus is very warm and dry, and composed mainly by carbon dioxide (CO_2, 96.5 %) and nitrogen (N_2, 3.5 %). Sulfuric acid droplets form the thick cloud layer, covering the planet at $\sim$ 50 to 70 km altitude and with hazes up to at least 80-85 km altitude (de Kok et al., 2011). The origin of the droplets seems to be the photochemical oxidation of SO_2 at the clouds top and condensation at the bottom of the clouds deck (Esposito et al., 1983). Sulfur-bearing trace gases, carbon and chlorine compounds and water vapor are also present in the atmosphere in amounts from few to few hundred parts per million (de Bergh et al., 2006).

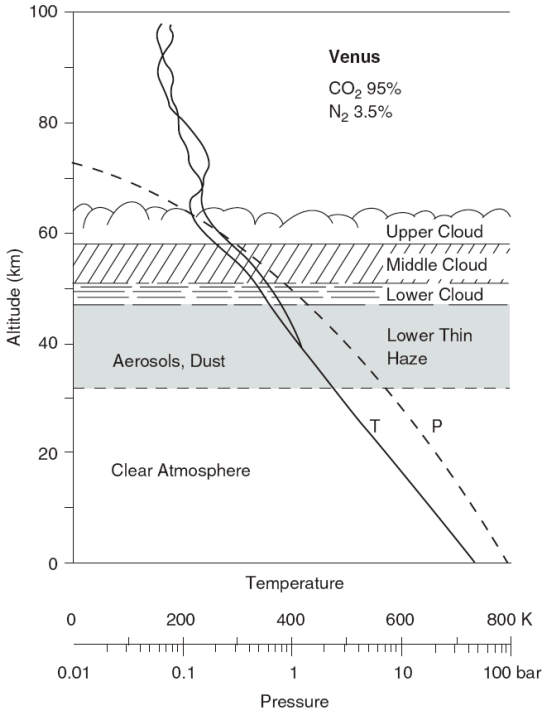

Figure 1.1: Temperature and pressure profile of the Venus atmosphere up to 100 km based on Pioner Venus orbiter. The location of the haze layer and clouds is also symbolically represented. (Russell et al., 2006)

According to its energetic and thermal structure, the atmosphere of Venus is roughly divided into three main regions: the *troposphere* (0-60 km) up to the cloud top, the *mesosphere* (60-120 km) with a fairly monotonous decline in the temperature, and the *thermosphere* (above 120 km) where temperature increases steadily with altitude. Figure 1.2 illustrates this atmospheric division.

The temperature and pressure profiles most commonly used in the literature follow the Venus International Reference Atmosphere (VIRA) for altitudes up to 100 km (Seiff et al., 1985). At higher altitudes data are usually taken from the model of Hedin et al. (1983)

(see Figure 1.2). The transition between the two can be performed by interpolating the temperature and reconstructing the pressure though the hydrostatic law. Since the publication of the VIRA volumes (1982-1983) progress in the atmospheric composition, density and thermal structure came from observations both from the ground and from space.

Early in-situ observations of the lower atmosphere (0-60 km) already showed that the temperature below 30 km altitude is fairly constant all over the planet (Seiff et al., 1985). However, those measurements were limited to low latitudes. At higher latitudes we lack conclusive data although we know that Venus has an unusual latitudinal distribution of outgoing thermal flux. Due to its small inclination to the ecliptic the solar energy reaches the planets at low latitudes and emits a considerable portion of it to space from the poles. This implies a significant role of atmospheric dynamics in the heat transport.
Above the top of the troposphere, in the mesosphere, the atmosphere starts to be optically thiner and the temperature tends to a fairly constant decrease with height (see Figure 1.1 and 1.2). To a first approximation the atmosphere is in radiative equilibrium, determined by the balance between the absorption of upwelling IR from the surface and troposphere and cooling to space, if no significant absorption of direct solar energy takes place (Taylor, 2006). Above about 90-95 km the solar absorption by CO_2 in its vibrational combination bands in the near-IR (1-5 μm) increases with altitude, with a maximum around 110-120 km (Dickinson, 1973; Roldán et al., 2000). At the low density of these altitudes, the CO_2 vibrational states that result pumped after the solar excitation present a non-local thermodynamic equilibrium (non-LTE) behavior: the energy gained follows a competition between collisional quenching and radiative re-emission to space. Also, the CO_2 vibrational states of lower energy, which give rise to important cooling rate at 15 μm, are under non-LTE conditions, cooling at a little higher energy altitudes than the solar heating. As a consequence, radiative equilibrium models predict a significant temperature variation between 90 and 120 km, with a possible mesopeak, or local temperature maximum at about 110 km (Dickinson, 1973; Ramanathan, 1974; Bougher et al., 1986; Roldán et al., 2000). Such a mesopeak is not present in the VIRA profile, although the few measurements available at those altitudes were highly uncertain at the time (López-Valverde et al., 2008).
In this work we refer to this region as *upper mesosphere* (see Figure 1.2, bottom panel). Notice that some authors (Clancy et al., 2003) locate the mesopause at $\sim$ 90 km, approximately the top of our *lower mesosphere*. They observed a nighttime mesopeak around 94 km, and increasing temperatures during daytime above that altitude, although these regions are close to their upper limit and are subject to significant uncertainties. Given the diversity of arguments and dataset used by different authors, it is important to clarify the nomenclature of each work.
Above the mesopause, the thermosphere is generally characterized by temperatures that increase dramatically with height because of heating by solar extreme-UV and UV, and approach an asymptotic and maximum value at the exobase ($\sim$ 180 km) (Bougher, 1995).

In the remaining part of this section, we will review observational information related to a few important aspects of the composition and dynamics in the troposphere and lower mesosphere, while data on the upper mesosphere/lower thermosphere will be presented in more detail in Section 1.1.1.
Nowadays radio ground based observations of Venus are performed frequently to sound the Venus mesosphere, and they are very useful to supply winds and distribution of minor

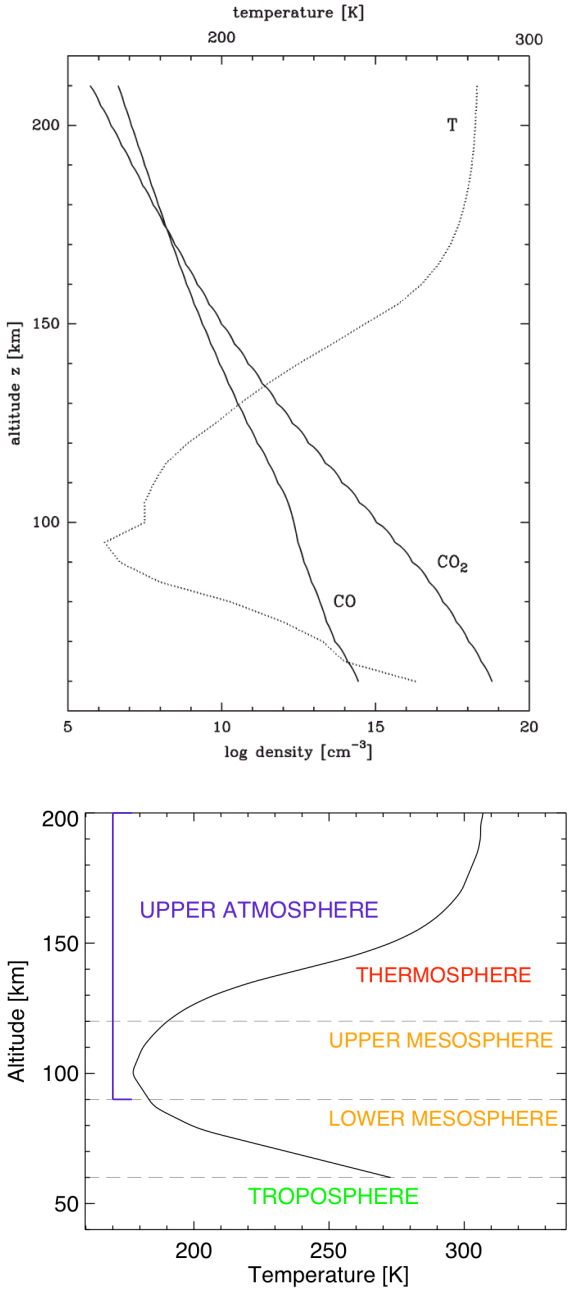

Figure 1.2: Top panel: CO and CO_2 densities and temperature profiles from the VIRA model (Keating et al. 1985) at the subsolar point for altitudes $100 < z < 250$ km, and from Seiff (1983) for altitudes below 100 km, after Crovisier et al. (2006). Bottom panel: Schematic view of the vertical thermal structure up to the thermosphere (from VIRA) to illustrate the division in atmospheric layers used in this work. The thermosphere depicts a daytime profile, at nighttime it is much colder.

compounds, very difficult to measure otherwise. They include H_2O and HDO above the clouds (Encrenaz et al., 1995; Sandor and Clancy, 2005) and CO at slightly higher altitudes, between 75 and 105 km (Clancy and Muhleman, 1991; Clancy et al., 2008, 2012), to mention a few of them. On the other hand, radio occultation measurements from Pioneer Venus (Jenkins and Steffes, 1991), Magellan (Steffes et al., 1991; Jenkins, 1998) and VEx (Tellmann et al., 2009) have provided the most accurate and comprehensive dataset of the atmospheric density and temperature in the altitude range 40-90 km.
In the ultraviolet, there have been measurements from Pioneer Venus (Esposito et al., 1997) as well as from VEx (Marcq et al., 2010; Piccialli et al., 2010). They provided new information on SO_2 above the clouds, detected and measured SO and have been used to obtain direct observations of winds at the cloud top.
Near-infrared radiation of the nightside provided information on the mixing ratios of CO, H_2O, SO_2, and the D/H ratio in water vapor below the cloud deck, some of which are sources of abundance at higher altitudes (Taylor et al., 1997; Marcq et al., 2006; Cotton et al., 2012). Daytime near-infrared measurements from Venera also gave SO_2 (Zasova et al., 1993) and H_2O mixing ratio (Ignatiev et al., 1999) around 60 km altitude on both the day and nightsides. Regarding CO, measurements by satellite (Pioneer Venus, Venera 12, NIMS/Galileo) and by ground-based telescopes in the near infrared seem to indicate the presence of a gradient in its mixing ratio in the altitude range sounded, between 20 and 65 km (von Zahn et al., 1983; Collard et al., 1993).

Several of the minor constituents exhibit striking amounts of temporal and spatial variability, indirectly revealing major characteristics of the planet, its atmospheric circulation and meteorology (Taylor, 2006). In particular, during the Galileo flyby in 1991, near IR measurements revealed an equator-to pole gradient in the abundances of tropospheric carbon monoxide (Collard et al., 1993), which Taylor (1995) interpreted as result of an hemispherical Hadley circulation that extends from the lower thermosphere at around 120 km all the way down to the surface.
Regarding the dynamics of the atmosphere of Venus, its global view is probably one of the most enigmatic and unpredictable processes analyzed by both models and data. Data from most previous missions and ground-based observations showed that the general circulation of the atmosphere can be divided into two regimes: a retrograde west-to-east zonal superrotation (RZS) in the region from the surface of the planet to the top of the cloud deck at $\sim$ 70 km (Gierasch et al., 1997) and a relatively stable mean subsolar to antisolar flow (SS-AS) across the terminator in the thermosphere, above 120 km (Bougher et al., 1997). The responsible for this dominant SS-AS pattern is the inhomogeneous heating by solar radiation (EUV, UV and IR) in the mesosphere/thermosphere which generates large pressure gradients (Dickinson and Ridley, 1977; Schubert et al., 1980; Bougher et al., 1997). The transition between the two regimes appears to be a steady reduction of the super-rotation with altitude up to 100 km, which might be produced by some easterly acceleration, perhaps form the upward propagation of waves (Mueller-Wodarg et al., 2006). No attempt to model the superrotation has been completely successful so far, indicating that the basic mechanisms of the phenomenon are still unclear (Svedhem et al., 2009). In addition to this, another dynamical phenomena are particularly enigmatic, as for example the complex dipole-shaped vortex at the north pole observed briefly by PVO (Limaye and Suomi, 1981; Taylor et al., 1979) and recently by VIRTIS/VEx (Piccioni et al., 2006).

Despite extensive Venus exploration in past decades, numerous open issues in its atmosphere could be remarked. Significant gaps in our knowledge of global energy balance between the incoming and outgoing radiation still remain. Other key questions concern: 1) the detailed distribution of heat sources in the atmosphere that drives the dynamics, 2) the impact of gases and aerosols and their variations on the greenhouse effect and on the efficiency of the radiative energy escape from the lower atmosphere via IR emissions, 3) the propagation of waves from the lower atmosphere and 4) the global and inter-hemispheric circulation, to mention a few of them.

The next sections are devoted to the description of the upper region of the Venus atmosphere, with a particular emphasis on the actual knowledge of CO density and temperature above 100 km, which is one of the main targets of this Thesis.

1.1.1 The upper atmosphere of Venus

In this work we focused on the upper mesosphere and the thermosphere of Venus (between $\sim$ 90 and 180 km), which we overall refer to as "upper atmosphere". Its study presents challenges to on-going global modeling efforts of the Venus atmosphere, therefore it is nowadays a highly unknown region in the scientific context of the terrestrial planetary atmospheres. The ultimate reason is that this rarefied portion of the atmosphere is difficult to observe. The understanding of its energy balance requires to take into account various physical and chemical processes, still poorly known or insufficiently constrained by observations (e.g absorption of solar radiation, energy transport, dissipation of wave disturbances, heating and cooling by radiative emissions). In the upper thermosphere, above 150 km, conditions are crucial for determining loss rates for atmospheric species and hence for understanding the global composition and the evolution of the atmosphere with time. At the highest altitudes, a number of additional processes are involved: dissociation, ionization, thermal and nonthermal escape, solar wind and cosmic ray erosion, meteoritic and cometary impacts. All of these are under active investigation, but they remain observationally very unconstrained. For determining the nature and extent of current losses, two key measurements are temperature and composition as a function of height in the upper atmosphere (Taylor and Grinspoon, 2009).

Most part of the upper atmosphere requires remote sounding techniques for its observation, because in-situ data can no be obtained in a systematic manner. Such a remote exploration should preferably be carried out in a limb-tangent geometry, since its longer path length and the cold space background permits retrieval of atmospheric parameters that, otherwise, could not be determined. This approach has been used extensively to determine the thermal structure and trace gas distributions in the Earth's stratosphere and mesosphere (Hanel et al., 2003). Moreover, if the instrumental field of view is sufficiently small, measurements tangential to the planetary limb can produce atmospheric profiles with a vertical resolution higher than that achievable in nadir viewing. However, there are two difficulties for the limb sounding of these layers. One is the obvious weakness of all the emissions, which usually means very noisy data. And the second is related to a typical condition of the upper atmosphere of a planet, characterized by low gas densities, and as mentioned above, is referred to as the breakdown of local thermodynamic equilibrium (LTE). Under such circumstances, the molecular emissions do not follow a Planckian source

function at the local kinetic temperature, but reflect a diversity of radiative, collisional and chemical processes which are specific of each molecular species and vibrational transition (Lopez-Puertas and Taylor, 2001). The strongest IR molecular emissions observed in the upper atmosphere of Venus are produced under non-LTE situations. Spectrally located at 2.7 μm, 4.3 μm and 4.7 μm, they correspond to the strongest rotational-vibrational bands of CO_2 and CO. Given the nature of these emissions, proper theoretical non-LTE models need to be used in their interpretation and analysis, and once they are well understood, they can also be used to derive other relevant atmospheric information. Hence, non-LTE emissions represent a useful tool on one hand, but a difficult one on the other, for sounding the upper atmosphere. The study of the CO non-LTE emissions at 4.7 μm and its interpretation in terms of abundance of CO and temperatures of the upper atmosphere constitutes the main goal of this work.

Regarding the thermal balance of the upper mesosphere, a pioneering study was conducted by Dickinson (1972) who derived the globally averaged radiative equilibrium temperature structure at altitudes between 66 and 130 km for a pure CO_2 atmosphere, i.e, in the absence of dynamics.

One of the most surprising results about the Venus thermosphere is that the nighttside temperatures are extremely cold compared to the counterpart on Mars or on Earth, and it is refereed to as the Venus "cryosphere". This, together with the small day-night contrast in exospheric temperatures, was a puzzle for long time in view of the proximity of Venus to the Sun, but it was essentially solved in the early 90s, after discovering that the rate of collisions between atomic oxygen and CO_2 was much larger than previously thought (Sharma and Wintersteiner, 1990). As a consequence, the 15 μm bands of CO_2 have a more powerful role as a cooling agent than previously assumed (López-Valverde et al., 2008; Lopez-Puertas et al., 1992).

This region is also dynamically and photochemically very active, but up to now it has been poorly observed, being both satellite and ground-based observations very limited in spatial and temporal coverage (Carlson et al., 1992; Clancy et al., 2003, 2012; Lellouch et al., 1994; Bertaux et al., 2007a; Drossart et al., 2007b, i.e). Also in-situ measurements, either from balloons or during the periapsis of satellite orbits, are very scarce. The RSZ and SS-AS patterns mentioned in the previous section are presumed to be superimposed in the altitude range of 70-120 km, but specific mechanisms occurring in these layers remain undetermined (Clancy et al., 2003). Complex processes like exchanges among a time variable equator-to-pole pressure gradient, thermal tides and gravity wave momentum deposition (Alexander et al., 1992) may significantly affect the dynamical stability within the Venus mesosphere.

Observational and theoretical constraints on this dynamical transition have been very limited until recently, and the Venus mesosphere (70-120 km) has long been an "information gap" region (Lellouch et al., 1994), being specific mechanisms still undetermined. Our knowledge about the processes and dynamics in the atmosphere of Venus was greatly improved in recent years due to the European space mission Venus Express (VEx). The arrival of VEx (see Section 1.2.1) on April 2006 marked the start of an exciting period with new data from a systematic sounding of the Venus atmosphere from orbit (Svedhem et al., 2007; López-Valverde et al., 2008).

After the latest findings by VEx we are starting to understand that this region is more

variable than thought before (Drossart et al., 2007b; Brecht et al., 2011). In particular, the interaction between the two main circulation patterns seems to produce modifications to the general flow in the upper atmosphere, which also vary with altitude and with solar cycle variations (Brecht et al., 2011; Schubert and Covey, 2007). Ground based observations have been carried out during a programmed validation campaign in support of VEx operations. They extended from the visible and near-IR to the microwave domains, and some of them provided useful complementary observations of the upper atmosphere (Sonnabend et al., 2008, 2010).
For example, a clear transition to the thermosphere, with an isothermal or inversion layer equivalent to the Earth's mesopause, is not as well marked on Venus as it is on Earth (López-Valverde et al., 2008). Not only there seem to be changes from day to night temperatures, but also between recent VEx measurements and previous data. The Venus Thermospheric General Circulating model (VTGCM) predicts a nighttime warm layer near 100 km (Bougher, 1995) which is probably associated with the dayside warm region in the lower thermosphere produced by solar absorption in the CO_2 near-IR bands (Brecht et al., 2011). This inversion layer is robust in the VTCGM for solar mimimum conditions and on the dayside seems to be displaced upwards (around 120 km). This nightside layer seems to be confirmed by stellar occultation measurements with SPICAV/VEx (Bertaux et al., 2007a) and also recently by microwave ground-based observations (Sonnabend et al., 2010, 2011), although these data were very noisy. However, these results seem incompatible with other studies, in particular with all previous nightside Venus upper mesospheric temperatures from sub-millimiter CO line observations (Clancy et al., 2003, 2008). This point seems to be inconclusive at the moment, requiring a better quality and a longer-term sounding for its final clarification.

1.1.2 CO density and temperature in the Venus upper atmosphere.

The aim of this section is to summarize the current understanding of CO density and temperature in the upper atmosphere of Venus, considering what was learnt from measurements before the arrival of VEx, from the latest results during VEx era, and from the 2-D models and 3-D GCM predictions. The knowledge of these physical parameters in the upper atmosphere has been noticeably improved in the last years thanks to the implementation of more and more sophisticated instruments, both from ground and from satellite, capable of detecting the weak signal emitted in those rarefied layers of the atmosphere.

Before VEx

The information about minor atmospheric constituents like CO, their concentration, reactions, sources and sinks is incomplete above 100 km, since most measurements have been performed below 100 km, in the lower mesosphere , and below the cloud tops.
The first investigations in the past, especially from millimeter-wave observations focused on the horizontal and vertical distribution of carbon monoxide and showed that the CO mixing ratio increases with altitude in Venus' mesosphere (Kakar et al., 1976). Since then we know that the primary source of CO in the atmosphere of Venus is the photo-dissociation of CO_2 by solar UV at altitudes higher than 120 km (von Zahn et al., 1983; Huebner et al., 1992).

This was confirmed by observations of microwave lines of CO which yielded CO mixing ratio for altitudes between 75 and 105 km (Clancy et al., 2008).
Other studies were mostly concerned with the diurnal variability of mesospheric CO (Schloerb et al., 1980; Wilson et al., 1981). The most detailed measurements were carried out by Clancy and Muhleman (1985, 1991), and successively by Clancy et al. (2003, 2008) who used sub-millimeter line observations of ^{12}CO and ^{13}CO to constrain CO mixing ratio and temperature profile in the mesospheric region (70-100km). All these studies inferred that in the upper mesosphere ($z > 95km$), CO is larger on the nightside than on the dayside, whereas the opposite happens in the lower mesosphere. Clancy and Muhleman (1985) interpreted these variations in terms of general circulation and suggested that the near-midnight maximum above 95 km was due to the penetration of the strong thermospheric subsolar-to-antisolar flow into the mesosphere. On the other hand, the morning maximum at lower altitudes would result from the combination of the SS-AS flow with a tropospheric zonal retrograde flow (Lellouch et al., 1994). CO not only exhibits a significant diurnal variation but also strong year to year variations (Clancy and Muhleman, 1991; Clancy et al., 2003; Gurwell et al., 1995). Clancy and Muhleman (1991), based on Pioneer Venus (Taylor et al., 1985; Kliore and Mullen, 1988) and CO millimeter observations, observed secular variability between 1978 and 1986, probably associated with large mesospheric temperature (> 40 K) and dynamical variations between 90 and 100 km.

Regarding the thermal structure of the upper atmosphere, the measurements of temperature above 100 km are also very scarce, and even more if we focus on daytime observations (see Table 1.1.2). The vertical 1-D thermal structure of reference above 50 km are taken from the empirical model of Hedin et al. (1983). This is based on Pioner Venus Orbiter (PVO) data from the Orbiter Neutral Mass Spectrometer (ONMS) (Niemann et al., 1980) and on entry probe density measurements which were normalized to the Orbiter Atmospheric Drag (OAD) data (Keating et al., 1980). Temperatures on the dayside remain virtually constant throughout the solar cycle at values around 170 K between 50 and 80 km, and above 100 km they begin to rise sharply. In addition to the peculiarities of the cryosphere and the mesopeak, and to the open debate about the mesopause variability, all of them mentioned above, another result which is noticeable on Venus, is the relatively small variability of the dayside temperatures in the thermosphere with the solar cycle, as compared to Earth or Mars, both of which are further from the Sun and might hence be expected to react more weakly to the solar EUV forcing. The causes of this behavior are once more linked to the effective cooling by CO_2 mentioned above.

VEX Era observations

For the first time a systematic study of the upper layers of the Venus atmosphere is possible with new VEx observations. Two specific instruments on VEX focus on measurements in this region: the Spectroscopy for investigation of Characteristics of the Atmosphere of Venus SPICAV/Soir and the Visible and Infrared Thermal Imaging Spectrometer (VIRTIS). A third instrument, VEnus RAdio science (VERA), which operates in radio occultation, achieves a very good vertical resolution and sensitivity, but is very noisy above 90 km. The description of VIRTIS is presented in Section 1.2.3. Here we briefly review the main results by the dual SPICAV/SOIR instrument.

Method	Temperature (K)	Altitude (km)	Reference
Sub-mm CO line ground obs.	181-107	100-106	Clancy et al. (2012)
Sub-mm CO line ground obs.	190-200	100-106	Clancy et al. (2003)
Mid-IR CO2 line ground obs.	250 ± 10 (SSP)	100-120	Sonnabend et al. (2010)
Mid-IR CO2 line ground obs.	220 ± 10 (Mid N lats)	100-120	Sonnabend et al. (2010)
Mid-IR CO2 line ground obs.	180 ± 10 (High N lats)	100-120	Sonnabend et al. (2010)
IR CO line ground obs.	189± 8	105± 5	Crovisier et al. (2006)
IR CO line ground obs.	257± 16	135± 10	Crovisier et al. (2006)
	CO vmr		
Sub-mm CO line ground obs.	2.9E-04- 3.5E-04	100-102	Clancy et al. (2012)
Sub-mm CO line ground obs.	2.3E-04	100-102	Clancy et al. (2003)

Table 1.3: Summary of Temperature and CO measurements for the Venus dayside above 100 km available so far.

Regarding the temperature, SPICAV provides repeated measurements of vertical profiles of atmospheric temperatures from the cloud top ∼60 to 150 km via solar and stellar occultation, respectively, with very high vertical resolution (Bertaux et al., 2007a; Vandaele et al., 2008).
Measurements by SPICAV on the night side revealed a noticeably warm layer around 100 km and a high temperature variability between 95 and 100 km, with an observed temperature range from ∼185 K to ∼ 240 K (Bertaux et al., 2007a; Brecht et al., 2011).
Ground based observations have recently complemented VEx. Rengel et al. (2008) compared a single temperature profile for one nightime observations with Bertaux et al. (2007a) and they found temperatures ∼ 185 K at 100 km, consistent with the cold limit of the SPICAV results. Submillimeter observations have also been reviewed by (Clancy et al., 2008) after compiling several previous campaigns (Clancy et al., 2003; Clancy and Muhleman, 1991) and they systematically found cooler temperatures than Bertaux et al. (2007a) and Rengel et al. (2008). Nevertheless, Clancy et al. (2008) also found occasionally a small temperature inversion, much smaller than that from SPICAV; in fact, their inversion is marginally outside their error bars (typically 5-7 K). They suggest that this temperature increase is caused by a diurnal radiative balance, in other words, either a local time effect which varies with altitude, or stochastic turbulent changes upon a general trend. On the contrary Bertaux et al. (2007a) propose that large inversions are possible at nightime and they are due to localized compressional heating from the down-welling of the day to night thermospheric circulation. A qualitative similar behavior has long been predicted by the Venus Thermospheric GCM (Brecht et al., 2011).
Further studies derived nightside temperatures maps from O_2 ($a^1\Delta_g$) and IR nightglow (Bailey et al., 2008; Ohtsuki et al., 2008) and they both observe a nightside warm layer and a correlation with the peak O_2 nightglow. This lead them to the same conclusions than Bertaux et al 2007 about its origin, in other words, as a result of down welling from the thermosphere along the SS-AS global circulation. However, the inversion layer observed is not as large as that of SPICAV.
Sonnabend et al. (2010) retrieved temperature from direct observations of non-LTE emis-

sion by CO_2 at 10 μm, predicted to be originated at an altitude around 110 km, with an uncertainty of 10 km (López-Valverde et al., 2011). Those authors found a strong local time and latitude dependence. Even though those high values are in disagreement with the prediction of the VIRA model, they area consistent with the recent observations by SPICAV (Bertaux et al., 2007a).
In contrast, the VIRA model is much cooler than what is currently being observed. However, it should be noted that VIRA is a diurnally averaged empirical model making use of only two profiles above 100 km, one for daytime and other for night conditions, but as the authors claimed (Keating et al., 1985), this is a simple division due to the lack of information on local time or latitudinal variations at the time of the measurements. Moreover, and for the purpose of comparison with VIRA, it should be remarked that Pioneer Venus measurements correspond to solar maximum conditions, while during VEx observations the solar activity was near a minimum.

Regarding the CO density, the observational record of CO is incomplete in spatial coverage, particularly on the day side and at altitudes above 100 km, as shown in Table 1.1.2. These correspond mainly to ground-based observations of the night side and indicate substantial temporal and spatial variability in the mesosphere (Clancy et al., 2012). One result from those microwave observations is a distinct (20-50 %) increase in the CO abundance during the night above 90 km.
Latitudinal variability of CO has been investigated in the lower mesosphere, around the cloud top, by Irwin et al. (2008) using VIRTIS data in the nightside. They found a fairly constant value with latitude, except for a tentative gradient with increasing CO toward the pole around 70 km. These are in contrast with the distinct positive latitude gradient obtained from microwave data at higher altitudes, and might be similar to the small (10 %) enhancement below the clouds (Marcq et al., 2006).

On board VEx, also SPICAV/SOIR measured a number of CO profiles during sunset or sunrise (Mahieux et al., 2010; Vandaele et al., 2008), and as typically in occultation data, they have a very good vertical resolution. The few profiles published so far by Vandaele et al. (2008) extend form 75 to 125 km and do not show a large variability, nor they are far from the PVO or the microwave abundances. The most interesting feature of the SOIR profiles is a clear minimum around 85 km, which is not present in ground-based data. The steady increase with altitude starts again above 90 km in the SPICAV/SOIR data. Whether this is a systematic or a singular result is waiting for more SOIR retrievals. In addition to this, there are measurements of the 4.7 μm 1-0 band of CO from higher altitudes with VIRTIS on VEx, with sufficient S/N up to the thermosphere (Gilli et al., 2009, 2011). These are non-LTE daytime fluorescent emissions, and there are model predictions about its behavior (López-Valverde et al., 2007). The study of those upper layers during daytime requires a non-LTE model and is the objective of this work. This is the first time that a non-LTE retrieval has been deveped to sound this unknown region of the Venus atmosphere.

Model predictions

The observed diurnal density, temperature and airglow variations on Venus atmosphere are not very well reproduced by existing GCMs, if an unique set of wind fields, eddy diffusion coefficients and wave drag parameters is used (Bougher et al., 1997). This may reflect

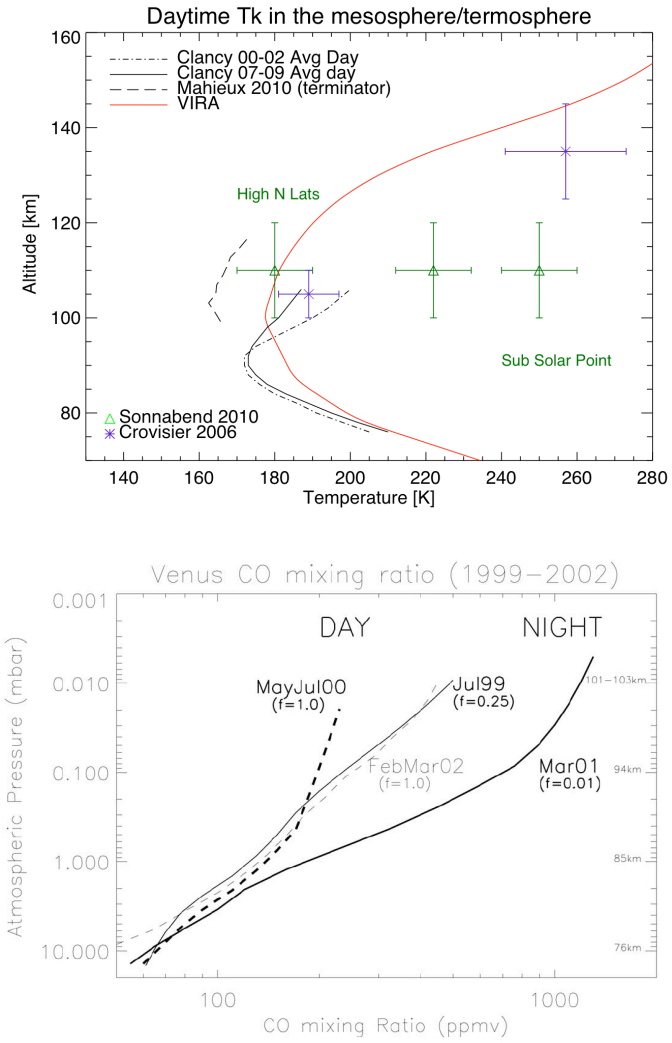

Figure 1.3: Top panel: Daytime temperature measurements of Venus upper atmosphere by ground base observations from the literature. A profile of temperature from SPICAV/VEx measurements is also plotted, but it correspond to the terminator (dashed line). VIRA thermal profiles is indicated with a solid red line as reference. Bottom panel: Variations of the CO mixing ratio from the microwave observations by Clancy et al. (2003).

missing physical processes or inputs, and in general, the existence of too many free parameters so far. The modeling task would be greatly improved if simultaneous measurements of winds, temperature and density in the region above the cloud tops (65∼200 km), along with the quantification of gravity wave parameters could be done (Bougher et al., 2006).

Pioneer Venus (PV) observations provided the information that was used for the development of global empirical models of the thermospheric structure for solar maximum

conditions (Hedin et al., 1983; Keating et al., 1985), which characterize the Venus International Reference Atmosphere (VIRA). Also, simpler models developed for heating efficiencies (Hollenbach et al., 1985) or mean subsolar-to antisolar circulation (Bougher et al., 1986), exploited additional work based on PV data.
A three-dimensional (3D) extension of the first model used by Bougher et al. (1986) was developed by Bougher et al. (1987), who built a Venus Thermospheric General Circulation Model (VTGCM) which provides a fully self-consitent and quantitative description of the Venusian upper atmosphere. In those pilot studies the neutral density (e.g CO_2, O, He and H) and temperature distribution observed by the PV orbiter were examined in order to constrain general circulation model simulations from which SS-AS and RSZ winds could be extracted (Brecht et al., 2011). Minor species distribution, especially CO have also been used to constrain upper atmospheric wind patterns (Lellouch et al., 1997).
The VTGCM predicts a diurnal variation of exospheric temperatures and densities at 160 km, which is symmetric in Local Time around the noon, as expected. Furthermore, CO_2, CO and O all exhibit dayside bulges with the CO2 showing the greatest variation.This result also suggests that superrotation has little influence upon the day-night distributions of heavy species and temperatures above 140 km. Below 130 km the VTGCM predicts that the supperrotation provides for little change in the distribution of winds or densities and temperature (Bougher et al., 1987), The symmetric nature of the VTGCM temperatures agree with VIRA, despite the fact that VIRA dayside temperatures are cooler.
Recently, the VTGCM has been updated and revised in order to address three key observations from VEx in the upper atmosphere: O_2 IR nightglow, NO UV nightglow and night-side temperatures, all of which should contribute to a comprehensive understanding of the global dynamics and circulation patterns above $\sim$ 90 km (Brecht et al., 2011). The "mean" simulations of this 3D model reproduce several interesting characteristics observed by VEx (see Figure 1.1.2). The predicted thermal structure present a warm region (about 207 K) near 112 km at the sub solar point (12h local time), mainly created by near IR heating, and on the nightside the dominating adiabatic heating produces a warm layer around 103 km. Brecht et al. (2011) suggested that the nightside warm region is associated with the day side warm region (in the lower thermosphere) and is resulting from the day-to-night global circulation, which produces dynamical heating near midnight. These simulations seem to explain the warm nightside temperature near 100 km observed at midnight by VEx (Bertaux et al., 2007a) and by Sonnabend et al. (2011). Above 130 km on the nightside, the VTGCM temperatures remain cold at about 114 K, reproducing the nightside cryosphere depicted by PVO observations and by previous modeling (Keating et al., 1980; Bougher et al., 1997).

1.1.3 Comparative aeronomy of the terrestrial planets

Nowadays the comparative planetology has a large and increasing interest also for the case of the Earth: as an experimental laboratory this field permits to represent similar physical systems in very different conditions, and therefore it is fundamental to understand common processes and the common evolution of the three terrestrial planets on a large scale. This also applies to their atmospheres. We will not discuss here all the specific processes that are suited for interesting inter-comparison between the atmosphere of the

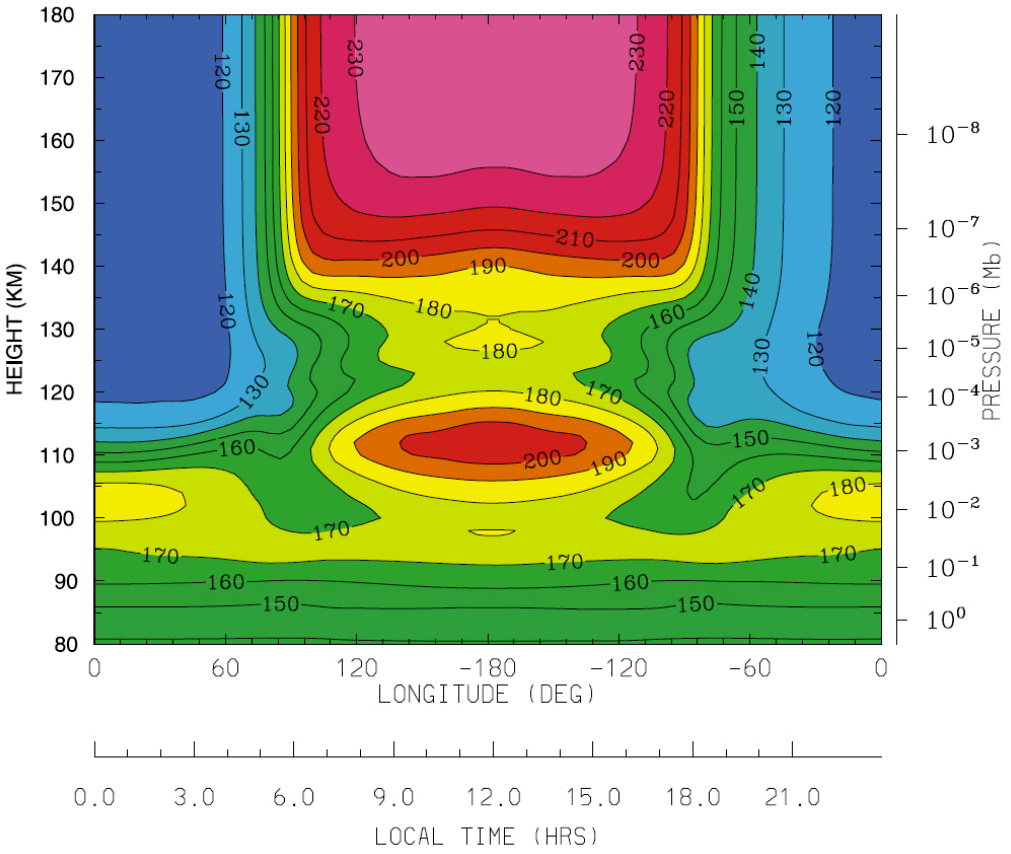

Figure 1.4: Cross section of the thermal structure of the Venus upper atmosphere produced by the VTGCM for mean VEx conditions (solar minimum fluxes). Local time values correspond to the 2.5ºN longitude. After Brecht et al. (2011).

three terrestrial planets but we will concentrate on some basic features of Mars, Venus and Earth atmospheres, and with focus on their upper layers.

The atmospheres of Earth Venus and Mars have similar origins and they are likely the result of similar out-gassing of volatiles from their interiors, but their obviously different evolutionary pathways may be ultimately due to their different masses and distances to the Sun (Krasnopolsky, 2006; Gladstone et al., 2002). As en example, almost all the water on Venus may have been lost by hydrodynamic escape, leaving a large reservoir of carbon in the atmosphere. On Earth, atmospheric CO_2 was dissolved in the ocean and formed carbonates, which represents the largest store of carbon. However, on on Mars most of the water may have been lost in reaction with iron or buried in the permafrost, after severe climate changes, and most of its CO_2 atmosphere may have also been lost by this mechanism, and by the intense meteorite impacts (Krasnopolsky, 2011).
In the three planets, the structure and dynamics of the upper layers (including temperature, pressure compositional distribution and wind distribution) are primarily determined by direct absorption of solar electromagnetic radiation in the short-wave spectral range

(Mendillo et al., 2002). In the upper portion of the middle atmosphere and, and especially in the thermosphere temperatures experiment large day-night changes, since the primary energy exchange is caused by the absorption of radiation, in the ultraviolet and soft X-ray range in the thermosphere and in the IR in the mesosphere. The main differences between the upper atmosphere of Venus and Mars must eventually be caused by the solar radiation and gravity acceleration (Krasnopolsky, 2011). The former is weaker on Mars than on Venus by a factor of 4.5, the latter is larger on Venus than on Mars and perhaps these factors contribute to the fact that the atmosphere of Mars is geometrically thinner, although the climate evolution must have played a role too.
In contrast to processes on Earth's upper atmosphere, where oxygen and nitrogen play a decisive role, processes occurring in the upper atmosphere of Venus and Mars are mainly controlled by the photochemistry of carbon dioxide. It is expected that O and CO are more abundant on Venus than on Mars by approximately a factor of 10 and this agrees with the observations. The more abundant atomic oxygen produces a stronger cooling of the upper atmosphere of Venus, due to the thermal-to-vibrational collisions with CO_2 via $O + CO_2 \rightarrow CO_2^* + O$ (Krasnopolsky, 2011). Subsequently, the vibrationally excited CO_2^* losses this internal energy by emission in different hot and combination vibrational bands, in the 15 μm spectral region.

Another puzzling aspect of the atmosphere of Mars and Venus is that their CO_2 atmosphere is stable (except for the known seasonal changes on Mars). CO_2 can be destroyed by photolysis ($\lambda \leq 0.2$ μm) on a relatively short time scale on both planets, and its stability seems to be guaranteed only with the assumption of heterogeneous processes that have to recycle CO_2 (Atreya and Gu, 1994). On Mars, the main catalytic role is played by the hydroxyl radicals (OH), by recycling CO and O or CO and O_2 into CO_2, while on Venus this mechanism fails, since the content of hydrogen is smaller (Baines et al., 2006). In addition to this, the oxygen is primarily consumed by CO_2 recombination and by the formation hygroscopic sulfuric acid (H_2SO) (Yung and Demore, 1982). On Venus, however, photolysis of HCl in the upper stratosphere provides a major source of odd hydrogen and free chlorine radicals, and Yung and Demore (1982) suggested that chlorine might play a catalytic role in Venus similar to OH in the Martian atmosphere.

1.2 Remote sounding in the infrared

The term *remote sensing* refers to any technique used to make measurements on a system without the use of in situ instruments. For instance, the analysis of the characteristic spectral signatures of the different molecular species and their associated vibration-rotation and electronic bands obtained with this technique in different wavelengths, provide precise measurements (Payan et al., 2005). The main roto-vibrational transitions of several molecules present in planetary atmospheres occur in the IR spectral domain [$\lambda = 1 - 100$ μm]. Moreover, compared to the UV and visible spectral domains, IR and microwave observations have the advantage of great accessibility from ground-base telescopes (Drossart, 2005) and consequently this allows long time series of measurements, useful to establish long-term trends and with high signal to noise ratio and high spectral resolution. In the content of planetary observations, high resolution spectrometers represent nowadays one

of the most powerful remote sensing tools. However, the ground-based observations are hindered by two main factors, the vertical resolution and the opacity of the atmosphere of the planet, limiting the measurements only to those in the most transparent windows.
On the other hand, remote sensing from satellite is very suitable to monitor the whole atmosphere of a planet because it provides global observations. In particular, limb sounding from space has proved to be a valuable technique for atmospheric composition measurements in the stratosphere and mesosphere, since good vertical resolution and large optical paths provide a high sensitivity to low concentration species (Payan et al., 2005). The common limitations of the observations from satellites are well known: the short-term coverage of a single spot and the limited spectral resolution.

A preliminary knowledge of absorbing and emitting properties of the target molecules is required before applying remote sensing techniques, and these properties are tabulated as spectroscopic parameters (e.g line positions, intensities, widths) and included in data bases such as HITRAN (Rothman et al., 2005). Those properties are usually derived from experimental and/or theoretical spectroscopic studies.Regarding Venus, unique infrared studies form space were provided by Galileo Venus flyby in 1990. This experiment benefited from the recent, at that time, discovery of the IR windows in the Venus atmosphere (Allen and Crawford, 1984). On board Galileo the instrument NIMS obtained spectacular views of the deep cloud structure, and detected surface features in the near IR window at 1.18 μm(Drossart et al., 2007c). Despite its short duration, this flyby provided new results on the cloud structure, the atmospheric composition, and even the dynamics (Carlson et al., 1992).
After a gap of about 20 years of missions to Venus, Venus Express and its six instruments on board was launched in November 2005 and its infrared measurements, some of which are the subject of this thesis, are providing unique insights into the upper layer of the atmosphere of Venus.

1.2.1 The Venus Express (VEx) mission

For more than a decade, after the emphasis for investigations of the terrestrial planets shifted from Venus toward Mars in the late 1980s, Venus was a forgotten planet. Space missions to Venus have not been very numerous since the mid 1980s, and for a long time, many studies had o be confined to re-analysis of data obtained form previous missions (de Bergh et al., 2006).
At last, in 2001 the European Space Agency (ESA) approved Venus Express (VEx), as part of its program for the exploration of the inner solar system. The satellite was equipped with a combination of instruments employing completely new techniques as well as improved versions of conventional instruments, partly inherited from Mars Express (Wilson and Chicarro, 2004) and from Rosetta (Coradini et al., 1999).
The payload included three spectrometers: SPICAV/SOIR, a high resolution UV and near IR spectrometer for stellar and solar occultation (Bertaux et al., 2007a), PFS, an high resolution IR spectrometer (Formisano et al., 2005) and VIRTIS, an imaging and high resolution spectrometer for the visible and infrared spectral range (Drossart et al., 2007a; Piccioni and VIRTIS/Venus Express Team, 2009). The optical package was complemented by a miniature Venus monitoring camera operating in the visible and near-IR

range (Markiewicz et al., 2007b,a). VEx included other three experiments suited for the upper atmosphere: ASPERA, to investigate plasma and neutral energetic particles around Venus (Barabash et al., 2007b,a), MAG for magnetic field studies (Zhang et al., 2006) and a radio science experiment, VeRa (Häusler et al., 2006). Unfortunately, a mechanism that controls the mirrors failed on PFS since the launch, and in spite of many attempts it was not possible tho move the scanner, making the instrument unusable.
Figure 1.5 shows the location of the instruments on the spacecraft, and compare their FOV relative to the disk of the planet.

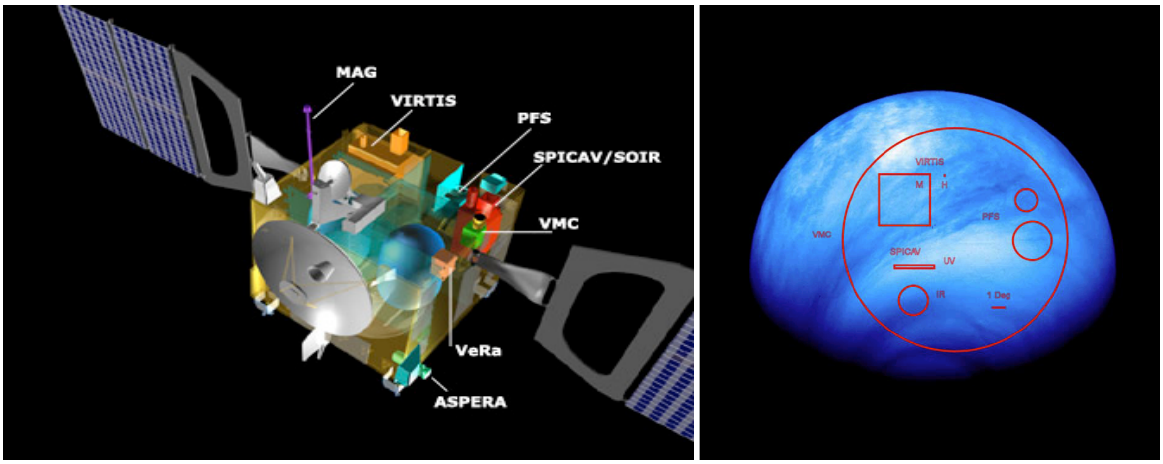

Figure 1.5: Left: Artistic diagram of the internal disposition and the relative sizes of the seven remote sensing instruments on board Venus Express. The size of the satellite main body is 1.65m x 1.75m x 12.4m, solar panels excluded. Right: Comparison of the fields of view (FOV) of the VEx instruments at a distance of 20,000 km form Venus. The background image was taken by VMC at ultraviolet wavelengths from about 35.000 km. The south pole is at the the bottom of the image. At the apocenter (60,000 km) the VIRTIS-M FOV is about one third of the planet. Credits ESA

Venus Express also benefited from the considerable experience accumulated by ground-based observations and it has a number of clear advantages to previous Venus missions. These extend from the technological improvement and the duration of the orbital mission, longer than any other, to the higher spatial resolution due to the proximity of the spacecraft to the planet. In addition to this, its near polar orbit permits to sound regions hardly accessible by previous missions, or from Earth observations (López-Valverde et al., 2008). VEx was launched in November 2005 and since June 2006 it is providing valuable information to understand processes responsible for current climate on Venus and its evolution over the time. VIRTIS investigations are intended to make systematic use of the transparent infrared spectral windows in order to probe the atmosphere in four dimensions: the three spatial dimensions plus time (Svedhem et al., 2009). After four years of "nominal" plan the mission extension was approved and was it is expected to last at least until the end of 2014, when the present funding runs out (Svedhem and Titov, 2011).

1.2.2 Main results from Venus Express

Although many successful measurements were taken since 1960 from data collected by more than 25 spacecrafts, which greatly advanced our description of Venus, a list of fundamental problems in the physics of Venus remain unresolved (Titov et al., 2006). For more than 5 years Venus Express (VEx) and its six instruments have continuously provided high quality data of Venus with the hope to address some of the topics.
The overall scientific objective of the Venus Express is to carry out a global, long-term remote and in situ investigation of the atmosphere, the plasma environment and some aspects of the surface of Venus from orbit (Titov et al., 2006; Svedhem et al., 2007). Its 24 hour polar orbit permitted extended global studies of the southern hemisphere and in particular of the southern vortex structure and dynamics; in addition to analysis of chemical composition throughout the atmosphere, and dedicated observations of the structure and dynamics of the cloud layers (Svedhem and Titov, 2011).

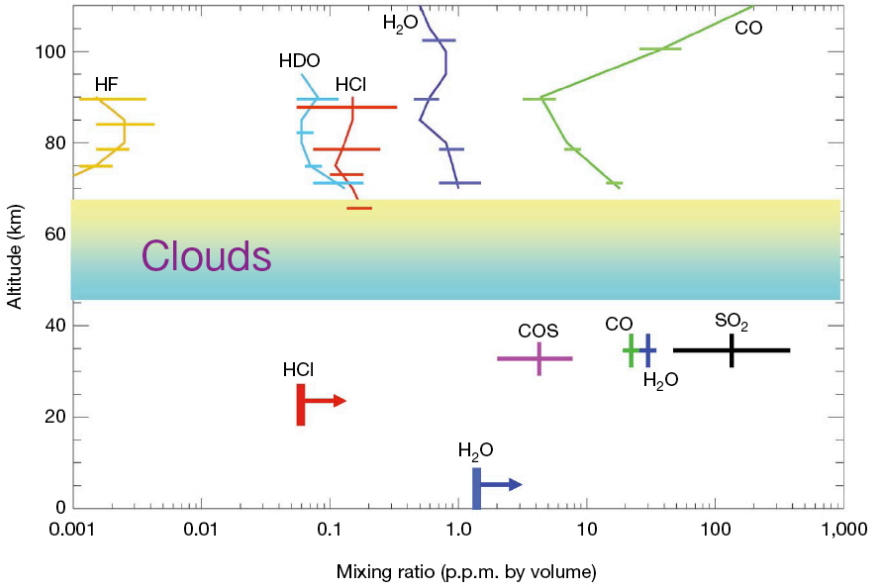

Figure 1.6: The abundance of the most important minor gases in the atmosphere of Venus from Venus Express observations. Credits Svedhem et al. (2007).

Among the main results obtained during the whole mission, we mention here only a few of them, which are also relevant for the topic of this thesis. First of all, the discovering by SPICAV of an unexpected warm layer at the mesopause ($\sim$ 100 km), interpreted by Bertaux et al. (2007b) as adiabatic heating of descending air. Let us also recall the remarkable latitudinal temperature variations found at the cloud tops (Lee et al., 2012), as well as the presence of a convective region within the "cold collar" all over the planet observed by VIRTIS and VMC (Titov et al., 2008). A global north/south symmetry is suggested by the temperature field obtained in the mesosphere of the southern hemisphere, similar to that observed in the northern hemisphere by earlier missions (Piccialli et al., 2012). The observations by VMC in the ultraviolet also showed evidences of convection in the cloud layer at

low latitudes (Titov et al., 2012). The detailed observations of the cloud morphology and dynamics, together with the polar orbit of VEx, led to the discovery and characterization of the complex "eye" of the southern polar vortex for the first time (Piccioni et al., 2007; Luz et al., 2011)
O_2 and NO airglows observed in the UV and near-IR approximately at the mesopause level and in the equatorial region, indicate a thermospheric solar-anti solar component in the atmospheric circulation. Vertical profiles of CO, H_2O, HDO, HCl, HF and SO_2 between 70-100 km shed light on the composition in the mesosphere together with global mapping of CO, COS, H_2O and SO_2 in the lower atmosphere (see Figure 1.6). Those results provide powerful tests of dynamical and chemical models of the Venusian atmosphere.
In addition to this findings in the atmosphere, it should be remarked that VIRTIS also performed thermal mapping of the surface of Venus in the near-IR spectral windows on the nigthside, in order to search for surface emissivity anomalies and possible signs of active volcanism (Smrekar et al., 2010)

Recently atmospheric drag campaigns have been carried out, and up to june 2001 a set of 15 data points down to an altitude of 165 km have been sampled (Svedhem and Titov, 2011). Those experiments offer the possibility to probe *in-situ* the atmospheric density in the altitude range 165-200 km, which is difficult to sound with remote measurements. Nowadays, more then 3.5 Tbit of science data has been downloaded to ground. The VEx mission is currently extended up to 2014 and continued measurements in the coming years will provide new insight to the importance of the solar activity for the different processes already studied at low solar activity (Svedhem and Titov, 2011).

1.2.3 The instrument VIRTIS on Venus Express

The Visible and Infrared Thermal Imaging Spectrometer (VIRTIS) on board Venus Express provided the data set used in this work. This section is devoted to describe the main characteristic of the instrument. A more detailed technical description is given in Piccioni et al. (2006) and in Table 1.4 from Drossart et al. (2007a).
VIRTIS was proposed for the Rosetta mission (Coradini et al., 1999) to study the properties of a cometary surface and the coma, and thanks to the high versatility of the observing modes the specification of VIRTIS were also found suitable for the study of the atmosphere of Venus. It is a dual instrument which combines two unique channels of data in one compact instrument:

- **VIRTIS/M**: a mapping spectrometer working in the visible (VIRTIS-M-vis from 0.3 to 1 μm) and in the infrared (VIRTIS-M-IR from 1 to 5 μm), with moderate spectral resolution (R $\sim$ 400).
- **VIRTIS/H**: a high-resolution echelle (R $\sim$ 1800) spectrometer with a spectral range in the infrared 2-5 μm.

The instantaneous field of view (IFOV) of VIRTIS-M over the whole slit is 0.25 x 0.64 mrad/pixel, corresponding to about one-third of the diameter of Venus at apoapsis ($\sim$ 60000 km from the planet). VIRTIS-H has a FOV slightly larger than a pixel of VIRTIS-M (0.5 x 1.5 mrad), which is particularly useful for limb-viewing observations (see also Figure

1.5, right panel). VIRTIS operates in nadir/disc viewing when VEX is a far from Venus (apoapsis), but also in a limb sounding geometry near and during periapsis.
The observations are stored in data-cubes, available in the PDS standard format (McMahon, 1996). They contain two spatial dimension and one spectral. There are usually three kind of cubes: the *. QUB files containing the raw images, the *.CAL files for the calibrated images and the *.GEO files with geographical and navigation information. For the first time on Venus, investigations make systematic use of the transparent infrared spectral windows in order to probe the atmosphere in four dimensions: three spatial dimensions plus time.

Parameter	VIRTIS-M		VIRTIS-M
	Visible	Infrared	Infrared
Spectral range (μm)	0.27-1.1	1.05-5.19	1.84-4.99
Spectral sampling (nm)	1.9	9.8	0.6
FOV (mrad^2)	64 x 64		0.58 x 1.75 per 3 pixeles
Pupil diameter (nm)	47.5		32
F #	5.6	3.2	2.04
Slit dimension	3.8 μm x 9.53 mm		29 x 89 μm
Detector format (p x)	512 x 1024	270 x 438	270 x 438
Saturation charge (Me)	¿ 0.4	¿2	¿ 2

Table 1.4: Main characteristics of the instrument VIRTIS. After Drossart et al., 2007)

VIRTIS is addressing a large number of scientific questions and has generated striking images and video sequences of the south polar vortex, non-LTE emission patterns, profiles of abundances of several atmospheric gases, wind field maps and temperature profiles over the southern hemisphere, images of cloud structure at several altitudes and surface temperature and emissivity, to mention just a few (Svedhem et al., 2009; Svedhem and Titov, 2011). It also provided valuable measurements of the IR emission of CO_2, the main component of the atmosphere of Venus, together with other trace spaces like CO and O_2. The objective directly related with our work is the sounding of the mesosphere and thermosphere of Venus by non-LTE IR emission with special emphasis on the CO emission at 4.7 μm and the CO_2 emission at 4.3 μm.

VIRTIS strategy and planning of observations

During normal operations, the strategy of observation of VIRTIS is divided into two categories:
1) *Spectral mode (spacecraft altitude* $<$ 12000 *km)*. This mode permits a partial coverage of the disk, although a statistically significant part of the planet could be covered after about seven orbits. Thanks to the proximity to the planet a reduced FOV is achieved, and these observations are ideal for tangent limb measurements and to study the variability of the atmospheric composition in the upper layers. Both VIRTIS-M and VIRTIS-H can be operative.
2) *Spectra-imaging mode (spacecraft altitude* $>$ 12000 *km)*. This mode was specifically designed for VIRTIS-M mosaic global imaging of the Southern hemisphere in order to

obtain images up to know unique of Venus (Titov et al., 2006). These observations would complement VMC imaging and SPICAV measurements, thus favoring the synergy between VEx instruments.

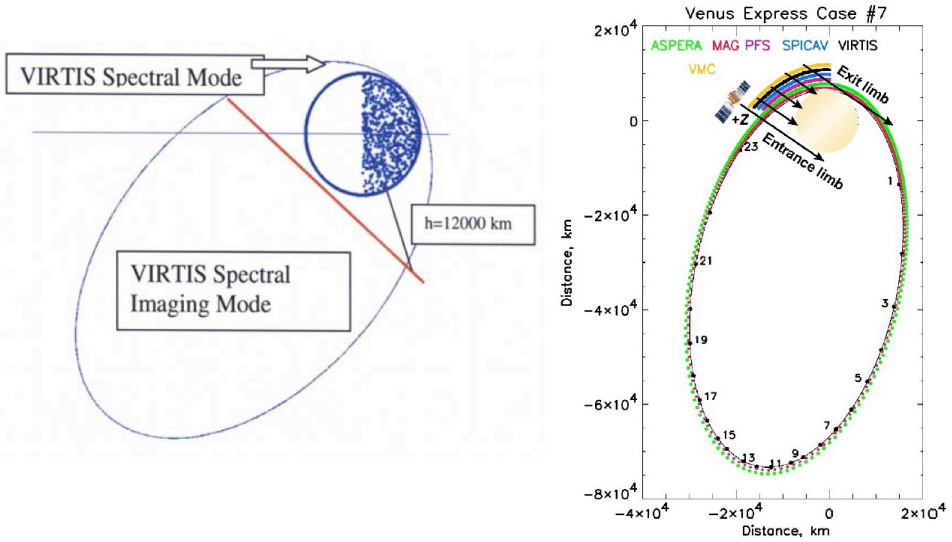

Figure 1.7: *Left panel*: Observation modes of VIRTIS: Spectral mode versus spectral imaging mode (see text for details) *Right panel*: Case 7 "Tangent limb". Each orbit around Venus corresponds to one terrestrial day. There are 24 divisions along the orbit, marked with asterisks, that correspond to the 24 hours of a complete orbit. (Credits: Venus Express, Mission definition Report, 2001)

Included in those two categories of observations there are 10 typical mode of observations, called "science cases", that differ by their science goals, geometry of observations and experiments involved (Titov et al., 2006).
The dataset that we used here belong mainly to the Case # 7 (Limb observation), and during the first stage of our analysis we also studied data from Case # 3 (Global spectro-imaging from apocenter). The right panel of Figure 1.7 shows an sketch of the orbit of Venus Express for Case # 7, and the list of instruments operating in each part of the orbit.

Even though the main goal of the Venus Express was to give a global and systematic survey of the atmosphere of Venus, the science planning prioritized areas with poor coverage from past missions, like the Southern hemisphere. This, together with the very elliptic polar orbit of VEx, makes the coverage of the Northern hemisphere very limited. The total number of VIRTIS spectral images over the southern hemisphere during about 2 years is shown in Figure 1.8, as a function of local time and latitude. Notice that the coverage from

the south pole to 50º S latitude is very good, but mid-latitudes and the equatorial region during daytime unfortunately have a poor coverage (Svedhem et al., 2009).

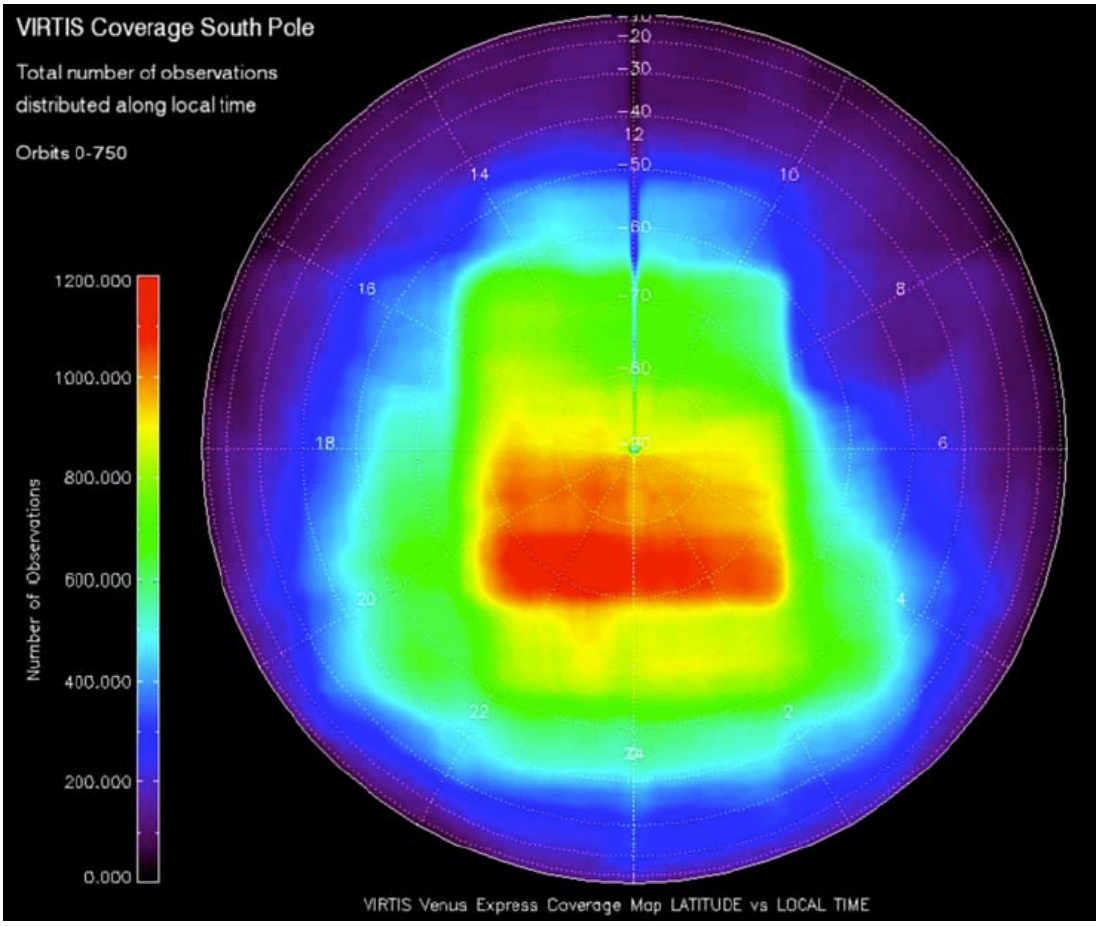

Figure 1.8: Coverage of the VIRTIS-M images of the southern hemisphere as a function of latitude and local solar time, from the orbit 0 to 750 (June 2006-May 2008). The scale on the left indicates the number of the observations (red is large, blue is poor). The coverage of the latitudes between 50º S and the south pole is very good, while the coverage at the equator and northward of the equator is very limited. After Svedhem et al. (2009)

1.3 Motivation and objectives of this work

The state of the upper mesosphere/lower thermosphere of Venus is poorly known because of the lack of regular measurements and validated models at those altitudes. Several interesting physical and chemical processes, like heating and cooling by radiative emissions, energy transport, dissipation of wave disturbances, etc., occur in this upper region and they are crucial for the understanding its energy balance. However, the low gas density of these regions makes them difficult to observe. They require sophisticated remote sounding techniques, preferably in limb-tangent geometry, i.e with precise pointing and stability, and with strong signals (solar occultation) and/or long integration times (emission observations).
Furthermore, these rarefied layers of the atmosphere of Venus are characterized by the breakdown of local thermodynamic equilibrium (LTE), and this is common to all planetary atmospheres. Under such circumstances, the ro-vibrational bands of molecules like CO_2 and CO produce strong emission in the IR (Lopez-Puertas and Taylor, 2001). Therefore, on one hand non-LTE emissions represent an advantage to sound the upper atmosphere, and on the other it adds a difficulty because they require proper non-LTE models for their interpretation and analysis. Once the main features and variability of those emission are well understood, with the help of the non-LTE models, the measurements may be used to derive relevant atmospheric parameters.

The arrival of the Venus Express (VEx) in June 2006 offered a unique opportunity to study systematically the non-LTE emissions on Venus, to validate the theoretical tools needed for their analysis, and to learn about the upper atmosphere of Venus. In particular, the instrument VIRTIS (Drossart et al., 2007c; Piccioni et al., 2006) on board VEx, has been measuring strong daytime IR emissions of CO_2 and CO, around 2.7 μm, 4.3 μm and 4.7 μm, respectively, with unprecedented spectral and spatial resolution.

The major objective of this Thesis is the scientific exploitation of VIRTIS dataset in order to make progress in the knowledge of the atmosphere of Venus above 100 km altitude. This goal has been pursued via a detailed data analysis and a specific theoretical study of the recent non-LTE VIRTIS measurements. For this purpose, a couple of theoretical tools were used: a non-LTE model of CO_2 and CO emissions in the Venus atmosphere (Roldán et al., 2000; López-Valverde et al., 2007), and a line-by-line radiative transfer code originally developed for the Earth's upper atmosphere (Dudhia, 2000). Also, a number of numerical tools were developed during the course of this Thesis, including data handling and averaging programs and a retrieval scheme specially devoted to these VIRTIS limb data.
The retrieval of atmospheric parameters was carried out in the final phase of the Thesis, from the CO emissions only. These data present a ro-vibrational structure well captured by the VIRTIS spectral resolution, and offered a large potential to test the scheme developed and to extract the maximum information from the data, deriving both kinetic temperatures and CO abundances.

The novel tool developed during this work, the retrieval scheme, required a special effort in order to test it and to gain confidence on its performance and error analysis. The peculiarities of these VIRTIS data suggested to build such retrieval on a χ^2 minimization strategy. A second steep was introduced as well, a linear inversion around the results of the minimization, in order to evaluate and constrain the error analysis further. Thanks to

this work, this retrieval code is in a suitable form to be exported to similar studies of limb observations, like PFS and OMEGA measurements of CO and CO_2 non.LTE emissions in the Mars atmosphere from Mars Express , and to nadir observations as well, like the VIRTIS mapping of the CO_2 4.3 μm non-LTE emission in Venus

1.3.1 Outline of this Thesis

This work is presented as a compendium of publications based on my PhD Thesis, carried out at the *Instituto de Astrofisica de Andalucia (IAA-CSIC)*, in Granada. This is in compliance with the normative *Artículo 27 de la Escuela de Posgrado de la Universidad de Granada*, concerning the content of the PhD thesis. Three of them have already been published between 2009 and 2011, and constitute the cores of chapters 2 and 3 of the present Thesis, while the last one, that forms the main part of chapter 4, is ready to be submitted. At the beginning of each chapter, and as a mode of introduction, a description of the work that led to the corresponding publication is presented, with a summary and a discussion of its main conclusions. Some results which have been fundamental for the development of this thesis, but were not included in the mentioned papers, have also been presented and discussed in more depth in those Chapter's introductions.

Starting with Chapter 2, this is centered in the description and analysis of the VIRTIS/VEx data during the first 4 months of the mission. Specifically, they were analyzed all the limb measurements in the upper atmosphere of Venus in the infrared window, where strong non-LTE emissions by CO_2 and CO permit the sounding of high altitudes during daytime conditions. It is the first time that observations of non-LTE emission have been performed in the atmosphere of Venus systematically and with high spectral resolution and good spatial coverage.

Chapter 3 is focused on the validation of the non-LTE model for Venus using CO_2 and CO emission observed by VIRTIS/VEx at 4.3 μm and 4.7 μm, respectively. A comparative study with non-LTE models for the Earth and Mars atmospheres is also performed. This consists of a common analysis of the most recent space observations of similar IR emission on the Earth's mesosphere, from MIPAS/Envisat, and on the Mars mesosphere from PFS/Mars Express.

The most ambitious part of the Thesis, which consists of the simultaneous derivation of CO density and temperature in the Venus upper atmosphere above 100 km, is presented in Chapter 4. There, first of all we described the precise criteria (small FOVs, daytime limb observations, etc) for the selection of data from the whole dataset of VIRTIS (from June 2006 to November 2010) which were going to be used for the retrieval. Several tests, including sensitivity and consistency tests, the error analysis and a comparison with previous results in the literature are presented in this chapter.
In the last chapter of the thesis, the conclusions obtained are summarized, and some ideas to expand this work and to be tackled in the future are proposed.

Chapter 2

VIRTIS/VEx observations and data analysis

In this chapter a description of the infrared (IR) measurements of the upper mesosphere and lower thermosphere of Venus (90-170 km) obtained by VIRTIS on board Venus Express (VEx) is presented. In the IR and during daytime conditions, the strong non-LTE emissions by CO_2 and CO offer the possibility to sound the atmosphere up to high altitudes (Lopez-Puertas and Taylor, 2001; López-Valverde et al., 2007). With this goal in mind, the analysis of these non-LTE limb observations was intended to understand the dataset, describe its variability, noise levels and data quality, identify the main emissions and to evaluate their potential for retrieval purposes. This detailed analysis focused on the first 4 months of observations of the VEx mission (June 2006 - September 2006). Part of this work was published in 2009 in the *Journal of Geophysics Research*, Volume 114, in a Special Issue dedicated to the first results by Venus Express, and is entitled: *Limb observations of CO_2 and CO non-LTE emissions in the Venus atmosphere by VIRTIS/Venus Express*. This paper forms the core of this chapter and is attached below.
Here, a summary of that work is presented, with a brief discussion of some of its main points and conclusions, and their relevance for the goals of this Thesis.

As mentioned in Section 1.2.3, the instrument VIRTIS supplies two signals, VIRTIS-H and VIRTIS-M, the former provides higher resolution spectra in the IR (2-5 μm) and the latter spectra and images to obtain global map of the disk of the planet in the visible (0.3 -1 μm) and near-IR (1-5 μm) ranges. The measurements of our interest are the ones taken during daytime (SZA between 0^{o} and 90^{o}) and above the cloud layer (from 60 -70 km upwards), where strong emissions by CO_2 at 4.3 μm and by CO at 4.7 μm were clearly observed. The signal-to-noise of an individual VIRTIS-H spectrum is good enough to detect CO_2 and CO emission up to about 160 km and $\sim$120 km, respectively. The weaker non-LTE CO_2 emission around 2.7 μm was also detected by VIRTIS-H around 120 km. In contrast to the CO_2 emissions, the VIRTIS-H spectral resolution permits the identification of the individual rotational lines of the CO(1-0), or fundamental band (FB), and of the CO(2-1) or first hot band (FH) around 4.7 μm, showing that this emission in the upper mesosphere (90-120 km) is mainly dominated by the optically thinner FH band.
Since the polar orbit of VEx is extremely elliptic and the periapsis is located near the

northern hemisphere, most of the observing time of VIRTIS was devoted to the southern hemisphere and to observations in a nadir geometry. Nevertheless, the instrument also provided tangential limb measurements during and close to the periapsis of VEx, which are the focus of this work. Those data are more suitable to study the uppermost layers of the atmosphere of Venus.
A typical periapsis orbit studied in this work is shown in Figure 2.1. The top-left panel shows a direct image of VIRTIS-M when the satellite was at about 650 km, during the orbit # 43, in the proximity of the periapsis. In the following panels the transformation of this map to the usual coordinates of altitude on the limb and distance on the surface of the planet is illustrated. The right-top panel shows a sphere, as a 3-D view of Venus, where the red lines represent the position (in latitude-longitude coordinates) of the pixels on the tangent point, which follows the satellite movement. The *pixel vs. pixel* image is converted into a 2-D map of radiance (bottom-right panel), to study the variation of the emission with physical parameters (tangent altitude, latitude, SZA, local time, etc). This map shows the strong emission of CO_2 at 4.3 μm in the limb of the planet, with its emission peak at altitudes around 120 km. Let us recall here that VIRTIS-M is a "dual" instrument which combines two spatial dimensions with a third spectral dimension, and therefore it permits to extract one spectrum in each spatial point of the image. These kind of *data-cubes* at different wavelengths are of great interest because they provide simultaneously 2-D maps of spatially distributed emissions and high vertical resolution profiles, for the first time on the dayside of Venus. VIRTIS-H also took measurements during this orbit, together with this VIRTIS-M map, and their data would be one individual spectrum per each strip of VIRTIS-M spectra, located at the centre of each vertical line. It is shown in the Figures 3 and 8 of Gilli et al. (2009).

A considerable amount of work has been especially devoted to the understanding of the behavior of VIRTIS-H and VIRTIS-M, from both the periapsis and the apoapsis. As explained in the manuscript, several strategies were followed: the correlation of the observations between the two channels, the revision of the theoretical or "nominal" noise values, the search for and the characterization of possible systematic effects, etc. In the case of VIRTIS-M mapping, it was proposed a correction to the so called "smiling effect" that produces an apparent bending of the images, especially the limb observations from the apoapsis. This correction is based on theoretical predictions of non-LTE CO_2 emission around 4.3 μm, plus some geometrical assumptions The effect is of the order of one pixel size, but at the distance of the apoapsis the error introduced in the tangent altitude registration is significant (section 2.5.2 of the manuscript). Another difficulty of VIRTIS-M data, especially a the longer wavelengths is a serious contamination, which produces unexpectedly strong emissions, as described in more detail in Chapter 4.
The geographical views which are possible with VIRTIS-H are unfortunately much more disperse than with VIRTIS-M, due to its slightly poorer vertical resolution, and most of all due to its obviously poorer spatial mapping. However, the information provided by the spectrograph VIRTIS-H is also fundamental for non-LTE studies and has the advantage of its high spectral resolution, which is very useful to scrutinize the ro-vibrational structure of the emitting molecules. In addition to this, VIRTIS-H data beyond 4.5 μm do not present any strong contamination. For these reasons, the rest of the work is devoted to the VIRTIS-H dataset.

Although we discuss the model-data validation in the next chapter, the manuscript attached in this chapter also contains a few validation studies. The shape of the bands and the peak intensities of the CO_2 and CO emissions were contrasted with a non-LTE model for Venus (Roldán et al., 2000; López-Valverde et al., 2007) and a general good agreement was found. The main variability observed in the data with SZA and altitude is also predicted correctly by the model simulations. We also studied the potential of VIRTIS data to retrieve atmospheric parameters, like densities and temperature, including a first attempt to determine the kinetic temperature from the CO emission rotational lines (section 2.3.3 of the manuscript). For this purpose the different lines observed were associated to the two mayor bands of CO, the fundamental and the first hot, and a couple of spectra were compared to proper numerical simulations. The main difficulty appeared to be how to select two different and strong lines of a given band (the FH for example) with very different quantum rotational numbers. It was concluded that the temperature should be a very important goal, if an adequate retrieval scheme able to fit the rotational structure were developed. This was apparently an easy task at that moment, however, an important aspect was overlooked, which became critical during the development of the non-LTE inversion in a later phase of the thesis. The noise of the CO spectra is high, and is crucial to characterize the overall shape of a band, which is were the information about the temperature comes from. As it is discussed in Chapter 4, this produces very large uncertainties during the inversion of the atmospheric temperature.

The main conclusions of this data analysis and the paper are summarized as follows:

- Strong emissions in the limb with both VIRTIS-H and VIRTIS-M were clearly identified at 4.3, 2.7 and 4.7 μm, and attributed to non-LTE daytime solar excitations of CO_2 and CO, respectively.

- Good signal-to-noise individual spectra are detectable up to above 160 km and 120 km in the case of CO_2 and CO, respectively.

- The nominal noise values are confirmed from "space" views of the non-LTE signals and from averaging of the wings of the bands, and they are used through the rest of the Thesis work.

- The comparison of VIRTIS-M and VIRTIS-H spectra, where the signals are coincident, show a good agreement in the 4.3 μm emission. Except for a few bad pixels, and the strong emission below 90 km, surely due to the scattering in the upper hazes, no serious systematic issues are found in the VIRTIS-H data set around 4.7 μm.

- The basic non-LTE features predicted by the non-LTE Venus model (López-Valverde et al., 2007), like the altitude and SZA variation of CO_2 and CO fluorescence, are observed by VIRTIS.

- The four months of VIRTIS observations studied in this Chapter are very useful not only to study the non-LTE processes but they may also supply interesting information about atmospheric variability in the lower thermosphere, when applied to a more extended dataset. Such extension was possible in the final phase of the Thesis, and is presented in Chapter 4.

- The development and application of non-LTE retrieval techniques to these measurements is very promising to derive atmospheric parameters in the upper mesosphere and lower thermosphere of Venus, such as densities and temperatures from the 4.7 μm CO emission, or densities from the 4.3 μm CO_2 data.

The publication included in this Chapter, represents the first analysis of the first extensive set of CO_2 and CO non-LTE measurements in the IR in the upper atmosphere of Venus, and should be useful to any further study using such database.

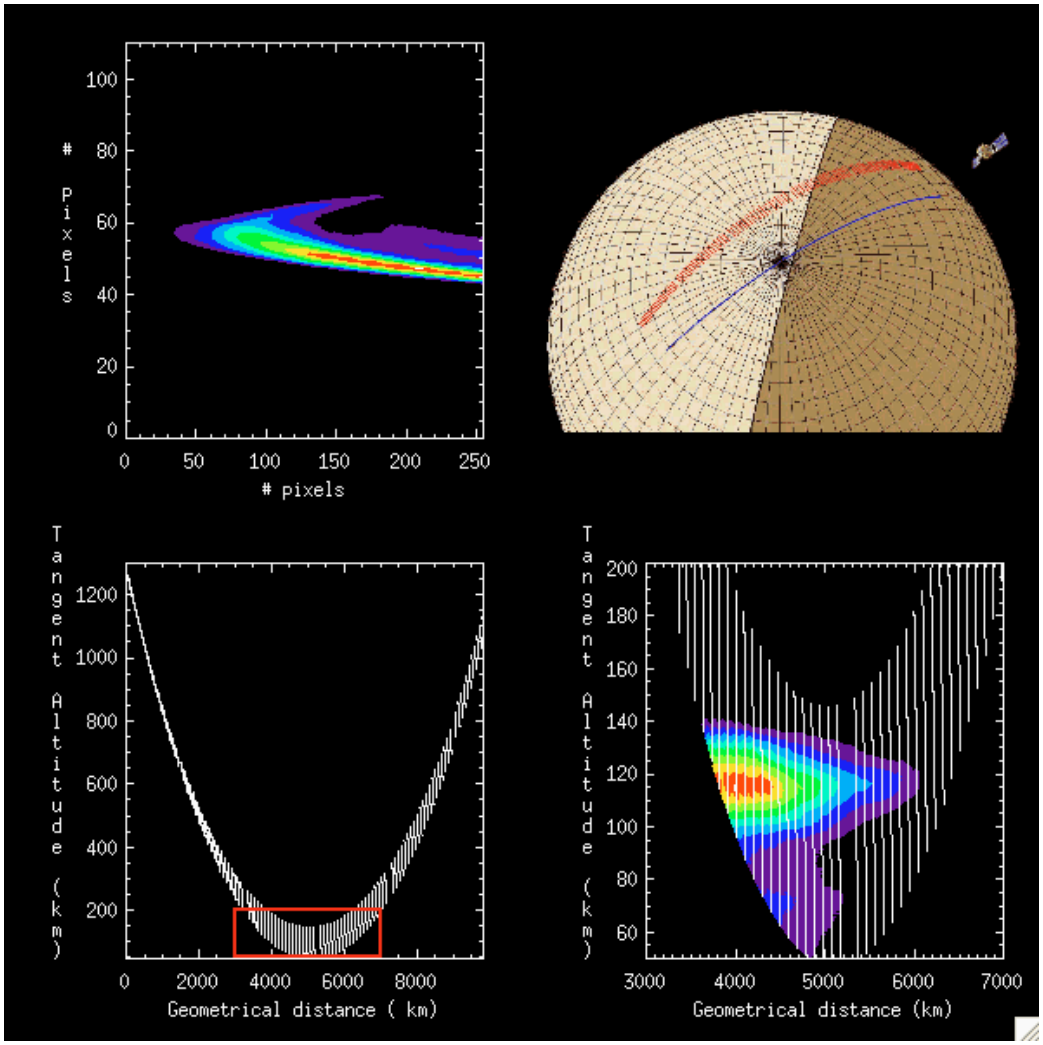

Figure 2.1: Example of images obtained by VIRTIS-M during the periapsis (day # 43). *Left top panel*: Direct image (pixels vs. pixels) of the data cube of VIRTIS-M. *Right top panel*: 3-D image of the planet to map a few characteristic of the periapsis. The terminator divides the night side (dark brown) from the dayside (light brown). The solid blue lines represents the trajectory of the satellite over the planet, while the red points represent the pixels' positions (latitude vs. longitude) at the tangent point. Each raw of 256 pixels compose the slit of the instrument, which is moving together with the satellite along the orbit. *Left bottom panel*: Position of the pixels versus geometrical distance (km) and tangent altitude scanned by the VIRTIS-M slit during the periapsis. *Right bottom panel*: Zoom of the measurements in the spectral region around 4.3 μm taken in the proximity of the planet and represented in a 2-D cross section (geometrical distance vs. tangent altitude).

JOURNAL OF GEOPHYSICAL RESEARCH, VOL. 114, E00B29, doi:10.1029/2008JE003112, 2009

Limb observations of CO_2 and CO non-LTE emissions in the Venus atmosphere by VIRTIS/Venus Express

G. Gilli,[1] M. A. López-Valverde,[1] P. Drossart,[2] G. Piccioni,[3]
S. Erard,[2] and A. Cardesín Moinelo[3]

Received 11 February 2008; revised 29 October 2008; accepted 13 November 2008; published 7 March 2009.

[1] We report and analyze here observations of strong infrared emissions from the limb of the Venus upper atmosphere during daytime, taken by the Visible and Infrared Thermal Imaging Spectrometer (VIRTIS) aboard Venus Express. We focus on the measurements taken during the first 4 months of nominal operations. The emissions observed at 4.3 μm and at 2.7 μm are attributed to CO_2 fluorescence of solar radiation and are detected up to about 160 km and 130 km, respectively, while the CO fluorescence at 4.7 μm is observed up to about 120 km. The emissions are detected in both the channels of VIRTIS, at different spatial and spectral resolutions (resolving powers about 1800 and 400), for the periapsis and the apoapsis of the Venus Express orbit. From these data sets we built up 2-D maps of the emissions as well as vertical profiles, which are then studied in order to characterize their variations with geophysical parameters, like solar illumination and emission altitude. Several analyses are performed in order to understand the VIRTIS behavior, to determine systematic effects in the data, and to propose appropriate corrections. We also present comparisons with a theoretical nonlocal thermodynamic equilibrium (non-LTE) model of the Venus upper atmosphere. The agreement is very encouraging, in general, and the main variability observed in the data, with solar zenith angle and altitude, can be understood with the model. We conclude that the present data set opens brilliant perspectives for deriving densities and rotational temperatures in the upper mesosphere and lower thermosphere of Venus.

Citation: Gilli, G., M. A. López-Valverde, P. Drossart, G. Piccioni, S. Erard, and A. Cardesín Moinelo (2009), Limb observations of CO_2 and CO non-LTE emissions in the Venus atmosphere by VIRTIS/Venus Express, *J. Geophys. Res.*, *114*, E00B29, doi:10.1029/2008JE003112.

1. Introduction

[2] The European mission Venus Express arrived at Venus in April 2006, and started its scientific phase in June 2006, being the first mission in more than 20 years to study the Venus atmosphere systematically from orbit [*Svedhem et al.*, 2007]. In contrast to the Earth's mesosphere and lower thermosphere, the equivalent density layers on Venus from about 90 to 150 km, are regions scarcely observed using remote sounding in the infrared (IR). The most abundant species CO_2, is well known to present strong IR vibrational-rotational bands, and more than 25 years ago, Pioneer Venus made systematic nadir observations using the fundamental band of CO_2 at 15 μm in order to retrieve atmospheric temperatures in the mesosphere of Venus [*Taylor et al.*, 1980]. Also, NIMS/Galileo permitted a sounding of the lower mesosphere temperature at 4.3 μm in nadir and nighttime [*Roos-Serote et al.*, 1995]. However, at higher altitudes, these emissions are expected to be out of thermodynamic equilibrium, with particularly large deviations during daytime, owing to solar pumping of the corresponding vibrational states [*Dickinson*, 1972; *Deming et al.*, 1983; *Roldán et al.*, 2000]. As a consequence, their inversion in terms of geophysical parameters is not straightforward, or in other words, their thermodynamic information content is limited [*López-Puertas and Taylor*, 2001]. The understanding of these non-LTE emissions is important, not only for its own interest, but also they can give rise to a large radiative heating, or cooling, of the atmosphere. In the case of Venus, they are a key ingredient of the energy balance between 80 and 150 km [*Bougher et al.*, 1994]. *Roldán et al.* [2000] showed that the CO_2 bands at 4.3 μm and the ones at 2.7 μm dominate the solar heating at those altitudes; much less important are the CO absorptions at 4.7 μm, given the lower atmospheric abundance of CO. Further observational problems challenged an infrared sounding of these layers from the Venus orbit so far; among them, the pointing in the limb (the optimum geometry of observation at these low atmospheric densities) and the sensitivity of the infrared detectors.

[3] Progress toward limb sounding of planetary atmospheres has been made during the last 2 decades, both theoretically and observationally. Triggered by ground-based

[1]Instituto de Astrofísica de Andalucía, CSIC, Granada, Spain.
[2]Observatoire de Paris, Meudon, France.
[3]IASF, INAF, Rome, Italy.

0148-0227/09/2008JE003112$09.00

observations of CO_2 laser bands at 10 μm, a number of non-LTE models for atmospheric IR emissions were developed for Mars and Venus in the 1980s [*Deming et al.*, 1983; *Gordiets and Panchenko*, 1983; *Stepanova and Shved*, 1985]. Later, more comprehensive tools were developed in preparation for sounding of the Martian atmosphere in the IR during the 1990s [*López-Valverde and López-Puertas*, 1994], which were adapted later to the Venus atmosphere [*Roldán et al.*, 2000]. These models, which included many more radiative bands and CO_2 energy states, represent adequate tools for simulation and analysis of limb data. Some of the few non-LTE observations available so far, and amenable for such studies, were taken by the Near Infrared Mapping Spectrometer (NIMS) instrument [*Carlson et al.*, 1992] on board the Galileo sounder, during its flyby of Venus in 1990 [*Carlson et al.*, 1991]. A few limb spectra of the CO_2 4.3-μm band were obtained during daytime and were explained recently using an improved version of the non-LTE model of Roldán and colleagues [*López-Valverde et al.*, 2007] (hereinafter LVEA). Recent analysis of CO_2 non-LTE emissions have also been carried out for Mars using data from the Planetary Fourier Spectrometer (PFS) on board Mars Express [see *López-Valverde et al.*, 2005; *Formisano et al.*, 2006], which helped to partially validate the non-LTE model. Regarding CO, non-LTE emission lines in the near-IR were first discovered in the Venus atmosphere about 20 years ago by *de Bergh et al.* [1988]. They were recently modeled and analyzed by *Crovisier et al.* [2006], who identified the fundamental CO(1-0) and the first hot CO(2-1) vibrational-rotational bands, derived rotational temperatures from them, and predicted that the instrument VIRTIS/Venus Express might detect these emissions.

[4] VIRTIS is one of the instruments aboard Venus Express with capabilities to sound the upper atmosphere of Venus [*European Space Agency* (ESA), 2001; *Titov et al.*, 2006]. It is an imaging spectrometer in the visible and near infrared, inherited partly from the Rosetta mission [*Coradini et al.*, 1998]. VIRTIS is devoted to a large number of investigations at Venus, like the cloud deck morphology and dynamics, the lower atmospheric composition, and the derivation of the temperature structure in the lower mesosphere. First studies of these aspects are presented in companion papers in this issue. Most of these studies are carried out by nadir observations. However, VIRTIS is designed to perform limb observations aboard Venus Express as well [*Titov et al.*, 2006]. This mode of observation represents the first systematic sounding of the upper layers of the Venus atmosphere in the infrared, and is devoted to understand the Venus high-atmosphere emissions [*Drossart et al.*, 2007b]. The detection of the non-LTE CO_2 4.3-μm band by VIRTIS at thermospheric altitudes has been confirmed by *Drossart et al.* [2007a], in consonance with the theoretical expectations.

[5] In this paper, we focus on a detailed and systematic analysis of VIRTIS observations of CO_2 and CO non-LTE emissions from the upper atmosphere of Venus using such a limb geometry. This is a unique data set, and our goals include, first of all, performing an internal validation of the data of our interest, second, characterizing the behavior of the instrument during limb sounding, and also describing the data set available, its quality and quantity, and its scientific potential. These CO_2 non-LTE emissions have also been observed by VIRTIS in nadir, which show signatures of gravity waves propagation into the thermosphere, as studied in a companion work in this issue [*García et al.*, 2009]. The study of the O_2 infrared system in the Venus mesosphere is also presented by *Hueso et al.* [2008] and in this issue (G. Piccioni et al., Near IR oxygen nightglow observed by VIRTIS in the Venus upper atmosphere, submitted to *Journal of Geophysical Research*, 2009).

[6] In this paper we also present and discuss comparisons with the non-LTE model results in LVEA, using both their published results and a small number of specific simulations performed here with such model. Although a more detailed comparison between model and data is under preparation, this is the first time that this model is confronted with an extensive data set of such a high spectral and spatial resolution. This work is, therefore, also devoted to test the model's main theoretical predictions, and to identify improvements and lines of exploration for non-LTE models.

[7] In section 2, we first describe VIRTIS observations in the limb, including the presentation of 2-D maps and vertical profiles of radiances. Their validation analysis, including consistency tests, actual noise level determination, as well as internal correlations and comparisons with the non-LTE model, are presented in section 3. Further discussions, future prospects and conclusions, are presented in section 4.

2. VIRTIS Observations

[8] VIRTIS on Venus Express is an imaging spectrometer whose precursor is currently en route to comet 67P/Churyumov-Gerasimenko, as part of the scientific payload of the Rosetta mission. Its detailed description and calibration can be found elsewhere [*Coradini et al.*, 1998; *Piccioni et al.*, 2006; *Titov et al.*, 2006] and see also the companion papers in this issue. We briefly describe here those characteristics and mode of operation on board Venus Express which are needed for our analysis.

2.1. VIRTIS/VEX Characteristics and Data Set

[9] The instrument consists of two channels: VIRTIS-M (hereinafter V-M), a mapping spectrometer at a resolving power $R \sim 400$, working in the visible (0.3–1 μm) and in the near infrared (1–5 μm), and VIRTIS-H (hereinafter V-H), a high-resolution spectrometer ($R \sim 1800$) working in the spectral range 2–5 μm. Table 1 of the work by *Drossart et al.* [2007b], summarizes their main characteristics; let us recall some of them here. The nominal field of view (FOV) is 64 $\times$ 64 mrad^2 for V-M (whole frame, with 256 spatial pixels in each direction), and 0.58 $\times$ 1.75 mrad^2 for V-H. The V-M spectral range is sampled at 432 spectral wavelengths, while a typical V-H spectrum obtained in the nominal mode contains a sequence of 3456 measurements. The nominal noise equivalent radiance (NESR), for 1 second of integration time, is 5000 μW m^{-2} sr^{-1} μm^{-1} in both channels, according to the *ESA* [2001]. All V-H and V-M data taken during one orbit, or terrestrial day, are stored in the so-called "qubes." The V-M ones generally contain a set of data in 3 dimensions, 2 spatial and 1 spectral. During each orbit the number of V-H/V-M data qubes

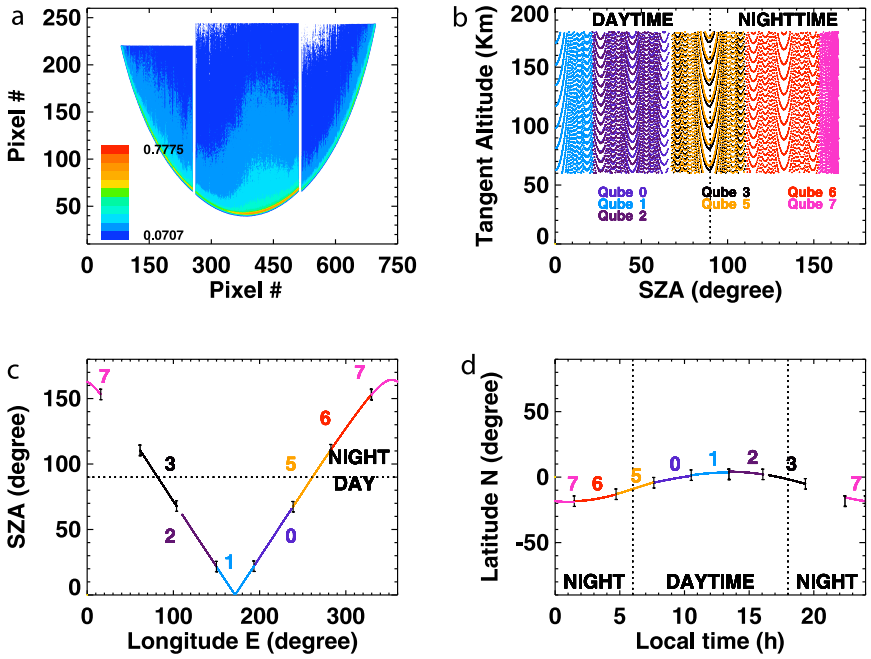

Figure 1. Geographical coverage with VIRTIS-M (V-M) during orbit 25, from apoapsis. (top, left) Map of radiances at 4.32 μm from qubes 0, 1, and 2. (top, right) Altitude-SZA location of all the limb data above the cloud layer (all pixels of seven qubes of this orbit); (bottom) Location of the data in SZA, longitude, latitude, and local time. The numbers identify the different qubes.

obtained varies from 1 to 20. A detailed description of data handling and archiving is presented by *Drossart et al.* [2007b].

[10] VIRTIS observations are separated into two categories, corresponding to distances of Venus Express to the planet lower than 12,000 km (Spectral Mode) or higher (Spectral Imaging Mode). During the Spectral Mode only a partial coverage of the surface is normally obtained, but thanks to the proximity to the planet, a very small field of view (projected) is achieved, ideal to study atmospheric variability and composition, and for tangential limb observations. Several instruments on board Venus Express share this operation mode. The Spectral Imaging Mode permits unique and unprecedented maps of the disk of Venus, and has been used to obtain global observations from apoapsis ("mosaic construction"). We will show below how these VIRTIS 2-D images contain useful information on the limb of the planet as well.

[11] A note regarding the distinction between limb and nadir observations is needed in order to clarify that, in a general sense, a data qube from VIRTIS will contain both kind of observations. Our distinction merely tells whether the line of sight touches the disk of Venus (nadir data) or crosses its atmospheric limb. Therefore, some pixels may represent actual limb sounding while nearby pixels in the same V-M image will supply "disk" observations. This will become clearer in section 2.5. For this reason, analysis of nadir observations, described in companion papers of this issue, share similar difficulties to our study and all of them are beneficial to the overall validation of VIRTIS data.

2.2. Geographical and Temporal Coverage

[12] At present, V-M data are available in calibrated form up to the orbit 631 (13 May 2006 to 1 Jan 2008), but in this work we focused our analysis on a selected number of orbits up to orbit 295 (10 February 2007). For V-H, at the time of preparing this paper, the data from orbit 23 to 127 (13 May 2006 to 25 August 2006) were already calibrated, so we focused on them, while only a fraction was calibrated and available for the rest of the mission. As mentioned above, our purpose is to perform an exploration of V-M and V-H limb data in the Venus upper atmosphere, from the cloud top, around 60 km, up to upper thermospheric layers. With this aim, we made a catalog of orbits/qubes/pixels with actual limb sounding and a number of diagrams of the geometrical and spatial coverage of all limb data obtained. Examples are shown and commented next.

2.2.1. VIRTIS-M

[13] Starting with V-M, Figures 1 and 2 show two examples of the V-M coverage for two different observational geometries, both sampling the Venus limb, one from orbit 25 (15 May 2006), during the apoapsis, and the other from orbit 43 (2 June 2006) near the periapsis. They can be considered as representative of the two principal VIRTIS modes of observation (see section 2.1).

[14] The first orbit, from apoapsis, contains 8 qubes of V-M data (7 with limb data), each one consisting of set of pixels, or a 2-D image at each wavelength, as mentioned above. Let us recall that each pixel is associated to one individual spectrum. In Figure 1a, data at the wavelength of 4.32 μm from three of the qubes, building up a map of radiances; we will discuss them below. Each qube includes a

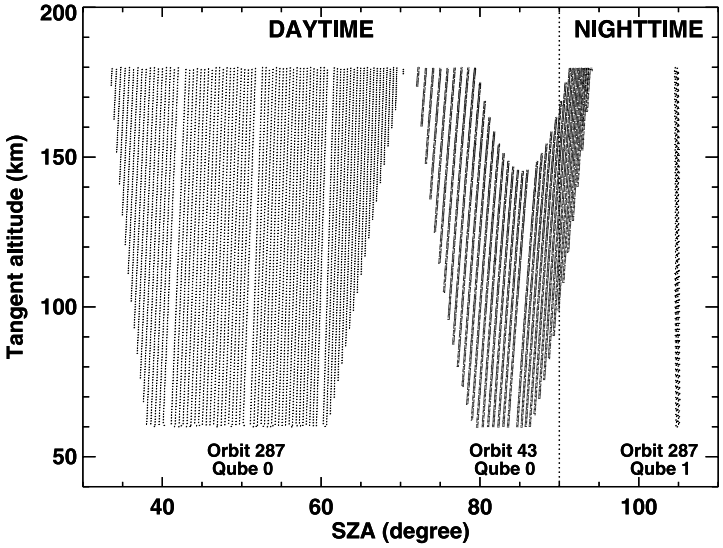

Figure 2. V-M coverage in tangent altitude versus SZA during periapsis of orbits 43 and 287. Data are shown between 60 and 180 km only.

large number of pixels (245 × 256), and the fraction of those pixels with actual pointing to the Venus limb are shown in Figures 1b–1d. We see that when the 8 qubes are considered, the latitude, longitude, and local time of the data cover an ample range of values. In this work we pay particular attention to the altitude and solar zenith angle (SZA) coverage. These two parameters are expected to produce the maximum variation in the non-LTE emission of both CO_2 and CO in the atmosphere, according to the model of LVEA. The most intense signal is expected between 90 and 140 km, and for low SZA values; for nighttime the signal would be very low, and we confirmed all of this with VIRTIS data. Figure 1b shows that the number of limb daytime spectra is large for this orbit. The vertical resolution from each row of pixels (for each qube) is between 15 and 20 km, typically. This is larger than an atmospheric scale height, but the superposition of adjacent rows may improve significantly this resolution, as we will show below. Also the SZA sampling is not completely even, but the large density of points permits suitable averaging if they are needed.

[15] Figure 2 illustrates the V-M coverage in the qube 0 of orbit 43 (2 June 2006), during the periapsis of Venus Express and in the qubes 0 and 1 of the orbit 287 (1 February 2007). We use again altitudes at the tangent point versus SZA, which describe our preferred data set for limb sounding. The available daytime limb data during the orbit 43 are about 5410 while this number is larger for the 287 (about 8000). The vertical resolution obtained at the limb from one single row of pixels (∼300 m), improves by a very large factor with respect to the apoapsis case, and is therefore particularly useful for studying the vertical variation of the non-LTE emissions and testing the theoretical predictions.

2.2.2. VIRTIS-H

[16] Observations of the limb of the planet by VIRTIS in the Spectral Mode are not as frequent as in the Spectral Imaging Mode owing to pointing constraints; the field of view of the V-M frame is much larger than the V-H. The amount of V-H spectra which actually touches the limb of the planet is therefore very limited in most orbits, sometimes only 2 or 3 spectra of our interest are available per orbit.

[17] Figure 3 illustrates the V-H geometrical coverage at the limb, again as a function of SZA and tangent altitude, combining all the orbits during the first four months of operation. A total of 651 points are shown, each one representing a V-H spectrum. We have marked 4 specific orbits (43, 76, 80, and 88) to indicate 4 different special observational coverages. The first one corresponds to a special limb case, the so-called "Tangential Limb Scenario" [see *Titov et al.*, 2006], where the satellite is fixed pointing to the limb of Venus during the periapsis. This is a specially useful kind of orbit for limb sounding and for non-LTE studies, given the high rate of tangent point observations. Orbit 76 (6 July 2006) corresponds to a "stellar occultation" case, where again a large number of observations is obtained at the limb, but they correspond to the nighttime hemisphere. They do not show a distinct emission level and have not been considered in the analysis. The other two orbits correspond to the most common limb scenario.

[18] For a number of studies, averaging of these data may be required, in order to achieve a good SZA or altitude coverage. From the 651 V-H limb spectra available, a total of 145 are daytime observations (SZA < 90°), and 44 of these correspond to strong solar illumination conditions (SZA < 60°). The last ones are, in principle, optimum for non-LTE studies. Let us recall that, within Venus Express, V-H data are the measurements with the highest spectral resolution. The latitude and longitude coverage of the daytime spectra are shown in Figure 3 as well. Except for orbits 43 (2 June 2006) and 80 (10 July 2006), with high-latitude sampling of nearby points, all others are disperse, with a preference for low latitude.

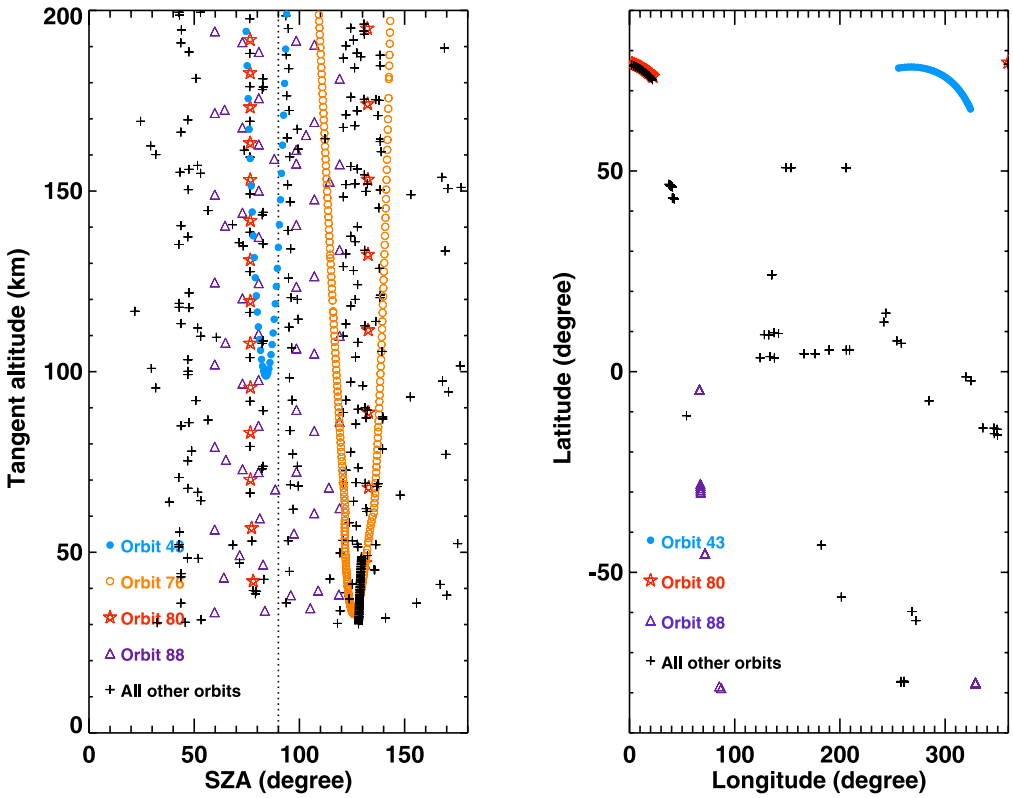

Figure 3. (left) Coverage in tangent altitude and SZA of the VIRTIS (V-H) data available from all the orbits from 23 to 127. Some orbits are indicated with special symbols. (right) Latitude-longitude location of the data, for daytime only. Symbols as in the left. See section 2.2.2 for details.

2.3. VIRTIS-H Spectra and Profiles

[19] We describe here typical V-H limb spectra which show strong non-LTE signals, and we build up vertical profiles also, in order to characterize the emissions. We focus on three emission bands, those at 4.3 μm and 2.7 μm both due to CO_2, and that at 4.7 μm, due to CO. All of them are suitable to be contrasted with the recent non-LTE model predictions of LVEA.

2.3.1. CO_2 4.3 μm Emission

[20] Figure 4 (left) shows a sample of seven V-H spectra in the 4.3-μm region, corresponding to different orbits, and pointing at different tangent altitudes. The selection corresponds to orbits 33, 40, and 47 (24 May, 31 May, and 7 June 2006, respectively) and to a SZA interval from 20° to 30°. First, it is noticeable an intensity of the signal well above the noise level at all wavelengths between 4.20 and 4.50 μm. The emission falls to zero shortward and longward of these values, respectively, where the small oscillation observed can be considered as the measurement noise and which seems to be close to 2000 $\mu W\ m^{-2}\ sr^{-1}\ \mu m^{-1}$. Only the two lowest altitude spectra show signal in the wings, though surely from solar scattering in the clouds. At the uppermost altitude shown in Figure 4, 167 km, the spectrum is still above noise level, which demonstrate that V-H can sound up to those thermospheric altitudes in Venus before averaging.

[21] It is clear that the spectral shape of the 4.3-μm band, the peak intensity, and the wavelength of the peak of the band, vary with altitude. The maximum emission is obtained in this sample around 110 km tangent altitude. This is close to the altitude predicted by the CO_2 non-LTE model by LVEA. Also the spectral shape is similar to the model prediction, with three clear peaks in the 110 km spectrum, around 4.28, 4.32 and 4.35 μm. According to the model, the first peak is due to the second hot band of the main CO_2 isotope; the mechanism being solar absorption at 2.7 μm, exciting CO_2 states which later relax radiatively, emitting in the 4.3-μm region. The second peak, around 4.32 μm, is produced by radiative relaxation of the CO_2 vibrational states excited after solar absorption at 2.7 μm and 2.0 μm. The third peak is mostly due to solar pumping at 2.0 μm. The non-LTE model predicts that at high tangent altitudes the 4.3-μm band would change this shape to a simpler two emission peaks separated by a dent around 4.29 μm, due to the dominance of the 2.7 μm solar pumping. This is indeed observed in Figure 4, above about 130 km. At higher altitudes, the model predicts a further change, due to the direct solar absorption in the fundamental band of the main isotope, whose central dip at 4.26 μm is observed in Figure 4 in the 167 km spectrum.

[22] Vertical profiles can be constructed combining spectra at different altitudes. They, however, will not represent

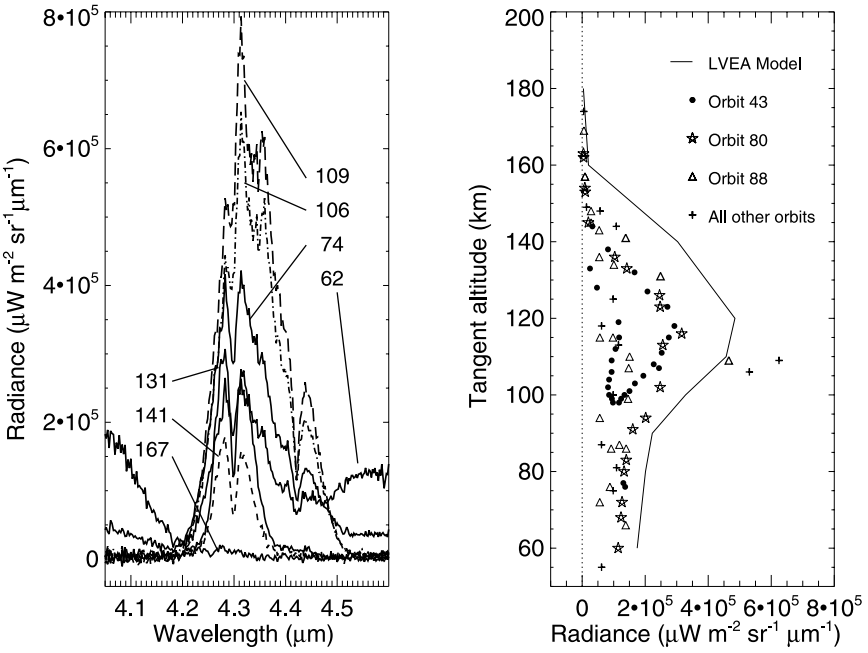

Figure 4. (left) Selection of seven V-H spectra from orbits 33, 40, and 47 at different altitudes and for 20° < SZA < 30°. (right) Vertical distribution of the 145 daytime measurements at 4.32 μm from orbits 23 to 127 (May–August 2006). The solid line on the right represents a model simulation. Orbits and symbols as in Figure 3.

real 1-D profiles of the Venus atmosphere. Only a couple of orbits (43 and 80) contain a sufficient number of limb spectra to build a vertical profile for one single orbit; in general, data from different dates and geographical locations will be combined. This will have to be taken into account when performing detailed comparisons with non-LTE models, which usually provide the radiance structure at a single geographical location. In Figure 4 (right) we combine diverse data at 4.32 μm. The data and the symbols correspond to those in Figure 3. A tentative grouping by SZA values did not show any clear trend, given the scarcity of data; the SZA variation is better observed in V-M data and discussed below.

[23] The cloud of V-H data presents a dispersion not present in the 1-D radiance simulations by LVEA, also shown in Figure 4. The model simulation corresponds to SZA = 80° similar to that of orbit 80. This orbit can be considered as a good 1-D profile extending from 30 to 200 km. Notice that data from orbit 43 can also be used to build vertical profiles, but only above about 100 km. Both data and model present a clear increase with altitude in the lower mesosphere and a peak emission around 120 km. Above this altitude, the emission declines quickly to zero, following the decrease in atmospheric density. The actual atmospheric density profile is critical in determining the precise altitude of the peak emission, and this is the most likely reason for the mismatch with the prediction of LVEA. Regarding the peak radiances, not much comparison can be performed at this stage, as it should be the topic of a more rigorous comparison of the non-LTE model, and should account for suitable atmospheric variability in the density profiles.

2.3.2. CO_2 2.7 μm Emission

[24] According to LVEA, CO_2 emissions at 4.3 μm and at 2.7 μm are both produced by solar pumping. The emission level at 2.7 μm is, however, much lower and we have only found a small number of cases/spectra with a distinct emission above noise levels. Figure 5 shows two of those spectra, which correspond to SZA of about 45° and 60°. One of them presents a bias, which is not corrected here. A non-LTE model simulation has been performed for these solar illumination conditions, using the VIRA reference atmosphere, and is also presented in Figure 5. The spectral shape of the two fundamental bands of the main CO_2 isotope can be discerned, by comparing with the non-LTE model simulation. The data are very noisy for further conclusions at this stage. Hopefully, a more extended data set of V-H spectra will be obtained during the rest of the mission, and a statistically sounded comparison with the theoretical prediction will be a good test for non-LTE models. This 2.7 μm non-LTE emission has also been detected in the V-M signal, as we discuss in section 3.2.

2.3.3. CO 4.7 μm Emission

[25] Figures 6 and 7 illustrate a similar study for the 4.7-μm spectral region which, according to LVEA is dominated by non-LTE emissions of CO in the upper mesosphere and lower thermosphere. The emission observed is lower than the CO_2 emission, and the number of V-H CO spectra with good signal to noise ratio is much smaller. About 20 spectra, out of the 145 available at the limb during daytime, show a clear signal. Many of them show a small signal above the noise level or above the daylight scattered by the aerosols and clouds. This is why it is difficult to detect this non-LTE

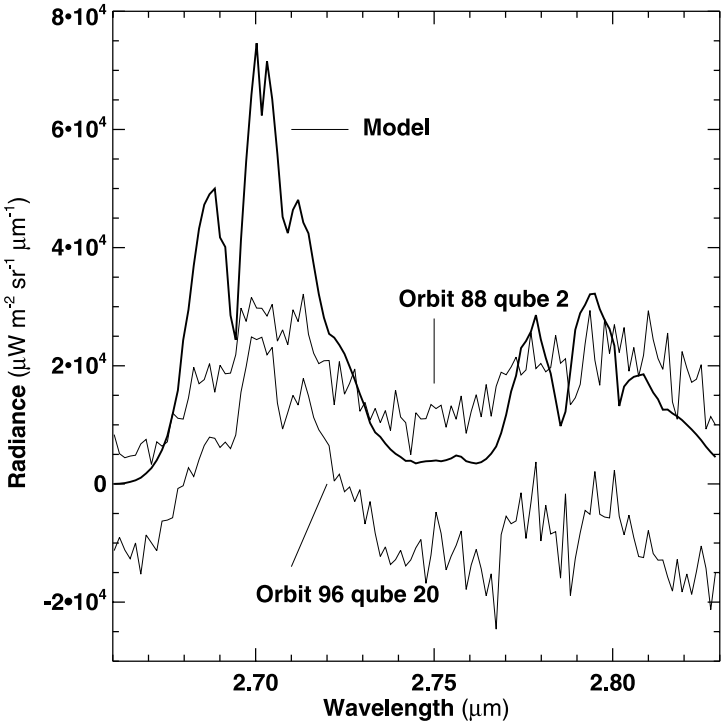

Figure 5. Two selected spectra at 2.7 μm observed by VIRTIS-H (thin lines) compared to a non-LTE model simulation (thick line). The upper spectrum is from orbit 88, qube 2 at an altitude of about 107 km and SZA about 60°. The lower spectrum is from orbit 96, qube 20 at an altitude of 118 km and SZA about 45°. The theoretical simulation has been performed at 110 km and for similar solar illumination conditions. No shift has been applied to the observed data. See section 2.3.2.

emission below about 70 km. The highest altitude where the emission can be clearly identified is about 120 km.

[26] Three of the most interesting spectra are shown in Figure 6 (top). The two spectra with the strongest emission correspond to two observations at approximately the same tangent height, around 85 km, but for SZA of 60° and 76°. The third one, shifted downward for clarity, is the spectrum at the highest altitude available in the data set explored so far, about 120 km. In spite of the noise level, very noticeable in the high-altitude spectrum, and which amounts to ~5000 μW m^{-2} sr^{-1} μm^{-1}, in all of them we can see two branches of what seems a typical vibrational-rotational band. The simulations of LVEA for the CO(1-0), or fundamental band (FB), of the main isotope showed such structure as well. However, their prediction has a minimum emission at the FB center, at 4.67 μm, while the spectra in Figure 6 present their central minimum around 4.73 μm. This points to a different band of CO, the CO(2-1), or first hot (FH), of the main isotope, as responsible for these data. Such emission was not simulated by LVEA, who focused their analysis in the FB. These V-H measurements indicate that, if the fundamental transition is present, its intensity is smaller than the first hot. A similar effect was observed with ground-based measurements at much higher spectra resolution [see *Crovisier et al.*, 2006].

[27] The spectral resolution of V-H allows to identify individual lines of the P and R branches of the FH CO band, and this is shown Figure 6 (bottom). A number of vertical lines are drawn at the wavelengths of the spectral lines centers of the two bands, according to HITRAN [*Rothman et al.*, 2005]. For clarity, we focus on the spectral interval occupied by the P branch of the FH band. We can identify most of the lines of the P branch, up to P20 at least. It is interesting to notice, however, that in the center of the FH P branch, at 4.727 μm, a weak emission line is observed, which coincides with the line P7 of the CO fundamental band. No FH lines are present there. Moreover, all the 5 lines observed around this wavelength are better fit by the P5–P9 lines of the FB than by the FH band. In other words, the emission from the FB seems to be also detected in the central portion of the FH band. The absence of FH lines may be due to the smaller strength of the lines with low rotational number. This is a tentative explanation which requires careful quantitative modeling.

[28] As previously done by *Crovisier et al.* [2006], it might be possible to derive temperatures from this emission after a correct model fit. This is not possible with the model of LVEA in this moment, but we have attempted to estimate the rotational temperature from some VIRTIS data. First, we assumed that the rotational levels of CO are in thermal equilibrium at the pressures of relevance. Then, the usual expression for the rotational temperature, given by the ratio of line intensities (see an example for the Venus atmosphere by *Deming et al.* [1983]), was applied to the spectrum shown in Figure 6 (bottom). A selection of lines from the P branch of the FH band is required. The criteria we

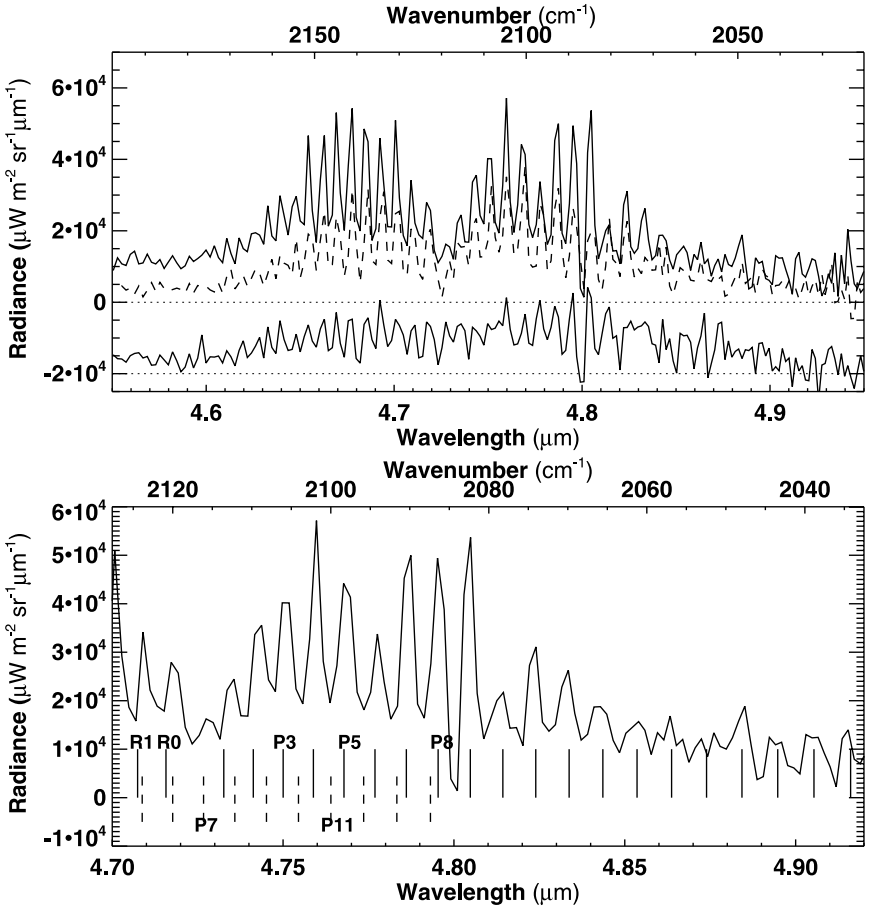

Figure 6. (top) Selection of three V-H spectra at 4.7 μm. The two closer ones correspond to about 85 km and to SZA of 60° (solid line) and 76° (dashed line). The lowest spectrum, shifted 20,000 radiance units downward for clarity, corresponds to a tangent altitude of 118 km and SZA of 46°. (bottom) Zoom of the SZA 60° spectrum, with lines marking the positions of the Hitran line centers for the fundamental (dashed marks) and first hot (solid marks) bands of CO.

followed were a small overlapping with the FB lines and a peak emission well above the noise levels. This method rules out high and low J lines. Also, adjacent rotational lines should be avoided in order to reduce numerical error. For this spectrum, the best subset of lines that we found are those between P3 and P8. By forming pairs between the more extreme ones, P3, P4 and P7, P8, several values of rotational temperature were found, all around 237 K, but with uncertainties of 50 K or larger. This large error is due to the large sensitivity to the peak intensity in the center of the lines. This intensity value is uncertain because it is not directly available from the data, given the V-H spectral resolution and sampling, but obtained by an extrapolation to the radiance values in the centers of the selected lines. Notice that the P branch of this spectrum apparently has a maximum at P9 and a local minimum at P6; we have excluded these two lines in this analysis since they seem specially affected by the V-H sampling and noise. This error in the lines intensities can be reduced in the future, by using a non-LTE model simulation for the FH band, as was done by *Crovisier et al.* [2006].

[29] Regarding the vertical variation, profiles can be constructed from the two dozens of spectra with good S/N ratio. They are shown in Figure 7 at 4.678 μm. The data have a clear dispersion, and in contrast to the model prediction for the FB, it does not show any clear peak: the plateau between 95 and 120 km, at about 6000 μW m^{-2} sr^{-1} μm^{-1} is very close to the noise level. As it happened with the CO_2 data in Figure 4, the small number of points does not allow to discern a clear SZA variation.

2.4. VIRTIS-M Maps During Periapsis

[30] In this section we present measurements of V-M from the periapsis, where the maximum spatial resolution can be achieved, as shown in Figure 2. In the Spectral Mode, near periapsis, the V-M slit is fixed, no scanning is performed, and a row of pixels is taken. Therefore, the mapping is composed of a set of successive "V-M slit frames," each one taken about 10 s apart, while the spacecraft is moving along the orbit.

[31] This is illustrated in Figure 8, where we plotted a map of CO_2 radiances at 4.32 μm, in the center of the strong

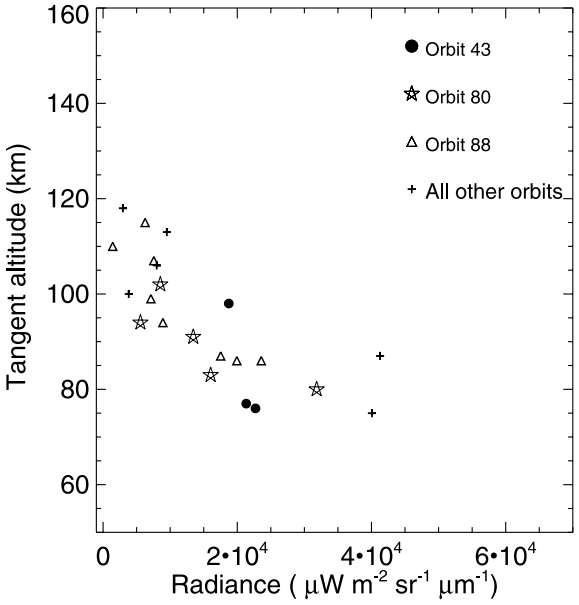

Figure 7. Vertical distribution or V-H radiances at a central wavelength of the 4.7-μm band of CO. Orbits and symbols as in Figure 3. See section 2.3.3.

CO_2 bands system. The vertical lines correspond to the actual pointing of each pixel, similarly to Figure 2. We will build similar maps with V-M data but from apoapsis observations, in the next section.

[32] Two strong variations are observed in the radiances, one along the vertical axis and the other along the horizontal, and both can be explained by the non-LTE model. Considering first the vertical, a peak emission is observed, in the lower thermosphere, 110–120 km. As the SZA varies along the track (from 70° to nighttime), the peak intensity, and the whole profile, decrease. This is predicted by the non-LTE model and this data set offers a perfect benchmark for a quantitative validation of the model; a work which is in progress.

[33] This is the first time that maps of IR radiation with this geometrical resolution are obtained in the Venus upper atmosphere. In order to illustrate more clearly such a resolution, we constructed a vertical profile with data from a single slit view, that indicated with an arrow in Figure 8. They are shown in Figure 9 (right), at three wavelengths. A log scale is used for the radiances, to confirm that a good signal to noise is achieved even at 160 km from one single spectrum. These data correspond to SZA $\sim$ 75°–80°, a value typical of daytime observations at high latitudes. The altitude of the peak is maximum in the center of the band, at 4.32 μm, and it is lower in the wings, at 4.25 and 4.40 μm, according to model expectations. Figure 9 (left) shows three V-M spectra at three tangent altitudes. The spectral resolution is lower than V-H, but the change in the overall shape of the band with altitude is clearly observed, as discussed in the previous section. We have also tried to build up maps of radiances in the 2.7-μm and 4.7-μm region. Unfortunately such V-M maps are very noisy at all altitudes, contain a very strong component of scattering up to 90 km, and are not further studied here.

2.5. VIRTIS-M Maps and Profiles During Apoapsis

[34] V-M observations from the apocenter of the Venus Express orbit are good examples to show the large potential of an imaging instrument like V-M for mapping large portions of the Venus disk. However, some images also contain information about atmospheric limb emissions, and

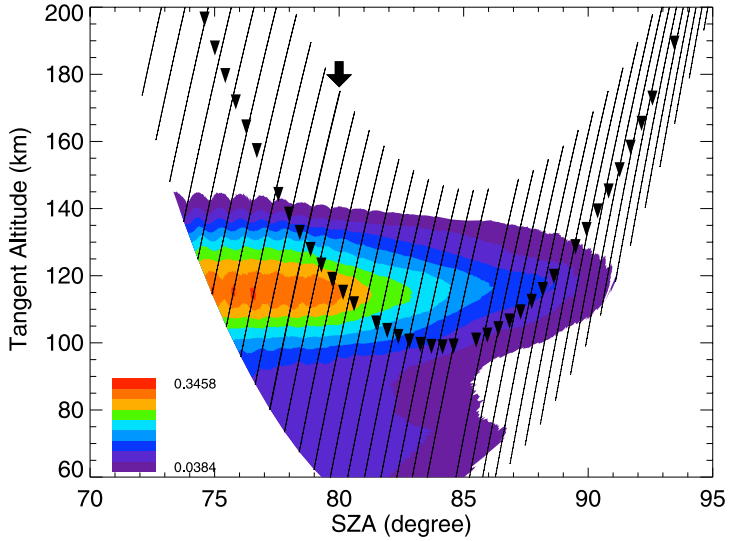

Figure 8. Map of V-M radiances from periapsis (orbit 43) at 4.32 μm versus SZA and tangent altitude. The color code ranges from 0.03 to 0.34 μW m^{-2} sr^{-1} μm^{-1}. Each line corresponds to a column of pixels along the V-M slit. V-H data for the same orbit are overplotted (triangles). The arrow indicates the column of pixels from which the vertical profiles in Figure 9 have been extracted.

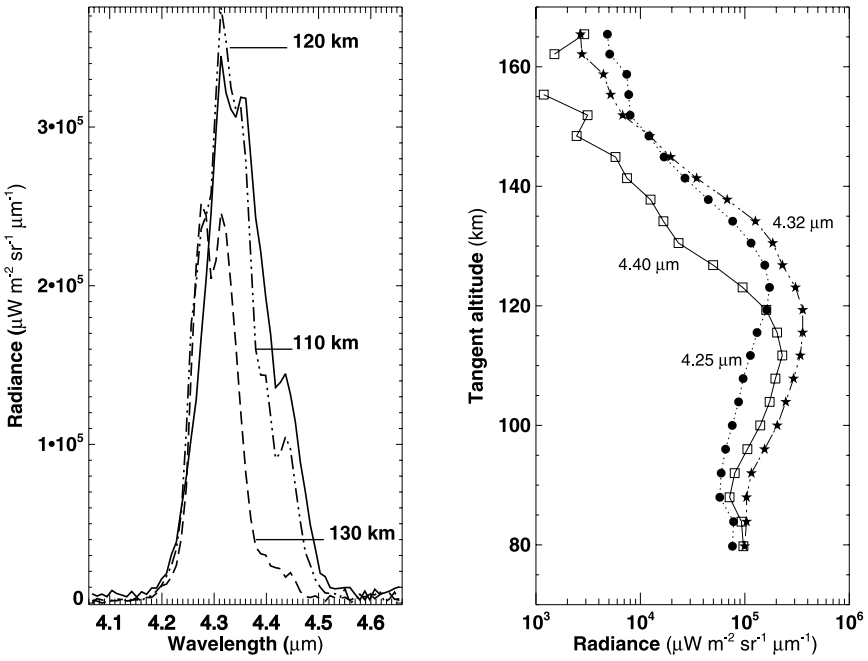

Figure 9. V-M spectra and profiles at 4.3 μm from periapsis, orbit 43. (left) Spectra at three different altitudes, as indicated. (right) Profiles at three wavelengths extracted from the pixels indicated in Figure 8. See section 2.4 for details.

allowed us to extract vertical profiles with an excellent vertical resolution.

2.5.1. 2-D Images From Apoapsis

[35] Figure 10 shows a map of V-M radiances at 4.32 μm, built up with the data from three consecutive qubes or V-M images (2, 1, and 0) of orbit 25, all of them acquired from apoapsis, at about 66,000 km from the center of Venus [*Svedhem et al.*, 2007]. The instrument takes about 10 min to take every qube, or image, before the satellite pointing switches to the next. The three images coincide with the data qubes shown in Figure 1a. The current map looks very different for two main reasons. First, now we are plotting

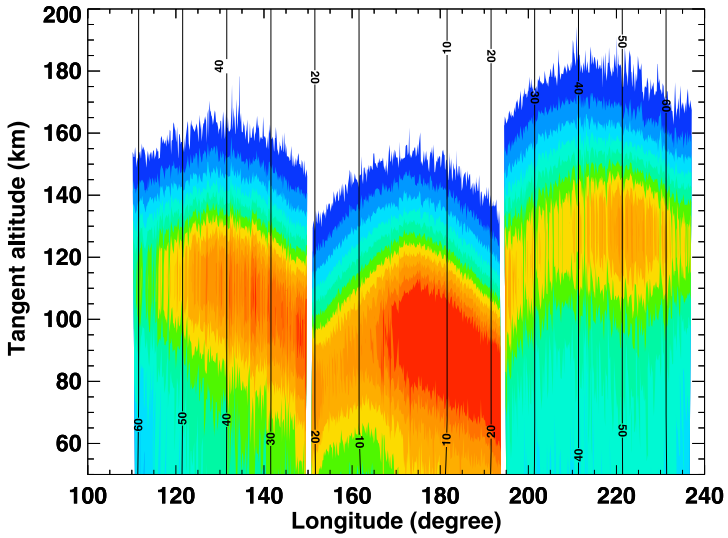

Figure 10. Maps of V-M limb radiances at 4.32 μm from apoapsis, from the three qubes of orbit 25 shown in Figure 1, as a function of tangent altitude and longitude. Vertical lines indicate SZA in degrees. Color scale is given in Figure 11.

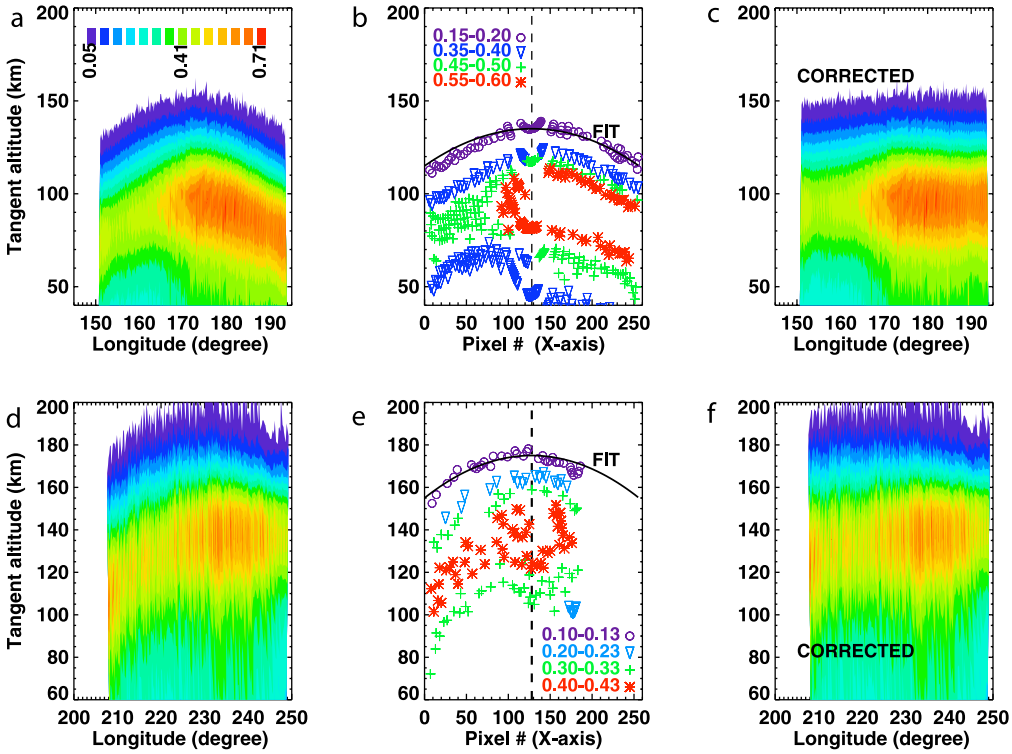

Figure 11. Smiling effect in V-M images from apoapsis and its correction for two cases: (top) qube 1 of orbit 25 and (bottom) qube 0 of orbit 29. (left) Original map of radiances at 4.32 μm. (middle) Location of pixels with radiance between the ranges indicated, and fit of a parabolic line to the cloud of pixels. (right) Corrected maps. See section 2.5.2 for details.

just the portion of the image which corresponds to actual limb sounding, i.e., tangent altitudes above about 60 km. And second, instead of pixel number, in Figure 10 we used altitude above the surface for the y axis, and a geographical parameter, longitude, in the x axis. Since the latitude is almost constant for all these limb data, Figure 10 represents a geometrically realistic view of such altitude-longitude cross section of the Venus upper atmosphere.

[36] Although the data acquisition and the image construction are different, this map is similar to the map from periapsis shown in Figure 8. Again, we observe a strong emission in the lower thermosphere, with a peak around 110–120 km. Also a large variation is observed in the horizontal axis. The SZA variation is, however, very small in each of the three qubes/images shown in Figure 10. Therefore, the horizontal variation may be of a different nature than that seen in the periapsis case, and might indicate a real atmospheric variability.

[37] However, extreme care is required before such an interpretation. The observations are taken from very far away, in a geometry which the instrument was not optimized for limb sounding; the data might contain some geometrical effects. First of all, these maps contain what appears to be a systematic bending of the radiances in the central part of the image. This bump has also been observed at other wavelengths, qubes, and dates, and it seems to be systematic. It is specially apparent in the uppermost layers. A second problem is shown by the sharp change in radiance between adjacent qubes. The three qubes shown here were taken with some minutes apart, and there is no obvious physical reason to expect changes of that magnitude between them. Investigation of these instrumental effects is ongoing. A likely explanation for the "smiling effect" is discussed in the next section. A probable cause for the second problem could be some flat field effect not yet identified.

2.5.2. Geometrical Correction of V-M Images

[38] The apparent bending observed in Figure 10 is of the order of 20 km, precisely the vertical resolution per pixel from the apoapsis, in other words, this error is within the size of one pixel. Although we cannot rule out small variations of the spacecraft pointing, the effect may be due to a slight bending of the V-M slit. This "smiling effect," which cannot be avoided, is of special importance for this limb sounding. Fortunately, some correction is possible, precisely by using these limb non-LTE emissions. We basically used two theoretical predictions of these emissions: first their strong decrease with tangent altitude, and second their variation with SZA, as explained below. The idea is to fit the bending observed with a simple function and then use that function to replot the radiances. We illustrate two examples of such a correction in Figure 11.

[39] Figures 11a and 11d show two different V-M images, those for orbit 25 (15 May 2006), qube 1 and orbit 29

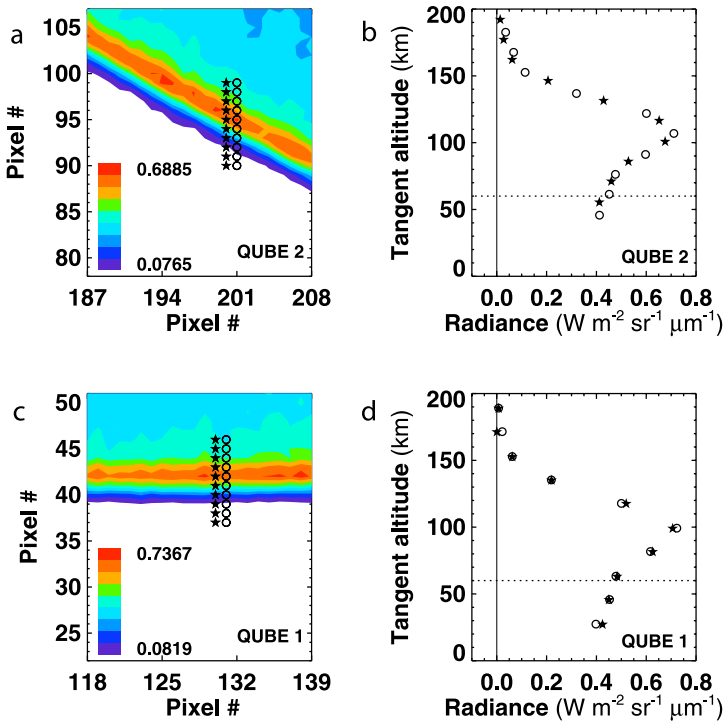

Figure 12. Vertical profiles of V-M radiance at (right) 4.33 μm after combining the (left) rows of pixels. (top) Qube 2 of orbit 25. (bottom) Qube 1.

(19 May 2006), qube 2; these are the original maps to transform. The correction has to be applied to them on a pixel basis, as we will assume it to be symmetric around the central pixel of the frame 128. Then we have selected all those pixels with radiances within a small bracket of values; they are marked with crosses in Figures 11b and 11e. According to the non-LTE model, if the atmospheric densities and the SZA illumination do not change very much, a given limb radiance corresponds to a given tangent altitude. Actually, this is the reason why we discovered this smiling effect. We can observe how the crosses marking the 0.15–0.20 radiance interval indicate a bending approximately symmetric around pixel 128. We fit a simple parabolic function to this cloud of pixels, and used it to correct for the tangent altitude of all the 256 pixels in each row of the frame. A perfect fit cannot be obtained owing to the different sources of error, which produce some dispersion in the measurements. In addition, the cloud of data does not present a random distribution but a peculiar dispersion produced by the particular geometry of the observations, which is specific for each qube. Some atmospheric variability cannot be ruled out either. For these reasons, we aim here at a first-order correction. Let us notice, also, that it will be difficult to find a single fit function with matches all the radiance intervals of all the orbits and qubes. In our example, the radiance maps resulting after the correction are shown in Figures 11c and 11f. The bending of about 20 km is greatly reduced. This correction function introduces some uncertainty in the absolute pointing altitudes. In the center of the frame, around pixel 128, the correction is very small, but the pointing may be inaccurate by around 5 km for the pixels at the extremes of the V-M frame. Still, we believe that the corrected images can be used for scientific studies, like atmospheric variability, possible dependence of the emissions on non-LTE parameters, etc, which would be impossible without this geometrical correction. In the VIRTIS team we are considering the implementation of this procedure in future operational processing.

2.5.3. Vertical Profiles From V-M 2-D Images

[40] Lets analyze now the vertical profiles of radiance from the limb that can be obtained from these V-M images at the apoapsis. As an example, Figure 12 shows two vertical profiles extracted from two different data qubes, already shown in Figure 1, qubes 2 and 1 of orbit 25. The profiles, at the wavelength of 4.32 μm, are shown on the right, while on the left we plot a small portion of the qube/image and marked the precise pixels used to build the profiles. The portion of the Venus disk selected corresponds to an almost constant solar illumination, with a small change of SZA, from 10° to 20°. To build up the profiles, we considered two adjacent sets of 10 pixels, taken at the same time, from two adjacent rows of the V-M frame. The selected pixels are pointing at varying altitudes, from the planet's surface up to the Venus thermosphere, with a vertical resolution around 15 km, and symbols in Figure 12 just point to the center of each pixel. If the orientation of the limb of Venus is optimum, as we can see in Figures 12a and 12b, a very good altitude resolution can be achieved by mixing adjacent pixels; otherwise, the gain in vertical resolution is lower or nonexistent. The improvement of

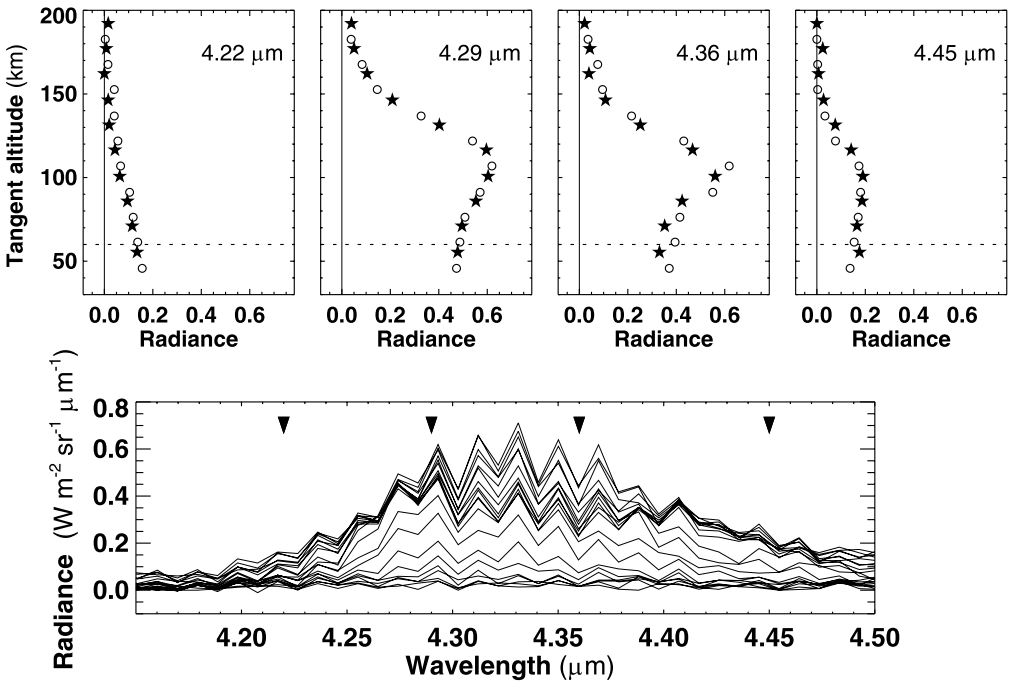

Figure 13. (top) Vertical profiles of V-M radiances at four wavelengths for qube 2, orbit 25. (bottom) Spectra of the 20 pixels composing the vertical profiles shown on the top; they belong to 2 adjacent rows of pixels, marked with stars and circles as in Figure 12. Four triangles mark the wavelengths of the four vertical profiles.

the vertical resolution is at the expense of losing horizontal resolution, obviously.

[41] Other four vertical profiles are shown in Figure 13 (top), obtained from the same rows of pixels in the top of Figure 12 but at four different wavelengths in the 4.3-μm region. The wavelength values are marked in Figure 13 (bottom), which shows the 20 spectra considered. We can get a lot of useful information about the non-LTE emissions from an image like this, since it combines spectral and vertical variations. For instance, the peak altitude is shown to vary with wavelength, being higher at 4.29 μm or 4.33 μm (see Figure 12) than in the wings of the band. This was predicted by the non-LTE model, and was observed also in periapsis observations. Although the qualitative behavior seems to agree with the model, the vertical profile at 4.45 μm does not coincide with the model, but this suggests a much lower emission compared with the center of the band. We think this may be solved by increasing the number of weak CO_2 bands in the non-LTE model, a task for a forthcoming revision of the non-LTE model that we are currently undertaking.

[42] A systematic problem in V-M data can be noticed in Figure 13 (bottom). There seems to be an oscillation in the spectral domain, with high and low values of intensity from one spectral point to the next. We checked that this "odd-even effect" is present at all VM near-IR wavelengths, from 2 to 5 μm, and it amounts to about 0.05 radiance units in Figure 13, or 50,000 μW m^{-2} sr^{-1} μm^{-1}, which is about 10 times larger than the measurement noise. The technical cause of the odd-even seems to be an asymmetry of the Read-Out Integrated Circuit (ROIC) of the Focal Plane Array (FPA) of the instrument; see *Coradini et al.* [1998] for a more detailed description of the instrument. In particular, there is an asymmetry in the clock feedthrough and the unit cells between pixels in odd columns and pixels in even columns, which causes some differences in gain and offset. Most part of this effect is corrected through the radiometric calibration where the responsivity of each pixel is taken into account. However, there seems to be also a problem of the offset/reset being dependent with the signal, which makes the difference of the odd-even effect bigger for extreme conditions, which is the case of very high signals or very low exposure times. During periapsis, for example, the exposure time is about 10 times larger than in apoapsis. This is the reason why the odd-even effect is much smaller (at or below the noise level) in Figure 9. Let us recall that odd-even effects are common in imaging spectrometers, in the spectral or spatial domains [*Moutou et al.*, 2003; *Siebenmorgen et al.*, 2007]. We will return to this point in the next section.

3. Validation Analysis

[43] Validation analysis traditionally comprises direct comparisons with independent observations. This is not possible with our VIRTIS limb data, although eventually, some indirect comparisons with related measurements by other Venus Express instrument, like neutral densities from VERA and SPICAV, will be possible. At this stage, however, our analysis focused on other aspects. These include (1) internal consistency tests and comparison with averages,

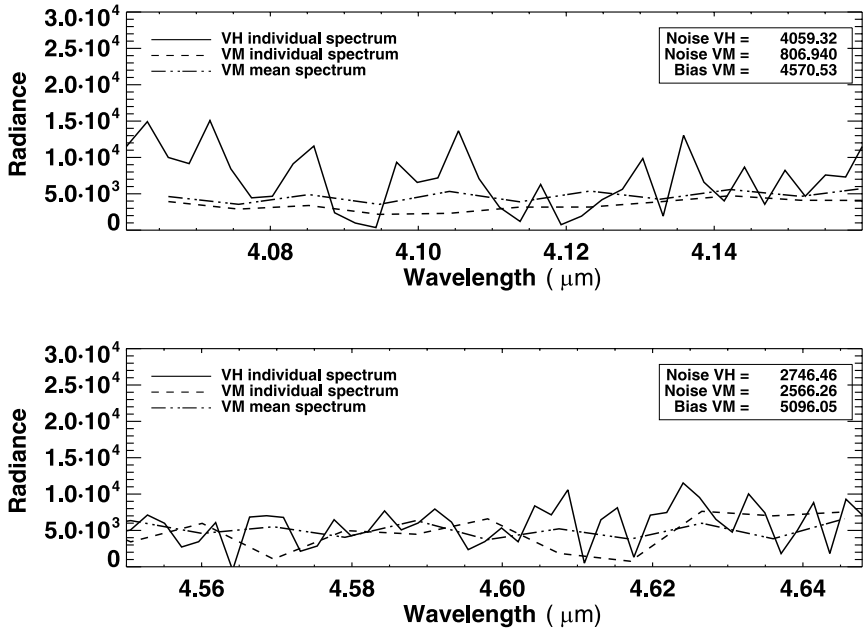

Figure 14. V-H and V-M noise and bias in a selection of spectra around 4.3 μm from periapsis, at a tangent altitude of 118 km. Radiance units are μW m^{-2} sr^{-1} μm^{-1}. See section 3.1 for further details.

(2) estimation of noise/data quality, (3) cross correlation between the two VIRTIS signals, (4) qualitative comparisons with theoretical non-LTE models, and (5) examination of the repeatability and variability of the measurements. The goal is to characterize the behavior of the VIRTIS instrument, to confirm that the measurements are physically meaningful, and to detect potential bias or systematic errors. The most important of these analysis, and their conclusions, are presented next.

3.1. Noise and Bias in V-H and V-M

[44] One of our basic objectives was to evaluate the measurement noise in orbit, in the spectral ranges and emissions of our interest, to compare it with the nominal one obtained by ground calibration, and at the same time, to analyze possible systematic effects. A first step was the examination of individual spectra for the orbits with limb data. A second task was to average homogeneous sets of data, considering appropriate boxes in SZA and tangent altitude, and to calculate their mean radiance and dispersion.

[45] For the evaluation of the noise level and the bias in the 4.3-μm region, we looked at the two wings of this CO_2 system of bands, shortward and longward of 4.20 and 4.50 μm, and at altitudes where no significant emission is expected there. The mean radiance of each spectrum can be considered as the bias, and its standard deviation (SD) as an estimation of the noise. An example for orbit 43 (periapsis) is shown in Figure 14, where two individual spectra are shown, one from V-H and a nearby one from V-M. The tangent altitude is around 120 km.

[46] Regarding V-H, the noise values obtained for this particular example are similar in the left and right wings of the band, and slightly lower than the nominal noise of 5000 μW m^{-2} sr^{-1} μm^{-1}. We have evaluated these values for a diverse set of spectra, for different orbits, solar illumination conditions and tangent altitudes, and have found that they are basically constant up to orbit 47 (7 June 2006) and decrease to about half those values after orbit 79 (8 July 2006). This is probably related to the spacecraft thermal evolution along the mission, with higher noise levels at the beginning of the mission, when the cold box temperature was higher.

[47] Regarding the V-M data, the noise in this example is also lower than the nominal value, although there is a significant difference between the left and right wings of the band. Regarding its bias, the availability of a large number of spectra from V-M at a given position, allows us to estimate it for a close subset of pixels. In Figure 14 we added another spectrum, that obtained by averaging 25 V-M pixels/spectra within a small range of tangent altitudes (118–120 km) and SZA (78°–81°) around the V-M spectrum selected. The mean value coincides well with the bias obtained from one single spectrum.

[48] Similar noise and bias analyses for V-M at apoapsis are difficult at present owing to the large odd-even effect mentioned above, much larger than those parameters. In fact, the averaged V-M spectrum in Figure 14 shows more clearly such oscillation in the intensity than one single spectrum. This effect has a magnitude (amplitude between peaks) of about 2000 μW m^{-2} sr^{-1} μm^{-1}, of the order of the noise. The V-M calibration group of the VIRTIS team is currently working on this point, in order to reduce its impact on apoapsis data.

3.2. Correlation Between V-H and V-M Spectra

[49] There is a small number of observations in the Spectral Mode which correspond to the special Tangential Limb sounding, with simultaneous measurements of V-H

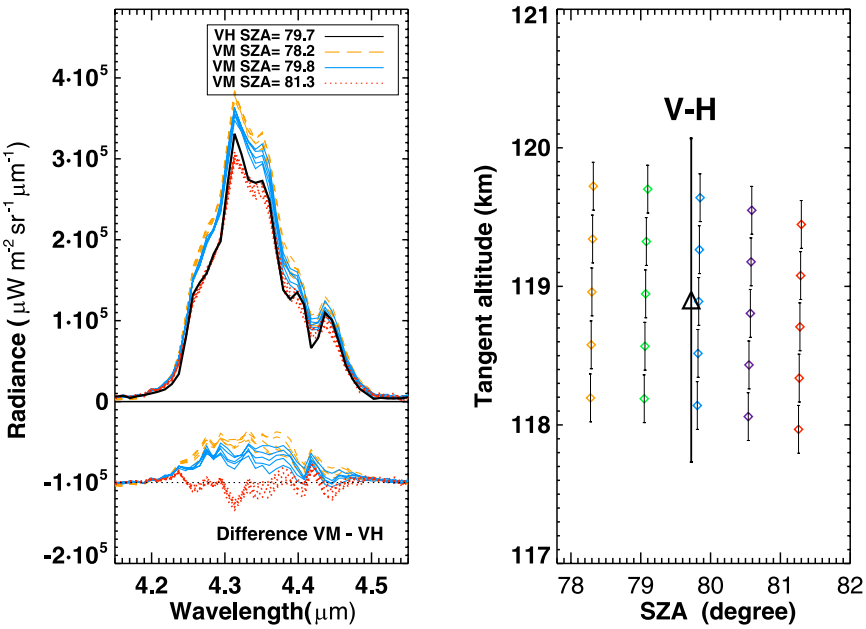

Figure 15. Correlation between V-M and V-H spectra taken during periapsis, orbit 43. (right) Location in tangent altitude and SZA, with approximate size of the V-H and V-M field of view. (left) Spectra of the 15 selected V-M pixels, those with SZA of 78.2°, 79.8°, and 81.3°, and of the V-H spectrum (convolved to V-M spectral resolution). Differences between V-H and V-M spectra are also plotted below. See section 3.2 for further details.

and V-M. The proximity to the planet during periapsis, allows for a precise geographical collocation of these profiles, and therefore, permits a specially appropriate comparison between them. Orbit 43 offers one example, and Figure 8 shows how close V-M and V-H measurements can be. Figure 15 shows a number of VM spectra close to one particular V-H spectrum, obtained at that orbit, around SZA = 80° and 119 km tangent altitude. Five adjacent slit images were considered, with five pixels on each. The vertical size of the pixel's FOV, about 300 m for V-M and 2 km for V-H, is shown on the right. On the left we plot 15 of the VM spectra, those from the groups at SZA of 78.2°, 79.9°, and 81.3°, and compare them with the V-H spectrum. This was degraded/convolved to the lower spectral resolution of V-M for the comparison. The shape of the whole CO_2 band is very well reproduced by all of them. We think the overall comparison seems fairly good, given the dispersion among the 15 V-M spectra plotted. These present, first of all, a small dispersion within each group, which is similar or slightly larger than typical noise and bias levels. In addition there is a small variation between the three groups, significantly larger than the noise, which is surely due to the small SZA difference between them; the radiance at larger SZA being smaller, as expected. Comparing the V-H spectrum with its closest V-M group of spectra, there is a small shift between them, of about 40,000 μW m^{-2} sr^{-1} μm^{-1} around the peak at 4.33 μm, larger than the noise and bias of both, V-H and V-M. However, this difference is only a factor 2 larger than the SD of this particular group of V-M data, and equivalent to a small fraction of a degree in SZA. This gives us a good level of confidence on both signals.

[50] The emission at 2.7 μm can also be used to test the V-H and V-M agreement. Although the number of spectra with good signal is very limited, we found some spectra in the orbit 43 which are useful for the present discussion. They are shown in Figure 16 and correspond to SZA = 80° approximately. Figure 16 (top) shows vertical profiles at three wavelengths in the 2.7 μm spectral region and show a neat altitude variation, with a clear peak around 115–120 km. This was predicted by the LVEA model. Figure 16 (bottom) shows the mean and standard deviation of a set of 15 V-M spectra, at altitudes around 120 km. The error bars of individual V-H and V-M are slightly larger than the nominal values, and they have been omitted in Figure 16. The agreement between V-H (convolved to V-M resolution) and V-M is good within error bars; there may be a slight mismatch around 2.8 μm but the data seem noisier there. Moreover, this emission is lower and noisier than that shown in Figure 5, at all wavelengths, since the solar excitation is lower now. We performed a simulation with the non-LTE model, also shown in Figure 16, for the same solar illumination conditions. The agreement is very encouraging, although the model seems to overestimate the radiance; this is due to the specific atmosphere structure assumed in the simulation, and therefore is of no relevance in this analysis.

[51] Related to this correlation, we investigated the correlation between different V-H spectra, wherever they can be collocated. The amount of V-H spectra is not large, but we identified a couple of interesting correspondences between spectra with good S/N ratio. On Figure 17 (left), they correspond to four consecutive V-H measurements (acquisition 84 to 87) obtained at the closest approach to Venus

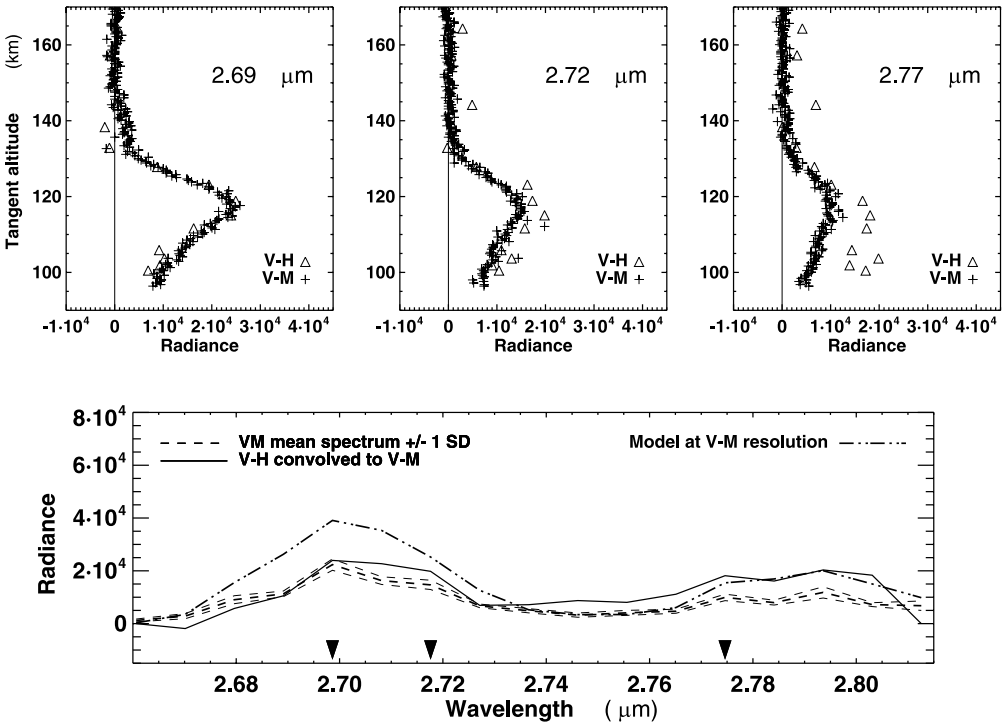

Figure 16. (top) Vertical profiles of V-H and V-M radiances at three wavelengths in the 2.7 μm for qube 0, orbit 43 and SZA around 80°. Triangles and crosses mark V-H and V-M data, respectively. (bottom) One V-H spectrum, convolved to V-M resolution (solid line) and comparison with the mean of 15 V-M spectra (dashed lines), from the data composing the vertical profile in the top, at a tangent altitude of 120 km. The dashed-dotted line represents a model simulation. Radiance units are μW m^{-2} sr^{-1} μm^{-1} in both the top and bottom. Three triangles in the bottom indicate the wavelengths of the three vertical profiles.

during orbit 43, and point to the lowest tangent altitudes for this orbit, around 99 km (as indicated in the picture) and around SZA = 83° (see Figure 8). The geometrical distance along the track of the satellite between the spectra 84 and 87 is about 250 km, and they correspond to latitudes of 73.0° and 71.8°, longitudes of 302° and 307°, respectively, and a difference in SZA of 1.4°. The four spectra are very similar, with differences of the order of the noise at almost all wavelengths, except in the central region. Around 4.3 μm there is a clear trend, from 84 to 87, the last one being about 30,000 μW m^{-2} sr^{-1} μm^{-1} lower than the former. We think, again, that this is due to SZA changes; close to the terminator small changes in SZA produce noticeable variations in the solar pumping of the CO_2 vibrational states. This reflects small changes in the atmospheric structure between those four locations.

[52] Figure 17 (right) presents another two V-H spectra, very closely located to each other, both at a latitude of 77.27°S and longitudes of 257.8°E and 260.8°E, respectively, but obtained 2 days apart, on orbits 40 and 42. Their tangent altitudes and SZA are also very close, at 108.4 and 107.8 km, and 82.7° and 82.3°, respectively. Their noise and bias levels are below 5000 μW m^{-2} sr^{-1} μm^{-1} and 8000 μW m^{-2} sr^{-1} μm^{-1}, respectively. It is surprising the excellent agreement between them in the overall shape and in the wings of the band; there is only a small difference, in the central portions of the CO_2 emission, with the spectrum of orbit 42 slightly larger than the other and the noise. Again, the small SZA differences is a possible candidate for the observed difference. This points, once more, to a relatively calm and stable atmospheric structure, fully repeatable in times scales of 2 days, at least in this case. It would be interesting to explore further coincidences of this type in future measurements of V-H, since the number of them available to date is small (see Figure 3).

3.3. Comparisons With a Non-LTE Model

[53] As discussed above, we have used in this work the non-LTE model of the Venus atmosphere developed at the Instituto de Astrofísica de Andalucía/CSIC, in Granada [*Roldán et al.*, 2000; *López-Valverde et al.*, 2007], to perform a small number of simulations. These simulations and those reported by LVEA have guided most of the analysis presented in previous sections. From these comparisons we found a good overall agreement with the predictions of the spectral shape of V-H and V-M data (Figures 4, 9, and 17), and with the altitude profiles of the radiances in the central part of the 4.3-μm band (Figures 4 and 9). Also the SZA variation of the peak radiance (Figures 8 and 15) qualitatively agrees with expectations. The vertical profiles of the CO_2 emission shown in Figures 9 and 13 do agree qualitatively with those of LVEA but a quantitative fit

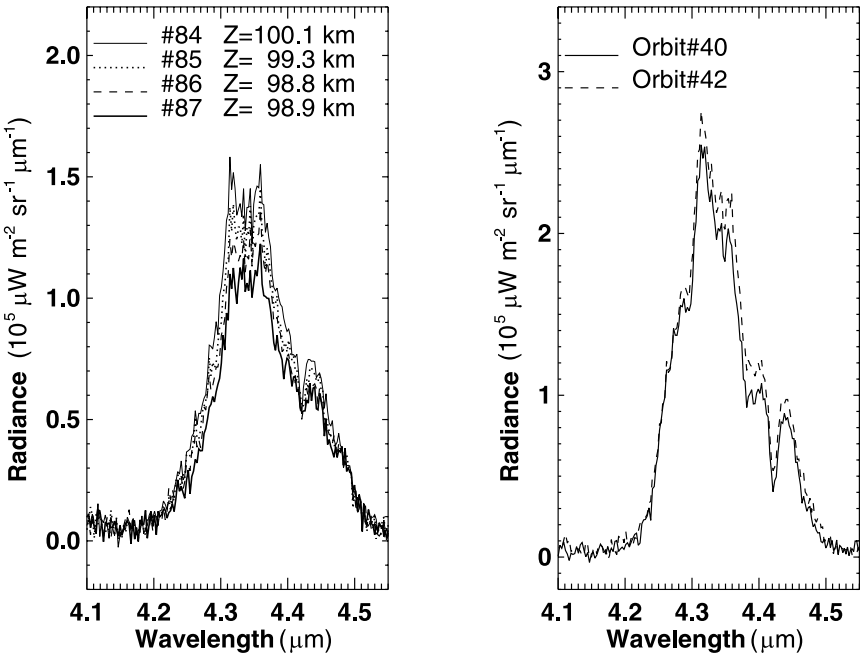

Figure 17. Geographical coincidences between different V-H spectra. (left) Four spectra from orbit 43, around 99 km. (right) Example of two spectra taken at very close points but 2 days apart. Variations attributable to SZA changes. See section 3.2 for details.

would be desirable and future work should focus on this aspect and exploit such fit, once the weak bands required are implemented into the model. Other non-LTE emissions predicted by LVEA have also been examined, detected and compared with the model. Figures 5 and 16 show simulations of the CO_2 2.7 μm bands for a given reference atmosphere; they indicate a good agreement in the spectral shape of the bands, and for both V-H and V-M spectral resolutions. Although these data are noisy, the main features are captured by the model, and the vertical profiles are also in agreement, with similar altitudes of the peak emission in the data and in the model. The absolute emission, as it happens with the 4.3 μm bands, is not considered in this comparison, since it depends on the actual atmospheric structure assumed in the non-LTE model. The third non-LTE emission detected and studied in this work, that of CO, contains a first hot component not simulated yet by the non-LTE model.

[54] Let us highlight here some other results which, either were not predicted or seem to pose interesting challenges to the theoretical modeling. One of them is the intensity in the longer wavelength wing of the 4.3 μm band, where contributions from weak, isotopic and hot transitions are expected. The predictions by LVEA produce a relatively minor contribution of that band's wings compared to the central band, but the VIRTIS spectra shown in Figures 4 and 9 indicate a more significant contribution. The model surely needs a larger number of CO_2 bands in this spectral region. Such a model extension is underway.

[55] Certainly, another extension of the non-LTE model is needed to include the first hot band of carbon monoxide, CO(2-1), in order to study the spectra shown in Figure 6. This is also a minor band compared to the strongest fundamental transition, but it seems to be highly excited by direct solar radiation, like the weaker transitions of CO_2 discussed above. As discussed in section 2.3.3, a proper simulation of the CO emission lines will be very valuable for the derivation of rotational temperatures. These could be obtained from this band's structure, but only after fitting a theoretical model which permits small radiance errors in the line peaks. This is the only molecular band detected by VIRTIS in this infrared portion of the spectrum with well isolated lines, and is therefore a very interesting data set.

4. Conclusions and Future Work

[56] VIRTIS on Venus Express is an innovative instrument which, combining imaging and spectroscopy in the near infrared, is obtaining very exciting new data on the upper atmosphere of Venus. We have analyzed the limb measurements taken by VIRTIS in the regions from 4 μm to 5 μm and around 2.7μm from both, the periapsis and the apoapsis of the Venus Express orbit, and in the two signals, V-H at high spectral resolution, and V-M at a lower resolution. We have focused in this work on a subset of VIRTIS data, which includes limb measurements with V-H taken at the periapsis from orbits 23 (13 May 2006) to 127 (25 August 2006), and a small sample of V-M data qubes between orbits 23 (13 May 2006) and 295 (10 February 2007). Extension of the analysis presented here to the rest of the data is ongoing.

[57] We clearly identified the strong emission by CO_2 at 4.3 μm in the upper mesosphere and lower thermosphere, and of the first hot band of CO at 4.7 μm in the upper

mesosphere. Individual spectra show good signal to noise up to above 160 km in the case of CO_2, and up to about 120 km in the case of CO. Single spectra show noise values slightly below the value expected from ground calibration, and a small bias too. We also showed that the V-H spectral resolution is good enough for a number of tests of our non-LTE models. The spectral resolution of V-M is lower, however the vertical resolution is much better from V-M data. During periapsis this is typically 300 m for a single row of pixels, while from apoapsis, the grouping of V-M adjacent rows of data permits a resolution at least two to three times better than the FOV of individual pixels, depending on the geometry of the V-M images and on the relative orientation of the limb of Venus. These observations characterize the Venus atmosphere directly, since they will permit to calculate densities and temperatures from measurements, and also indirectly, because they can give information about the collisional processes, energy transfer and the upper atmosphere energy balance, after a more detailed comparison with a non-LTE model.

[58] The variability observed by VIRTIS and mentioned previously by *Drossart et al.* [2007a] have been confirmed and analyzed here for the first time with this new and extended data set. The maps studied in this paper permit to describe altitude variations at several wavelengths, variations with SZA, and the detailed spectral shape of the CO and CO_2 bands. Actually, the good agreement between model and data, on the basic non-LTE features, indicates that our current understanding of the physical processes in the upper atmosphere is essentially correct. All these results will be perfect tests for future non-LTE models, and suggestions for more detailed future comparisons are given in section 3.3. We foresee that such detailed comparisons, specially of the shape of the V-H emissions, can give us information about non-LTE collisional parameters in the upper mesosphere and lower thermosphere, where these processes are specially relevant. Also, comparisons between spectra at similar conditions but obtained with a span of 2 days, and between data more than 200 km apart, show very good matches, which indicates a good behavior of VIRTIS. When applied to a future and extended data set, similar comparisons may supply interesting information about atmospheric variability in the lower thermosphere. The high density of points in the limb in some maps during periapsis offer excellent chances for derivation of density maps in the thermosphere. Such density profiles are foreseen to be obtained by a rigorous "retrieval" process which uses inversion techniques under non-LTE conditions, an exercise similar to other upper atmosphere experiment on Earth, like the MIPAS/Envisat data analysis [*Funke et al.*, 2005]. Densities of CO would be derived in a limited altitude range (90–120 km) owing to the low signal of the CO 4.7 μm emission (see section 2.3.3). However, densities of CO_2 can be derived in principle in a wider altitude range. Nevertheless, the accuracy of such derivation will depend on a sensitivity study to be performed with the revised non-LTE model. Limb views from V-M during apoapsis should also be very useful for density retrievals, although they are affected at present from a "smiling effect" which deforms the actual emission field by about 20 km, approximately the size of the projected FOV of one pixel. We showed how the non-LTE model has been essential to detect this effect which could be reduced in future processing thanks to a correction technique using these CO_2 non-LTE emission. These V-M data from apoapsis are also affected by a large odd-even effect, about 10 times larger than the noise level. During periapsis this effect is below noise due to the much larger exposure time there. This aspect requires further work within the VIRTIS team in the future.

[59] The study of the first hot CO(2-1) emission is also very promising, since the rotational structure is resolved and it can therefore be used to derive rotational temperatures in the upper mesosphere. This will be confined to daytime and to the altitude range 90–120 km, where such signal is strongest. This derivation does not require a full non-LTE retrieval but a fit of the shape of the CO emission band with the model, as explained in section 2.3.3. At present, uncertainties in individual lines of a CO spectrum produce very large temperature errors. Comparisons with temperatures obtained from ground-based measurements of these bands [*Crovisier et al.*, 2006] will also be interesting, as a validation exercise of these data and in order to future check the non-LTE models.

[60] VIRTIS/Venus Express will continue acquiring new data at least until 2009. The exploration of the new data and their analysis will continue, hopefully with a version of the non-LTE model extended to weaker bands, and with better understanding of some of the current uncertainties in the data that we highlighted here. The application of retrieval techniques and systematic search for atmospheric variability, makes the VIRTIS observations a very promising data set for studying the non-LTE processes and the structure of the upper atmosphere of Venus.

[61] **Acknowledgments.** We thank the space agencies ASI and CNES for their support. The work of the IAA-CSIC team has been carried out under project ESP2004-01556 and was partially funded by the project AYA2008-03498/ESP of the Spanish Ministery of Science and Innovation and by EC-FEDER funds. GG has been partially supported by a fellowship from Spanish National Research Council (CSIC-JAE Program).

References

Bougher, S. W., D. M. Hunten, and R. G. Roble (1994), CO_2 cooling in terrestrial planet thermospheres, *J. Geophys. Res.*, *99*, 14,609–14,622.

Carlson, R. W., et al. (1991), Galileo infrared imaging spectroscopy measurements at Venus, *Science*, *253*, 1541–1548.

Carlson, R. W., P. R. Weissman, W. D. Smythe, and J. C. Mahoney (1992), Near-Infrared Mapping Spectrometer experiment on Galileo, *Space Sci. Rev.*, *60*, 457–502.

Coradini, A., F. Capaccioni, P. Drossart, A. Semery, G. Arnold, and U. Schade (1998), VIRTIS: An imaging spectrometer for the Rosetta mission, *Planet. Space Sci.*, *46*, 1291–1304.

Crovisier, J., E. Lellouch, C. de Bergh, J.-P. Maillard, B.L. Lutz, and B. Bèzard (2006), Carbon monoxide emissions at 4.7 μm from Venus' atmosphere, *Planet. Space Sci.*, *54*, 1398–1414, doi:10.1016/j.pss.2006.04.027.

de Bergh, C., J. Crovisier, B. L. Lutz, and J.-P. Maillard (1988), Detection of CO infrared emission lines in spectra of Venus, *Bull. Am. Astron. Soc.*, *20*, 831.

Deming, D., F. Espenak, D. Jennings, T. Kostiuk, M. Mumma, and D. Zipoy (1983), Observations of the 10-um natural laser emission from the mesosphere of Mars and Venus, *Icarus*, *55*, 347–355, doi:10.1016/0019-1035(83)90107-0.

Dickinson, R. E. (1972), Infrared radiative heating and cooling in the Venusian mesosphere: I. Global mean radiative equilibrium, *J. Atmos. Sci.*, *29*, 1531–1556.

Drossart, P., et al. (2007a), A dynamic upper atmosphere of Venus as revealed by VIRTIS on Venus Express, *Nature*, *450*, 641–645, doi:10.1038/nature06140.

Drossart, P., et al. (2007b), Scientific goals for the observation of Venus by Virtis on ESA/Venus Express mission, *Planet. Space Sci.*, *55*, 1653–1672, doi:10.1016/j.pss.2007.01.003.

European Space Agency (ESA) (2001), Venus Express: An orbiter for the study of the atmosphere, the plasma environment, and the surface of Venus, *Eur. Space Agency Sci. Tech. Rep., ESA STR 6*, 46 pp.

Formisano, V., A. Maturilli, M. Giuranna, E. D'Aversa, and M. A. Lopez-Valverde (2006), Observations of non-LTE emission at 4–5 microns with the Planetary Fourier Spectrometer aboard the Mars Express mission, *Icarus*, *182*, 51–67, doi:10.1016/j.icarus.2005.12.022.

Funke, B., et al. (2005), Retrieval of stratospheric NO_x from 5.3 and 6.2 μm nonlocal thermodynamic equilibrium emissions measured by Michelson Interferometer for Passive Atmospheric Sounding (MIPAS) on Envisat, *J. Geophys. Res.*, *110*, D09302, doi:10.1029/2004JD005225.

García, R., M. A. López-Valverde, P. Drossart, and G. Piccioni (2009), Gravity waves in Venus atmosphere revealed by CO_2 non-LTE emission, *J. Geophys. Res.*, doi:10.1029/2008JE003073, in press.

Gordiets, B. F., and V. I. Panchenko (1983), Non-equilibrium infrared emission and the natural laser effect in the Venus and Mars atmospheres, *Kosm. Issled.*, *21*, 929–939.

Hueso, R., A. Sánchez-Lavega, G. Piccioni, P. Drossart, J. C. Gèrard, I. Khatuntsev, L. Zasova, and A. Migliorini (2008), Morphology and dynamics of Venus oxygen airglow from Venus Express/Visible and Infrared Thermal Imaging Spectrometer observations, *J. Geophys. Res.*, *113*, E00B02, doi:10.1029/2008JE003081.

López-Puertas, M., and F. W. Taylor (2001), *Non-LTE Radiative Transfer in the Atmosphere*, *Ser. Atmos., Oceanic, Planet. Phys.*, vol. 3, World Sci., Singapore.

López-Valverde, M. A., and M. López-Puertas (1994), A non-local thermodynamic equilibrium radiative transfer model for infrared emission in the atmosphere of Mars: 2. Daytime populations of vibrational levels, *J. Geophys. Res.*, *99*, 13,117–13,132.

López-Valverde, M. A., M. López-Puertas, J. J. López-Moreno, V. Formisano, D.Grassi, A. Maturilli, E. Lellouch, and P. Drossart (2005), Analysis of CO_2 non-LTE emissions at 4.3 μm in the Martian atmosphere as observed by PFS/Mars Express and SWS/ISO, *Planet. Space Sci.*, *53*, 1079–1087, doi:10.1016/j.pss.2005.03.007.

López-Valverde, M. A., P. Drossart, R. Carlson, R. Mehlman, and M. Roos-Serote (2007), Non-LTE infrared observations at Venus: From NIMS/Galileo to VIRTIS/Venus Express, *Planet. Space Sci.*, *55*, 1757–1771, doi:10.1016/j.pss.2007.01.008.

Moutou, C., A. Coustenis, J. Schneider, D. Queloz, and M. Mayor (2003), Searching for helium in the exosphere of HD 209458b, *Astron. Astrophys.*, *405*, 341–348.

Piccioni, G., et al. (2006), VIRTIS: The Visible and Infrared Imaging Spectrometer, *Eur. Space Agency Spec. Publ.*, *ESA-SP 1295*, 1–27.

Roldán, C., M. A. López-Valverde, M. López-Puertas, and D. P. Edwards (2000), Non-LTE infrared emissions of CO_2 in the atmosphere of Venus, *Icarus*, *147*, 11–25, doi:10.1006/icar.2000.6432.

Roos-Serote, M., P. Drossart, Th. Encrenaz, E. Lellouch, R. W. Carlson, K. H. Baines, F. W. Taylor, and S. B. Calcutt (1995), The thermal structure and dynamics of the atmosphere of Venus between 70 and 90 km from the Galileo-NIMS spectra, *Icarus*, *114*, 300–309, doi:10.1006/icar.1995.1063.

Rothman, L., et al. (2005), The Hitran 2004 molecular spectroscopic database, *J. Quant. Spectrosc. Radiat. Transfer*, *96*, 139–204.

Siebenmorgen, R., et al. (2007), Very large telescope paranal science operations CRIRES user manual, *Rep. VLT-MAN-ESO-14500-3486*, 56 pp., Eur. South. Obs., Garching, Germany.

Stepanova, G. I., and G. M. Shved (1985), Radiation transfer in the 4.3-μm CO_2 band and the 4.7-μm CO band in the atmospheres of Venus and Mars with violation of LTE: Populations of vibrational states, *Sov. Astron., Engl. Transl.*, *29*, 248–422.

Svedhem, H., et al. (2007), Venus Express: The first European mission to Venus, *Planet. Space Sci.*, *55*, 1636–1652, doi:10.1016/j.pss.2007.01.013.

Taylor, F. W., et al. (1980), Structure and meteorology of the middle atmosphere of Venus infrared remote sensing from the Pioneer orbiter, *J. Geophys. Res.*, *85*, 7963–8006.

Titov, D. V., et al. (2006), Venus Express science planning, *Planet. Space Sci.*, *54*, 1279–1297, doi:10.1016/j.pss.2006.04.017.

A. Cardesín Moinelo and G. Piccioni, IASF, INAF, via del Fosso del Cavaliere 100, I-00133 Rome, Italy.

P. Drossart and S. Erard, Observatoire de Paris, F-92195 Meudon, France.

G. Gilli and M. A. López-Valverde, Instituto de Astrofísica de Andalucía, CSIC, Camino Bajo de Huetor 50, E-18008 Granada, Spain. (gilli@iaa.es)

Chapter 3

Non-LTE model validation with VIRTIS/VEx data

As it is mentioned in the previous Chapter the non-LTE model used in this work to analyze the infrared emissions by CO and CO_2 on Venus was originally developed by Roldán et al. (2000) at the Instituto de Astrofísica de Andalucía based on a previous model for the Martian atmosphere (Lopez-Valverde and Lopez-Puertas, 1994) and it was updated and used to make predictions on some of the VIRTIS emissions by López-Valverde et al. (2007). As it is discussed in the next Chapter, this code is a central part of the forward model and the inversion scheme developed during this Thesis for the retrieval of temperature and CO in the Venus atmosphere.
In addition to these applications, VIRTIS on board Venus Express supplied a unique set of infrared measurements in the limb of Venus, which also includes a systematic sounding of the non-LTE emissions of its upper atmosphere, for the first time. This represents an unprecedented opportunity to test and validate such non-LTE theoretical tool and this is one of the main goals of this Thesis. Numerous comparisons between data and simulations have been performed during the course of this work, some of which were mentioned in the previous Chapter, and a few others will be presented in the next Chapter. However, there is a specially interesting validation exercise in the broader context of Comparative Planetology, which is possible nowadays and it is discussed in the present Chapter. It consists on a comparison of the different planetary versions of the non-LTE model (Mars, Earth and Venus) with similar data on the three terrestrial planets. This is possible nowadays since a number of analogous experiments to VIRTIS, measuring similar IR emissions in an equivalent observational geometry, is available on Earth and Mars. The results of these validation exercises were first presented in the International Conference on Comparative Planetology: Venus-Earth-Mars (43rd ESLAB Symposium, May 2009) and then published in 2011 in two separate papers on *Planetary and Space Science* journal, Volume 59. Those works are entitled: *"Modeling the atmospheric limb emission of CO_2 at 4.3 μm in the terrestrial planets"* and *"Non-LTE CO limb emission at 4.7 μm in the upper atmosphere of Venus, Mars and Earth: Observations and modeling"*. They are attached below.

The dataset selected for those studies are limb measurements of the Earth, Mars and Venus atmosphere by MIPAS/Envisat, PFS/Mars Express and VIRTIS/VEx, respectively.

Those observations were contrasted with non-LTE models developed for the three planets at Instituto de Astrofisica de Andalucia (IAA), Granada, Spain. One of the main objective was to perform a common analysis of these recent space observations with similar and consistent theoretical tools, in order to highlight similarities and differences among those planets, and to detect possible biases in the models (i.e, as a powerful validation exercise). Specifically we used the latest version of the non-LTE model for Venus (López-Valverde et al., 2007), for Mars (Lopez-Valverde and Lopez-Puertas, 1994) and for the Earth (López-Puertas et al., 2005). The essential aspects of the modeling are similar in the three planets: the statistical equilibrium and the radiative transfer equations of CO and CO_2 are solved simultaneously, within proper approximations (see Lopez-Puertas and Taylor (2001). In the upper atmosphere of the three terrestrial planets, high energy states of these molecules are very excited during daytime by the same pumping mechanism, the direct absorption of the solar flux in their respective resonant wavelengths in different ro-vibrational bands in the near-IR (1-5 μm), thus producing the strong emissions studied.

The first paper included in this chapter is devoted to explain the main peculiarities of the recent observations of the 4.3 μm CO_2 limb emission in the upper atmosphere of the terrestrial planets detected by the mentioned instruments. Sensitivity studies were also performed to evaluate the impact of small perturbations in temperature and density on the radiances. Those emissions were examined in a global planetary view using large averages of data, comparing their dependence on geophysical parameters and evaluating their potential for retrieving atmospheric properties.
The second paper is focused on the comparative study of non-LTE emission of CO at 4.7 μm on Venus, Mars and the Earth. As for the CO_2 emission study, this is a strong test for the non-LTE models, since a detailed analysis of the CO emission and their different contributing bands permits to gain insight into the governing mechanisms of different CO and CO_2 states, under varying conditions of the same physical processes.

As explained in the two papers, the models can explain satisfactorily the main spectral features of the measurements and the variation of those radiances with two key-parameters: the solar zenith angle and the altitude. This confirms the results obtained by (Gilli et al., 2009) and mentioned in the previous chapter. To elaborate further, Figure 3.1 shows as an example, a map of simulated and measured radiances in the region of 4.7 μm as a function of these two parameters, in the case of a strong line of the CO emission. The peak of emission is located around 100 km and the larger emissions correspond to lower SZAs, as expected. Let us recall that simulations like these are valid only for the reference atmosphere used as input. A more detailed quantitative comparison between model and data would require the knowledge of the actual thermal structure of the Venus atmosphere, which is unknown. The data presents variations with SZA not seen in the simulations and this may indicate spatial variations in the actual Venus atmosphere not present in the VIRA model, used as reference in the simulations, although some of these variations may be close to the noise level, especially for high SZA. Moreover, the data also shows a steeper decline with altitude, possibly indicating different scale heights, smaller than in VIRA, which could be suggestive of an overall colder thermosphere.

The main conclusions of the two papers can be summarized as follows:

- For the first time an inter-comparison of the non-LTE emissions of CO_2 and CO of

the IR limb of the three terrestrial planets was performed.

- Regarding the CO_2 4.3 μm region, the CO_2 relative abundance and the distance to the Sun are the two key parameters driving the excitation and the strength of this emission.
- These emissions are useful to constrain rate coefficients of collisional exchanges between energy states which are poorly known.
- In the case of the CO emission, the fundamental band dominates the observations on Earth, while the FH band is the dominant component on Mars and Venus, due to lower abundance of CO on Earth on the same pressure level.
- All the previous results are well reproduced by the non-LTE models, without altering the main assumptions and the internal scheme of transitions and collisional interactions, which gives confidence on capturing correctly the essential mechanism on the three planets.

In addition to these published results, a number of theoretical studies devoted to improve the comparison model-data, and to correct possible instrumental effects were carried out. Those studies form an integral part of the development of this Thesis, and most of them are discussed briefly in the previous chapter (Gilli et al., 2009) and in the next one (Gilli et al. 2012, in preparation). Here a few others which are also relevant for the model-data comparison and for the retrieval results of the Thesis are mentioned. Among the aspects that required extensive discussion, are the spectral resolution and the instrumental line shape (ILS) of the actual VIRTIS-H data. Although the original ILS and resolution were determined before the flight, they have continuously been revised during regular operations throughout the VEx mission. The actual ILS is fairly complex (Grassi D., personal communication) but can be approximated to a Gaussian form with added lobules. This shape is not a critical parameter for our simulations; the synthetic spectra are not much affected by the actual shape, as far as the spectral resolution is correct. This last parameter does have a large impact, and it was found that the theoretical value of 1.3 cm^{-1} is completely inappropriate for realistic simulations in the spectral region of interest. Values between 1.7 and 2.2 cm^{-1} resemble the data more closely, as shown in Figure 7 of Gilli et al. (2011). The value finally used is 2.0 cm^{-1}, with an uncertainty of 0.3 cm^{-1}. Unfortunately, it is difficult to decide on a single value and this uncertainty has an important impact on the total retrieval error, as it is discussed in the next chapter.
Another result obtained and not discussed at length in the papers, is that no other CO bands are needed to explain the VIRTIS data around 4.7 μm. Isotopic bands and second hot bands of the main isotope were included, all giving negligible contributions.

Once the overall behavior and results of the non-LTE model are trusted, an important application of non-LTE models is their implementation and the use within the retrieval scheme of atmospheric parameters, like density and temperature. As it is customary, Earth's instrumentation and studies are pioneering in this field and Gilli et al. (2011) explain that MIPAS spectra have already provided CO_2 and CO abundances with good vertical resolution (Funke et al., 2009). It was demonstrated that similar non-LTE retrievals are also possible in the mesosphere of Mars and Venus, using data from Mars Express and VEx,

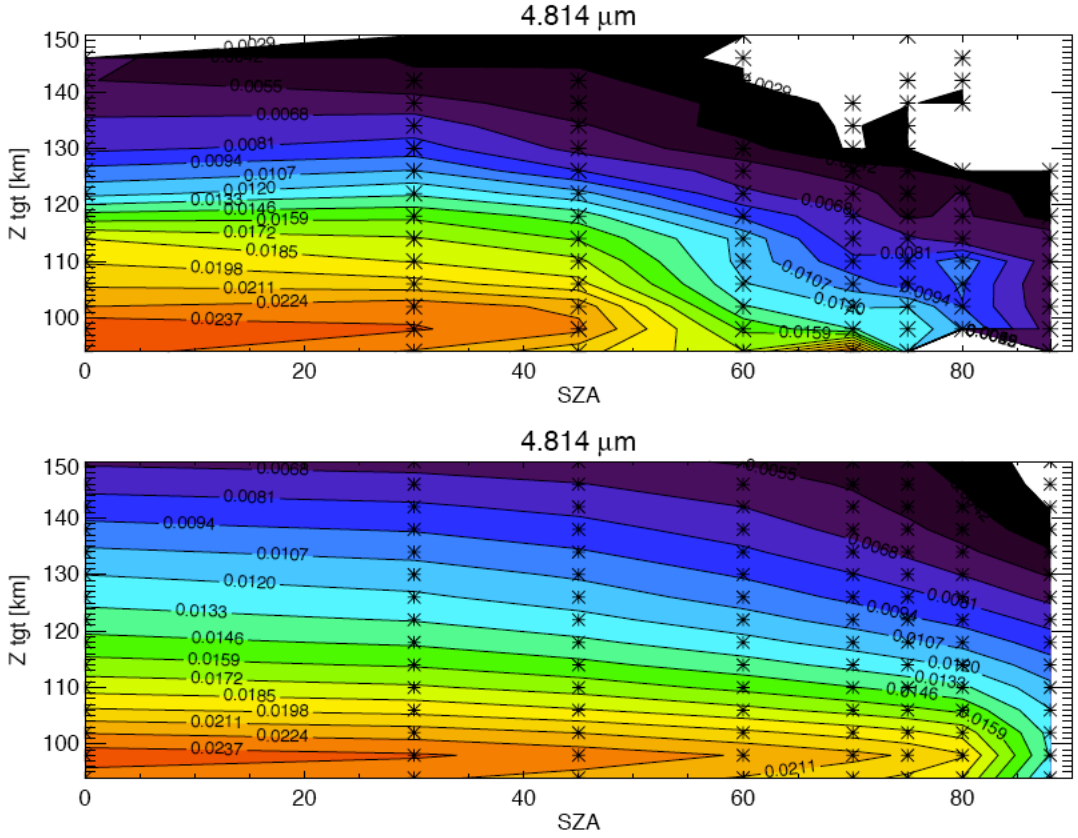

Figure 3.1: Variation of daytime CO radiances with SZA and tangent altitudes, observed by VIRTIS-H (upper panel) and in model simulations (lower panel) at 4.81 μm, which corresponds to the centre of the P10 line of the first hot band.

being more promising on Venus, due to the larger sensitivity of VIRTIS and the stronger non-LTE emissions in this planet. This task is addressed in the next chapter.

Planetary and Space Science 59 (2011) 988–998

Contents lists available at ScienceDirect

Planetary and Space Science

journal homepage: www.elsevier.com/locate/pss

Modeling the atmospheric limb emission of CO_2 at 4.3 μm in the terrestrial planets

M.A. López-Valverde [a,*], M. López-Puertas [a], B. Funke [a], G. Gilli [a], M. Garcia-Comas [a], P. Drossart [b], G. Piccioni [c], V. Formisano [d]

[a] Instituto de Astrofisica de Andalucia (CSIC), Apdo. 3004, Granada, Spain
[b] LESIA, Observatoire de Paris, France
[c] IASF/INAF, Rome, Italy
[d] IFSI/INAF, Rome, Italy

ARTICLE INFO

Article history:
Received 12 October 2009
Received in revised form
25 January 2010
Accepted 2 February 2010
Available online 16 February 2010

Keywords:
Planetary atmospheres
Aeronomy
Remote sounding
Infrared astronomy
Radiative transfer

ABSTRACT

The MIPAS instrument on board Envisat, in Earth orbit, the PFS and OMEGA instruments on Mars Express, and VIRTIS on board Venus Express are currently providing a dataset of limb measurements of the CO_2 atmospheric fluorescence emission at 4.3-μm from the upper atmosphere of the three planets. These measurements represent an excellent dataset to perform comparative studies between the terrestrial planets' upper atmospheres, and also to test our theoretical understanding of these emissions. In order to exploit these datasets, we apply a set of non-local thermodynamic equilibrium (non-LTE) models developed at the IAA/CSIC, in Granada, Spain, to a selection of data. In general, the models can explain the main spectral features of the measurements, and also the altitude and solar zenith angle variations. However, the simulations for Mars and Venus give an incorrect ratio of the emissions at two wavelengths, 4.4 and 4.32 μm. In order to explain this deficiency, a revision of the most uncertain non-LTE energy transfer parameters has been performed. The quenching rate of v_3 quanta of high-energy CO_2 states by CO_2 itself could reduce the model-data discrepancy if increased by a factor 2–4, still within its current uncertainty range. This factor, however, is subject to the uncertainty in the thermal structure. A number of simulations with the non-LTE models were also used to study and compare the role of radiative transfer in this spectral region in the three terrestrial planets. Sensitivity studies of density and temperature are also presented, and they permit an analysis of how the differences between the planets and between the three instruments affect their sounding capabilities.

1. Introduction

The upper mesosphere/lower thermosphere is an atmospheric region not well described in the three terrestrial planets, mainly because of its difficult accessibility, either by in situ or remote sounding. Non-local thermodynamic equilibrium (non-LTE) is a condition typical of the upper atmosphere of a planet, linked to the lack of efficient energy transfer by collisions between atmospheric species. Under such circumstances, the molecular emissions do not follow a Planckian source function at the local kinetic temperature, but reflect a diversity of radiative, collisional and chemical processes (López-Puertas and Taylor, 2001). These emissions can therefore be used to gain insight into such processes, and once they are well understood, they can also be used to derive other relevant atmospheric information. Hence the non-LTE emissions represent a useful tool for sounding the upper atmosphere. Carbon dioxide's ro-vibrational bands are responsible for well known atmospheric emissions in the 4.3-μm region, and when observed in a limb geometry become very intense.

Here we study and compare three sets of limb measurements of such emissions, one set for each of the three terrestrial planets. For the Earth upper atmosphere, we used data from MIPAS on board Envisat; for Mars, measurements by PFS on board Mars Express (MEx); and for Venus, data by VIRTIS on Venus Express (VEx). The three instruments are still operative at the time of writing this manuscript. There is a long history of observations of this intense emission band in the Earth's upper atmosphere, like the ISAMS instrument on board UARS (see López-Puertas and Taylor, 2001, and references therein). However, the MIPAS instrument has an unprecedented combination of high spectral resolution, sensitivity and regular limb sounding operations on board Envisat (Fischer et al., 2008). For Venus and Mars, only a few measurements were available. However, the PFS and OMEGA instruments on Mars Express (Formisano et al., 2006; Drossart

* Corresponding author. Tel.: +34 958121311; fax: +34 958814530.
E-mail address: valverde@iaa.es (M.A. López-Valverde).

0032-0633/$ - see front matter © 2010 Elsevier Ltd. All rights reserved.
doi:10.1016/j.pss.2010.02.001

et al., 2006; López-Valverde et al., 2005); and specially VIRTIS/VEX (Drossart et al., 2007a; Gilli et al., 2009) are supplying the first systematic sounding (nadir and limb) of these atmospheres in this spectral region. A few data on the dayside limb of Venus were previously taken by NIMS/Galileo during its fast fly-by of Venus in 1991 (Carlson et al., 1992). These data, which were shown to correspond to non-LTE emissions (López-Valverde et al., 2007), demonstrated the feasibility of using this strong signal for sounding the Venus upper atmosphere (Drossart et al., 2007a, b). A special mention should be made to the first VIRTIS instrument, on board the ESA/Rosetta mission, which also measured this emission during its flybys of Earth and Mars (Drossart et al., 2009).

Given the nature of these emissions, proper non-LTE models need to be used in their interpretation and analysis. Most theoretical efforts devoted to study non-LTE situations in the past were carried out to understand the Earth's upper atmosphere, but a number of them have also been extended to the Mars and Venus upper atmospheres (Dickinson, 1972; Deming and Mumma, 1983; Stepanova and Shved, 1985; Crovisier et al., 2006).

In the IAA/CSIC we have acquired a long experience in the development of atmospheric non-LTE models for the most interesting atmospheric molecular emission bands in the infrared. The essential aspects of the modeling are similar in the three planets. The models need to solve the statistical equilibrium equations and the radiative transfer simultaneously within proper approximations. Since the models can reproduce correctly the measurements, it will be useful to compare key modeling aspects in the three terrestrial planets' atmospheres, and the goodness of those approximations under these diverse conditions. Another advantage of comparing similar observations in different planets using similar theoretical tools is to highlight the relevance of various excitation processes under different conditions.

Our objective is, therefore, to apply state-of-the-art non-LTE models to explain the main peculiarities of the most recent measurements of the 4.3-μm limb emission in the upper atmospheres of Earth, Mars and Venus; to explain and compare them in a global planetary view; and to derive conclusions about their dependence on geophysical parameters and the potential for retrieving atmospheric properties.

We describe the sets of measurements used in this study in Section 2. Section 3 summarizes the non-LTE model characteristics and the numerical simulations performed. Sensitivity tests and retrieval perspectives are presented in Section 4, and the conclusions are presented in Section 5.

2. Limb measurements at 4.3-μm

2.1. Earth observations by MIPAS/Envisat

Fig. 1 illustrates a typical Earth limb spectra obtained by MIPAS at mesospheric altitudes. MIPAS spectral resolution is 0.035 cm^{-1} (unapodized), and the noise level for a single spectrum is 3 nW/(cm^2 sr cm^{-1}), about 800 times smaller than the peak emission for the co-added spectrum shown in Fig. 1. The inset panel in the figure zooms to a smaller spectral subinterval in order to illustrate in more detail the high spectral resolution achieved with this instrument. MIPAS is operating from the nearly circular polar orbit of Envisat, nominally observing in a limb geometry, between the tropopause and the lower mesosphere, with a 3 km field of view. Given its high spectral resolution and low noise level, beyond current observing satellites on other planets, it is an ideal instrument to retrieve chemical species in the Earth stratosphere and mesosphere. The retrieval scheme used in our group is based on the forward model Karlsruhe Optimized and Precise Radiative

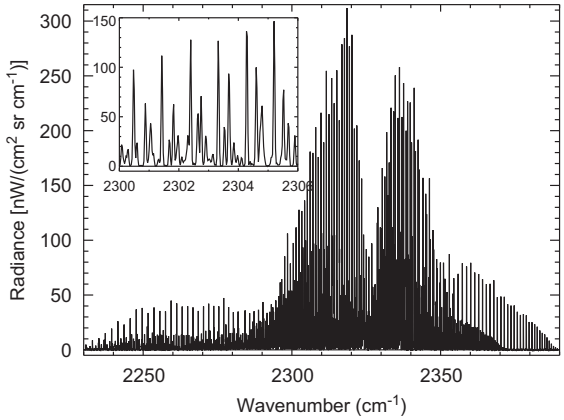

Fig. 1. Average of 156 daytime spectra of MIPAS for a tangent altitude of 67 km. The axis in the inset panel have the same units as in the main window.

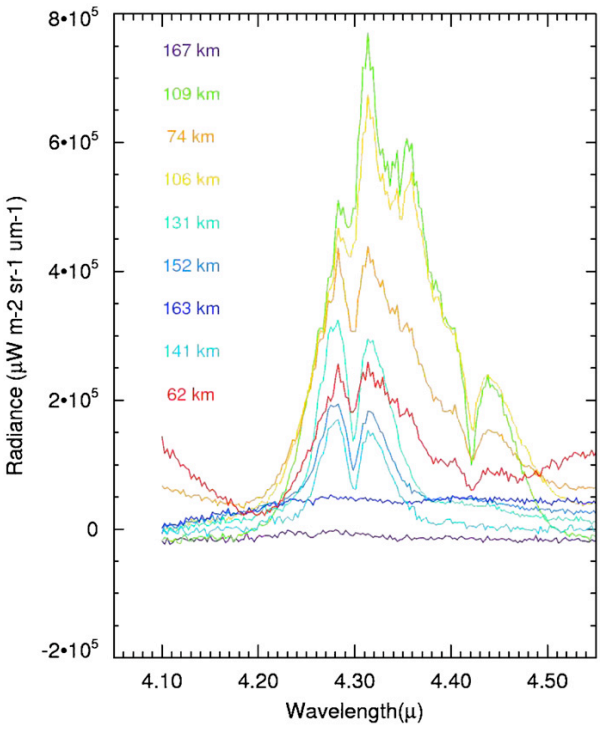

Fig. 2. Single spectra from Venus upper atmosphere taken by VIRTIS/VEx at different tangent altitudes, as indicated.

Transfer Algorithm (KOPRA) (Stiller et al., 2002), which makes use of a generic non-LTE model, the Generic Radiative Transfer and non-LTE population Algorithm (GRANADA) (Funke et al., 2002), in order to account for non-LTE effects and/or retrieve parameters from non-LTE emissions (López-Puertas and Taylor, 2001; Funke et al., 2009).

2.2. Venus observations by VIRTIS/Venus Express

Fig. 2 shows typical individual spectra at 4.3-μm from VIRTIS for varying tangent altitudes in Venus. VIRTIS operates with a

nominal spectral resolution of 1.5 cm^{-1} in this spectral region. The noise level is about 150 times smaller than the peak emissions shown in Fig. 1. The data shown correspond to the so-called "VIRTIS-H" signal, the higher spectral resolution mode of VIRTIS (Drossart et al., 2007b). VIRTIS looks at Venus mostly on a nadir geometry during the apoapsis of a high eccentricity orbit of Venus Express. Most tangent observations are taken during scans which occasionally cross the limb of the planet, except for a number of special limb inertial observations (Drossart et al., 2007a). Compared to MIPAS, VIRTIS cannot resolve individual ro-vibrational lines, however, contributions from some bands or groups of bands can be discerned (López-Valverde et al., 2007). The envelope shape observed in Fig. 2 changes with altitude, as explained by López-Valverde et al. (2007) and Gilli et al. (2009). This point is also discussed below.

2.3. Mars observations by PFS/Mars Express

Fig. 3 shows two spectra typical of the PFS sounding of the upper Martian atmosphere at this wavelength region. PFS was designed to measure mostly in a nadir view from the highly elliptic orbit of Mars Express (Formisano et al., 2005). Limb data were taken during special orbits, with fixed inertial pointing and with lowest altitude of the FOV close to the upper mesosphere. MEx and VEX have similar orbital characteristics around their host planets, and this mode of operation of PFS is entirely similar to some of VEX soundings during periapsis. The PFS field of view (FOV) is about 30 km during closest approach, much larger than VIRTIS and than MIPAS. The first clear evidences of non-LTE emissions were studied by Formisano et al. (2006), like the two spectra shown in that Figure. Due to the scarcity of those special orbits, the amount of limb data is lower than with VIRTIS, but nowadays there is a much larger dataset of limb spectra. The PFS nominal spectral resolution is 1.3 cm^{-1}, higher than other instruments on Mars Express like OMEGA, and permitted the detection of different band contributions (López-Valverde et al., 2005; Formisano et al., 2006). The data shown in Fig. 3 correspond to one orbit and two altitudes, and show a clearly different emission structure at the two altitudes, with a larger number of bands contributing to the emission at the lowest altitude. Notice also the noise levels and the space signal (dotted line in the figure).

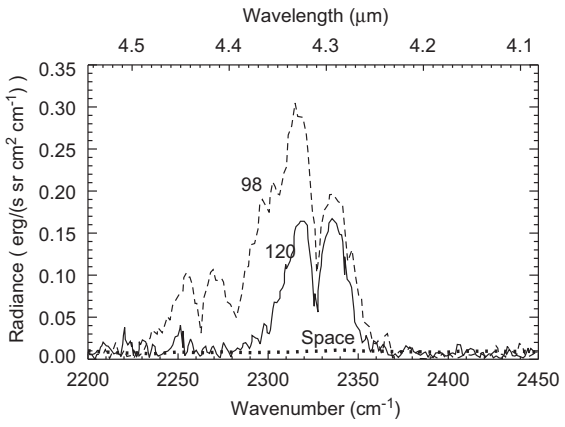

Fig. 3. Two limb single spectra from PFS/Mars Express in the upper atmosphere of Mars, at 98 and 120 km tangent altitudes, together with a typical space signal from this orbit. Figure adapted from Formisano et al. (2006). Published with permission.

3. Model results and comparisons

3.1. Non-LTE model description

For the Earth simulations we used the model GRANADA, mentioned above. The model builds upon previous versions for the CO_2 molecule and has been extensively compared to other non-LTE models and measurements (see López-Puertas and Taylor, 2001 for details). For Mars and Venus, the non-LTE models used were also developed at the IAA/CSIC, and were originally described by López-Valverde and López-Puertas (1994a, b) and by Roldán et al. (2000), respectively. A number of improvements were introduced later in both Mars (López-Valverde et al., 2005) and Venus (López-Valverde et al., 2007) codes, and a joint version for both planets is used in this work. The Earth/Mars/Venus models are very similar in most aspects, but differ in the number of high energy states, in the radiative transfer calculations, and the collisional processes involving the relevant atmospheric species on each planet.

Fig. 4 shows a diagram of levels and processes of the main isotope (CO_2-626) which are most important for the emissions at 4.3-μm. This scheme is a subset of the models' full scheme. Similar vibrational levels are implemented for the other three most abundant isotopes (636, 628 and 627). Energy transfer between the different CO_2 states by molecular collisions (thermal and non-thermal) are represented by dotted lines. Although not shown in the figure, collisional exchanges with excited states of other molecular species are also included. Those with CO(1) have some importance on Mars and Venus but not on Earth, while on our planet the collisions with $N_2(1)$ are very important. It is important to recall that not all the rate coefficients are well determined by laboratory experiments, and therefore, they lead to uncertainties in some of the model results. See López-Puertas and Taylor (2001) for details.

The higher energy states shown in the figure are directly excited during daytime by direct absorption of the solar flux in their respective wavelengths. They are responsible for the strongest near-IR (1−5 μm) emissions from the upper atmospheres of these planets. The first excited state of the asymmetric stretching mode (0 0 1) is the upper state of the fundamental transition at 4.3-μm (FB). The first hot (FH) and second hot bands (SH) arise from higher energy states, the later strongly populated by absorption in the 2.7-μm bands, as indicated in the figure.

In general, for any vibrational state with an enhanced population, the initial excitation can be radiated away, quenched down, re-absorbed and re-emitted at other altitudes, or exchanged between the different states and isotopes by non-thermal collisions. All these mechanisms need to be implemented correctly in the non-LTE models in order to obtain a solution for the resulting stationary conditions in each planet. Although the absorptions and emissions of our interest do affect the atmospheric temperatures, normally the thermal structure is given as input to the non-LTE models, and the results are, in principle, only valid for such a reference atmosphere. Fig. 5 shows the atmospheric structure assumed for the three terrestrial planets in the present simulations, plotted on the same pressure scale.

The Venus profile corresponds to the mean VIRA daytime reference, and the Mars reference was extracted from the Mars Climate Database version 4.3 (Millour et al., 2008) for the latitude, solar longitude and local time appropriate for the PFS observations. Mars and Venus have clear similarities in these profiles, with colder conditions at Mars at all the altitudes shown here; this impacts some results. On Earth, in addition to the distinct stratopause and the warmer thermosphere, the volume mixing ratio (VMR) of CO_2 and CO are much lower than on Mars and Venus, and this affects also the CO_2 IR emissions. Although the

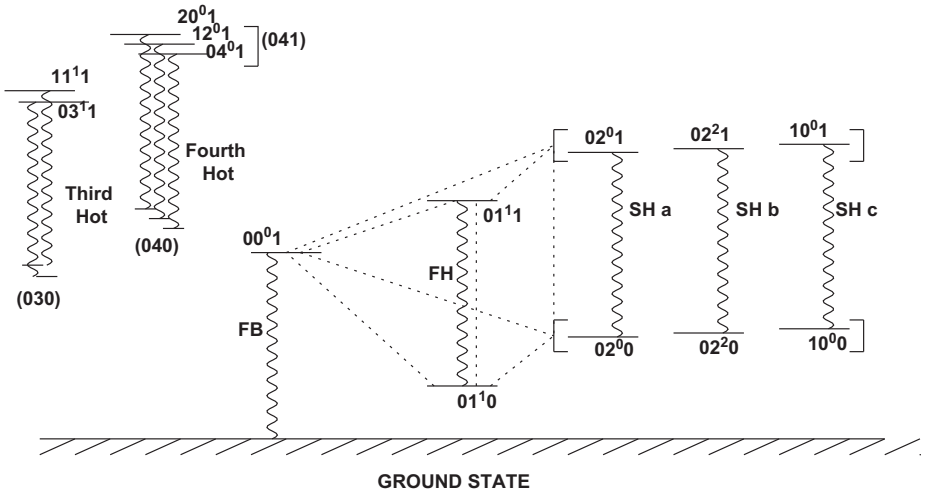

Fig. 4. Schematic diagram of CO_2 states relevant for the 4.3-μm emissions, including important radiative transitions and collisional links between vibrational states. Dots: collisional exchanges and arrows: radiative bands.

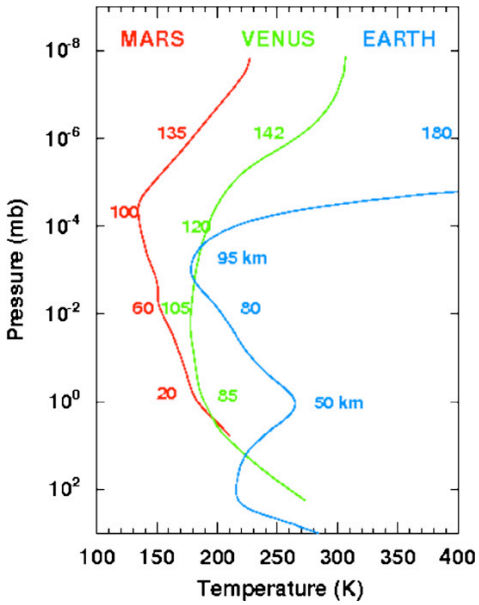

Fig. 5. Vertical temperature profiles on the same pressure scale during daytime assumed in this work for Earth, Mars and Venus. The altitudes above the planets surfaces are indicated for easy reference. Red, green and blue lines for Mars, Venus and Earth, respectively. (For interpretation of the references to color in this figure legend, the reader is referred to the web version of this article.)

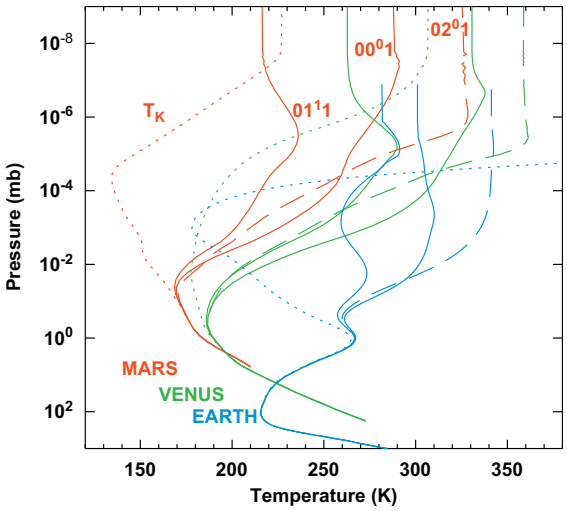

Fig. 6. Vibrational temperatures of the selected CO_2 states for the three planets, as indicated, including the kinetic temperature (dotted lines, labeled Tk). Solar maximum illumination and nominal non-LTE assumptions. Red, green and blue lines for Mars, Venus and Earth, respectively. (For interpretation of the references to color in this figure legend, the reader is referred to the web version of this article.)

selected profiles are arbitrary, they correspond to typical situations during daytime and mid-latitudes in the three planets. They have also been used in two other companion papers (Gilli et al., 2010; López-Valverde et al., 2010).

3.2. Nominal results for the state populations

Fig. 6 presents the results of the non-LTE models for nominal conditions and zenith solar illumination (SZA=0). The population of a state is expressed in terms of the vibrational temperature, which matches the kinetic temperature in LTE, and is larger the more populated a given state is (López-Puertas and Taylor, 2001).

The solid lines track the (0 0 1) state, or the fundamental band of the main isotope. The general behavior is similar in the three planets: at low altitudes the efficient collisional quenching due to high atmospheric densities maintains an LTE regime. The departure from LTE occurs in a similar pressure range in Mars and Venus, around 0.1 mb, and slightly lower in Earth (1 mb). In the three planets the vibrational temperature increases rapidly with altitude above that layer. This increase follows the growing absorption of solar radiation at mesospheric altitudes. At the top of the atmosphere the vibrational excitation is constant since the solar flux is unaffected at those altitudes. Comparing between the three planets, the top value of the vibrational population of this

state decreases from Venus to Earth to Mars, following their increasing distance to the Sun.

The main excitation process for the $(00^{0}1)$ state in the three planets is the direct solar pumping in the 4.3-μm fundamental band, "FB" in Fig. 4. However, in the CO_2 atmospheres of Mars and Venus, other indirect excitations of the $(00^{0}1)$ state can be important. These other routes start with solar absorption in many other CO_2 transitions in the near-IR, which excite higher energy states, and these later relax radiatively and collisionally to $(00^{0}1)$. This indirect pumping of the $(00^{0}1)$ state can be very important compared to the direct pumping in the 4.3-μm FB in the lower mesosphere, around the altitude of LTE departure. The reason is the large optical thickness of the 4.3-μm FB, whose maximum absorption occurs very high in the Martian/Venusian thermosphere; it therefore gives rise to a relatively small absorption at these low mesospheric altitudes. On Earth, due to the lower CO_2 abundance, the direct pumping in the FB is still strong at those altitudes; the indirect pumping is also noticeable, but to a lesser extent. $N_2(1)$ plays a major role in the Earth as an intermediate agent between the $CO_2(0, v_2, v_3)$ levels excited in the near-IR and the $(00^{0}1)$. Excitation via $O(^{1}D)\rightarrow N_2\rightarrow CO_2(00^{0}1)$ is also important at mesospheric altitudes on Earth.

Another noticeable difference among the three atmospheres is the different altitude where the maximum absorption of solar energy takes place. This is manifested in the strong decrease of the $(00^{0}1)$ vibrational temperatures in the mesosphere. At Mars and Venus this occurs around 10^{-5} mb. At Earth, this occurs at lower altitudes, at pressures about 1000 times larger. This factor corresponds to the ratio of CO_2 densities between the atmospheres. As a consequence, the solar heating in the upper mesosphere and lower thermosphere, associated to these CO_2 absorption bands (and also the thermal cooling), is much larger on Venus and Mars than on Earth.

3.3. Radiance simulations

We present here a number of simulations of the emerging radiances at 4.3-μm at the top of the three planetary atmospheres in nadir. Our radiance calculations consist of three steps. First, the 1-D profiles of non-LTE populations are calculated for the given reference atmosphere, as described above. Secondly, those populations are fed into a radiative transfer line-by-line forward model which computes the radiation at the specified observing geometry of the instruments. The final step is to convolve the obtained spectra to the lower spectral resolution of each instrument.

In this work we use two different line-by-line codes. For the Earth we use the KOPRA algorithm, mentioned above. For Mars and Venus we used the so-called reference forward model (RFM) (Dudhia, 2000). Both have been extensively validated against each other and with atmospheric measurements (von Clarmann et al., 2003).

3.4. SZA variations

A key parameter for the non-LTE excitation is the solar illumination. Here we examine the effect of the solar zenith angle on the measurements on the three planets. Fig. 7 shows this effect on the radiance simulations at a given pressure level, around 0.01 mb, which corresponds to tangent altitudes around 80, 60 and 100 km for our Earth, Mars and Venus atmospheres, respectively. To ease the comparisons, the MIPAS simulations are shown after convolution with a 5 cm^{-1} wide boxcar, as it is done also for VIRTIS and PFS, and which is a bit lower than the resolution of the latter.

The SZA is varied from zenith to 88°, and the impact of this variation is essentially similar in the three planets, with small variations up to 40° (perhaps a little smaller on Earth) and acute effects beyond 80°. The effects also change with altitude (not shown here). All this follows from emissions dictated by solar pumping. Clearly the variation due to SZA is very large when large changes in the solar flux occur. This effect has to be considered carefully when sounding the atmosphere using this emission at high SZA angles or close to the terminator (Funke et al., 2007).

The convolution of the MIPAS measurements permits a comparison of the shape of the system of bands in the 4.3-μm region. It is clear that the CO_2 emission presents a spectrally double structure in the three planets, with a big dent around 2325 cm^{-1}, which coincides with the second hot bands of the main isotope. The calculations performed for the arrival of VIRTIS at Venus by López-Valverde et al. (2007) showed that those bands should indeed dominate the limb emission, but also that there should be other non-negligible contributions from weaker bands (hot and isotopic), and particularly at lower tangent altitudes. That is shown here for Venus, and for Mars too. On Earth, due to the low CO_2 VMR, such emissions must be comparatively smaller when pointing at a similar density layer, as we did in this study, and this is the reason for the different envelope shape between Mars (or Venus) and the Earth.

3.5. Altitude variation

We studied also the variation of the emitted spectrum with altitude, on the three planets. Fig. 8 shows them, again adding a spectral convolution of 5 cm^{-1} to the MIPAS data to get it down to comparable spectral resolutions to those of VIRTIS and PFS. In all these runs the SZA was fixed at 30°. The Mars and Venus panels show model simulations. The variations obtained in these simulations for Venus follow well what is observed by VIRTIS (Gilli et al., 2009), and an example is presented in Fig. 2.

The maximum emission is observed around 77, 100 and 110 km on Earth, Mars and Venus, respectively. In the three cases it is due to the P and R branches of the CO_2-626 second hot bands, whose upper states (0201 and 1001) are highly excited at 2.7-μm by solar absorption. Those altitudes are equivalent in pressure coordinates for Mars and Venus (about $1–3\times10^{-5}$ mb), but about 1000 times larger/denser for Earth (around 2×10^{-2} mb). Again this can be explained by the lower CO_2 VMR on Earth. This peak altitude essentially responds to the transition region where the SH bands become optically thin. Comparing Mars and Venus, the emission in Mars is lower by a factor 5, which is approximately the ratio given by the (0201 and 1001) vibrational temperatures in their respective atmospheres, about 40 K lower in Mars (see Fig. 6). Therefore, this ratio is due to the lower solar flux at Mars.

At the highest altitudes, in the upper thermosphere, the emissions decrease strongly with altitude, as shown above in Fig. 2 for Venus. This is typical of full optically thin conditions, and the emission is directly proportional to the CO_2 number density. Similar CO_2 column densities on both planets should produce similar emissions, except for the solar flux factor. This is what was found during the fly-by of VIRTIS on Mars, a peak emission in the P and R branches of the SH bands about 4 times lower than in the Venus data (Drossart et al., 2009).

Note also that the shape of the emission spectra changes with altitude, showing different contributions from different bands. The lower the limb pointing, the larger the contribution from weaker bands is. A good example of these bands is the isotopic 636 SH, centered around 2260 cm^{-1} (4.42-μm), and clearly seen in the MIPAS, PFS and VIRTIS data (Figs. 1–3).

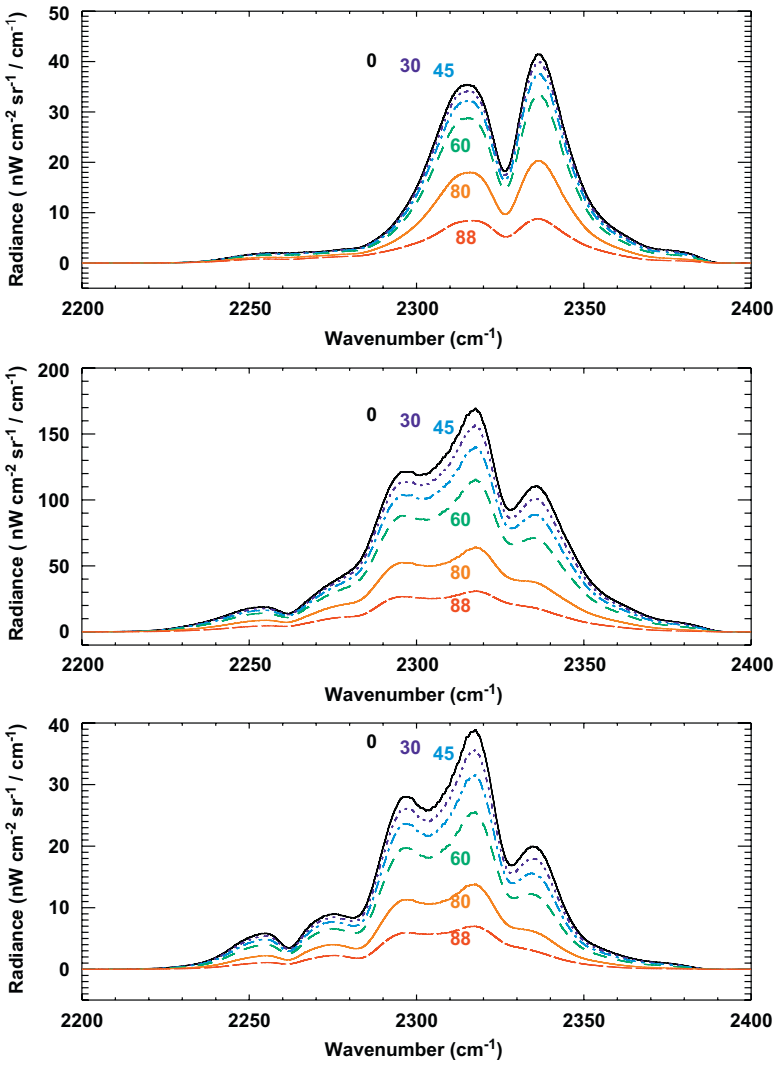

Fig. 7. Effect of SZA on simulations of the limb radiance for Earth (top panel), Venus (middle) and Mars (bottom panel) at 5 cm^{-1} spectral resolution. SZA in degree.

Although the model simulations seem to explain well most of the features observed in the three planets, on Mars and Venus the overall shape of the whole spectral region is not fully reproduced. We fail reproducing the correct strength of the emissions around 2250–2270 cm^{-1} (4.40–4.45 μm) compared to the peak emission at 2310–2325 cm^{-1} (4.30–4.33 μm). The 4.40 μm emission seems specially prominent in the Venus lower mesosphere, according to VIRTIS, but in our simulations its ratio to the peak emission at 4.32 μm is a factor 2 smaller than in the data. A similar situation occurs on Mars, comparing our simulations with the PFS data in Fig. 3. In the Earth atmosphere those weak emissions are small and are well reproduced by the model. Since the shape of the overall region depends on several bands' contributions, a quantitative analysis of the Mars and Venus spectra is very interesting, and may permit gaining insight into the excitation mechanisms of different CO_2 states, which can be a strong test for the non-LTE models. This has been done in the case of Earth by López-Puertas et al. (2005).

The 4.40 μm region seems dominated by the emission of the isotopic 636 SH bands. We eliminated the isotopic abundance as a possible reason for this apparent discrepancy. We are using the terrestrial values for the 636 abundance, in agreement with observations, and with uncertainties lower than 10% (von Zahn et al., 1983).

Therefore, we forsee three possibilities. The first one is that our simulated 4.40 μm emission is too low; another is that our peak emissions at 4.28 and 4.32 μm are too large. A third solution comes from the fact that the SH bands of the main isotope are optically thick for mesospheric tangent paths, which means that we are actually sounding higher atmospheric altitudes when using those bands. Our input reference atmosphere may be very different from the actual atmospheres at the time of the measurements. Still, the same discrepancy seems to be systematic in most VIRTIS measurements (Gilli et al., 2009), in the PFS data observed so far, and even in a few spectra taken by NIMS/Galileo of the limb of Venus (see e.g. López-Valverde et al., 2007). For these reasons, we think that this effect may indicate a caveat in our current non-LTE modeling of the Mars and Venus atmospheres, and that even a full knowledge of the thermal structure might not account for this difference. Moreover, we made runs for

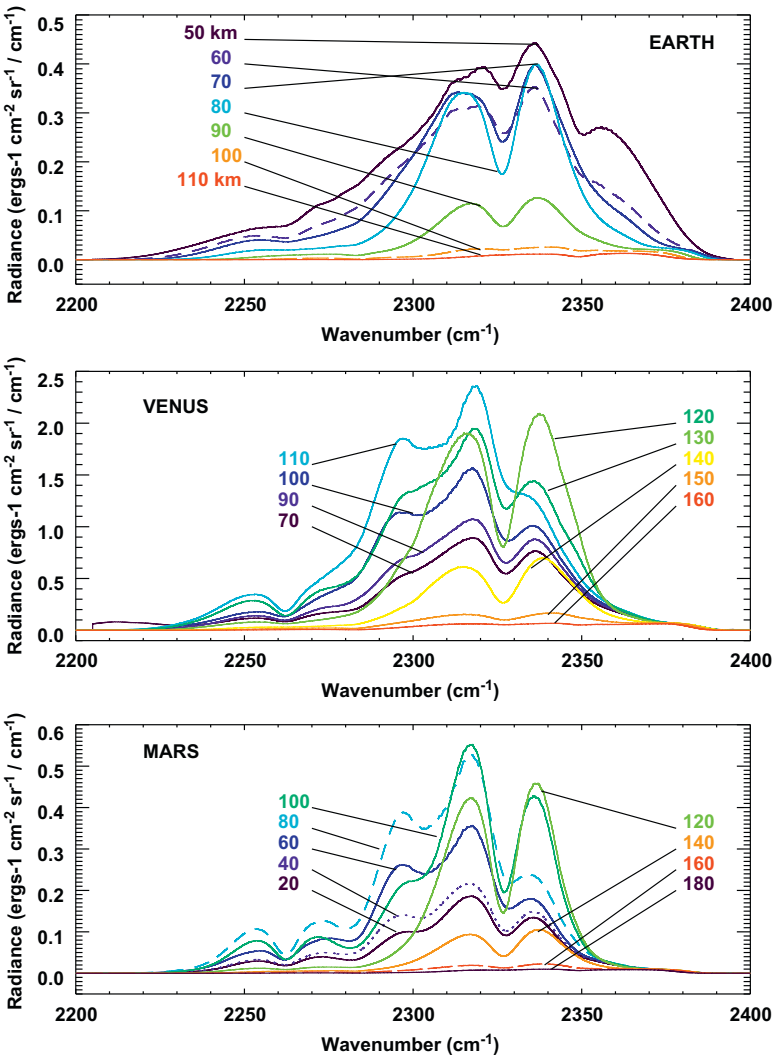

Fig. 8. Altitude variation in simulations of limb radiance for Earth (top panel), Venus (middle) and Mars (bottom panel) at a 5 cm^{-1} spectral resolution. SZA=30° in all runs. Altitudes in km.

a couple of extreme thermal structures for Mars, extracted from the Mars Climate Database, obtaining a similar overall shape. Therefore, we discuss below the first two options, and analyzed the model in the search for possible ways to solve or minimize the discrepancy.

Regarding the first suggestion, it could be that a number of very high energy CO_2 states, not yet included in our Mars/Venus models, are relaxing down after solar excitation, in many weak hot bands in this spectral region, adding some contribution (a factor 2) to the 636 SH bands. We have performed estimations for some of the possible high energy states which could be excited by solar absorption, without success so far.

Regarding the peak emission, at 4.32 μm, two major contributions to such emission were identified by López-Valverde et al. (2007) at mesospheric altitudes. They are the SH bands mentioned above, and also two other systems of bands: three weaker bands absorbing around 2.0 μm, exciting three CO_2 states which can be collectively called as (0 4 1), and two absorptions in 2.7-μm FH bands exciting two states which can collectively be called (0 3 1). The first ones originate the 4.3-μm fourth hot bands and the second states emit in the third hot bands. They are also shown in Fig. 4. Since the SH bands are well reproduced in the upper atmosphere, both in Mars and Venus, we are rather confident that they are well modeled. The other two solar excitations share a common problem, the collisional relaxation of the excited $CO_2(v_1, v_2, v_3)$ states is not well known; the value of the rate coefficient used for *V–V* relaxation is subject to large uncertainties (López-Valverde and López-Puertas, 1994b; López-Puertas and Taylor, 2001). Therefore, we have evaluated the effect of this parameter.

4. Effects of the CO_2 *V–V* collisional relaxation rates

In the collisional relaxation of high-energy combination states of CO_2, an increase in their rates produces a reduction in their state populations (López-Valverde and López-Puertas, 1994b), and hence, a reduction in their 4.3 μm emission. Another

consequence is an increase of the solar heating of the atmosphere, by increasing the thermalization of the initial solar absorption. These latter effects were computed by López-Puertas and López-Valverde (1995) for Mars and by Roldán et al. (2000) for Venus.

The uncertainty bracket used for this rate coefficient in those studies (see processes VV1 in Table 1 of López-Valverde and López-Puertas (1994a), and discussion therein) is a factor of 10 larger and smaller than the nominal value. This ample bracket follows from the uncertainties in a rate coefficient which has never been measured for the transitions of interest. Even for the lowest CO_2 states its temperature dependence and its variation with the quantum numbers v_1, v_2 and v_3 are not known. In our models for Mars and Venus we use the value and the temperature dependence measured by Shved et al. (1978) and Moore (1973): $k_{VV} = 6.8 \times 10^{-12}\sqrt{T}\,\mathrm{cm^3\,s^{-1}}$, where T is the atmospheric kinetic temperature. For the variation of k_{VV} with v_3 (López-Valverde and López-Puertas, 1994a) assumed a harmonic oscillator approach, and we keep such variation here.

The results obtained for increase factors 2 and 10 are shown in Fig. 9 for two tangent altitudes. As expected, an increase of the rate coefficient reduces the emission at the peak, while maintaining the 636 SH bands emission. A change of a factor 10 seems too large, while changes of a factor 2 or 3 seem more plausible and would bring our simulations closer to the VIRTIS measurements. The calculations show that the maximum effect does occur at the peak emission altitude. Other tangent altitudes do not show such a larger change. In particular the thermospheric emission, dominated by the 626-SH bands, is completely unaffected.

Focusing on the Venus spectrum at 110 km altitude we notice that the shape of the band envelope may help to constrain the rate coefficient. The local maximum around 2335 $\mathrm{cm^{-1}}$ is dominated by the 626-SH, unaffected by this rate coefficient, while the local maximum at 2290 $\mathrm{cm^{-1}}$. We observe in Fig. 9 that the nominal rate produces a maximum at 2290 $\mathrm{cm^{-1}}$ much larger than at 2335 $\mathrm{cm^{-1}}$. However, an increase of a factor 10 reduces the 2290 $\mathrm{cm^{-1}}$ too much, compared to the other. A simple comparison with Fig. 2 informs us that the optimum relative magnitudes between the two bands is obtained for a rate coefficient increase of a factor 3.

This variation in this rate coefficient (VV1 in López-Valverde and López-Puertas, 1994a) would have a very small impact on the Earth simulations, since the major collisions take place with N_2. On Mars, our calculations show that a larger value of the rate coefficient also brings the simulation closer to the measurements. And also in this planet an increase of a factor 10 seems too large, as it would almost eliminate the local peak around 2290 $\mathrm{cm^{-1}}$.

In summary, this analysis suggests that a rate coefficient in the bracket 1.5–3.0 $\times 10^{-11}$ gives the best fit to the VIRTIS and PFS measurements.

Let us recall that there still remains the uncertainty in the actual thermal structure on both Mars and Venus. Ideally, this analysis should be carried out for sounding at locations and times where independent determinations of the thermal/density structure are available. Such possibility may partially come from other instruments on Venus Express, like VeRa, which is sounding the lower mesosphere of Venus up to about 90 km altitude (Patzöld et al., 2007; Tellmann et al., 2009). For Mars, we would need to rely on climatological averages.

5. Sensitivity to atmospheric variables

An important application of non-LTE models is the retrieval of atmospheric parameters like density and temperature, once the models are fully trusted. Emissions with strong departures from non-LTE contain limited information on temperature but they depend on density. In addition, collisional rate coefficients affecting the population of the emitting levels can also be obtained, but this requires the density of the emitters to be well known or determined by other means. Both strategies have been followed in Earth remote sounding using data from instruments like MIPAS/Envisat (López-Puertas et al., 2005) and AIRS/Aqua (DeSouza-Machado et al., 2007), and are in progress for the Mars and Venus missions mentioned above.

In this section we illustrate the dependence of the emissions on CO_2 VMR, or density, and temperature. Our strategy was to compute and study the Jacobians, in other words, to evaluate how the radiances change to small perturbations in the input atmospheric parameters.

5.1. CO_2 volume mixing ratio

Fig. 10 shows the sensitivity of the emerging limb radiance at three tangent altitudes in Venus, Mars and Earth to 1% CO_2 VMR increase at those tangent altitudes. The perturbation consists of a

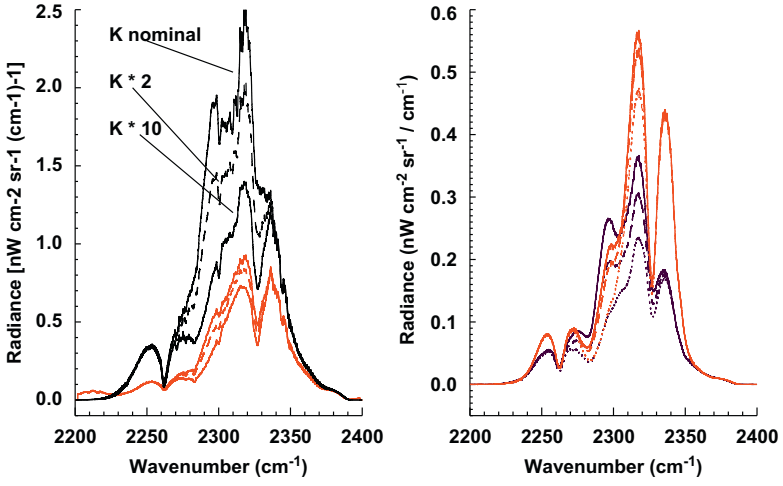

Fig. 9. Effect of changing the *V–V* collisional rate on the 4.3-μm limb emission in Venus (left panel) and Mars (right panel). The rate was multiplied by factors 1, 2 and 10, as indicated. The tangent altitudes in Venus are 70 and 110 km, and in Mars 60 and 100 km. See text for details.

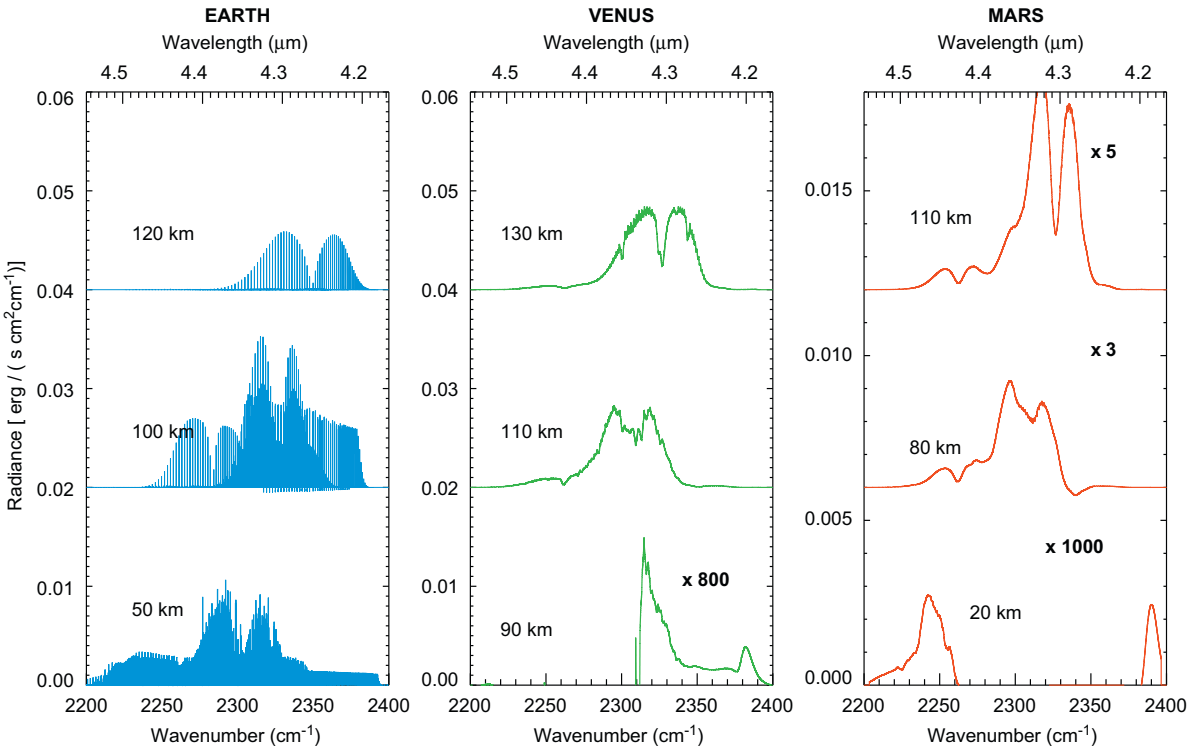

Fig. 10. Jacobians or radiance changes in Earth, Venus and Mars for perturbations of 1% CO_2 VMR at the three altitudes indicated. A multiplication factor and vertical shifts are applied to the spectra for better visualization. Notice also the different radiance axis.

simple triangular function, 10 km thick centered at the tangent altitude (HWHM of the change at 5 km above and below the pointing height). In the calculations for the Earth, Venus and Mars we used the spectral resolutions of MIPAS, VIRTIS-H and PFS, respectively. We show the radiance increase obtained for such a perturbation, which should be compared to the sensitivity (noise) of the instruments. The noise level for a single spectrum is around 3 nW/[cm^2 sr (cm^{-1})] for MIPAS and around 1 nW/[cm^2 sr (cm^{-1})] for VIRTIS and PFS.

On Venus, when pointing at 90 km, only the wings of the lines in the 4.3 um region show a change, and it is very small (notice the large increase factor of 800). But at 110 (around the maximum emission) and at 130 km the change is about 0.8 radiance units, comparable to the measurement noise. Larger changes in the CO_2 VMR to those introduced in this numerical exercise, 5–10% for example, should be easily detected by VIRTIS at those altitudes.

The calculations for Mars with PFS resolution and noise levels indicate that their largest sensitivity occurs between 80 and 110 km, but is smaller than the noise levels for this perturbation in VMR. The larger emission (solar flux) in Venus, compared to Mars, makes an important difference, and the density in Venus can therefore be derived with VIRTIS with better precision and in a much wider altitude range than with PFS on Mars.

On Earth, notice first that the effect obtained is much lower than in Mars and Venus, and this is because of the lower CO_2 abundance. When considering this VMR factor, which is around 1000, and assuming a linear response for the sake of simplicity, we find that the sensitivity of the instrument MIPAS is about one order of magnitude larger than that of VIRTIS, and therefore, MIPAS would be better suited than VIRTIS for detecting variations in CO_2 abundance if it were placed on Venus Express. Notice that this better fit of MIPAS for density changes occurs in spite of having a similar sensitivity/noise level to VIRTIS. The result is merely an effect of the larger spectral resolution of MIPAS, about 20–30 times better than VIRTIS.

The MIPAS measurements of the non-LTE Earth's emission at 4.3 μm are under study by our team, and have already been used to derive preliminary CO_2 abundances at mesospheric altitudes. The CO_2 VMR obtained shows a distinct increase towards the winter polar regions, similar to that obtained by GCM simulations for solstice conditions.

5.2. Atmospheric temperature

A similar numerical exercise to obtain the sensitivity of the emerging radiance to temperature changes is presented in Fig. 11 for the three planets, and using the noise and spectral resolution of the three instruments MIPAS, VIRTIS and PFS. The perturbations for 1 K in the temperature at the indicated three tangent altitudes are shown, again with a perturbation function 10 km wide. The tangent altitudes selected correspond to three distinct regimes, all of them with very similar behavior in the three planets, except for the different spectral resolution of the three instruments. A first case corresponds to lower mesospheric tangent altitudes (50, 60 and 70 km on Mars, Earth and Venus, respectively), where the main bands are blocked due to the large optical thickness; the sensitivity for changes at the tangent altitude is very small. A second case where the main emission bands (SH bands) are optically thin, in the upper mesosphere/lower thermosphere (120, 80 and 130 km, in Mars, Earth and Venus, respectively); here the response to temperature changes mimics the spectral shape of the

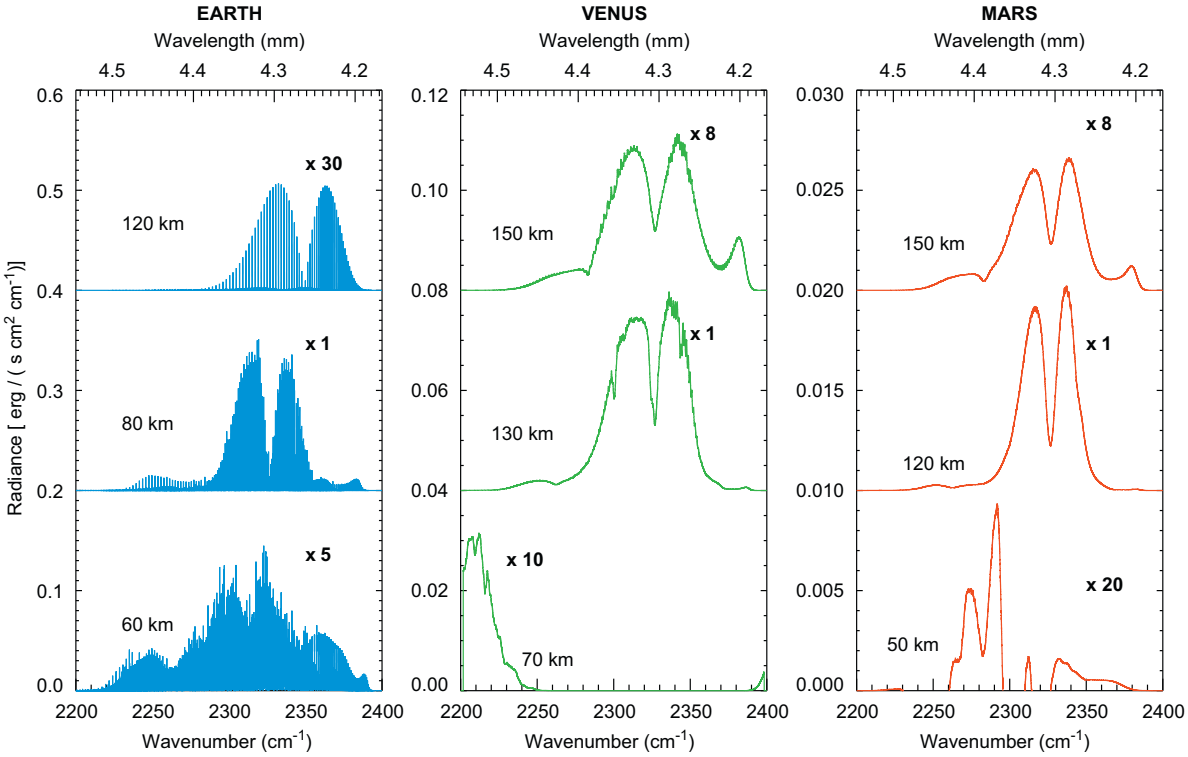

Fig. 11. As Fig. 10 but for temperature perturbations of 1 K. The spectra are also shifted in the radiance axis for clarity. See text for details.

emission, dominated by the P and R branches of the SH bands. The third situation is at altitudes where the wings of the FB become optically thin (150, 120 and 150 km in Mars, Earth and Venus).

On Mars, these temperature perturbations produce radiance changes at the tangent altitude a little smaller than the PFS noise between 80 and 120 km, for this Martian reference atmosphere. At all other altitudes, the response is smaller. For example, for pointing at 150 km it is 10 times smaller than the noise, and at tangent altitudes below 70 km the maximum change occurs for temperature perturbations around 90 km and is about 6 times smaller than the noise value.

On Venus, the sensitivity for the VIRTIS spectral resolution and noise level is larger than the same for Mars and PFS characteristics. The maximum radiance change for the 1 K perturbation is obtained at the tangent altitudes of 110–130 km and is 4 times larger than the VIRTIS noise. For limb pointings below about 90 km, the peak sensitivity occurs for temperature perturbations also around 110–130 km, and is of the order of the VIRTIS noise. And at tangent altitudes around 170 km, with the present reference profile, the radiance response is about 10 times smaller than the VIRTIS noise, and 50 times smaller than the radiance itself.

On Mars and on Venus, the present temperature perturbation and the previous VMR perturbation both have their maximum responses at the tangent altitudes of the maximum emission, and both affect the envelope shape of the 4.3 μm emission in a similar way. In principle, one of these two parameters need to be assumed or known in order to derive the other, unless approximations like hydrostatic equilibrium is used in a full vertical profile to relate both parameters. Unfortunately, the sounding of a vertical profile with PFS and VIRTIS-H has never been done explicitly, and climatological values may be needed. Such retrieval work is underway for the two planets using the datasets from VIRTIS-H and PFS.

6. Conclusions

All together, these three datasets set up a first-time data set comprising similar CO_2 non-LTE emissions in the three terrestrial planets. This data set offers an excellent chance to improve our theoretical models in three distinctly different physical situations, and we are starting to exploit such potential in this work. A systematic bias between model and data found at Venus and Mars is the relatively small emission at 4.40 μm compared to the peak emission at 4.32 μm. Although it may be possible that the atmospheric structure may be systematically colder than our daytime references profiles, an alternative solution could be achieved by changing the vibrational-vibrational relaxation of high-energy CO_2 states in intra-molecular V–V collisions. We suggest a value for such coefficient of $k_{VV}=2\times10^{-11}\sqrt{T}$, where T is the atmospheric temperature, with a possible bracket between $1.5-3.0\times10^{-11}\sqrt{T}$; this rate is about 3 times larger than the rate previously used in non-LTE models for Mars and Venus. Such a modification will produce a small increase in the near-IR solar heating in the Martian and Venusian mesospheres.

The different density and temperatures in the three terrestrial planets, together with the CO_2 relative abundance and the distance to the Sun, are the key parameters which determine the non-LTE excitation of the relevant CO_2 states and the strength of the 4.3 μm emission observed in their upper atmospheres. Mars, with a lower atmospheric density and further away from

the Sun, has a lower emission at 4.3 μm. We have demonstrated that the retrieval of atmospheric densities from these non-LTE limb emissions is possible in the mesosphere of the three planets, being more promising on Venus than on Mars, and also it can be performed over a wider altitude range, assuming identical instrumentation on both planets.

Noise levels are key to determining the sensitivity of a given instrument to the 4.3 μm signal, but also the spectral resolution is important. Both are much better for Earth-observing instrumentation, like MIPAS, compared to planetary missions like Venus and Mars Express. When those conditions are met, these CO_2 emissions uniquely validate our theoretical understanding of the non-LTE processes in the upper atmosphere, and suitable models can be used to invert the radiances and determine important quantities like CO_2 abundance and non-LTE model collisional parameters. Not only CO_2 but also a number of rate coefficients for exchanges between different CO_2 states are derived from MIPAS spectra (López-Puertas et al., 2005). Results like these show the large amount of information contained in the high resolution and wide range of MIPAS spectra, containing many lines of different CO_2 bands.

Acknowledgments

The work of the IAA/CSIC team has been partially funded by the Project AYA2008-03498/ESP of the Spanish Ministry of Science and Innovation and by EC FEDER funds.

References

Carlson, R.W., Weissman, P.R., Smythe, W.D., Mahoney, J.C., 1992. Near-Infrared Mapping Spectrometer experiment on Galileo. Space Sci. Rev. 60, 457–502.

Crovisier, J., Lellouch, E., de Bergh, C., Maillard, J.-P., Lutz, B.L., Bézard, B., 2006. Carbon monoxide emissions at 4.7 μm from Venus atmosphere. Planet. Space Sci. 54, 1398–1414.

Deming, D., Mumma, M.J., 1983. Modeling of the 10-micron natural laser emission from the mesospheres of Mars and Venus. Icarus 55, 356–368.

DeSouza-Machado, S.G., Strow, L.L., Hannon, S.E., Motteler, H.E., Lopez-Puertas, M., Funke, B., Edwards, D.P., 2007. Fast forward radiative transfer modeling of 4.3 μm nonlocal thermodynamic equilibrium effects for infrared temperature sounders. Geophys. Res. Lett. 34, 1802.

Dickinson, R.E., 1972. Infrared radiative heating and cooling in the Venusian mesosphere. I. Global mean radiative equilibrium. J. Atmos. Sci. 29, 1531–1556.

Drossart, P., López-Valverde, M.A., Garcia-Comas, M., Fouchet, T., Melchiorri, R., Bibring, J.P., Langevin, Y., Gondet, B., 2006. Limb observations of infrared fluorescence of CO_2 from OMEGA/Mars Express. In: Forget, F., et al. (Eds.), Second Workshop on Mars Atmosphere Modelling and Observations. LMD, IAA, AOPP, CNES, ESA, Granada, Spain, February 27–March 3, p. 611.

Drossart, P., López-Valverde, M.A., Piccioni, G., Coradini, A., Cappacioni, F., Gilli, G., López-Puertas, M., Erard, S., 2009. Carbon dioxide non-LTE emissions in the upper atmospheres of Mars, Venus and Earth from VIRTIS observations. In: International Conference on Comparative Planetology: Venus-Earth-Mars. ESA, ESTEC, Noodwijk, Holland, 11–15 May, p. 131.

Drossart, P., et al., 2007a. A dynamic upper atmosphere of Venus as revealed by VIRTIS on Venus Express. Nature 450, 641–645.

Drossart, P., et al., 2007b. Scientific goals for the observation of Venus by VIRTIS on ESA/Venus express mission. Planet. Space Sci. 55, 1653–1672.

Dudhia, A., 2000. Michelson Interferometer for Passive Atmospheric Sounding (MIPAS) Reference Forward Model (RFM) Software User's Manual. Oxford University, Oxford, UK.

Fischer, H., Birk, M., Blom, C., Carli, B., Carlotti, M., von Clarmann, T., Delbouille, L., Dudhia, A., Ehhalt, D., Endemann, M., Flaud, J.M., Gessner, R., Kleinert, A., Koopman, R., Langen, J., López-Puertas, M., Mosner, P., Nett, H., Oelhaf, H., Perron, G., Remedios, J., Ridolfi, M., Stiller, G., Zander, R., 2008. Mipas: an instrument for atmospheric and climate research. Atmos. Chem. Phys. 8 (8), 2151–2188.

Formisano, V., 2005. The Planetary Fourier Spectrometer (PFS) onboard the European Mars Express mission. Planet. Space Sci. 53, 963–974.

Formisano, V., Maturilli, A., Giuranna, M., D'Aversa, E., López-Valverde, M.A., 2006. Observations of non-LTE emission at 4.5 microns with the planetary Fourier spectrometer aboard the Mars Express mission. Icarus 182, 51–67.

Funke, B., López-Puertas, M., Bermejo-Pantaleón, D., von Clarmann, T., Stiller, G.P., Höpfner, M., Grabowski, U., Kaufmann, M., 2007. Analysis of nonlocal thermodynamic equilibrium co 4.7 m fundamental isotopic and hot band emissions measured by the Michelson interferometer for passive atmospheric sounding on Envisat. J. Geophys. Res., 112.

Funke, B., López-Puertas, M., García-Comas, M., Stiller, G.P., von Clarmann, T., Höpfner, M., Glatthor, N., Grabowski, U., Kellmann, S., Linden, A., 2009. Carbon monoxide distributions from the upper troposphere to the mesosphere inferred from 4.7 m non-local thermal equilibrium emissions measured by Mipas on Envisat. Atmos. Chem. Phys. 9 (7), 2387–2411.

Funke, B., Martin-Torres, F.J., López-Puertas, M., Hoepfner, M., Hase, F., López-Valverde, M.A., Garcia-Comas, M., 2002. A Generic Non-LTE Population Model For Mipas–Envisat Data Analysis. EGS XXVII General Assembly, Nice, 21–26 April 2002, Abstract #4915 27, 4915.

Gilli, G., López-Valverde, M.A., Drossart, P., Drossart, P., Piccioni, G., Erard, S., Cardesín Moinelo, A., 2009. Limb observations of CO_2 and CO non-LTE emissions in the Venus atmosphere by VIRTIS/Venus Express. J. Geophys. Res., 114.

Gilli, G., López-Valverde, M.A., Funke, B., Lopez-Puertas, M., Drossart, P., Piccionic, G., Formisano, V., 2010. Non-LTE CO limb emission at 4.7 μm in the upper atmosphere of Venus, Mars and Earth: observations and modeling. Planet. Space Sci., this issue.

López-Puertas, M., Funke, B., Gil-López, S., López-Valverde, M.A., Clarmann, T.v., Fischer, H., Oelhaf, H., Stiller, G., Kaufmann, M., Koukouli, M.E., Flaud, J.-M., 2005. Atmospheric non-local thermodynamic equilibrium emissions as observed by the Michelson interferometer for passive atmospheric sounding (MIPAS). C. R. Phys. 8, 848–863.

López-Puertas, M., López-Valverde, M.A., 1995. Radiative energy balance of CO_2 non-LTE infrared emissions in the martian atmosphere. Icarus 114 (1), 113–129.

López-Puertas, M., Taylor, F.W., 2001. Non-LTE radiative transfer in the atmosphere. In: López-Puertas, M., Taylor, F.W. (Eds.), Non-LTE Radiative Transfer in the Atmosphere. Series on Atmospheric Oceanic and Planetary Physics, vol. 3. World Scientific, Singapore, ISBN 9810245661.

López-Valverde, M.A., Drossart, P., Carlson, R., Mehlman, R., Roos-Serote, M., 2007. Non-LTE infrared observations at Venus: from NIMS/Galileo to VIRTIS/Venus Express. Planet. Space Sci. 55, 1757–1771.

López-Valverde, M.A., López-Puertas, M., 1994a. A non-local thermodynamic equilibrium radiative transfer model for infrared emission in the atmosphere of Mars. 1: theoretical basis and nighttime populations of vibrational levels. J. Geophys. Res. 99, 13093–13115.

López-Valverde, M.A., López-Puertas, M., 1994b. A non-local thermodynamic equilibrium radiative transfer model for infrared emission in the atmosphere of Mars. 2: daytime populations of vibrational levels. J. Geophys. Res. 99, 13117–13132.

López-Valverde, M.A., López-Puertas, M., López-Moreno, J.J., Formisano, V., Grassi, D., Maturilli, A., Lellouch, E., Drossart, P., 2005. Analysis of CO_2 non-LTE emissions at 4.3 μm in the Martian atmosphere as observed by PFS/Mars Express and SWS/ISO. Planet. Space Sci. 53, 1079–1087.

López-Valverde, M.A., Sonnabend, G., Sornig, M., Kroetz, P., 2010. Modelling the atmospheric CO_2 10-μm laser emission in Mars and Venus at high spectral resolution. Planet. Space Sci., this issue.

Millour, E., Forget, F., González-Galindo, F., Spiga, A., Lebonnois, S., Montabone, L., Lewis, S.R., Read, P.L., López-Valverde, M.A., Gilli, G., Lefèvre, F., Montmessin, F., Desjean, M.-C., Huot, J.-P., The McD/Gcm Development Team, November 2008. The Latest (Version 4.3) Mars Climate Database. LPI Contributions 1447, 9029.

Moore, C.B., 1973. Vibration–vibration energy transfer. In: Prigogine, I., Rice, S.A. (Eds.), Advances in Chemical Physics, vol. 23. Wiley, New York, pp. 41–83.

Patzöld, M., Hausler, B., Bird, M.K., Tellmann, S., Mattei, R., Asmar, S.W., Dehant, V., Eidel, W., Imamura, T., Simpson, R.A., Tyler, G.L., 2007. The structure of Venus' middle atmosphere and ionosphere. Nature 450, 657–660.

Roldán, C., López-Valverde, M.A., López-Puertas, M., Edwards, D.P., 2000. Non-LTE infrared emissions of CO_2 in the atmosphere of Venus. Icarus 147, 11–25.

Shved, G.M., Stepanova, G.I., Kutepov, A.A., 1978. Transfer of 4.3 μm co_2 radiation on departure from local thermodynamic equilibrium in the atmosphere of the earth. Atmos. Oceanic Phys. 14, 589–696.

Stepanova, G.I., Shved, G.M., 1985. Radiation transfer in the 4.3-micron CO/2 band and the 4.7-micron Co/ Band in the atmospheres of Venus and Mars with violation of LTE—populations of vibrational states. Sov. Astron. 29, 422.

Stiller, G.P., von Clarmann, T., Funke, B., Glatthor, N., Hase, F., Höpfner, M., Linden, A., 2002. Sensitivity of trace gas abundances retrievals from infrared limb emission spectra to simplifying approximations in radiative transfer modelling. J. Quant. Spectrosc. Radiat. Transfer 72 (3), 249–280.

Tellmann, S., Pätzold, M., Häusler, B., Bird, M.K., Tyler, G.L., 2009. Structure of the Venus neutral atmosphere as observed by the radio science experiment VeRa on Venus Express. J. Geophys. Res. (Planets) 114 (E13).

von Clarmann, T., Ceccherini, S., Doicu, A., Dudhia, A., Funke, B., Grabowski, U., Hilgers, S., Jay, V., Linden, A., López-Puertas, M., Martín-Torres, F.-J., Payne, V., Reburn, J., Ridolfi, M., Schreier, F., Schwarz, G., Siddans, R., Steck, T., 2003. A blind test retrieval experiment for infrared limb emission spectrometry. J. Geophys. Res. 108 (D23), 4746.

von Zahn, U., Kumar, S., Niemann, H., Prinn, R., 1983. Composition of the Venus atmosphere. In: Hunten, D.M., Colin, L., Donahue, T.M., Moroz, V.I. (Eds.), Venus. University of Arizona Press, Tucson, AZ, pp. 299–430.

Planetary and Space Science 59 (2011) 1010–1018

Contents lists available at ScienceDirect

Planetary and Space Science

journal homepage: www.elsevier.com/locate/pss

Non-LTE CO limb emission at 4.7 μm in the upper atmosphere of Venus, Mars and Earth: Observations and modeling

G. Gilli [a,*], M.A. López-Valverde [a], B. Funke [a], M. López-Puertas [a], P. Drossart [b], G. Piccioni [c], V. Formisano [d]

[a] Instituto de Astrofísica de Andalucía-CSIC, Camino Bajo de Huétor 50, Granada, Spain
[b] LESIA, Observatoire de Paris, Meudon, France
[c] IASF-INAF, Via del Fosso del Cavaliere, Rome, Italy
[d] IFSI-INAF, Via del Fosso del Cavaliere, Rome, Italy

ARTICLE INFO

Article history:
Received 28 September 2009
Received in revised form
17 June 2010
Accepted 23 July 2010
Available online 4 August 2010

Keywords:
Planetary atmosphere
Aeronomy
Remote sensing
Infrared emission
Terrestrial planets
Non-LTE

ABSTRACT

We report here on CO limb observations in Mars, Venus and Earth and their model simulations. A comparative study of the CO emission, including the most recent spacecraft observations of the three planets' atmospheres, has been performed. Strong daytime emissions near 4.7 μm have been recently observed in the limb of the upper atmosphere of the three terrestrial planets by the Planetary Fourier Spectrometer on Mars Express (Formisano et al., 2005), the Visible and Infrared Thermal Imaging Spectrometer on Venus Express (Drossart et al., 2007), and the Michelson Interferometer for Passive Atmosphere Sounding on Envisat (Fischer et al., 2008). Those emissions are produced by solar pumping of molecular vibrations and non-local thermodynamic equilibrium (non-LTE) models are used to explain them in a consistent framework for the three atmospheres. The maximum of the 4.7 μm emission occurs on Venus between 90 and 110 km, on Mars above 60 km, and on Earth around 68 km. The observations show that the fundamental band dominates the CO non-LTE emission on Earth, while on Venus and Mars the larger contribution comes from the first hot band transition. The main goal of this study is to understand those differences and similarities with the help of theoretical simulations with optical thickness considerations, and compare the capability of space instrumentation for the remote sounding of the atmospheres in this spectral region.

1. Introduction

The upper atmospheres of the terrestrial-like planets are similar in terms of physical processes, in spite of important differences in temperature, density and composition. A basic property of these upper layers, particularly relevant to our study, is the low gas density that is also responsible for situations of breakdown of local thermodynamic equilibrium (LTE). These are specific for each molecular species and each vibrational transition, and result in populations of the molecular energy states not dictated by the Boltzmann statistics at the local kinetic temperature (Lopez-Puertas and Taylor, 2001). This non-LTE effect occurs when molecular collisions are so infrequent that other processes (radiative transfer, for example) become important for the determination of those states' number populations. In the terrestrial planets, and for the main molecules and infrared emissions, those layers usually correspond to their mesospheres and thermospheres. Since non-LTE emissions originate in the upper atmosphere, they are commonly used to sound those altitudes, preferably with a limb observational geometry.

At thermospheric altitudes, solar EUV heating and thermal conduction are the main processes controlling the energy balance, while in the mesosphere, absorptions and emissions by atmospheric molecules with active ro-vibrational bands in the infrared usually play a dominant effect on the thermal structure (Gladstone et al., 2002). Despite these similarities, the resulting thermospheric temperatures on Earth are much higher than on Mars and Venus. This is in part a consequence of larger carbon dioxide (CO_2) concentrations in the atmosphere of the Venus and Mars: cooling by radiative emission from CO_2 at 15 μm is much stronger (Gladstone et al., 2002). Also, the presence of a strong magnetic field on Earth's produces a strong heating of the its atmosphere by auroral and Joule processes. For a detailed comparison of the three planets thermospheres, see e.g. Bougher and Roble (1991). In addition to this, on Earth's upper atmosphere oxygen (O) and nitrogen (N) chemical reactions play a crucial role, while on Venus and Mars the photochemistry of CO_2 dominates, producing O and carbon monoxide (CO) by UV photolysis

* Corresponding author. Tel.: +34 958 230626.
E-mail address: gilli@iaa.es (G. Gilli).

0032-0633/$ - see front matter © 2010 Elsevier Ltd. All rights reserved.
doi:10.1016/j.pss.2010.07.023

(Yung and Demore, 1999). This partially explains why CO is more than 3 orders of magnitude more abundant on Venus and Mars than on Earth in the thermosphere.

CO has been detected on the upper atmosphere of the terrestrial planets both by ground-based observations and by remote sensing experiments.

Several satellite measurements on Earth mesosphere have been obtained in the sub-millimetre and microwave (Dupuy et al., 2004; Filipiak et al., 2005), in the infrared (López-Valverde et al., 1996; Funke et al., 2007), and with solar occultation techniques (Gunson et al., 1990; Clerbaux et al., 2005).

The first CO detection on Venus dates back to the late 1970s (Gulkis et al., 1978; Schloerb et al., 1980) and most of CO measurements on the Venusian mesosphere/thermosphere are in the sub-millimeter and microwave and during nighttime (Lellouch et al., 1994; Clancy et al., 2003; Gurwell et al., 1995). On Mars, CO was first definitively detected spectroscopically by Kaplan et al. (1969), who were able to identify several lines in the (2, 0) and (3, 0) bands.

Non-LTE CO emissions have been observed on Earth by rockets and by several satellite missions, i.e. CIRRIS (Dodd et al., 1993), ISAMS (López-Valverde et al., 1996) and Michelson Interferometer for Passive Atmosphere Sounding on Envisat (MIPAS/Envisat) (Funke et al., 2007). These measurement at 4.7 and 2.4 μm have also been successfully used to retrieve CO concentration by remote sensing experiments (López-Valverde et al., 1996; Funke et al., 2009).

On Mars and Venus, however, only a few measurements are available. High resolution infrared observations of Mars at 5 μm showed CO vibrational lines for the first time (Billebaud et al., 1991), some CO limb measurements by the OMEGA experiment on Mars Express were reported by Drossart et al. (2005) and Planetary Fourier Spectrometer on Mars Express (PFS/MEx) observations from two orbits were described and analyzed by Formisano et al. (2006). On Venus, the atmospheric CO infrared emission at 4.7 μm was detected for the first time by de Bergh et al. (1988) using ground base observations at very high spectral resolution, and only recently it has been observed from orbit, both in nadir and in the limb by Visible and Infrared Thermal Imaging Spectrometer on Venus Express (VIRTIS/VEx) (Gilli et al., 2009).

Given the non-LTE nature of the CO emissions at 4.7 μm, a proper modeling is required for their interpretation and analysis. Several non-LTE theoretical models have been developed to analyze these emissions and they all show that absorption of solar radiation by CO itself in its fundamental band (FB) is the major excitation mechanism in the upper atmosphere of Earth (Lopez-Puertas and Taylor, 2001), Mars (Stepanova and Shved, 1988; Lopez-Valverde and Lopez-Puertas, 1994) and Venus (Crovisier et al., 2006; López-Valverde et al., 2007). Different non-LTE radiative transfer schemes have been applied to those models, although without significant alteration of the resulting non-LTE populations. Solar absorption also occurs in other near-IR bands, at 2.3 and 1.6 μm, exciting higher CO vibrational levels, which can be subsequently relaxed by spontaneous emission or quenched down to the lowest CO states. Hence these models show that the emissions can be explained by solar fluorescence occurring not only in the fundamental but also in overtones and hot bands (see Lopez-Puertas and Taylor, 2001).

The present paper is not aimed at presenting new data, nor at giving a detailed review of Non-LTE processes in the three planetary atmospheres, but it compares those CO emissions, focusing on recent limb observations by VIRTIS/VEx, PFS/MEx, and MIPAS/Envisat, and analyzes them theoretically. This is the first time a comparative study of this kind is performed highlighting the differences and similarities among the three planetary atmospheres. In Section 2 we report on the data-sets and the principal characteristics of those instruments. The theoretical models used to understand those observations are described in Section 3 and the analysis and the discussion of the results is presented in Section 4. Most of this work is part of an ongoing effort devoted to retrieve CO abundances in the three planets. This goal is in its final stage for the Earth (Funke et al., 2009), while it is an intermediate phase for both Mars and Venus and their final retrieval results will be presented elsewhere.

2. 4.7 μm limb measurements on Earth, Mars and Venus

Fig. 1 shows a selection of measurements obtained with PFS/MEx, VIRTIS/VEx and MIPAS/Envisat. The CO emissions observed in the three planets appear as a typical double peak of a diatomic molecule, in which the line structure is discerned (or not) according to the spectral resolution of each instrument, as described next.

PFS on board Mars Express has two channels, the long wavelength (LW) and the short wavelength (SW) channels, covering the spectral range 250–1700 and 1700–8200 cm^{-1}, respectively, with a nominal spectral resolution of 1.3 cm^{-1}. A detailed description of the instrument can be found in Formisano et al. (2005).

In this work we used only measurements from the SW channel during two limb-tracking orbits as reported in Formisano et al. (2006). Fig. 1 (panel a) shows three averaged spectra at different tangent heights with significant CO limb emissions between 4.80 and 4.63 μm. In these observations, due to the small signal to noise (S/N), a large averaging was required. Formisano et al. (2006) reported an emission peak around 85 km, although it should be remarked that PFS instantaneous field of view (FOV) is about 30 km in these observations. The red curve is the instrumental signal when looking at the deep space. Since this should be very close to zero, this measurement represents the instrumental offset, which should be subtracted from the intensity of the measured emissions at all tangent heights. The noise equivalent spectral radiance (NESR) is similar of the deep space offset (Formisano et al., 2006). These spectra show a two-branches band centered around 2115 cm^{-1}, which corresponds to the center of the first hot (FH) band of the main CO isotope.

VIRTIS is a mapping spectrometer on Venus Express and also supplies two signals: VIRTIS-M, covering the visible (0.3−1 μm) and the near infrared (1−5 μm) at a resolving power $R \sim 400$, and VIRTIS-H, at higher resolution ($R \sim 1800$) covering the IR range (2−5 μm). VIRTIS-M nominal noise level is better than 1000 $\mu W/(sr\,m^2\,\mu m)$ and for VIRTIS-H it is about 5 times larger. A complete technical description of the instrument is presented elsewhere (Drossart et al., 2007; Piccioni et al., 2006). Since the beginning of the mission a large number of CO spectra with good S/N have been obtained both in nadir and limb geometries. Due to the large eccentricity of the Venus Express orbit, the FOV projected to the limb changes continuously during each orbit. In this work only limb data from VIRTIS-H with a small FOV (less than 5 km) were used, counting with more than 5000 daytime spectra between 70 and 180 km from about 750 limb orbits, most of them taken during the periapsis.

VIRTIS-H observations provide an excellent opportunity to analyze CO non-LTE emission in the upper mesosphere and lower thermosphere of Venus. Emissions between 80 and 120 km tangent heights were clearly detected even with individual VIRTIS-H spectra. The emission peak is located between 85 and 110 km, in agreement with model predictions (López-Valverde et al., 2007). Above 120–130 km, the spectra are noisier and a proper averaging is needed. Selected spectra were averaged in boxes of 7 km of tangent altitude for consistency with the FOV and

measurements from both north and south hemispheres have been included to improve the S/N. Fig. 1 (panel b) shows two examples of averaged spectra: the first (upper panel) includes 35 measurements from 96 to 103 km and the second (lower panel) 43 measurements between 145 and 152 km. The standard deviations are also plotted. The solar zenith angle (SZA) varies between 0° and 30° in both averages.

Two interesting features are clear in these observations. First, the central minimum of the emission band observed around 100 km is approximately at 4.73 μm, which corresponds to the first hot (FH) vibrational transition of CO, while the spectra around 150 km show a clear minimum around 4.67 μm, the center of the fundamental band (FB), both from the main CO isotope. Individual ro-vibrational lines can be identified even in the noisier FB emission with VIRTIS data, marked by the short lines in the figure, which denote their spectral positions according to the Hitran 2004 database (Rothman et al., 2005).

Secondly, as reported by Gilli et al. (2009), the FH band gives a larger contribution than the FB in a broad altitude range in the Venus mesosphere, and only at thermospheric altitudes the FB is larger. This was also obtained for a nadir geometry at high spectral resolution by Crovisier et al. (2006) with ground based observations. These two features were not initially predicted by López-Valverde et al. (2007), who focused their attention to fundamental bands, but a revised version of their Venusian non-LTE model, including several hot bands, is able to reproduce those observations (see Section 4).

MIPAS on ENVISAT is a mid-infrared limb emission Fourier transform spectrometer designed for the measurement of atmospheric trace species of the Earth's atmosphere from space (Fischer et al., 2008). MIPAS provides very high resolution spectra (0.035 cm^{-1} unapodized) and observes the atmosphere during day and night with global coverage from pole to pole. A selection of measurements taken between 19 and 27 September 2002 as described in Funke et al. (2007) was used for our analysis.

Fig. 1 (panel c) shows a plot adapted from Funke et al. (2007). It is an example of coadded daytime spectra taken by MIPAS at a mesospheric tangent height of 68 km, with a FOV of about 3 km. The NESR of the coadded spectra is 1.8×10^3 μW/(m² sr μm). Unlike on Venus and Mars, the CO emissions observed on the Earth are mainly produced by the CO (1–0) FB, which is about 10 times larger than the weaker first hot band.

Limb observations obtained with MIPAS are particularly useful for non-LTE studies and more advantageous than VIRTIS and PFS measurements for two main reasons. First, MIPAS observes the limb of the Earth continuously, while PFS and VIRTIS only have limb 'passes' during the brief periapsis period. Secondly, MIPAS spectral resolution is about 40 times better than VIRTIS-H and PFS, and such a high spectral resolution is beneficial also because contributions from different ro-vibrational bands can be separated.

Those three instruments are providing very different data-sets, which represent an excellent benchmark to test our non-LTE models. A detailed comparison of the radiances of the three planets is presented in Section 4.

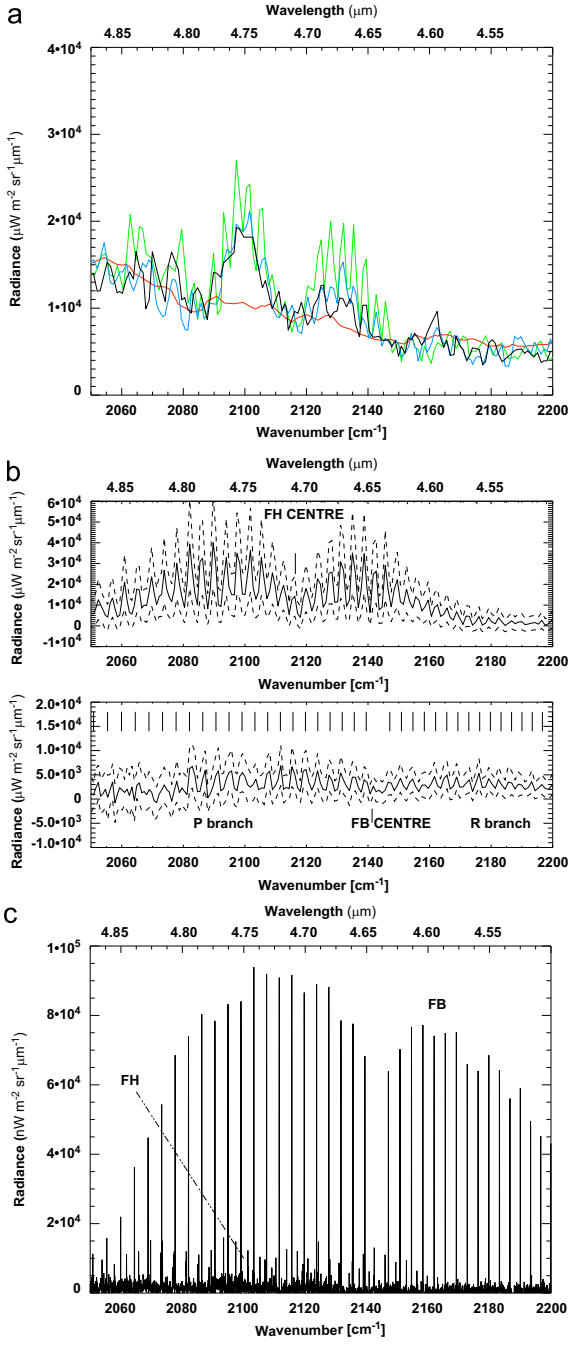

Fig. 1. CO non-LTE limb emissions at 4.7 μm observed in the three terrestrial planets. (a) Observations of Mars by PFS adapted from Formisano et al. (2006). The three average spectra represent measurements from 110 to 180 km (black line), from 80 to 110 km (green line) and from 80 to 120 km (blue line), at the latitudes ranges 56°–47°N, 46°–35°N and 35°–20°N, respectively. Red line indicates the deep space signal (similar to the noise level). See Formisano et al. (2006) for more details. (b) Observations of Venus by VIRTIS-H. Averaged spectra (solid line) and standard deviations (dashed line) of measurements at tangent heights between 96 and 103 km (top panel) and between 145 and 152 km (bottom panel). SZA is between 0–30° in all of them. (c) Observations of the Earth by MIPAS extracted from Funke et al. (2007). Coadded daytime spectra around 4.7 μm at tangent height of 68 km and at equivalent latitudes 10°–29°N (defined in terms of potential vorticity, see Funke et al., 2007 for more details). The noise equivalent spectral radiances of the coadded spectra is 1.8×10^3 μW/(m² sr μm^{-1}). (For interpretation of the references to color in this figure legend, the reader is referred to the web version of this article.)

3. Non-LTE simulations

Once the emissions are identified as produced by CO at high altitudes and during daytime, our goal is to perform precise

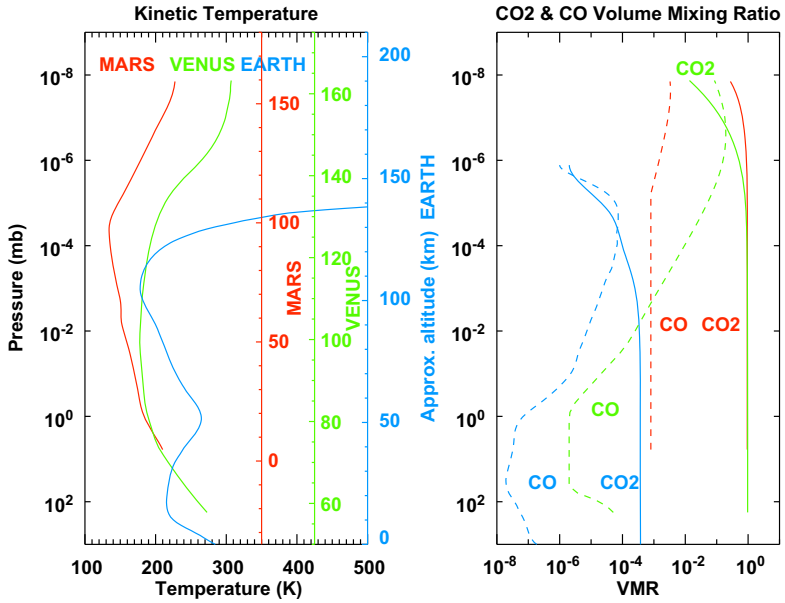

Fig. 2. Reference atmospheres used in this study. Kinetic temperature profiles (left panel), and volume mixing ratio (right panel) of CO_2 (solid line) and CO (dashed line) for Mars (red), Venus (green) and Earth (blue). (For interpretation of the references to color in this figure legend, the reader is referred to the web version of this article.)

simulations with appropriate non-LTE models for each planet, to describe and understand the data.

The simulation of CO non-LTE populations for the Earth is performed with the Generic Radiative Transfer and non-LTE population Algorithm GRANADA (Funke et al., 2002). This model has been extensively tested against other non-LTE models, has been used to analyze diverse satellite observations in the upper atmosphere, and is also included in retrieval schemes, operational nowadays, like the IMK/IAA scientific MIPAS data processor (von Clarmann et al., 2003). Limb radiances were calculated with the Karlsruhe Optimized and Precise Radiative Transfer Algorithm (KOPRA) (Stiller et al., 2002).

Regarding Mars and Venus, during the last 15 years a non-LTE model for Mars (Lopez-Valverde and Lopez-Puertas, 1994) and for Venus (Roldán et al., 2000) have also been developed at the Instituto de Astrofísica de Andalucía (IAA/CSIC) in Granada, Spain. These models are similar and have been revised recently during their application to the analysis of PFS and VIRTIS (López-Valverde et al., 2005, 2007, this issue). The simulation of non-LTE radiances is performed in two steps. First, the populations of the vibrational levels of CO are computed with those non-LTE models. Secondly, the Reference Forward Model (RFM) (Dudhia, 2000) line-by-line radiative transfer code was used to compute the emerging radiance.

For these simulations, input reference atmospheres are needed. The reference profiles (kinetic temperatures and CO and CO_2 volume mixing ratios, VMR) used in the calculations are shown in Fig. 2. The Earth thermal profile is taken from Funke et al. (2007) and, in contrast to Venus and Mars, it was retrieved at the location of the observations studied here. The Mars profile was extracted from the latest version of the Mars Climate Database (Millour et al., 2008) for the latitudes, solar longitudes and local time of the PFS data. The Venus profile is taken from the Venus International Reference Atmosphere (VIRA) for daytime mean condition (Seiff, 1983).

It is worth to remark that the accuracy of the agreement model-data depends on the knowledge of the thermal and density structure in the location of the observations which is not available so far for Mars and Venus. Therefore, we did not pursue to obtain a perfect fit here but to identify and compare the main features.

In this work we discuss the breakdown of LTE in the vibrational levels of CO, and assume that LTE holds in the rotational distribution within each vibrational state. There are theoretical and observational reasons to support this assumption. First, all the states studied here present large excitations after absorption of solar radiation in fundamental bands, i.e. with the ground state as their lower state. The absorption of the solar photons by a thermalized ground state population does not impose deviation from the LTE rotational distribution of the upper state CO(1) and we expect the CO fluorescence to deviate very little from the rotational-LTE distribution. Second, we obtained good fits to the observations by the rotational LTE approach. Hence, this approximation may fail at very high altitudes (Shved, 1974), but the error expected at the altitudes of our interest here is very small.

Fig. 3 illustrates a schematic diagram of the CO vibrational states and radiative transitions included in our non-LTE models for Mars and Venus. We present here results from an extended and improved version of non-LTE model by López-Valverde et al. (2007). In addition to the fundamental and first hot bands of the CO^{26}, already included by López-Valverde et al. (2007), which dominate and appear clearly in the measurements, two other higher energy states were introduced, $v=3$ and 4. They are excited via solar absorption at 1.57 and 1.18 μm, respectively; their contribution, however, is very small (less than 0.3%). Furthermore, three isotopic levels were also added ($CO^{36}(1)$, $CO^{36}(2)$, $CO^{36}(3)$). We found that none of their bands is important for the emerging radiance at 4.7 μm, with a total radiance about 1% of the dominating bands. The $CO^{36}(1)$ level was also included in the Earth's model.

Vibrational–vibrational (V–V) collisional exchange and vibrational–translational (V–T) processes were also included in the models (dashed lines in Fig. 3). The rate coefficients involving the states $CO(v \leq 2)$ of the main isotope are summarized in Lopez-Puertas and Taylor (2001) and Funke et al. (2007) for the

Earth and in Lopez-Valverde and Lopez-Puertas (1994) and López-Valverde et al. (2005) for Mars and Venus. In the Martian and Venusian models the most important V–V collisions of CO(v) are with CO_2(0 0 0 1 1) (López-Valverde et al., 2007). For the isotopic CO^{36}, the rates for the V–T and V–V collisions with CO_2 were assumed the same as for the main isotope, given the similar nature of the collisions and energy gaps involved. The inter-isotopic V–V relaxation of CO^{36}(2) follows Stepanova and Shved (1988). For the CO^{26} ($v>2$) states we use the harmonic oscillator approximation. All these assumptions involve a degree of uncertainty in the populations of the states but since the contributions of these weak bands are so small, they do not alter significantly the results presented here.

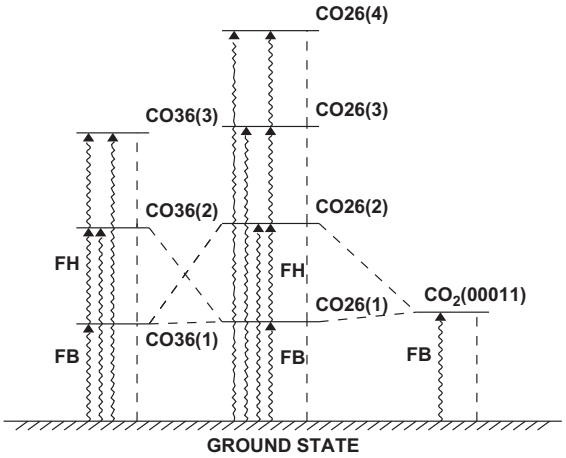

Fig. 3. Diagram of the CO energy states, with the most relevant emission bands at 4.7 μm included in the Martian and Venusian non-LTE models. The states are labeled following the Hitran nomenclature. Arrows indicate ro-vibrational transitions with significant solar absorption. Fundamental band (FB) and first hot band (FH) of CO and isotope CO^{36} are indicated, as well as the 4.3 μm FB of CO_2. The collisional energy transfers between CO levels themselves and with CO_2 (0 0 0 1 1) are indicated with dashed lines. See text for details.

On Earth, direct collisional exchanges with CO_2(0 0 0 1 1) are less important since CO ($v=1, 2$) is connected with N_2 ($v=1$) and subsequently with CO_2 (v_3) (Funke et al., 2007).

Fig. 4 shows the vibrational temperatures for the three planets, for the excitation of the CO(1), CO(2) and isotopic CO^{36}(1) states during typical daytime conditions, together with the kinetic temperatures. The departure from LTE for the CO(1) state occurs around 1 mb, which approximately corresponds to 20 km on Mars, about 90 km on Venus and 50 km on Earth and it is produced mainly by the absorption of solar radiation in the FB. The solar pumping at 2.3 μm, which populates the level CO(2), is about a factor 1.6 larger than at 4.7 μm. The LTE breakdown for this vibrational level occurs at lower altitudes than for the CO(1). The strong pumping of CO(2) at 2.3 μm also produces larger vibrational temperatures of this state and this behavior is observed in the three planets: above 1 mb they are about 100 K higher than the CO(1) vibrational temperature.

The vibrational temperatures used in this study agree very well with previous models for the Earth (López-Puertas et al., 1996; Kutepov et al., 1997), Mars (Stepanova and Shved, 1988), and Venus (Crovisier et al., 2006). The vibrational temperatures of the CO states at the top of the thermosphere are constant in the three planets because solar flux reaching those layers is almost unaffected. Since Venus is closer to the Sun, those temperatures are the largest, and on Earth those values are intermediate. In the lower atmosphere, at higher densities, collisions start to dominate and the vibrational temperatures decrease and tend to follow the kinetic temperature.

These results are introduced in the forward radiance codes to calculate the emerging radiances. In the next section we compare simulated and measured radiances on the upper atmosphere of the three planets.

4. Comparative analysis of limb radiances

In the absence of a detailed knowledge of the thermal structure and composition at the time of the measurements for Mars and Venus, this study does not aim to obtain an excellent fit to the data nor to retrieve the CO abundance. Our purpose is to better understand the spectral shape and the contributions of the

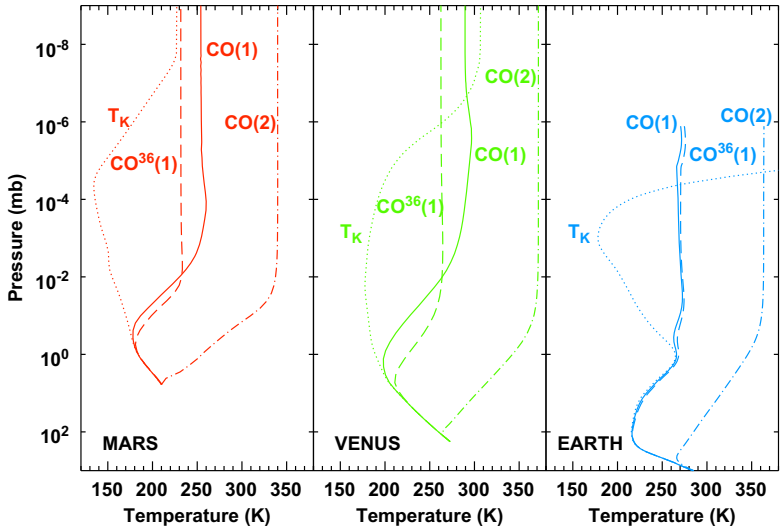

Fig. 4. Vibrational temperatures for the CO(1) (solid), CO(2) (dashed-dotted) and CO^{36}(1) (dashed) levels for Mars, Venus and Earth for mean daytime conditions. T_k stands for kinetic temperature, shown for reference.

different bands to the observed non-LTE CO emission in the three terrestrial planets. As expected, at approximately the same pressure levels (10^{-2} mb), 65 km on Mars and 100 km on Venus, the denser atmosphere of Venus produces a larger CO emission (about a factor 2) than the Martian atmosphere (see Fig. 1). The spectrum of Earth shown in the figure is not directly comparable with PFS and VIRTIS-H spectra because MIPAS resolution are different.

In order to compare the contribution of individual CO bands we have performed a series of calculations, shown in Fig. 5. Simulated non-LTE radiance profiles for the FB, FH and the FB isotopic CO bands, integrated in the spectral range 4.55–4.90 μm have been obtained for the three planets.

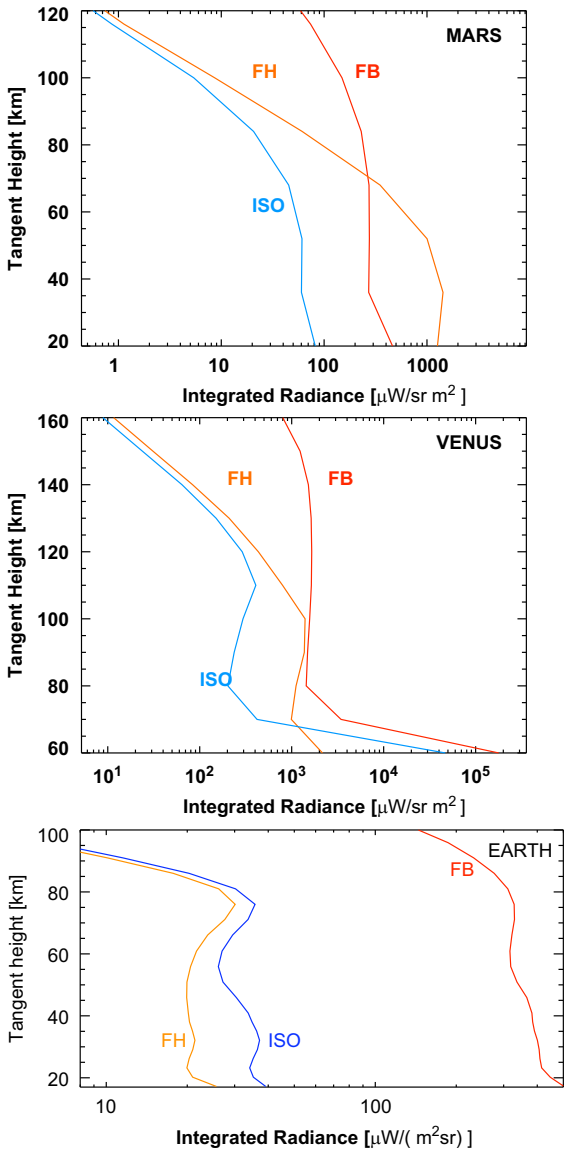

Fig. 5. Simulated profiles of the 4.7 μm limb radiance integrated over the spectral range of Fig. 1 for Mars (top), Venus (middle) and Earth (bottom, adapted from Funke et al., 2007) and for the daytime atmospheric conditions, as in Fig. 2. The contributions of the fundamental band (FB) (red), first hot (FH) (orange) and fundamental isotopic (ISO) (blue) are shown. Note the different *x*-axis range in the three panels. (For interpretation of the references to color in this figure legend, the reader is referred to the web version of this article.)

At the top of the altitudes shown in the figure, the Martian and Venusian profiles have a similar behavior and their radiances are also similar in order of magnitude. In optically thin conditions, the emitted radiance is proportional to the number of emitters, and the emission decreases with decreasing density (increasing altitudes). Since CO(1) has a larger population than CO(2), its contribution is also larger. Note that this is not in contradiction with the vibrational temperatures shown in Fig. 4 (much higher for the CO(2) than for the CO(1)), since the number density of a given vibrational (or rotational) upper state $n_{v,r}$ is proportional to $n_0\, e^{-E_{v,r}/kT_{v,r}}$, where $E_{v,r}$ is its energy, $T_{v,r}$ its vibrational (or rotational) temperatures, n_0 is the number density of the lower state and k is the Boltzmann constant (Lopez-Puertas and Taylor, 2001).

At mesospheric tangent altitudes, as the amount of absorber in the atmosphere above increases, the bands become optically thicker. As can be seen in Fig. 5 this occurs for the FB below 10^{-5} mb (about 100 km on Mars and 140 km on Venus) and for the FH below 10^{-2} mb (about 60 km on Mars and 100 km on Venus). The FB lines saturate and the radiation in the FB cannot escape. This is why the emission by the weaker FH becomes comparatively very important at those tangent altitudes, and it can be similar or even larger that the FB. On Venus the FH contribution is comparable to that of the FB below 100 km while on Mars the FH contribution is about 5 times larger than the FB below 70 km. Under optically thick conditions, the emitted radiance of the bands approximately follows the Planck function at the vibrational temperatures of the layers where they become optically thin. As can be seen in Fig. 4, those values are similar to the vibrational temperatures at the top of the atmosphere. The FB vibrational temperatures on Venus are about 30 K (12%) larger than on Mars and produce radiances about 6 times larger. On the contrary, the FH vibrational temperatures on Mars are only 3% smaller than on Venus and their radiances profiles are therefore very similar.

For the Earth, the situation is different because neither the FB nor the FH become saturated at any mesospheric altitude and their emissions are essentially proportional to the populations of their upper states. Since the CO(1) population is everywhere larger than that of CO(2), the FB has a much larger contribution. The shape of the contributions' profiles depends on the source function and on the concentration of CO. On Earth's middle atmosphere there is a strong increase of CO VMR with altitudes above about 40 km, which produces a different profile than in Mars or Venus, with radiances slightly increasing up to 80 km. The vertical VMR gradient decreases again above about 80 km and the radiances show the usual fall with the atmospheric density above this altitude. It is also noticeable that the peak of the FB on Earth's upper mesosphere is about one order of magnitude lower than those on Mars and Venus, reflecting the difference in CO VMR in the three planets at the same pressure level (at approximately 10^{-2} mb).

Comparisons between simulated and measured spectra in the three planets are presented in Figs. 6–8. For Mars, a simulation at 85 km containing the 30 km nominal FOV of the instrument was first compared with the observed PFS average spectrum between 80 and 110 km. This is the only set of PFS data in a limb geometry available at 4.7 μm to contrast our non-LTE model so far. We found that our simulation at this altitude did not reproduce the measurements correctly: in contrast to the PFS data, the CO simulated emission was dominated by the FB band. This PFS average spectrum is better described by a simulated spectrum at a tangent altitude around 68 km, as shown in Fig. 6 (upper panel). To clarify the comparison, the offset has been removed

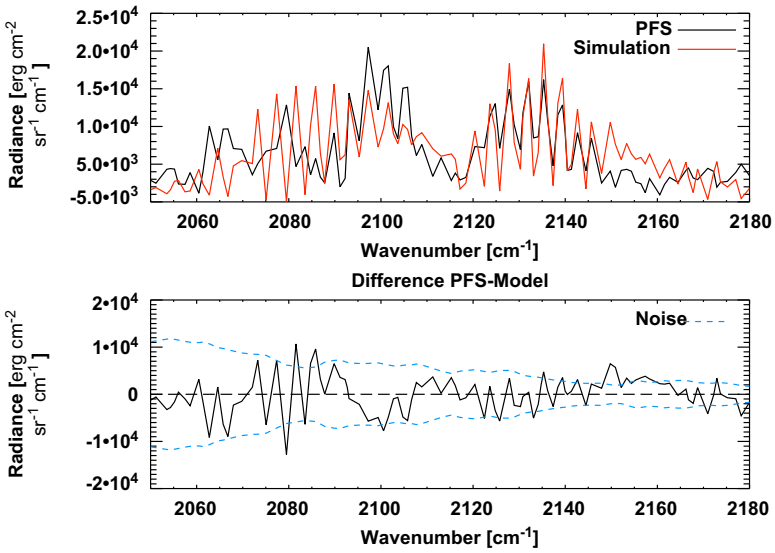

Fig. 6. Top panel: comparison between the PFS averaged spectrum (black) of the limb 4.7 μm CO band radiance on Mars between 80 and 110 km tangent heights after offset removal, and its non-LTE simulation at 68 km (red). Bottom panel: difference between model and data together with the noise level (dashed line, similar to the deep space offset). See text for details. (For interpretation of the references to color in this figure legend, the reader is referred to the web version of this article.)

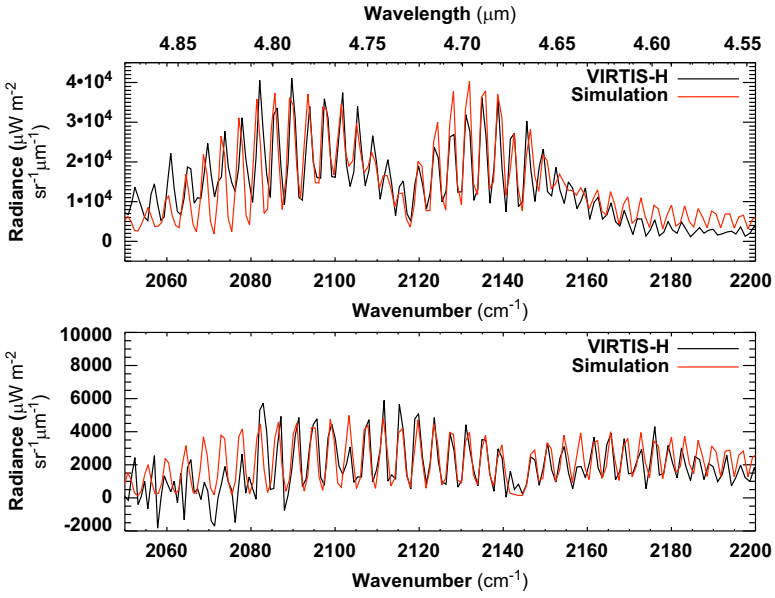

Fig. 7. Comparison between VIRTIS-H averaged limb spectra (black) and non-LTE simulations (red) for the tangent altitudes of 100 km (top panel) and 150 km (bottom panel). (For interpretation of the references to color in this figure legend, the reader is referred to the web version of this article.)

from the PFS spectrum. The agreement is reasonably good in the R branch and at the center of the P branch but differences are observed in two spectral regions, 2150–2170 cm^{-1} and especially 2060–2090 cm^{-1}, where the PFS signal is noisier. It is shown in the lower panel of Fig. 6 together with the difference between model and data, which is approximately within these noise values.

A fine-tuning of the input reference atmosphere is required to find a better agreement but this is part of an ongoing retrieval procedure and is beyond the scope of this study.

For Venus, two simulations performed at 100 km and at 150 km are compared with two VIRTIS-H averaged spectra in the same altitude ranges (see Fig. 7). The FOV of the instrument was taken into account in the simulated radiances, although we found that the FOV effect for values below 5 km is very small. To improve the comparison at 100 km, we also modified the thermal structure, decreasing the VIRA reference daytime temperature in about 40 K in the altitude range of interest (90–130 km). For the 150 km spectrum the reference atmosphere was unaltered. The overall agreement is very good: the simulations clearly reproduce

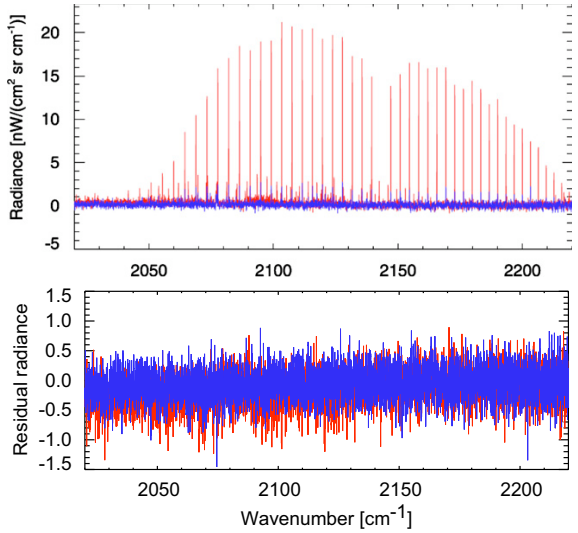

Fig. 8. Comparison between MIPAS daytime (red) and nighttime (blue) coadded limb observations and non-LTE simulations in the latitude band 10–29°N at 68 km (extracted from Funke et al., 2007). Difference between simulated and measured radiances are shown in the bottom panel. (For interpretation of the references to color in this figure legend, the reader is referred to the web version of this article.)

FH band lines at tangent altitudes around 100 km and the FB lines at 150 km, as observed in VIRTIS-H data. Other hot and isotopic bands give very small contributions and are not discernible in the figure.

For the Earth, Fig. 8 shows 60 coadded spectra taken by MIPAS observing the Earth's limb at 68 km (top panel) during daytime (red) and nighttime (blue) and the difference between simulated and measured radiances (lower panel). In contrast to the comparisons for Mars and Venus, a better fit is obtained because the CO VMR used in the simulation was that retrieved from the measured spectra. Residuals are generally in the order of the instrumental noise (0.4 nW/(sr cm^2 cm^{-1}), after coadding), except for tangent heights below 35 km (see Funke et al., 2007 for more details). This non-LTE model for the Earth has been successfully used in the of CO abundances from MIPAS (Funke et al., 2009).

5. Summary and conclusions

We presented here a comparative study of the CO non-LTE limb emissions observed around 4.7 μm in the upper atmospheres of Mars, Venus and Earth, using measurements by PFS/MEx, VIRTIS/VEx and MIPAS/Envisat, respectively. The goal of this work is to perform a common analysis on these recent space observations with similar theoretical tools, and highlight differences and similarities among the three planetary atmospheres. New data from VIRTIS-H were also analyzed, and a model-data comparison together with a quantitative contribution from the bands identified by Gilli et al. (2009) were performed here.

Furthermore, this study allows to compare the capability of different space instrumentation to extract geophysical information from atmospheric emissions in similar spectral region. In fact, the typical ro-vibrational double peak structure of the CO diatomic molecule is a common feature observed in the emission spectra of all terrestrial planets, while the rotational structure is identified according to the spectral resolution and sensitivity of the three instruments. Earth observations by MIPAS clearly show individual rotational lines whereas only the strongest lines can be identified with VIRTIS-H on Venus, and this is possible on Mars only after a proper large averaging with PFS. Another interesting difference is that both Mars and Venus spectra at mesospheric altitudes, show a central minimum of the emission at 4.73 μm, which corresponds to the center of the FH band, while the CO emission on Earth is clearly dominated by the FB band. A similar structure has also been observed by ground-based measurements (Crovisier et al., 2006) on Venus. On Earth, the FH is also present but has a very low contribution (Funke et al., 2007). All this is in good agreement with the general purpose of our non-LTE models, which are also able to describe non-LTE emissions by CO_2 taken on Venus (López-Valverde et al., 2007, this issue; Gilli et al., 2009), Mars (Formisano et al., 2006; López-Valverde et al., this issue) and on the Earth (Funke et al., 2007). This is the first time that CO measurements in this spectra region from PFS and VIRTIS-H are compared directly with non-LTE simulations, and the agreement is satisfactory, within measurements uncertainties.

In addition to the validation of the current non-LTE models, the CO 4.7 μm limb observations on Mars and Venus by PFS and VIRTIS are also of great interest because they are potentially useful to retrieve CO densities in their upper atmosphere, as it has been done with MIPAS data on the Earth (Funke et al., 2009). Furthermore, the rotational distribution of the CO emission at 4.7 μm could also be used to derive the kinetic temperature in the upper atmosphere of Venus, as previously done by Crovisier et al. (2006).

High spectral resolution and good sensitivity are fundamental to derive atmospheric parameters from remote measurements. The comparison between MIPAS, VIRTIS and PFS clearly manifests that the investigation on Earth is nowadays leading this field of research. Nevertheless, VIRTIS-H limb observations are also very promising for sounding the upper atmosphere of Venus. Non-LTE retrievals of CO density and temperature in the upper atmosphere of Venus from VIRTIS data are in progress. Furthermore, this work also advances in ways which are valuable to export ideas to the emerging field of exoplanetary atmospheres.

Acknowledgements

The IAA-CSIC team was supported by the Spanish MICINN under Project AYA2008-03498/ESP and EC FEDER funds and GG has been supported by a Spanish National Research Council (CSIC) Grant (BOE 16/08/2007).

References

Billebaud, F., Crovisier, J., Lellouch, E., Encrenaz, T., Maillard, J.P., 1991. High-resolution infrared spectrum of CO on Mars: evidence for emission lines. Planet. Space Sci. 39 (February), 213–218.

Bougher, S.W., Roble, R.G., 1991. Comparative terrestrial planet thermospheres. 1. Solar cycle variation of global mean temperatures. J. Geophys. Res. 96 (July), 11045–11055.

Clancy, R.T., Sandor, B.J., Moriarty-Schieven, G.H., 2003. Observational definition of the Venus mesopause: vertical structure, diurnal variation, and temporal instability. Icarus 161 (January), 1–16.

Clerbaux, C., Coheur, P.-F., Hurtmans, D., Barret, B., Carleer, M., Semeniuk, R.C.K., McConnell, J.C., Boone, C., Bernath, P., 2005. Carbon monoxide distribution from the ACE-FTS solar occultation measurements. Geophys. Res. Lett. 32.

Crovisier, J., Lellouch, E., de Bergh, C., Maillard, J.-P., Lutz, B.L., Bézard, B., 2006. Carbon monoxide emissions at 47 μm from Venus atmosphere. Planet. Space Sci. 54 (November), 1398–1414.

de Bergh, C., Crovisier, J., Lutz, B.L., Maillard, J.P., 1988. Detection of CO infrared emission lines in spectra of Venus. In: Bulletin of the American Astronomical Society, vol. 20. Bulletin of the American Astronomical Society, June, p. 831.

Dodd, J.A., Winick, J.R., Blumberg, W.A.M., Lipson, S.J., Armstrong, P.S., Lowell, J.R., 1993. CIRRIS 1A observation of (13)C(16)O and (12)C(18)O fundamental band radiance in the upper atmosphere. Geophys. Res. Lett. 20 (December), 2683–2686.

Drossart, P., et al., 2005. Atmospheric studies with OMEGA/Mars express. In: Mackwell, S., Stansbery, E. (Eds.), 36th Annual Lunar and Planetary Science Conference, vol. 36. Technical Report, Lunar and Planetary Institute, March, p. 1737.

Drossart, P., et al., 2007. Scientific goals for the observation of venus by VIRTIS on ESA/Venus express mission. Planet. Space Sci. 55 (October), 1653–1672.

Dudhia, A., 2000. Michelson Interferometer for Passive Atmospheric Sounding (MIPAS) Reference Forward Model (RFM) Software User's Manual. Oxford University, Oxford, UK.

Dupuy, E., Urban, J., Ricaud, P., Flochmoën, E.L., Lautié, N., Murtagh, D., de la Nöe, J., Amraoui, L.E., Eriksson, P., Forkman, P., Frisk, U., Jégou, F., Jiménez, C., Olberg, M., 2004. Strato-mesospheric measurements of carbon monoxide with the Odin sub-millimetre radiometer: retrieval and first results. Geophys. Res. Lett. 31, L20101.

Filipiak, M.J., Harwood, R.S., Jiang, J.H., Li, Q., Livesey, N.J., Manney, G.L., Read, W.G., Schwartz, M.J., Waters, J.W., Wu, D.L., 2005. Carbon monoxide measured by the EOS Microwave Limb Sounder on Aura: first results. Geophys. Res. Lett. 32.

Fischer, H., Birk, M., Blom, C., Carli, B., Carlotti, M., von Clarmann, T., Delbouille, L., Dudhia, A., Ehhalt, D., Endemann, M., Flaud, J.M., Gessner, R., Kleinert, A., Koopman, R., Langen, J., López-Puertas, M., Mosner, P., Nett, H., Oelhaf, H., Perron, G., Remedios, J., Ridolfi, M., Stiller, G., Zander, R., 2008. MIPAS: an instrument for atmospheric and climate research. Atmos. Chem. Phys. 8 (8), 2151–2188.

Formisano, V., et al., 2005. The planetary fourier spectrometer (PFS) onboard the European Mars express mission. Planet. Space Sci. 53 (August), 963–974.

Formisano, V., Maturilli, A., Giuranna, M., D'Aversa, E., Lopez-Valverde, M.A., 2006. Observations of non-LTE emission at 4–5 μm with the planetary Fourier spectrometer aboard the Mars Express mission. Icarus 182 (May), 51–67.

Funke, B., Martin-Torres, F.J., Lopez-Puertas, M., Hoepfner, M., Hase, F., Lopez-Valverde, M.A., Garcia-Comas, M., 2002. A generic non-LTE population model for MIPAS–Envisat data analysis. EGS XXVII General Assembly, Nice, abstract #4915 27, 21–26 April, p. 4915.

Funke, B., López-Puertas, M., Bermejo-Pantaleón, D., von Clarmann, T., Stiller, G.P., Höpfner, M., Grabowski, U., Kaufmann, M., 2007. Analysis of nonlocal thermodynamic equilibrium CO 4.7 μm fundamental isotopic and hot band emissions measured by the Michelson interferometer for passive atmospheric sounding on Envisat. J. Geophys. Res. 112.

Funke, B., López-Puertas, M., García-Comas, M., Stiller, G.P., von Clarmann, T., Höpfner, M., Glatthor, N., Grabowski, U., Kellmann, S., Linden, A., 2009. Carbon monoxide distributions from the upper troposphere to the mesosphere inferred from 47 μm non-local thermal equilibrium emissions measured by MIPAS on Envisat. Atmos. Chem. Phys. 9 (7), 2387–2411.

Gilli, G., López-Valverde, M.A., Drossart, P., Piccioni, G., Erard, S., Cardesín Moinelo, A., 2009. Limb observations of CO_2 and CO non-LTE emissions in the Venus atmosphere by Virtis/Venus Express. J. Geophys. Res. 114.

Gladstone, G.R., Yelle, R.V., Majeed, T., 2002. Solar System Upper Atmospheres: Photochemistry, Energetics, and Dynamics, p. 23.

Gulkis, S., Kakar, R.K., Klein, M.J., Olsen, E.T., Wilson, W.J., 1978. Venus—detection of variations in stratospheric carbon monoxide. In: Vallance Jones, A. (Ed.), Planetary Atmospheres Symposium, pp. 61–65.

Gunson, M.R., Farmer, C.B., Norton, R.H., Zander, R., Rinsland, C.P., Shaw, J.H., Gao, B.C., 1990. Measurements of CH_4, N_2O, CO, H_2O, and O_3 in the middle atmosphere by the atmospheric trace molecule spectroscopy experiment on Spacelab 3. J. Geophys. Res. 95, 13867–13882.

Gurwell, M.A., Muhleman, D.O., Shah, K.P., Berge, G.L., Rudy, D.J., Grossman, A.W., 1995. Observations of the CO bulge on Venus and implications for mesospheric winds. Icarus 115 (May), 141–158.

Kaplan, L.D., Connes, J., Connes, P., 1969. Carbon monoxide in the Martian atmosphere. Astrophys. J. 157 (September), L187–L192.

Kutepov, A.A., Oelhaf, H., Fischer, H., 1997. Non-LTE radiative transfer in the 4.7 and 2.3 μm bands of CO: vibration-rotational non-LTE and its effects on limb radiance. Journal of Quantitative Spectroscopy and Radiative Transfer 57 (March), 317–339.

Lellouch, E., Goldstein, J.J., Rosenqvist, J., Bougher, S.W., Paubert, G., 1994. Global circulation, thermal structure, and carbon monoxide distribution in Venus' mesosphere in 1991. Icarus 110 (August), 315–339.

Lopez-Puertas, M., Taylor, F.W., 2001. Non-LTE radiative transfer in the atmosphere. In: Lopez-Puertas, M., Taylor, F.W. (Eds.), Series on Atmospheric Oceanic and Planetary Physics, vol. 3. World Scientific, Singapore, ISBN 9810245661.

López-Puertas, M., Zaragoza, G., López-Valverde, M.A., Martín-Torres, F.J., Clarmann, T.V., Linden, A., Stiller, G.P., Wegner, A., 1996. An improved non-LTE quantifier for MIPAS. Technical Report.

López-Valverde, M.A., López-Puertas, M., López-Moreno, J.J., Formisano, V., Grassi, D., Maturilli, A., Lellouch, E., Drossart, P., 2005. Analysis of CO_2 non-LTE emissions at 4.3 μm in the Martian atmosphere as observed by PFS/Mars Express and SWS/ISO. Planet. Space Sci. 53 (August), 1079–1087.

Lopez-Valverde, M.A., Lopez-Puertas, M., 1994. A non-local thermodynamic equilibrium radiative transfer model for infrared emission in the atmosphere of Mars. 2: daytime populations of vibrational levels. J. Geophys. Res. 99 (June), 13117–13132.

López-Valverde, M.A., López-Puertas, M., Remedios, J.J., Rodgers, C.D., Taylor, F.W., Zipf, E.C., Erdman, P.W., 1996. Validation of measurements of carbon monoxide from the improved stratospheric and mesospheric sounder. J. Geophys. Res. 101 (April), 9929–9956.

López-Valverde, M.A., Drossart, P., Carlson, R., Mehlman, R., Roos-Serote, M., 2007. Non-LTE infrared observations at Venus: from NIMS/Galileo to VIRTIS/Venus Express. Planet. Space Sci. 55 (October), 1757–1771.

López-Valverde, M., López-Puertas, M., Funke, B., Gilli, G., Garcia-Comas, M., Drossart, P., Piccioni, G., Formisano, V., Modeling the atmospheric limb emission of CO_2 at 4.3 μm in the terrestrial planets. Planet. Space Sci., this issue, doi:10.1016/j.pss.2010.02.001.

Millour, E., Forget, F., González-Galindo, F., Spiga, A., Lebonnois, S., Montabone, L., Lewis, S.R., Read, P.L., López-Valverde, M.A., Gilli, G., Lefèvre, F., Montmessin, F., Desjean, M.-C., Huot, J.-P., The McD/Gcm Development Team, November 2008. The Latest (Version 4.3) Mars Climate Database. LPI Contributions 1447, 9029.

Piccioni, G., et al., 2006. VIRTIS: The visible and infrared thermal imaging spectrometer. European Space Agency Spec. Publ., ESA Publications Division, Noordwijk, The Netherlands. ESA-SP 1295, pp. 1–27.

Roldán, C., López-Valverde, M.A., López-Puertas, M., Edwards, D.P., 2000. Non-LTE infrared emissions of CO_2 in the atmosphere of Venus. Icarus 147 (September), 11–25.

Rothman, L.S., et al., 2005. The HITRAN 2004 molecular spectroscopic database. J. Quant. Spectrosc. Radiat. Transfer 96 (December), 139–204.

Schloerb, F.P., Robinson, S.E., Irvine, W.M., 1980. Observations of CO in the stratosphere of Venus via its $J=0$–1 rotational transition. Icarus 43 (August), 121–127.

Seiff, A., 1983. Thermal structure of the atmosphere of Venus. In: Venus. University of Arizona Press, Tucson, pp. 215–279.

Shved, G.M., 1974. Radiative transfer in the vibrational–rotational bands of linear molecules when local thermodynamic equilibrium is violated. Soviet Astron. 51 (August), 841–851.

Stepanova, G.I., Shved, G.M., 1988. Calculations of the limb emission of Venus and Mars in infrared CO_2 bands with allowance for breakdown of local thermodynamic equilibrium. Soviet Astron. 32 (December), 677–681.

Stiller, G.P., von Clarmann, T., Funke, B., Glatthor, N., Hase, F., Höpfner, M., Linden, A., 2002. Sensitivity of trace gas abundances retrievals from infrared limb emission spectra to simplifying approximations in radiative transfer modeling. J. Quant. Spectrosc. Radiat. Transfer 72 (3), 249–280.

von Clarmann, T., Ceccherini, S., Doicu, A., Dudhia, A., Funke, B., Grabowski, U., Hilgers, S., Jay, V., Linden, A., López-Puertas, M., Martín-Torres, F.-J., Payne, V., Reburn, J., Ridolfi, M., Schreier, F., Schwarz, G., Siddans, R., Steck, T., 2003. A blind test retrieval experiment for infrared limb emission spectrometry. J. Geophys. Res. 108 (D23), 4746.

Yung, Y.L., Demore, W.B. (Eds.), 1999. Photochemistry of Planetary Atmospheres. Oxford University Press, New York, QB603.A85 Y86 1999.

Chapter 4

Venus upper atmospheric CO and Temperature

In this chapter the retrieval scheme applied to the VIRTIS-H 4.7-μm non-LTE CO emissions to derive carbon monoxide and temperature in the upper mesosphere/lower thermosphere of Venus is described, and the results obtained are presented and discussed.
As mentioned in Chapter 1, the knowledge of atmospheric parameters such as temperatures and abundances in the Venus upper atmosphere is very scarce, especially during daytime. Venus Express (VEx) with its instruments on-board, increased significantly the number of measurements in the limb of the planet. In particular, VIRTIS/VEx sounded systematically the atmosphere of Venus in the IR window, and detected strong non-LTE emissions of CO_2 around 4.3 μm, and CO at 4.7 μm above 100 km altitudes. In this work they have been analyzed and interpreted with the help of a non-LTE model for Venus (Gilli et al., 2009, 2011; López-Valverde et al., 2011) as detailed in the two previous chapters.

Throughout this thesis, particular emphasis was given to the potential of VIRTIS-H to retrieve CO density and temperature from the CO non-LTE emission at 4.7 μm. When investigating the retrieval strategies to follow, one has to face with the characteristics and the overall quality of the data. The nature of the measurements, including spectral range and resolution, observational geometry and sigal to noise ratio (S/N), is always a limiting factor in the retrieval analysis (Hanel et al., 2003). All these aspects are crucial to build up a retrieval method capable to extract the maximum information possible from a given set of measurements. In our case, the low S/N in the spectral region of our interest, required large averages to increase it and to improve the sensitivity of the data to the retrieval parameters. Besides, VIRTIS-H limb measurements did not provide typical 1-D profiles, but a set of isolated limb spectra, and each of these single spectral acquisitions is not necessarily connected in time and space with the previous spectrum. In addition to this, the vertical profiles of those atmospheric parameters on Venus are not well known, so it is difficult and unpractical to build a-priori information for proper weightings with the actual measurements. Another important requirement, and limitation at the same time, was the inclusion of the non-LTE model into the retrieval code. This imposes constraints to the dataset since it requires averages within the limits of physically homogeneous conditions. This can be traduced to a careful use of data within relatively small brackets in parameters like SZA

and tangent altitude. Taking into account all these observational and theoretical aspects, it was developed a two-steps retrieval method capable to derive CO and temperature simultaneously, from sparse individual spectra.
A complete description of our non-LTE retrieval code, the selection of the VIRTIS-H data used for the retrieval and the error analysis we performed, is given in the manuscript attached to this chapter. The paper is entitled: *Carbon monoxide and temperature in the upper atmosphere of Venus from VIRTIS/Venus Express non-LTE limb measurements* and is foreseen to be submitted soon to *Planetary and Space Science*.
Next, the main results and the conclusions obtained are summarized, and some ideas discussed in the paper are expanded.

The method chosen for this work is not an iterative scheme but it makes use of a set of pre-computed synthetic spectra for a number of possible CO and temperature values, and at different SZAs and altitudes. A first approximate solution, the *first-fit*, was obtained by minimizing the (χ^2), calculated as the sum of the squared differences between the simulations and the measured spectrum, weighted as usual by the measurement error. The second step followed the theory of linear inversion , according to which the *best-fit* is obtained around the solution of the previous step, or reference state x_0. Following the nomenclature of Rodgers (2000):

$$\mathbf{x} = \mathbf{x}_0 + [\ (\mathbf{K}^T\ \mathbf{S}_\epsilon{}^{-1}\ \mathbf{K})^{-1}\ \mathbf{K}^T\ \mathbf{S}_\epsilon{}^{-1}\ (\mathbf{y}\text{- }\mathbf{F}(\mathbf{x}_0))\ ]$$

where $\mathbf{y}$ denotes the measurement vector, which in our case contains one element, the spectrum at one single altitude. The variable $\mathbf{x}$ is the state vector to be retrieved, which here contains two parameters, CO and temperature at the pointing altitude. $\mathbf{F}$ stands for the Forward Model, and $\mathbf{F}(\mathbf{x}_0)$ is the simulation for the reference state x_0 (our *first-fit*). $\mathbf{K}$ is the Weighting Function, a *Jacobian* matrix which provides information on the dependence of the radiance $\mathbf{y}$ on the retrieval parameters $\mathbf{x}$, usually computed by the first derivative of the forward model with the unknown state vector variable.

The retrieval error was calculated according to the covariance matrix, expressed by:

$$\mathbf{S} = \mathbf{K}^{-1}\ \mathbf{S}_\epsilon\ (\mathbf{K}^T)^{-1}$$

where $\mathbf{S}_\epsilon$ is the measurement's error matrix. The usual problem of deciding on the vertical correlation is eliminated, as this case deals with 1-element vectors. Regarding the correlation between CO and T errors, this is assumed to be very small. In other words, $\mathbf{S}_\epsilon$ is a diagonal matrix.

A first study, previous to the computation of the synthetic spectra, consisted on a detailed evaluation of the Weighting Functions. This study showed that the sensitivity peak of the CO radiances is around 100-110 km and 140-150 km, where the FH and FB bands become optically thin, respectively. In addition to this, it was found that most of the information comes from a 20-km wide layer above each tangent altitude. This result was used in the production of the set of pre-compute synthetic spectra, obtained by perturbations of the CO and temperature values of the VIRA reference atmosphere. The perturbation extended over 20 km above each tangent altitude, following the Weighting functions widths.

The manuscript enclosed includes a discussion on the retrieval errors and a table of the most important uncertainties. Here that discussion is elaborate in more depth. The basic

assumption in the error analysis is that the errors of a function y of several variables x_k can be treated following the Bayesian probabilistic theory, with a sum of squared errors in the form (d'Agostini, 2003):

$$\sigma^2(y) = \sum_k (\frac{\delta y}{\delta x_k})^2 \sigma^2(x_k)) + \text{correlation terms}$$

In our case, we assumed that all the error components are random, including the systematic terms of unknown sign, and that there are no significant correlation between them. Then, the problem is reduced to compute a number of *Jacobians*, or sensitivity matrixes, for each error source. This error analysis was applied only to the CO retrieval, since the retrieval errors in the temperature are very large, and did not merit further insight. In practice, since there are many possible sources of uncertainty, only two sensitivity matrices have been computed. A first sensitivity matrix evaluated the change in the retrieved CO for changes in the atmospheric CO. This matrix is usually called Averaging Kernel, and gives information on the actual vertical resolution of the inversion. The results obtained confirmed a resolution of the order of 15-20 km, in agreement with the criterion used in the perturbation study.
The second sensitivity matrix relates the CO retrieved to the radiance. This is useful for those error components whose effect can be converted to an impact on the spectrum and most error sources fall into this category. Two different cases were contemplated: changes in the spectrum proportional to the radiance (variable with wavelength), and constant changes in radiance (regardless of wavelength). The former was used to treat errors that produce an increase or decrease of the whole emission, and the latter to handle systematic errors like the background emission.

In addition to the terms discussed in the manuscript, one of the largest uncertainties came form the spectral resolution, fairly unconstrained observationally. In this work the equivalent to a Gaussian function with FWHM of 2.0 cm^{-1} is used, but values between 1.9 and 2.1 cm^{-1} would also explain the spectra. This uncertainty represents a continuous difference between simulations which amounts to 10-20 %of the total radiance, giving rise to an error in the retrieved CO of 15-40 %, depending on altitude. Figure 4 illustrates this effect for a synthetic spectra at 100 km.

For the final set of main error sources, see the table in the manuscript. Many other sources were evaluated, but their contribution was very small. Some of these are: uncertainties in the rate coefficients of the non-LTE model, size of the grid of synthetic spectra, ILS and FOV size and shape, and spectroscopic uncertainties and solar flux changes in the IR.

The main conclusions of this chapter and the manuscript, can be summarized as follows:

- The VIRTIS-H measurements at 4.7 μm have been extensively analyzed with a non-LTE Forward Model and with an inversion scheme specially developed to study them. These tools have been used to validate the non-LTE model and to derive CO and temperature in the atmosphere of the planet, between 100 and 150 km altitudes.

- Our results show [CO] latitudinal variations, with higher densities in the equatorial region during high solar illumination conditions. We also found a nearly factor 2 between noon and the near-terminator measurements, at all altitudes. Those variations

are consistent with a strong sub-solar source of CO from CO_2 photo-dissociation plus a sub-solar to anti-solar circulation, which transport the CO in the thermosphere. VIRTIS measurements of CO agree, within the error bars, with SPICAV/Soir measurements between 100 and 120 km altitude.

- A few daytime temperature profiles can be retrieved from a large average of data. A clear mesopeak is observed at high latitudes in the morning hours. This is in agreement with similar features near the terminator obtained by SPICAV/SOIR most recent results (A. C. Vandaele, personal communication). This mesopeak is not observed at the sub-solar point, in contrast to radiative equilibrium considerations and to ground-based measurements.

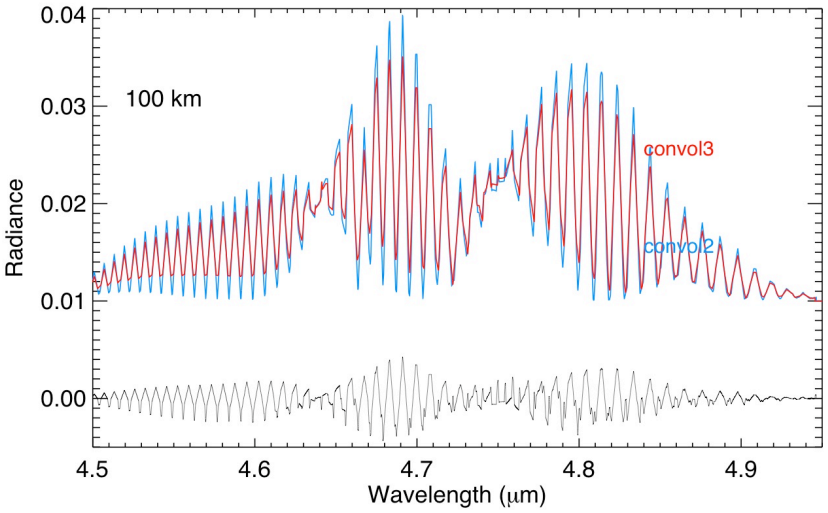

Figure 4.1: Effect of spectral resolution on a typical CO spectrum. Two spectra are shown, for convolutions with 1.7 cm^{-1} (blue spectrum) and 2.0 cm^{-1} (red spectrum).

Carbon monoxide and temperature in the upper atmosphere of Venus from VIRTIS/Venus Express non-LTE limb measurements

G. Gilli[a], M. A. López-Valverde[a], J. Peralta[b], P. Drossart[c], G. Piccioni[d]

[a] *Instituto de Astrofísica de Andalucía-CSIC, Glorieta de la Astronomía, Granada, Spain*
[b] *Observatório Astronómico de Lisboa, Tapada da Ajuda / 1349-018, Lisboa, Portugal*
[c] *LESIA,Observatoire de Paris, 5 place Jules Janssen, Meudon, France*
[d] *IASF-INAF, via del Fosso del Cavaliere 100, Rome, Italy*

Abstract

The upper atmosphere of Venus from 100 to 150 km seems to play a transition region in photochemistry, dynamics and radiation, but is still very poorly constrained observationally. The difficulty of its remote observation can partly be overcome by improving the measurements of the strong fluorescence emissions of some atmospheric species, a type of non-local thermodynamic equilibrium (non-LTE) situation that occurs at the low densities of the upper atmosphere during daytime. Since 2006 VIRTIS on board Venus Express has been obtaining limb observations of CO_2 and CO fluorescent infrared emissions in that altitude range in a systematic manner. This work is intended to exploit this dataset and to derive new information on the composition and temperature of the upper mesosphere and the lower thermosphere of Venus. The work is focused on the 4.7 μm emission of CO, which is shown to consist of two emission bands, the fundamental and the first hot of the main CO isotope. With the help of a non-LTE comprehensive model of this molecular emissions, a specific scheme for simultaneous retrieval of CO and of temperature is proposed. A forward model containing such non-LTE model is used at the core of an inversion scheme that consists of a minimization procedure of model-data differences, as a first step, and as a second part, of a linear inversion around the solution of the first step. The error analysis shows that the retrievals of CO and temperature are very noisy but can be improved by suitable averaging of data, consistent with the non-LTE nature of the emissions. Unfortunately the data binning process reduced the geographical coverage of the results. The retrieval results indicate a global distribution of the CO in the Venus dayside with a maximum around the subsolar point, and a decrease of a factor 2 toward the terminator. No morning to afternoon gradients are observed, nor latitudinal variations except those similar to the local time gradient. This supports a CO distribution controlled by dynamics in the lower thermosphere, with a sub-solar to anti-solar gradient. The thermal structure obtained presents a mesopeak around 115 km, in the early morning but not at noon. The presence of this mesopeak was also found by SPICAV measurements in the night and near the terminator. The variations in temperature suggest a mechanism different to the dynamical control of the distribution of CO and also inconsistent with an upper mesosphere in purely radiative balance.

Key words: Venus, upper atmosphere, remote sounding, CO, thermal structure, non-LTE

1. Introduction

The Venus upper mesosphere and lower thermosphere (~ 90 -150 km) constitutes a transition region between the zonal rotation of the lower atmosphere (below 70 km) and the sub-solar to anti-solar circulation of the thermosphere (above 100 km). It is claimed to be an important photochemical source region for the whole atmosphere (Clancy et al., 2008) and it is more variable than previously thought (Drossart et al., 2007; Brecht et al., 2011)

It is notorious that satellite and ground-based observations of the mesosphere and thermosphere of the planet (70-180 km) are both very limited in spatial and temporal coverage, and that in-situ measurements either from balloons or during the periapsis of satellite orbits are also very scarce (Carlson et al., 1992; Clancy et al., 2003, 2012; Lellouch et al., 1997; Bertaux et al., 2007). In the early 80s Pioneer Venus Probes and Orbiter provided a first-order examination of temperature and composition of the upper atmosphere, paving the way for the Venus International Reference Atmosphere (VIRA) model (Seiff et al., 1985; Keating et al., 1985). However, those observations were too restricted in local time (sunrise and midnight) and space to characterize proper averages of the diurnal or vertical behaviors of the atmospheric structure above 90 km (Clancy et al., 2003).

Temperature, carbon monoxide (CO) and wind measurements gathered in the past 30 years, together with model simulations with the Venus Mesosphere and Thermosphere General Circulation Model (VTGCM) have shown that CO, among other minor atmospheric constituents, is a good dynamical tracer in the upper atmosphere of Venus (Irwin et al., 2008; Gurwell et al., 1995; Clancy and Muhleman, 1991; Clancy et al., 2012; Bougher et al., 2006).

A number of investigations in the past, especially from millimeter-wave observations (Kakar et al., 1976) focused on the horizontal and vertical distribution of carbon monoxide and showed that the CO mixing ratio increases with altitude in Venus' mesosphere. According to photochemical models, it is produced at equatorial and mid-latitudes in the upper atmosphere during dayside by UV photolysis ($\lambda < 224$ nm) (von Zahn et al., 1983; Huebner et al., 1992), then it is thought to be transported toward the poles by the planet's Hadley circulation, and also rapidly transferred to the nightside by strong zonal winds (Irwin et al., 2008). Night side observations indicate substantial temporal and spatial variability in the mesosphere around 65-70 km, at the cloud tops (Irwin et al., 2008), and between 75 and 105 km (Clancy et al., 2012). However, the observational record of CO remains incomplete in spatial coverage, particularly on the day side and at altitudes above 100 km.

Those upper regions are also poorly constrained in terms of key physical properties such as temperatures and winds (Sonnabend et al., 2011). Regarding the temperature, the observed thermal structure responded to convective and radiative processes up to about 90 km, as expected (Lellouch et al., 1997; Crisp and Titov, 1997) but showed peculiar latitudinal variations with a positive gradient towards the poles in the region

between 70-90 km (Newman et al., 1984; Irwin et al., 2008). According to the VIRA profile the temperature presents a constant decrease with altitude from cloud top values of 240 K to 170 K at 90 km altitude, with it follows an increase with altitude above 120 km on the dayside of Venus. Temperature measurements of 189 ± 8 K and 257 ± 16 K were obtained by Crovisier et al. (2006) at two layers, 100-110 km and 125-145 km respectively, from the rotational distribution of the CO bands in 4.7 μm.
However, since the arrival of Venus Express (VEx) in 2006 both satellite and ground observations showed that the VIRA model is incomplete and that the situation is far more complex, including inversion layers at various altitudes and temporal changes on different time scales (Pätzold et al., 2007; Sonnabend et al., 2008, 2010; Drossart et al., 2007).
The mesospheric temperature retrieved by Sonnabend et al. (2010, 2011) with IR heterodyne high resolution measurements and associated to altitudes of 110 ± 10 km (López-Valverde et al., 2011), showed strong local time and latitude dependence. They found higher temperatures (about 250 K) at the sub solar point and values of 160 K close to the terminator and near the South pole. Those values disagree with VIRA reference predictions but they are consistent with earlier measurements from 2007 (Sornig et al., 2008) and with SOIR-SPICAV profiles (100-120 km altitude at terminator) (Mahieux et al., 2010).
Millimeter and sub-millimeter CO absorption lines also allow temperature profile retrievals over 75-115 km, indicating spatial and temporal variations in vertical and horizontal transport across the nightside upper atmosphere of Venus (Clancy et al., 2003, 2008, 2012). The symmetric zonal and SS-AS circulation of the thermosphere could be responsible of the the short-time scale variations (weeks) they found during 2000-2009 campaign. Regarding daytime, two global profiles are also available up to 105 km, from measurements during 2000-2002 and 2007-2009, which correspond to solar maximum and minimum conditions, respectively (Clancy et al., 2012). They found a diurnal variation for temperature in the lower thermosphere in the 2007-2009 period half as large as during 2000-2002.
A compilation of the daytime kinetic temperature above 90 km retrieved so far is shown in Figure 1.

Two instruments on board VEx offered a great opportunity to increase our knowledge of CO density and temperature of the Venus upper atmosphere. First, SOIR-SPICAV on VEx (Bertaux et al., 2007) provided several density and temperature profiles up to 120 km by the solar occultation technique with an excellent vertical resolution (Vandaele et al., 2008; Mahieux et al., 2010). Secondly, VIRTIS channels sounded during day and night, in nadir and limb geometries, the spectral region around 4.7 μm dominated by the strongest ro-vibrational CO bands in the IR. Regarding the night side, VIRTIS observations of the absorption of CO at 4.7 μm have been used to investigate the distribution of this gas just above the cloud tops (Irwin et al., 2008). During the day and above 100 km altitudes, those CO bands are affected by non-LTE processes (Dickinson, 1972), with a strong solar enhancement, which permits their detection up to the thermosphere (Gilli et al., 2009, 2011). However, this is also a further difficulty for their analysis, requiring the development and the use of sophisticated tools and specific non-LTE models.
The first analysis of the non-LTE CO limb emission observed by VIRTIS during day-

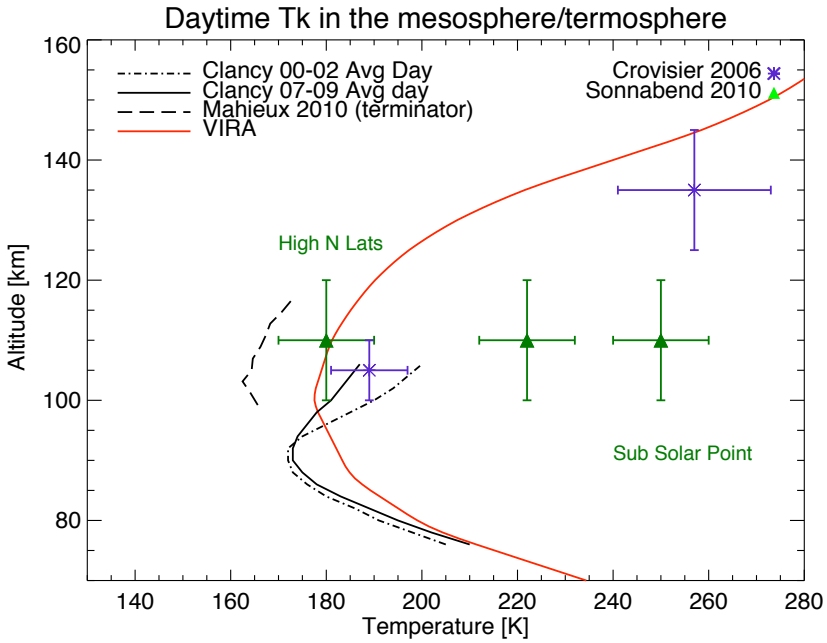

Figure 1: Upper mesospheric/lower thermospheric temperature from the recent measurements, together with the daytime VIRA reference profile (red solid line) for comparison. Daytime average profiles from sub-millimiter CO observations (Clancy et al., 2012) over 2000-2002 and 2007-2009 periods are in dash-dot black and solid black lines, respectively. One profile from SPICAV/SOIR (orbit 341) solar occultation (Mahieux et al., 2010) is plotted with dashed line. Temperature and error bars from ground-based observations by Sonnabend et al. (2010), around midday, are indicated with triangles, for the sub-solar point, mid-latitudes north, and high north latitude. Blue asterisks represent the temperatures form ground-based CO observations at 4.7 um by Crovisier et al. (2006).

time were performed by (Gilli et al., 2009, 2011) (hereinafter referred to as GEA09 and GEA11). They showed the potential of VIRTIS data to retrieve atmospheric parameters like densities and temperature up to high altitudes. GEA09 showed that the rotational structure of the CO band at 4.7 μm can be clearly identified in the VIRTIS higher resolution spectra. Also, depending on the altitudes the individual contributions from the CO (1-0) fundamental band (FB) and from the (2-1) first hot band (FH) can be discerned with the help of the non-LTE model (GEA11).

The objective of this work is two-fold. First, to carry out the analysis of the daytime IR signal observed by VIRTIS around 4.7 μm and its variability, with a focus on the understanding and characterization of this dataset . Secondly, to perform a joint retrieval of T and CO in the altitude range 100-150 km. The first task can be seen as a continuation of previous works by by López-Valverde et al. (2007) and GEA11, but extended now to a larger dataset and intended to further validate the non-LTE models and to understand the main features of the emissions. The second task is a truly new

step further, since a specific non-LTE inversion scheme for these VIRTIS-H measurements has been developed and a simultaneous retrieval of atmospheric temperature and CO abundances above 100 km in the Venus upper atmosphere has been performed. To clarify the nomenclature, in this work we refer to the upper mesosphere as the altitudes between 90-120 km, and to the lower thermosphere as the 120-150 km region.

The paper is organized in 5 main sections. Section 2 describes the instrument and the measurements used in this work; the non-LTE model simulations and the retrieval method are discussed in Section 3; and Section 4 is focused on the retrieval results and the comparison with previous studies. The conclusions are presented in Section 5.

2. VIRTIS-H observations

The main characteristics and technical specifications of the instrument VIRTIS (Visible and Infrared Thermal Imaging Spectrometer) on board Venus Express (VEx) have been described elsewhere (Piccioni and VIRTIS/Venus Express Team, 2009; Drossart et al., 2007; Titov et al., 2006). Let us recall here that VIRTIS is a dual instrument consisting of two channels VIRTIS-H and VIRTIS-M, the former being a high resolution echelle spectrometer (R $\sim$ 1200) with a spectral range in the infrared 1.8 - 5.0 μm, and the latter a mapping spectrometer working in the visible (0.27 - 1.1 μm) and in the IR (1.05 - 5.2 μm), with moderate spectral resolution (R $\sim$ 200).
This work is focused on the limb observations from VIRTIS-H, due to its higher spectral resolution, which makes it more suitable for joint temperature and CO retrievals. Besides, daytime VIRTIS-M data are excluded from this analysis because most spectra with $\lambda > 4.5$ μm showed an unexplained increasing emission toward the end of the spectral order, possibly related to some instrumental effect, still unresolved. Specifically, measurements taken during about 4 years (nominal and extended mission, 4 June 2006 to 2 October 2007 and until the end of 2010, respectively) have been used in this study. This basically represents the whole available dataset in the limb of the planet.
During that period, the pericenter of the very eccentric VEx orbit was located approximately above the north polar region at altitudes between 200 and 300 km above the ground, and the apocenter was above the south polar regions, reaching about 65000 km. For this reason, the instantaneous field of view (IFOV) of VIRTIS-H, which is 0.567 x 1.73 *mrad* (Drossart et al., 2007), projected onto the limb of the planet, changes dramatically along the orbit. It varies from few kilometers to dozens of kilometers, as the satellite moves from periapsis to the apoapsis. This variation is illustrated in Figure 2 (top-right panel), where the crosses represent the actual field-of-view (FOV) of the VIRTIS-H observations selected in this study. Those measurements are the extension of the data-set used by GEA9 and GEA11 and correspond to daytime (SZA between 0 and 90) limb measurements above the clouds layer (tangent altitude $\sim$ 70 km). The altitude-SZA distribution is also shown in Figure 2 (top-left panel). For retrieval purposes, to better constrain the information coming from the emission layer, only measurements with FOV smaller than 5 km have been selected (red asterisks in the figure). Notice that most of the data with FOV less than 5 km correspond to high SZA. Unfortunately, most data with SZAs lower than 50^o (higher solar illumination conditions) were usually taken very far away from the planet.
We also represent the geographical distribution of the data in latitude-tangent height

and local time-latitude maps in the bottom panels of Figure 2. Those panels show that limb observations in the southern hemisphere are very scarce, and most of the data between 10º and 30º latitudes have large FOV (> 5*km*). This is also due to the pointing strategies of VIRTS and VEx, being the mapping of the Venus disk carried out typically upon the southern region in nadir geometry, to obtain global observations from the apoapsis ("mosaic construction").
The correlation in the data distribution between latitude and SZA is not shown in the figure, but can be derived from the combination of latitude and local time. Northern latitude observations correspond to lower solar illumination condition (SZA 50º-90º) and equatorial latitude correspond to high solar illumination condition. This is a consequence of both the orientation of the satellite orbit mentioned above, and the orbit of Venus itself, almost perpendicular to the ecliptic plane (Drossart et al., 2007; Titov et al., 2006).
Let us recall that VIRTIS-H did not scan the atmosphere to obtain vertical profiles. Given the peculiar mode of operation of the instrument in the limb and with variable observing opportunities within the VEx observational strategies, most of the limb data correspond to single spectra in local time, space and tangent altitude, with no particular connection with the next acquisition. Only some orbits do correspond to a continuous acquisition of spectra in time, typically close to the periapsis, during an inertial-mode pointing of the limb, at whatever tangent altitude. These orbits can be clearly identified in Figure 2, by the parabolic-like line of crosses. Still, these sequences do not correspond to real vertical profiles, since the sub-track of the VIRTIS pointing along the limb draws a line of thousands of kilometers over the planet. However, limb-tracking orbits were also performed at the end of the mission, and they can be identified in the figure by the vertical line of crosses. Most of them were taken during nighttime conditions or near the terminator, but a few of them are also available for daytime conditions, especially in the equatorial region.
Figure 2 (left-bottom panel), shows different types of orbits, with most of the inertial limb cases occurring at high northern latitudes, near the periapsis. These orbits offer sometimes the best vertical sampling, ranging from 10 m to a few kilometers.

VIRTIS-H data are subdivided in 8 spectral orders of 432 elements, covering the wavelengths from 1.88 to 5.03 um (Drossart et al., 2007; Cardesín Moinelo, 2010). In this work we used order #0 covering 4.01 μm- 5.03 μm (2000-2500 cm^{-1}, approximately), where the strong non-LTE limb CO emission is observed. Typical VIRTIS-H spectral resolution is around 1 cm^{-1} but it varies along the spectral range and also within each spectral order, being higher at the lower wavelengths of each order. In the spectral range of our interest (4.5 μm- 4.9 μm) the resolution is about 2 cm^{-1} and the sampling step is around 1 cm^{-1}. The exposition time of VIRTIS measurements varied throughout the mission and this affects the noise equivalent spectral radiance (NESR). At the centre of the CO fundamental band, around 4.7 μm, measurements with 1 sec integration time have a NESR ~2.5e3 [μW m^{-2}sr^{-1} μm], and about a factor 2 higher for 250 msec integration (Grassi D. personal communication). The signal-to-noise (S/N) of the spectra analyzed in this work typically varies from values lower than 10 to about 20 for integration times of 250 msec and 1 sec, respectively.

As reported in previous work (GEA09, GEA11) VIRTIS-H spectral resolution allows to identify clearly the ro-vibrational structure of the main CO bands contributing

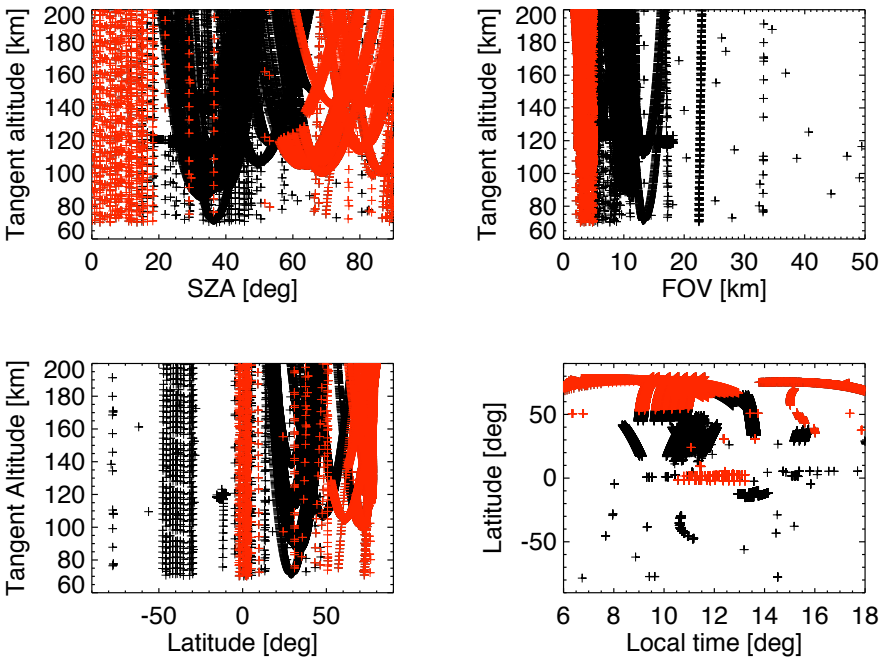

Figure 2: Distribution of the set of VIRTIS-H limb daytime observations used in this work: SZA *vs.* Tangent altitude (top-left panel); FOV *vs.* tangent altitude (top right panel); Latitude versus tangent altitude (bottom-left panel); Local time versus latitude (bottom-right panel). Red crosses represent measurements with FOV smaller than 5 km.

to the emission around 4.7 μm: the fundamental band (FB) ($1 \rightarrow 0$) and first hot band (FH) ($2 \rightarrow 1$) of the main isotope $^{12}C^{16}O$. Comparison with simulated non-LTE emissions by other CO bands, hot and isotopic, confirms that no other components are present in the spectra, with the averages studied in this work. The FB dominates the spectra at tangent altitudes above 140 km and the FH characterizes the CO strongest emission lines below those altitudes (see Figure 1 in GEA11). The lower the altitude of the limb pointing the larger the contribution from the optically thinner FH band. In other words, the shape and the intensity of the spectra changes with altitude (see Figure 7 in GEA11).

A typical VIRTIS-H spectrum at 4.7 μm, from an average of data at tangent altitudes between 100 and 110 km, is shown in Figure 3 (upper panel) with its standard deviation. The measurements were extracted from a single orbit, close to periapsis (day #712, cube #2) during high solar illumination conditions (SZA 25º-45º, local time 10-11h) and latitudes 20º-50º N. The integration time for these spectra was 250 ms. In the lower panel, the vertical variation of these radiances at five different wavelengths, from 85 to 150 km, is also plotted.

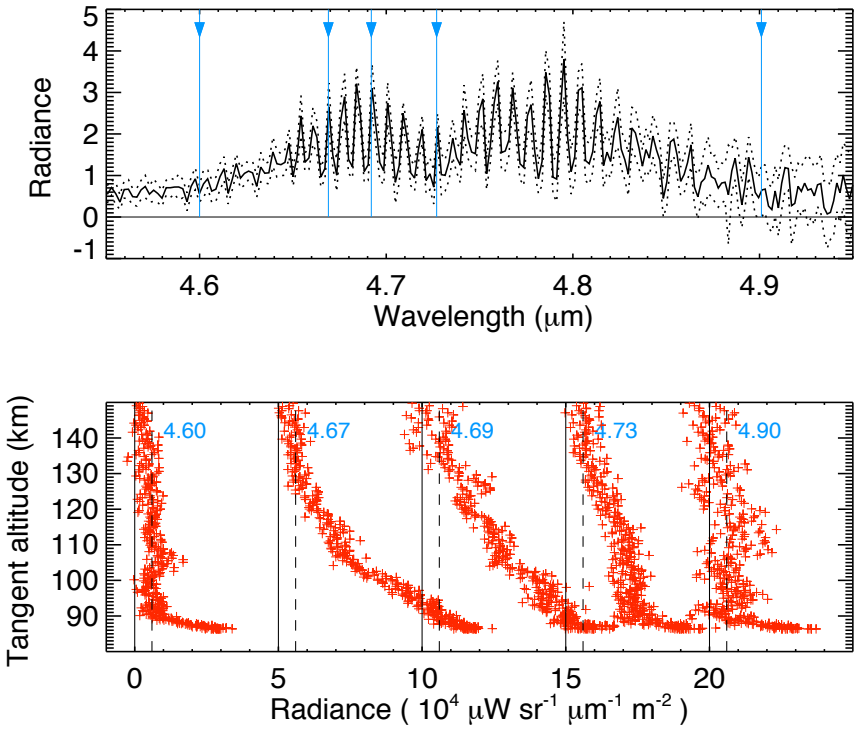

Figure 3: Top panel: VIRTIS-H average spectrum (solid line) between 100 and 110 km, with SZA 25°-45°. The standard deviation is also plotted (dotted line). The triangles mark the position of the VIRTIS-H wavelengths selected in the lower panel. Bottom panel: CO radiance profiles at five selected wavelengths extracted from 361 individual spectra in the altitude range 85 to 150 km during orbit 712. The nominal noise level is indicated with dashed lines. The radiances at 4.60 ad 4.90 μm represent the short and long wavelengths wings of the CO emission, respectively. The wavelengths at 4.67 and 4.73 μm are at the centre of the fundamental and the first hot band, respectively, and the line 4.69 μm is the result of the overlapping of FH and FB lines.

The long wavelength edge is noisier than the short wavelength region of the spectrum, as clearly seen by comparing the profiles for the extreme wavelengths 4.6 and 4.9 μm. The standard deviation increases with wavelengths in a similar manner than the noise and therefore, it may not indicate a real atmospheric variability within the selected spectra. The wavelengths at 4.67 and 4.73 μm are at the centre of the FB and the FH bands, and therefore they correspond to "pure" lines of the FH and FB bands, respectively. Both have strong emission up to the lower thermosphere. Another difference between them is the slope of the vertical variation, much larger in the FH line. The FB shows a nearly constant value through a large range of altitudes, in line with optically thicker conditions. Around 4.69 μm there is a "mixed" line, the R2 of the FH and the

P4 of the FB coincide, and the profile seems to present both features: a strong slope below 120 km and a smaller slope above. Strong overlapping also occurs in the nearby lines and in another region, around 4.80-4.83 μm, with a closest coincidence between the P11 line of the FH and the P16 line of the FB.
The strong emission below 95 km and the absence of a clear peak seems common to all wavelengths. This may be partly due to the scattering from the layers below 90 km, which seems present at all wavelengths. This conclusion is fully consistent with GEA09 and GEA11 results, obtained with a smaller amount of data.

All these results will be compared to non-LTE model simulations in the next section.

2.1. Data averaging

The behavior of the retrieval depends on several factors, and one of the most important is the S/N of the data. VIRTIS-H measurements are usually noisy in the spectral region around 4.7 μm, and to overcome this situation a large effort was devoted to obtain suitable averages.
The final dataset used for the CO and temperature non-LTE retrieval is a subset of all the VIRTIS-H limb spectra available from the whole mission (from day/orbit 1 to day/orbit 1435). The criteria for rejecting some spectra are discussed next. First, line-of-sight (LOS) pointing below 100 km and above 170 km have been excluded from the retrieval, to avoid possible scattering effects from the lower layers and for signal-to-noise ratio limitations, respectively. Second, we only selected daytime limb measurements with small FOVs (less than 5km), since larger FOVs produced larger standard deviations, due to the altitude variation of the radiances. This imposed a severe restriction on the number of the analyzed spectra: only the half of the about 9900 daytime limb spectra between 100 and 170 km fulfilled this FOV condition. Due to the shape of the Venus Express orbit described in section 2, this selection corresponds to a particular distribution of data in terms of latitude, local time and SZA. Figure 4 shows a map of limb radiances at one particular wavelength in the μm region, versus Local Time and Latitude coordinates, in the altitude range between 100 and 110 km. This is typically the location of the data used for our retrieval. Notice that the distribution in SZAs and latitudes is strongly correlated (higher latitudes, higher SZA), and no measurements correspond to the southern hemisphere, where the FOV is typically larger. The distribution of the this dataset is scarce and patchy, and unfortunately similar at all altitude ranges.

Before applying the retrievals to the above mentioned selection of VIRTIS-H measurements, the spectra were averaged in boxes of SZAs, tangent altitudes, latitudes and local times. Since the non-LTE radiances strongly depend on the solar illumination conditions and altitude of the emission, the size of the boxes was selected taken into account these two parameters. Specifically, the following boxes were used: the altitude box size is 5 km, stepped every 2.5 km, and the SZA boxes are [0-30º], [30-45º], [45-60º], [60-70º], [60-70º], [70-80º], [80-88º]. Spectra with radiances above 3σ have been discarded from the averaging and the number of individual spectra in each box varies, from 20-30 spectra at lower latitudes and high SZA, to more than 200 spectra in the northern latitudes region, where limb measurements were much more frequent (see Section 2).

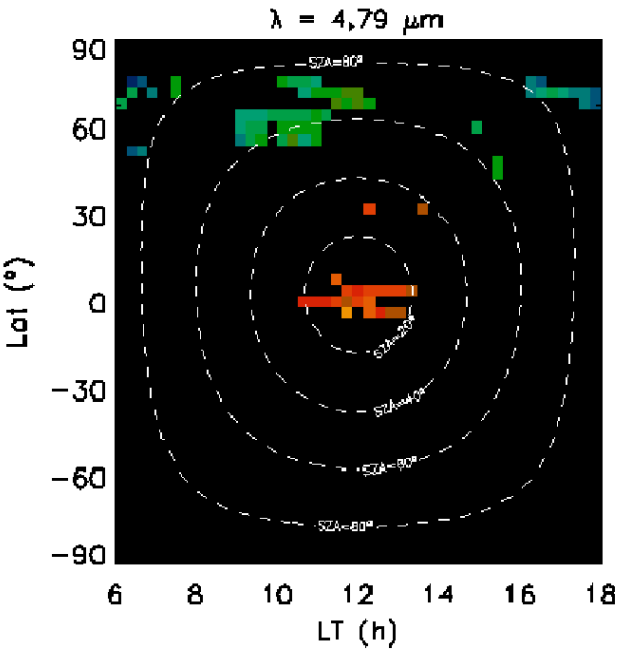

Figure 4: Location of the averages of VIRTIS-H limb daytime observations used for the non-LTE retrieval, between 100 and 110 km, in a Local Time (LT) versus Latitude map. The colors indicate the intensity of the radiance at 4.79 μm (red stronger, blue weaker). The SZA values (20^o 40^o, 60^o, 80^o) are also indicated with white dashed lines. The size of the boxing in LT and Latitude can be appreciated in the isolated points.

The total measurements uncertainty to be used in the retrieval was taken as the maximum between the standard deviation of the data and the "reduced" noise, or noise in the mean, at each wavelengths. As the number of data included in the bins increase, the standard deviation normally increases due to atmospheric variability but the reduced mean decreases with the square of the number of spectra.

3. Non-LTE retrieval method

The retrieval of CO abundances and temperature from the VIRTIS-H observations presents a challenging problem. First, the data are not actual 1-D profiles, but single measurements scattered in altitude, geographic and time domains, without a physical correlation between different sequential data acquisitions. Secondly, the emission contains a strong non-LTE component with contributions from different CO bands. This requires the use of a non-LTE forward model, properly implemented within the retrieval suite. This model also has to be used in the selection of data to build physically consistent averages of spectra (similar non-LTE features). Third, independent information on co-located temperatures or densities are not available from other VEx instruments,

and even the a-priori/climatological knowledge of CO above 100 km, especially during daytime is very scarce. Moreover, spectral contamination by clouds and aerosol particles is an important issue for the CO retrieval in the upper mesosphere and lower thermosphere (Titov et al., 2008).

The retrieval scheme used here was designed to tackle most of these difficulties. Others, like the scattering contamination of the lower mesosphere, are partially avoided by selecting spectra above 100 km.

Our retrieval method follows two steps. In the first one, a set of synthetic non-LTE spectra have been calculated, to obtain an approximate solution (let us call it *first-fit*), by minimization of χ^2 differences with the measured spectrum. In the second step, a linear inversion is performed around the previous solution (used as reference state) to obtain the *best-fit*, following the optimal estimation formalism (Rodgers, 2000).

Next we describe the forward model, the set of synthetic spectra and the behavior of the inversion code in some detail.

3.1. Non-LTE simulations

The forward model used here contains 2 modules. The first one is a non-LTE code for the populations of the CO vibrational states. The second uses those outputs and the information about instrument performance into a line-by-line radiative transfer code to compute the emerging atmospheric spectra.

Non-LTE models provide vibrational and rotational non-LTE populations for relevant atmospheric IR emitters, by solving iteratively the statistical equilibrium and radiative transfer equations with consideration of radiative, collisional and chemical excitation processes (Lopez-Puertas and Taylor, 2001). A description of the non-LTE population model for Venus was presented by Roldán et al. (2000) and López-Valverde et al. (2007), and an extended discussion of the CO vibrational temperatures calculated at typical geophysical conditions in the Venus upper atmosphere can be found in GEA11. Here we give a summary of those results. The most important processes affecting the CO 4.7 μm emission on Venus are radiative processes (spontaneous emission, absorption of solar radiation, and exchange of photons with the atmosphere) and also exchanges of vibrational excitation during collisions with CO_2. CO vibrational populations are largely controlled by absorption of solar radiation at 4.7 μm and 2.3 μm during daytime, leading to an important enhancement of the 4.7 μm CO emissions of more than an order of magnitude compared to LTE or nighttime conditions. The solar pumping at 2.3 μm, which populates the level CO(2), is about 1.6 times larger than at 4.7 μm (GEA11), and consequently the vibrational temperatures for the CO(2) level are larger than those for CO(1) by approximately the same factor, as can be seen in Figure 5 (upper panel). As already noticed by López-Valverde et al. (2007), the effect of solar excitation during the day, that produces the strong departure from LTE is very pronounced above 90 km for CO(1), while the LTE breakdown for CO(2) vibrational populations occurs at lower altitudes. Those authors also studied the impact of the variation of the solar illumination upon the CO_2 populations, in the 4.3 and 2.7 μm regions, but not upon the vibrational populations of CO at 4.7 μm. This effect is shown in Figure 5 (upper panel). The kinetic reference temperature is plotted together with the vibrational temperatures for the excitation of CO(1) and CO(2) states at seven SZAs between 60 and 200 km altitude. The variation of the state populations with SZA is

about a factor 5 larger for CO(1) than for CO(2), only when SZA is near the terminator (SZA = 88). The maximum variation of the vibrational temperatures occurs between 100 and 160 km altitude for CO(1) state, and around 100 km for the CO(2). All this is consistent with the different optical thicknesses of the FB and FH bands.
In these calculations, as in previous studies with the Venus non-LTE model, a daytime reference atmosphere extracted from VIRA (Seiff, 1983; Hedin et al., 1983) was used.

Regarding the radiative transfer model to calculate the emerging spectra, in this work we used the Radiance Forward Model (RFM, Dudhia (2000)). It handles non-LTE populations as inputs (following Edwards et al. (1993)) and has been extensively validated in the Earth's atmosphere (von Clarmann et al., 2003). RFM is flexible in terms of observing geometries, including limb and nadir, and allows for convolutions with FOV of arbitrary shape. The calculations performed in this work were first computed at a very high spectral resolution, followed by a post-processing which convolved the spectra with the theoretical instrumental line shape (ILS) of VIRTIS-H (D. Grassi, personal communication) and sampled them at the actual VIRTIS-H wavelengths.
As previously obtained by López-Valverde et al. (2007) and GEA09, two key-parameters affect most he emerging radiances: the tangent altitude of the pointing and the SZA. At a given pressure level, the stronger the solar flux (lower SZAs) the higher the CO non-LTE emission (see Figure 5, bottom panel).

3.2. Non-LTE model validation

Model simulations by GEA11 predicted that the CO limb emission peak is located around 100 km tangent altitude, for the VIRA reference atmosphere, corresponding to the region where the FH bands become optically thin. Above that altitude the limb radiance decreases, following the decrease in density. This is shown in Figure 6, where a set of simulated profiles at selected VIRTIS-H wavelengths are plotted. This behavior is very similar to what is observed in Figure 3 at the same wavelengths.

A key parameter in non-LTE fluorescence studies is the SZA, and the variation with this parameter is usually an important validation task in the field. The variation of the CO measurements could not be tackled by GEA09, given the smaller amount of spectra studied at the time. Now it is possible to make proper averages of measurements in similar geophysical conditions and to study such a variation. In Figure 7 measured averaged radiances at a given wavelength (4.70 μm) are plotted together with error bars and model predictions, at three different SZAs. The averages were obtained from all the spectra used in this work, with FOV <5 km.
The accuracy of the agreement model-data obviously depends on knowledge of the actual thermal and density structure at the location and time of the observations, which are not available for VIRTIS.

3.3. Sensitivity studies

Several sensitivity studies have been carried out in order to characterize the forward model, to determine the altitudes and spectral regions containing the most useful information on the retrieval parameters, and to generate an appropriate set of synthetic spectra. The effects that perturbations in temperature and CO density have on the non-LTE population and on the simulated radiances have been investigated.

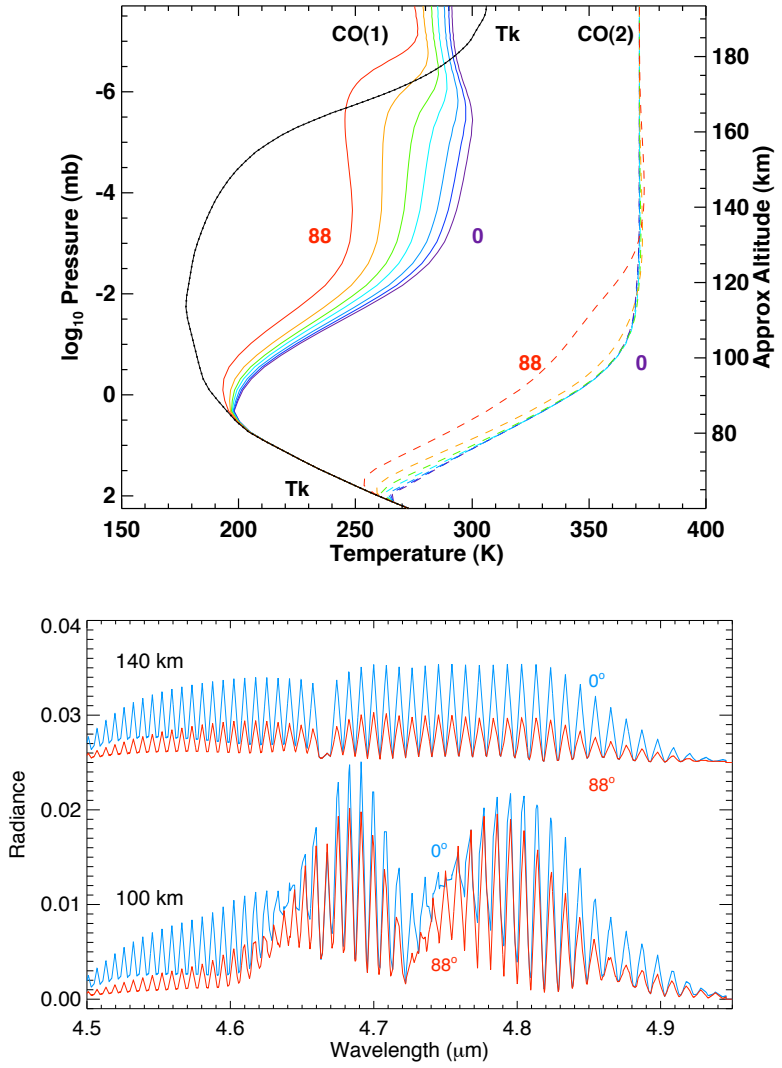

Figure 5: Top panel: Dependence of CO daytime vibrational populations on the solar zenith angle (SZA). Vibrational temperatures for levels CO(1)) and CO(2)) of the main isotope are plotted in solid and dashed lines, respectively. SZA values: 0º, 30º,45º, 60º, 70º, 80º and 88º. Kinetic temperature (black thick line) for the nominal (VIRA) atmospheric conditions is also shown as reference. Bottom panel: Simulated spectra at 140 km and 100 km altitudes, for SZA= 0º (blue spectra) and SZA=88º (red spectra).

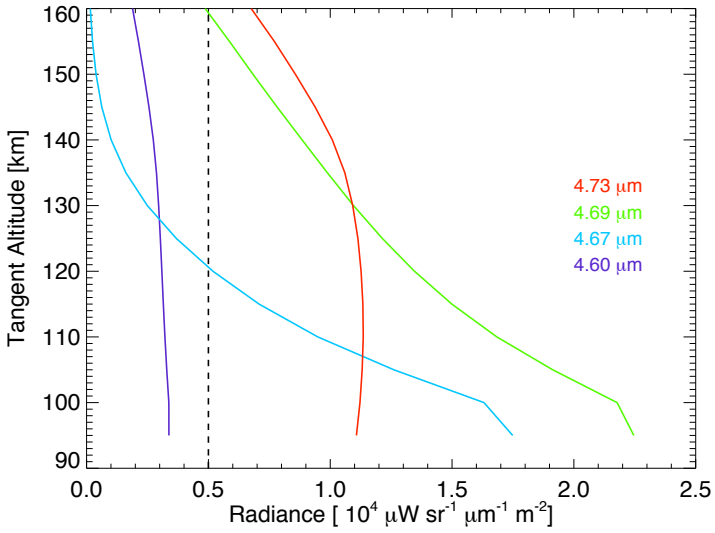

Figure 6: Simulated CO radiances profiles at 4 of the selected frequencies in Figure 3. The VIRA reference atmosphere for daytime conditions was used for these non-LTE radiance calculations. Dashed line: nominal noise of an individual VIRTIS-H spectrum.

Figure 8 shows some of these results in the form of vertical profiles of Jacobians. These correspond to changes in radiance at a given pointing altitude obtained by changing the CO abundance at all altitudes. Three Jacobians profiles are shown, for the three pointing altitudes of 100, 115 and 145 km. And they are shown at two wavelengths which represent the two basic behaviors through the 4.7 μmregion. The wavelength 4.73 μm indicates a FB line and 4.67 μm represents a strong FH line (R7 line) at the center of the FB, as can be seen in Figure 5. These jacobians show that for pointing at 100 km or below, the CO emission comes from layers above about 115 km, except for optically thinner spectral regions (i.e near the strong FH line at 4.67 μm) where the emitted radiation comes mainly from the tangent point. Although the layers below the emission peak also emit a small percentage of radiances, they did not contribute significantly to the observed radiances since they are below the line of sight. Optically thin conditions for the FB band are found only above 120-130 km (with the VIRTIS-H spectral resolution), and this is consistent with the bottom panels of the figure, where it is clear that the observed radiances come from the pointing altitude at the two selected wavelengths. In spite of the differences with wavelengths and altitudes, a general result approximately valid for all cases is that layers $\sim$ 20 km wide above the tangent point contains most of the emission in limb geometry with FOV of 5-10 km.

Figure 9 shows in more detail an example of perturbations of CO and kinetic temperature T_k in a 20 km layer located at 120 km and their impact on the vibrational

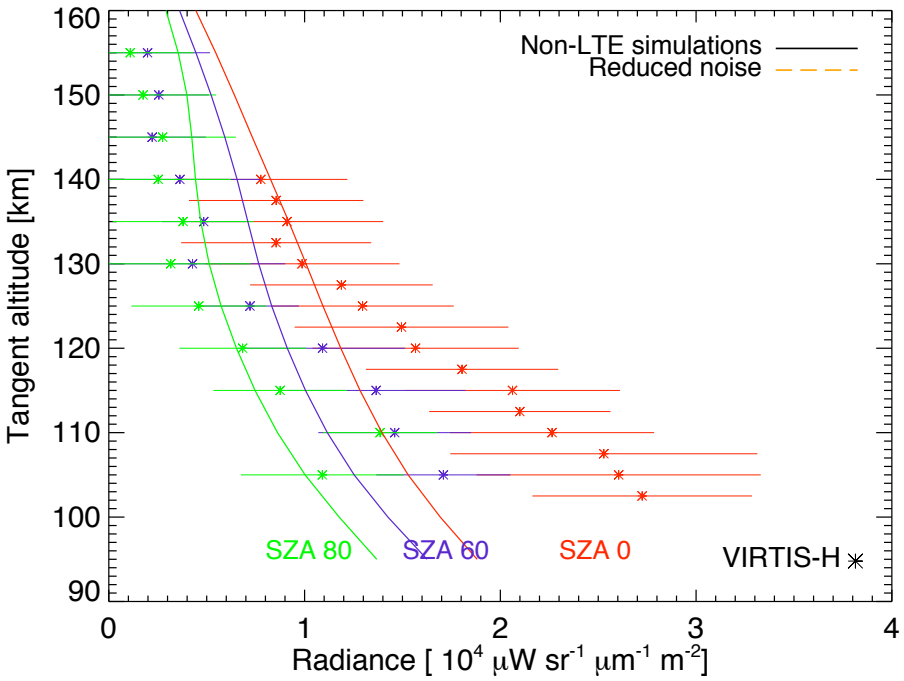

Figure 7: Variation of CO VIRTIS-H average radiances at 4.70 μm with tangent altitude and SZA, with error bars. Non-LTE simulations are also plotted for comparison. Note that the VIRTIS-H observations do not form actual 1-D vertical profiles. See text for details.

temperatures and on the emitted radiances. The increasing/decreasing of CO vmr by a factor 3 produces a small effect on the vibrational temperatures, at the most 2 K for the CO(1) state, and less than 1 K for the CO(2) state. A change of 30 K in T_k also barely affect the vibrational temperature of the CO(1) level (less than 2 K) and the impact on the CO(2) population is negligible.

The effect on the radiance is almost linear with the CO vmr (the more abundant is CO the larger the radiances) and not far from linearity for the temperature variations (a positive/negative increase of kinetic temperature produce a positive/negative variation of the synthetic radiances). Note that the CO spectra are sensitive to the abundance of CO through the strength of emission lines. However, the kinetic temperature influences the overall shape of every vibrational band. If temperature increases, the position of the maximum emission of the band moves from low J lines to higher J values (Hanel et al., 2003). However, the sensitivity of these radiances to temperature is very poor. Notice that such sensitivity in Figure 9 has been multiplied by a factor 10 to make it

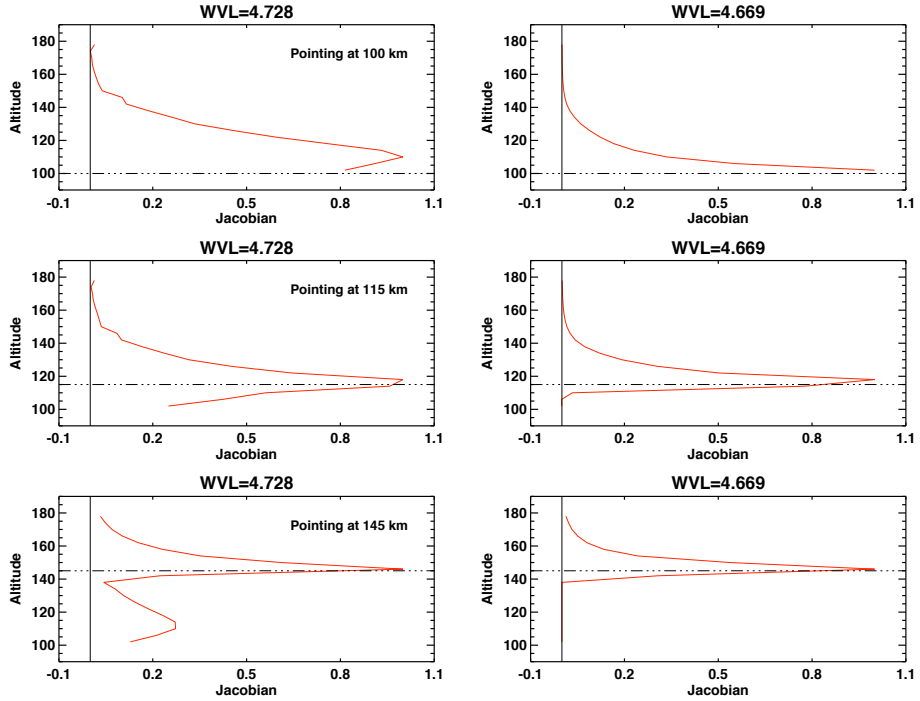

Figure 8: Normalized CO jacobian profiles for maximum solar illumination conditions (SZA= 0^o) pointing at 100 km altitude (top panels), at 115 km altitude (middle panels) and at 145 km altitude (bottom panels). The pointing altitude is indicated with an horizontal dashed line and the nominal noise level is also marked with vertical line. Each column corresponds to the sensitivity of the radiances at two different VIRTIS-H wavelengths: 4.728 μm and 4.669 μm, which are located around the centre of the FH band and a strong FH line, respectively. The maximum sensitivity of the CO radiances comes from a layer around 115-120 km and the region containing the maximum information of the unknown parameter is located about 20 km above the pointing altitude.

more visible. Large averages (i.e > 100 spectra) are required to increase the sensitivity to the temperature by a factor 10 and make them comparable to the sensitivity to the CO density.

3.4. Grid of pre-computed synthetic non-LTE spectra

The grid of synthetic radiances used into the retrieval code has been computed for a set of atmospheric conditions obtained by varying the two parameters to be retrieved, CO and temperature, in the VIRA reference atmosphere. The changes were applied in 13 altitudes, at 5 km steps between 100 km and 160 km, and extended to the 20-km-wide atmospheric layer just above each tangent altitude. That region contains most of the information from the limb emission, as described in the previous section.
The VIRA values of T_k and CO vmr are termed ”nominal” (thereinafter *Tnom* and

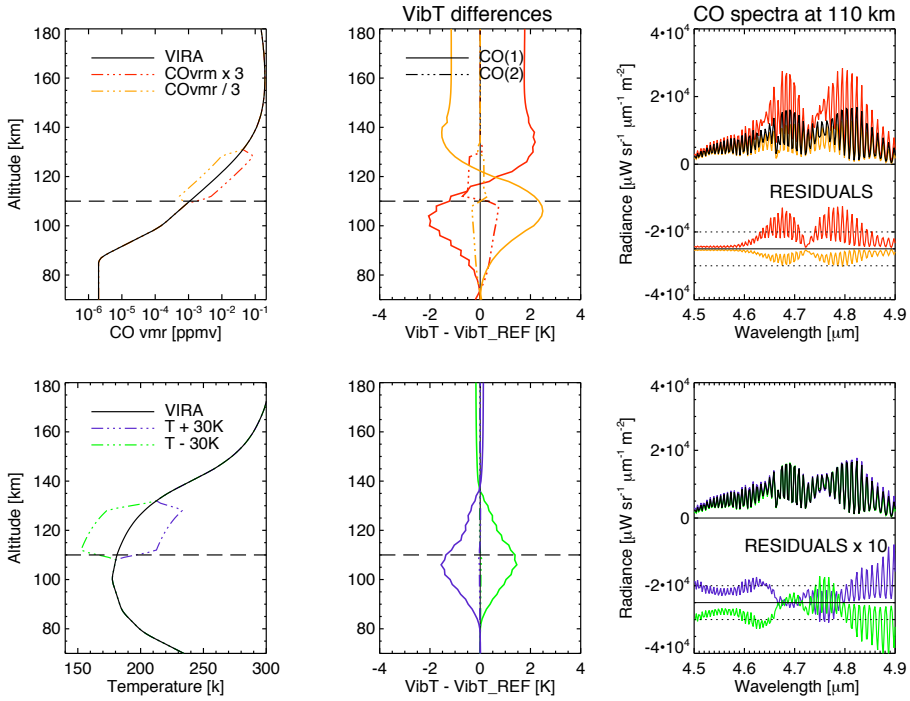

Figure 9: Left panels: VIRA reference profile (solid line) and perturbed profile (dashed-dotted lines) in a 20 km layer centered at 120 km altitude for CO vmr (top panel) and temperature (bottom panel). In this example, CO vmr has been increased/decreased by factor 3 and the temperature changed by ± 30 K. Middle panels: Impact of the changes on the vibrational temperatures for the CO(1) level (solid line) and the CO(2) level (dotted-dashed line) of the main isotope. Right panels: simulated VIRTIS-H non-LTE CO radiances at 110 km for VIRA (black solid line) and for the perturbed atmosphere (colored lines), as indicated in the legend. The residuals and the VIRTIS-H nominal noise level (dotted-line) are also indicated in each panel.

COnom, respectively), and the 2-D parameters grid consists of 9 different CO abundances and 7 different temperatures around the nominal case, at each altitude. The CO densities correspond to equidistant values in a log scale between *COnom*/9 and *COnom**9. In other words, 9 equidistant values of log (CO/COnom) between ± log(9) with step 0.238, which cover almost one order of magnitude up and down the nominal value. In temperature, the 7 equidistant values run between *Tnom* - 45 K and *Tnom* + 45 K, at 15 K steps. In addition to this, the radiances have been calculated for 7 values of SZA (0º, 30º, 45º, 60º, 70º, 80º, 88º), which correspond to an usual division in non-LTE studies. The total number of synthetic spectra in the grid is therefore 5733: 9(CO values) x 7 (Tvalues) x 7 (SZA values) x 13 (N layers). An alternative grid of radiances was also tested with similar extreme values, this one with 17 points in the CO space. The results of the retrieval were almost identical at all altitudes and SZA. This gives us confidence that a grid of 9 points in CO is enough for the present purposes,

and is also less computationally time-consuming.

3.5. Retrieval tests

Before applying the non-LTE retrieval method to VIRTIS-H measurements, several tests using synthetic spectra were carried out, in order to determine the overall behavior of the retrieval and an estimation of the errors propagation.

First, pure synthetic spectra obtained with the same forward model, but for different, arbitrary values of CO and temperature than the the ones used in the grid of pre-computed radiances were considered to test the convergence of the inversion. Secondly, a random component was added to the spectra, similar to the VIRTIS-H noise. In both cases, all wavelengths between 4.55 and 4.9 μm were considered during the χ^2 square "best-fit". Regarding the first test, the output of the retrieval was correct, within a margin smaller than half the space between grid points, even after the first step of the retrieval. The *best-fit* or output of the second step of the retrieval, was almost coincident with the *first-fit*. Regarding the addition of noise to the spectra, this had a large impact, reducing the sensitivity and accuracy of the χ^2 fit. These aspects and the behavior of the retrieval can be illustrated in Figure 10 , which shows some insight into a typical retrieval using a real VIRTIS-H spectrum. The spectrum chosen here corresponds to an average of VIRTIS-H measurements between 107 and 112 km tangent altitude and SZA 0-22º. A total of 30 spectra were combined, spreading from 10ºS-10ºN latitude and 10-14h local time. In this case, the standard deviation is larger than the noise, except in the long wavelengths wings.

The panel # 1 in the Figure 10 shows the χ^2 obtained when comparing the measurement with the synthetic spectra subset at 110 km tangent altitude. The map covers the whole range of values of the CO-T_k grid, whose points are indicated with black crosses. The green area shows the region where the χ^2 minimum value is reached, which is also indicated with a green diamond. In this example, the values of CO vmr and temperature of the *first-fit* are 273,2 [ppmv] and 179,4 K, respectively. The width of this green area illustrates the sensitivity of the minimization to changes in CO and temperature, the smaller this region looks, the more sensitive to those changes and accurate the method is. The variation of χ^2 with CO shows a clear minimum, while the sensitivity to temperature is much worse. The shape of the χ^2 surface at the first-fit point is better illustrated in panels 3 and 4, where the CO and T sections of the surface are plotted. The green area extends for a wide range of temperatures. It is frequent in data fitting to estimate the uncertainty of the minimization method by measuring this "minimum χ^2 area".This poor sensitivity to temperature is a common feature of all our retrievals. The reason behind this difficulty resides in the large noise of these VIRTIS-H data, which makes the CO band structure highly unconstrained, and it requires large temperature excursions for significant changes in the shape of ro-vibrational bands.

The result of the second step of the retrieval, the linear inversion, is indicated by the pink square in panel # 1 of Figure 10. Another outcome of the matrix inversion is the retrieval error, shown with pink lines in panels # 1, 3, and 4 of the figure. This is a measure of the numerical propagation of the measurement uncertainty or noise (Rodgers, 2000). In order to evaluate the quality of the final fit, we included in our scheme an extra non-LTE forward model calculation using the best-fit values of CO and temperature. The best-fit spectrum is shown in panel # 5 of Figure 10 together with the measured

one, while the residuals, or difference between both are shown in panel # 6. In both panels the measurement uncertainty is also shown, so that the residual significance can be evaluated.

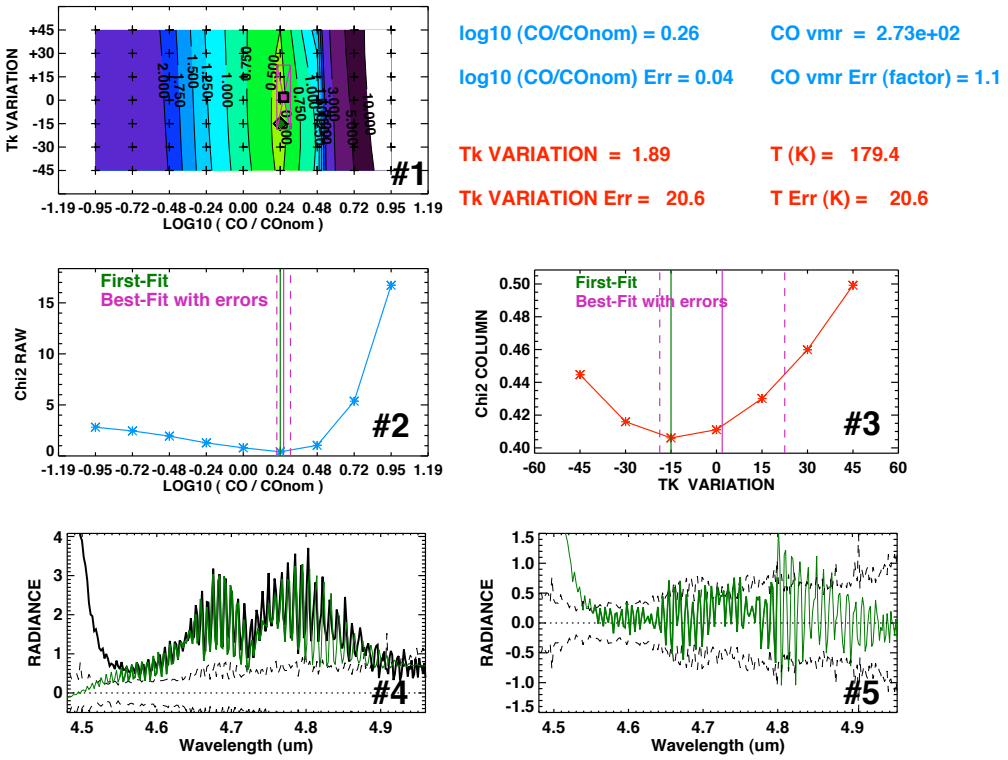

Figure 10: Example of non-LTE retrieval applied to a VIRTS-H average spectrum obtained between 107 and 112 km altitude, SZA 0º-20º, latitude 10ºS-10ºN and local time 10-14h. Left top panel: map of χ^2 covering the whole space of kinetic Temperature (T_k) and CO density of the synthetic radiances. The grid points are marked by crosses, and they represent the T-CO cases used in the simulations. The green rhombus marks "first-fit", or the point where χ^2 reaches its minimum; the pink square shows the result of the inversion, i.e the CO density and T_k obtained as best-fit, with their error bars. Central panels: sections of the χ^2 map at the first-fit point, showing the variation of χ^2 with CO (left panel) and Temperature (right panel). The first-fit and the best-fit are marked with vertical solid lines, and the retrieval errors are shown with dashed pink lines. Bottom left panel: Comparison of the best-fit spectrum (green line) with the VIRTIS data (black line). The dashed line shows the VIRTIS error level. Bottom right panel: Residuals (green line) or difference between the two spectra in the bottom left panel, compared to the VIRTIS noise level (dashed black line). The thickness of the spectra are increased to mark the spectral range actually used in the inversion, thin lines indicate data not used in the retrieval.

Since this scheme performs retrievals of temperature and CO, simultaneously, the initial strategy to build the error covariance matrix was to use the measurement's uncertainties in the diagonal of the matrix and null elements otherwise. In order to evaluate possible cross-correlation effects between the retrievals of CO and temperature, and

their impact on the retrieval error obtained, a set of test retrievals was carried out. These consisted in fixing one of the variables (CO for example) and changing the other (temperature in this case) running through all the values of the grid. In these calculations we considered realistic measurement noise, FOV and ILS, and used the same subset of wavelengths and retrieval parameters than in the nominal runs. The result of this numerical experiment demonstrates that the retrieval outputs of one of the two variables, were not much affected by the variation of the other. All CO values were very close to the correct solution, with a dispersion smaller than the retrieval error at all altitudes. At high altitudes, when the retrieval errors are very large due to very low S/N, the dispersion in the results were large, but still within the large retrieval errors. This result tells us that such a cross-talk between variables is minimal in this inversion method, and it justifies the initial approximation of using null values in the off-diagonal elements of the retrieval error covariance matrix.

3.5.1. Continuum background correction

During this work possible systematic effects which might produce residuals systematically larger than the measurement error were taken into account. One of the largest ones found was a systematic bias towards the longer wavelength edge of the spectral region of our interest, which produces measurements larger that the simulations, especially below 120 km. The residuals were sometimes larger that the noise by approximately a factor 2 at altitudes around 100 km. A systematic study of this offset showed that it decreases with altitude and becomes very small above about 130 km. A first candidate could be scattering from the clouds or hazes in the mesosphere, or some bias in the instrument performance. Several corrections were tested by adding blackbody curves at typical Venus mesospheric temperatures as well as solar photospheric values, with no success. Finally, we decided to apply an ad-hoc linear correction, between two values estimated near the edges of the spectral region, at 4.54 and 4.94 μm, so as to obtain a better match at these wavelengths. This correction is now part of the operational forward model but it is also a source of uncertainty in the retrieval outputs.

3.5.2. Wavelengths selection

The selection of the precise wavelengths to be used in the retrieval can be considered as an open parameter of the inversion method. The retrieval code allows for any set of wavelengths, and in principle, the larger the number of points, the better. However, test retrievals showed that the inclusion of noisy data (like the far wings) increased the retrieval error. We carried out tests using different subsets of wavelengths. The results showed that as far as the strongest lines of the FH band are included, and the distant wings excluded, not much difference exists in the outcome of the retrieval. The spectral region 4.55-4.80 μm was the one finally selected for retrievals at all altitudes, since it contains the strongest FH lines, which favours retrievals below 120 km, and also a significant amount of FB lines, which become relevant above 125 km. Beyond 4.8 μm the noise is particularly large, while the contamination from CO_2 non-LTE lines is very important around 4.45 μm, and both are conveniently eliminated with the chosen interval.

Figure 11 shows best-fits and residuals for arbitrary VIRTIS-H (averaged) spectra pointing at four different tangent altitudes. They include the background correction,

the selected subset of wavelengths, and the rest of nominal parameters of the retrieval. The strong non-LTE emissions by the 4.3 μm bands of CO_2 is clear at the low wavelengths edge, and the increase of the noise with wavelength is also clearly visible. As can be seen, some peaks of lines and valleys in between look more pronounced in the simulations than in the measurements, and this produces a spectrum of apparent lines in the residuals, but these are within the noise limit.

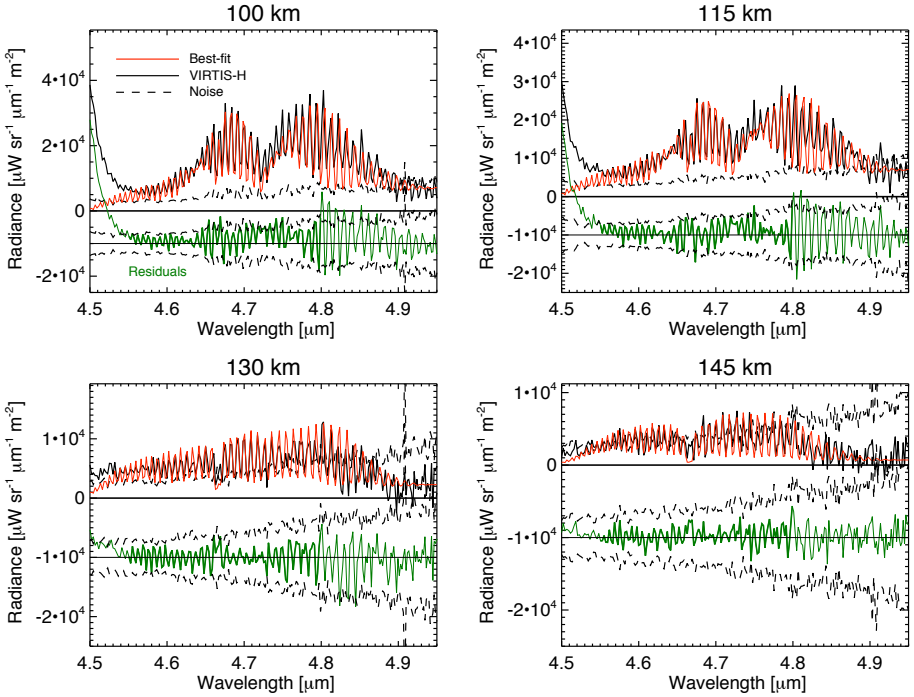

Figure 11: Examples of the spectral fit obtained during the simultaneous CO and temperature retrievals at four altitudes: 100 km, 115 km, 130 km and 145 km and for SZA 0-20º. For each altitude, VIRTIS-H average spectrum (black) is compared to the synthetic best-fit spectrum (red) line. The bottom part of each panel shows the residuals (observed - fitted radiances) in green, together with the noise level of the averages (dashed black lines). The thicker segment in the residuals represents the subset of wavelengths selected for the retrieval [4.55-4.80 μm].

3.6. Error analysis

In this work attention was paid to a number of uncertainties in the retrieval methodology and the impact of these uncertainties on the retrieved values, following the nominal retrieval scheme was evaluated. This was carried out by computing a number of sensitivity matrixes, of the form $\Delta(i, j) = \delta\hat{x}(i, j)/\delta x(i, j)$ where i, j denote different atmospheric layers, $\hat{x}$ is the retrieved value and x the other parameters.

Two main sensitivity matrixes were obtained, for two important parameters: the radiance and the true state vector. The former, is very useful to extend this error analysis to a large number of parameters or approximations in our method, since many uncertainties can be expressed or converted to an impact on radiances. The latter is also called Averaging Kernel matrix (AK) (Rodgers, 2000) and may be considered as an estimation of the vertical resolution of the inversion.

In order to test the application of this sensitivity matrix, we made a test by changing a few typical synthetic spectra by an amount similar to the measurement noise. The impact on the retrieval parameters was entirely similar to what the retrieval error suggested, which is given, as explained above, by the propagation of the measurement noise through the system. This propagation is therefore captured correctly by the matrix, and we conclude that the impact of the measurement noise is larger (more than a factor 3) on the temperature than the CO retrievals.

We present in Table 1 a selection of the most important parameters and their contribution to the total error. The different sources of uncertainty are very varied and contain random and systematic errors. We classified the major components into 3 groups: data handling, forward model and retrieval approximations. The measurement noise was left outside this classification to facilitate its comparison with the rest of the uncertainties. The total error is computed as the square root of the sum of the squares of all the individual contributions, including the systematic errors of unknown sign. One example of systematic errors of unknown sign is the uncertainty associated to the selection of the wavelength interval used in the retrieval, and mentioned in the previous section. This was evaluated with the difference between the nominal interval and another one, 4.62-4.80 μm, which excludes part of the FB wing. The change in the CO obtained with these two intervals, or with all pairs of intervals, is a systematic and variable difference, which depends on the pair of intervals chosen. Therefore it is treated as a random component.

As an example of the non-LTE complications arising in such an analysis, let us discuss the error component due to the reference atmosphere used in this study. The largest error may come from the assumption of the densities given by VIRA outside the altitude of actual sounding. Figure 9 illustrates a perturbation study which can be used to estimate this source of uncertainty. In that study the CO abundance was modified by a "moderate" amount, by a factor 3, around 120 km, and the impact on the vibrational temperatures of the CO(1) and CO(2) states, and on the simulated spectra at 120 km was shown and discussed. Although not shown in Figure 9, the change in the spectra when pointing at higher altitudes does not contain any component from the FH, since the vibrational temperature of the CO(2) states is unaltered, but contains a small component due to the small FB change observed. On the contrary, the spectra at altitudes below the perturbation altitude, contain basically a change of the form of the FH band. In the case o an increase of CO outside the altitudes studied, as in this example, the spectra are increased. The sensitivity matrixes were applied to these spectral changes to obtain the estimation of the contribution to the retrieval error at several altitudes below and above the sounding region (120 km), and summed up to obtain a total value for this component.

The resulting total error in the Table 1 contains, as its largest component, the measurement noise. Notice that the total error is about twice this term at 100 km, and

Sources		Type	Altitudes (km)			
			100	**115**	**130**	**145**
Measurement Noise		R	25	50	100	500
Data handling	Spectral Resolution	S	15	15	20	40
	Altitude Averaging	R	11	11	15	30
	SZA Averaging	R	4	4	18	100
	Total Data Handling		19	19	31	112
Non-LTE Forward Model	Rate coefficients	S	< 5	< 5	< 5	< 5
	Lower Boundary	S	20	20	5	5
	Total NLTE Forward Model		21	21	7	7
Retrieval Parameters	Size of perturb layers	R	30	30	45	90
	Reference atmosphere	R	10	10	15	30
	1-single layer perturbations	R	10	10	15	30
	Wavelength interval	R	10	2	20	25
	Total Retrieval Parameters		35	33	54	103
TOTAL ERROR			51	66	120	525

Table 1: Error components and total retrieval error, in percentage. The S and R types of error refer to systematic (of unknown sign) and random. Total error is obtained as the square root of the sum of the squares of al the contributions. When errors are estimated as smaller than an upper limit, this limit is used for its contribution. See text for details.

similar to it around 145 km. Other important contributions come form the size of the perturbation layers and the averaging of data into SZA and altitude boxes.

To compute the AK matrix we evaluated the response of the retrieval to a δ-function perturbation in the CO density profile. Specifically, we perturbed the CO density by a factor 3 at all altitudes, and the retrieval was performed at four pointing altitudes: 100, 115, 130 and 140 km. The raws of the matrix are shown in Figure 12, normalized to the peak at 115 km. The vertical resolution of the CO retrieval can be represented as the full width at half maximum of the averaging kernels. It is typically 10-15 km in the upper mesosphere (100-125 km) and slightly increases with altitude throughout the lower thermosphere. Higher AK values indicate a larger sensitivity to the CO abundance at the corresponding altitude. The maximum sensitivity is obtained for tangent altitudes around 115 km, where the FH strong lines become optically thin. It can be also observed a reduction of the vertical resolution when the sensitivity at the peak drops, showing a spread or redistribution of the information content within a wider atmospheric layer. Figure 12 also shows that the altitude of maximum information from the retrieval does not coincide with the actual pointing. The peaks of the AK profiles occur at approximately 10 km above the tangent altitude. This seems a bit smaller for pointings above about 125 km. These results are used in the discussion of the result in the next sections.

4. Non-LTE retrieval results

We present here the retrieval results for CO abundances and temperature obtained from a selection of VIRTIS-H data, as described in the next section. The results are presented as vertical profiles, although they do not correspond to actual 1-D structures,

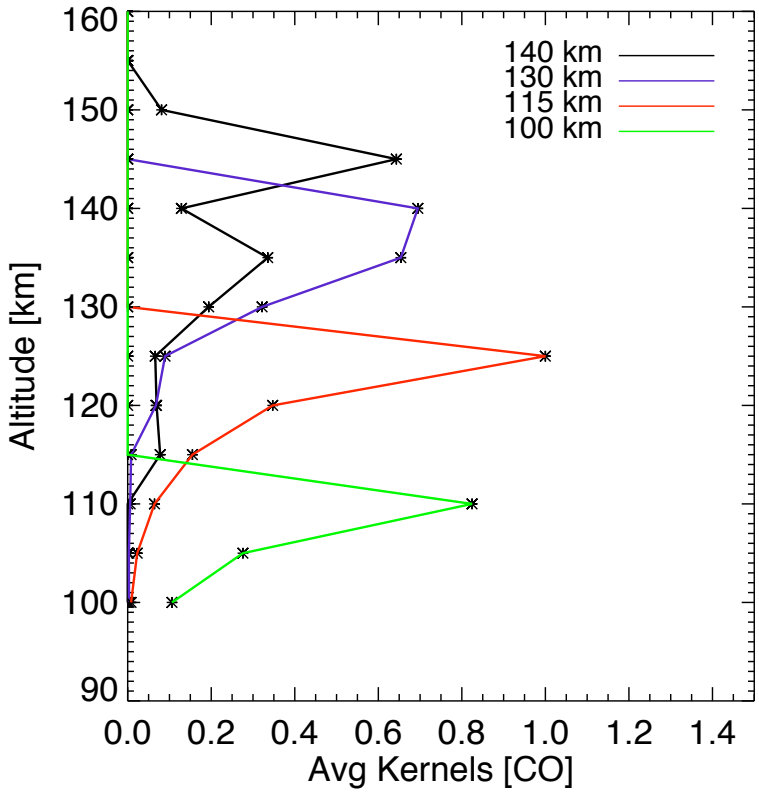

Figure 12: Averaging kernels of typical retrievals of CO densities at four sampling altitudes: 100 , 115, 130 and 140 km. The average vertical resolution is estimated as the full width at half maximum of the rows of each function.

as mentioned below. This facilitates their comparison with previous data and models. We payed special attention to the possible variations of the CO density with different geophysical parameters.

4.1. Carbon monoxide non-LTE retrieval

Figures 13 and 14 show the CO retrievals for a selection of boxes in latitude and local time, with the total error bars. The VIRA profile is shown for reference and two CO vertical profiles from SPICAV-Soir (Vandaele et al. 2008) are also plotted in the figures, for comparison. The data shown correspond to boxes in tangent altitude pointing every 2.5 km between 100 and 142.5 km, but have been displaced in altitude

following the vertical shift given by the Averaging Kernels as mentioned in the previous section. The vertical error bars, about 15 km at all altitudes, are omitted for clarity.
The right panel of Figure 14 shows the retrieval error obtained from the measurement noise after the inversion, as an illustration of the error propagation through the retrieval. This is an independent estimation of the measurement noise component, and basically agrees with the values in Table 1. This error component is usually smaller than 50 % below 120 km, but increases considerably with altitude above that layer as data become noisier.

The search for spatial and diurnal variation in the CO densities is difficult due to the irregular distribution of VIRTIS-H data. Regarding the latitudinal variation, Figure 13 shows the three latitude boxes [10°S-10°N], [50°N-70°N] and [70°N-80°N] for local times 10-14 h (left panel), and other three latitude boxes, [50°N-60°N], [60°-70°N], [70°-80°N], for local times 6-10h (right panel). These are the largest subsets of VIRTIS-H data that can be considered as optimal to tackle this issue.
The results for maximum solar illumination in Figure 13 indicate that CO densities decrease from equatorial regions to high latitudes. The decrease is around a factor two and is clearly observed at all altitudes. However, above 140 km this enhancement becomes doubtful, as it is within our larger error bars. Small variations of such enhancement with altitude below 130 km are also difficult to claim with the present dataset. This variation is smaller or inexistent (comparable to the retrieval errors) for local time 6-10 h, although the latitudinal bracket is smaller in this case, since no data for 10°S-10°N are available for this local time.
Regarding the local time variation, Figure 14 shows three CO density profiles during the morning, at noon and in the afternoon, between 55° and 75° N latitudes. No strong variations are observed, with the exception of a slight increase in CO density at noon, smaller than the size of the error bars at all altitudes. Considering the results in the two figures, it seems that the latitudinal gradient of CO appears to be confined to the local time around noon, and that no local time changes appear to exist at high latitudes. In other words, the gradient seems to exist between the sub-solar point and the terminator.

A comparison with a few recent results from other instruments on board VEx is possible. In particular SPICAV/Soir measurements provided reliable vertical CO densities (error bars < 6 %) between 100-120 km, and at high latitudes but at different local time than our data (during sunset). The two density profiles by SPICAV/SOIR shown in Figures 13 and 14 are about a factor 2 lower than VIRA, and VIRTIS results seem to be between the two. Considering the different local time and the VIRTIS error bars, there is a fair agreement between SPICAV/SOIR and VIRTIS. SPICAV/SOIR data are consistent with the small local time variation found with VIRTIS at these high latitudes, at least in the altitude range below 120 km.

4.2. Temperature retrieval

As described in section 3.3, CO non-LTE radiances at 4.7 μm are poorly sensitive to temperature variations. Most of the information about the temperature comes from the overall shape of the CO spectral bands, and high S/N measurements are needed. All VIRTIS-H limb measurements from June 2006 to November 2010 were considered and large averages were therefore used for the temperature retrieval. Figure 15 shows the temperatures retrieved in three selected boxes in latitude and local time

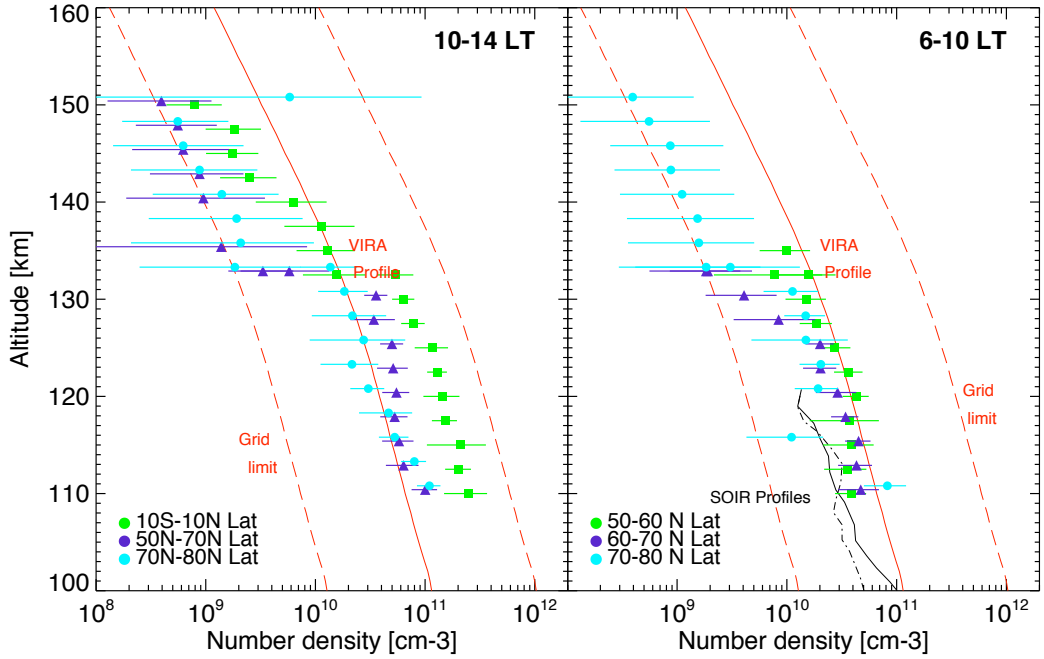

Figure 13: CO density retrieved from selected VIRTIS-H limb average measurements taken during 2006-2010. VIRA CO density (solid red line) and SPICAV-SOIR vertical profiles at 82°N (solid black line) and at 73°N (dashed black line) are also shown for comparison. Left panel: Local time between 10-14h and latitude 10°S-10°N (green squares), 50°N-70°N (purple triangles) and 70°N-80°N (light blue circles). Right panel: As left panel but for local time 6-10h and latitude boxes: 50°N-60°N (green square), 60°N-70°N (purple triangles) and 80°N-90°N (light blue circles).

[10°S-10°N] and [10-14h], [55°N-75°N] and [6-10h], [55°N,75°N] and [10-14h], respectively. Those boxes contain the largest number of available measurements needed to improve the S/N and increase the sensitivity to the temperature. The same vertical shift than for the CO retrieval has been applied to these data. Only results between 110 and 140 km have been plotted because the errors are very large especially above 130 km, where the uncertainty is larger than the size of our grid. Also, the retrieved temperatures at these altitudes are systematically outside the grid of synthetic spectra, which means that the code made extrapolations following the jacobians gradient. This is a risky mathematical solution, and these cases should contain extra uncertainties for this reason.

Despite the large errors, the temperature profile for local time [6-10h] presents a clear mesopeak between 110 and 120 km, while this is not present at noon, in none of the two selected latitudes boxes.

These results suggest that the temperature in the upper mesosphere does not follow

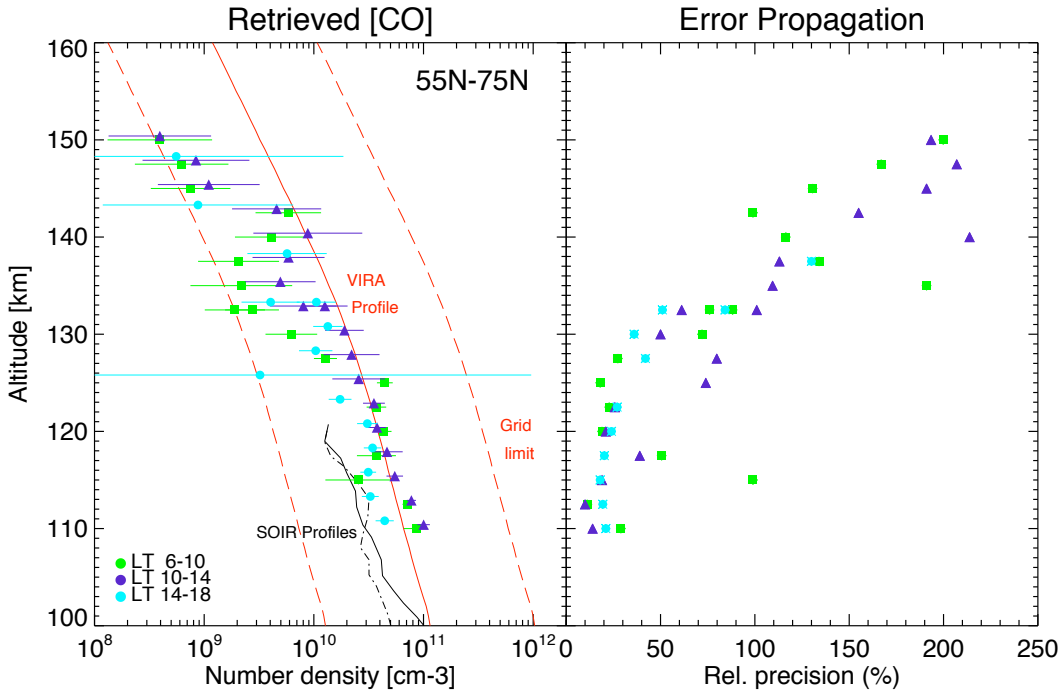

Figure 14: Same as Figure 13 but for a fixed latitude box [55°-75°N], and three local time boxes: green squares: local time 6-10h, purple triangles: 10-14h and light-blue circles: local time 14-18h. The right panel shows the typical measurement error propagation of the retrieval.

neither a clear latitudinal variation neither shows a SS-to-AS gradient, in contrast to the variation observed in the CO density. Unfortunately, the lack of VIRTIS limb data in the morning and in the afternoon in the equatorial regions makes it impossible to confirm this conclusion with more global data.

In the lower thermosphere between 120 and 130 km there is a local time variation at high latitudes, with higher temperature at noon. However, the temperatures at noon at the sub-solar point are colder, which is an unexpected result for a radiatively driven atmospheric layer.

We added a few results in Figure 15, from recent experiments and models, for comparison purposes. Regarding the VIRA reference values, our temperatures are consistent with them within the error bars below 125 km at noon, but not in the morning, when VIRTIS temperatures are warmer, with an increase of about 50 K.

Regarding the search for a mesopeak such as that reported by SPICAV (Bertaux et al., 2007), by ground-based observations (Sonnabend et al., 2010) (see Figure 1) and by the VTGCM (Brecht et al., 2011), and the most recent SPICAV/SOIR retrievals (A. C. Vandaele, personal communication) a mesopeak is indeed found with VIRTIS but at

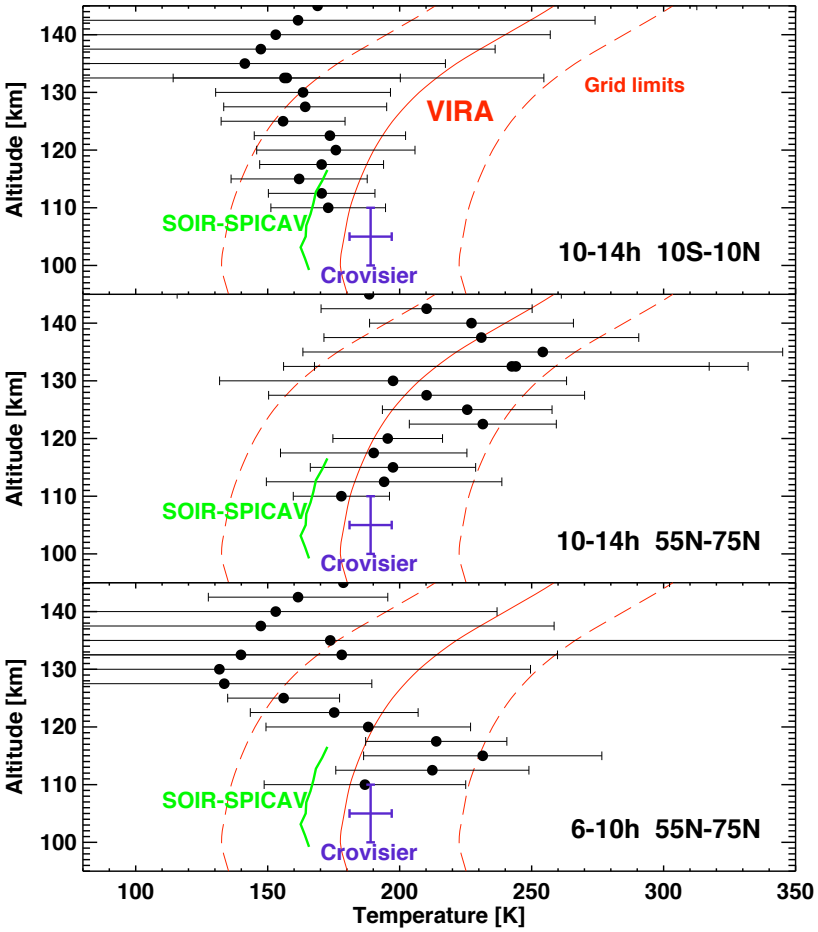

Figure 15: Non-LTE retrieved kinetic temperature with error bars from selected VIRTIS-H limb average measurements taken during 2006-2010. Top panel: Local time between 10-14h and latitude 10°S-10°N; Middle panel: Local time between 10-14h and latitude 55°N-75°N; Bottom panel: Local time between 6-10h and latitude 55°N-75°N. VIRA temperature profile (solid red line), and the grid limits (dashed red lines) are also plotted as reference. Results from Mahieux et al. (2010) (green dashed line) and Crovisier et al. (2006) (blue triangle with error bars) are shown for comparison.

the mesopeak obtained by Sonnabend et al. (2010) seem to agree with VIRTIS, within the large error bars of both measurements. This is surprising because their mesopeak is maximum in the sub-solar point where VIRTIS data do no show any enhancement. SPICAV/SOIR on VEx (Mahieux et al., 2010) also provided several profiles between 100 and 120 km, with error bars lower than 3K. These temperature values are colder then VIRA, and marginally agree with VIRTIS within error bars. However, neither

SPICAV/SOIR nor ground-based observations correspond to averages entirely comparable to the VIRTIS ones. For this reason, a more appropriate comparison, making use of similar geographical and temporal averages might only be possible with VTGCM results, after a careful extraction from this model. This task is foreseen in a near future.

5. Discussion and conclusions

A detailed study of the VIRTIS/VEx measurements of the non-LTE limb emissions of CO in the 4.7 μm region has been carried out. This required the development of a specific non-LTE inversion scheme with the goal of deriving CO abundance and atmospheric temperatures simultaneously. Guided by the solutions of a non-LTE model, our method starts with the calculation of a large set of pre-computed spectra for variations in CO and temperature, at different altitudes and SZA. The retrieval scheme then follows a χ^2 minimization procedure to obtain a first-fit solution, and proceeds with a linear inversion around the first-fit. A thorough error analysis is included. The results were discussed and compared with previous data and models and a summary of our conclusions follows next.

Starting with the carbon monoxide abundances, the geographical variations we found, with higher densities in the equatorial region, minor variations at high latitudes, and small or negligible latitudinal changes at low solar illumination conditions, are also expected by model predictions. CO densities obtained by VTGCM also drop from equatorial latitudes towards northern, but the magnitude of this variation is a factor 2 smaller than what we found (Bougher S., personal communication).
These variations are consistent with a strong sub-solar source of CO from CO_2 photodissociation plus a dynamical controlled distribution of CO, by a sub-solar to anti-solar circulation (Bougher et al., 1987). This would produce a decrease of CO of nearly a factor 2 from the morning to the terminator, at all altitudes considered here.
Within the uncertainty derived from our normally large retrieval errors, this is the first time that this sub-solar to anti-solar circulation is confirmed with a dynamical tracer like CO in the Venus upper mesosphere and lower thermosphere. Previous results showed similar results but at lower mesospheric altitudes in Venus.
One of the most detailed study was accomplished by Clancy and Muhleman (1985) that showed the night side versus dayside factor of 2-4 enhancement at 80-90 km and a similar in magnitude but reversed gradient in the morning. Later studies based on millimeter and submillimiter nightside observations (Clancy and Muhleman, 1990; Clancy et al., 2003, 2008, 2012), confirmed those results and also found secular variations and latitudinal variations (less than 20 %) over 50S-50N at the evening terminator. The appearance of nighside localized maxima is typically considered to be related to global dynamics, as a combination of the penetration of SS-AS thermospheric flow in the mesosphere near midnight and the tropospheric zonal retrograde flow in the morning side (Bougher et al., 1997; Clancy and Muhleman, 1991; Clancy et al., 2003, 2012).
The night-to-day increase factor obtained from microwave observations look consistent with our factor 2 increase from low terminator to equatorial regions. There might be an additional factor 3 from terminator to mid-night. An alternative is that this enrichment factor presents an altitude variation. Unfortunately we cannot see a clear variation, or it is within our uncertainties.

Regarding the temperature retrievals, these are particularly difficult as explained above. On one hand, the non-LTE nature of the emission makes these IR bands highly non-dependent on the thermal structure. On the other, the spectral shape of the CO bands is strongly masked by the large noise of individual spectra. Only large averages were amenable for stable solutions of our inversion method. The results presented here correspond to three vertical profiles of three large averages. Within the large error bars of the VIRTIS retrievals, there is a variation in lower thermospheric temperature with local time at high latitudes. In the upper mesosphere there is a mesopeak in the morning hours at high latitudes at least, with a peak around 230 K. The absence of a mesopeak at the sub-solar point, and at noon at high latitudes, suggest that the temperature in the upper mesosphere does not respond to a radiative equilibrium situation, nor is dynamically controlled by the same mechanism than determines the distribution of CO obtained. These VIRTIS results represent a challenging picture of the upper atmosphere of Venus, which may hopefully be tested against future data and may stimulate further development of the 3-D global models of the Venus atmosphere.

Acknowledgments

The IAA-CSIC team was supported by the Spanish MICINN under project AYA2008-03498/ESP and EC FEDER funds and GG has been supported by a Spanish National Research Council (CSIC) JAE-Predoc grant, co-funded by the European Social Fund (ESF).

References

Bertaux, J.-L., Nevejans, D., Korablev, O., Villard, E., Quémerais, E., Neefs, E., Montmessin, F., Leblanc, F., Dubois, J. P., Dimarellis, E., Hauchecorne, A., Lefèvre, F., Rannou, P., Chaufray, J. Y., Cabane, M., Cernogora, G., Souchon, G., Semelin, F., Reberac, A., van Ransbeek, E., Berkenbosch, S., Clairquin, R., Muller, C., Forget, F., Hourdin, F., Talagrand, O., Rodin, A., Fedorova, A., Stepanov, A., Vinogradov, I., Kiselev, A., Kalinnikov, Y., Durry, G., Sandel, B., Stern, A., Gérard, J. C., Oct. 2007. SPICAV on Venus Express: Three spectrometers to study the global structure and composition of the Venus atmosphere. *Planet. Space Sci.* 55, 1673–1700.

Bougher, S. W., Alexander, M. J., Mayr, H. G., 1997. Upper Atmosphere Dynamics: Global Circulation and Gravity Waves. In: S. W. Bougher, D. M. Hunten, & R. J. Phillips (Ed.), Venus II: Geology, Geophysics, Atmosphere, and Solar Wind Environment. p. 259.

Bougher, S. W., Gerard, J. C., Stewart, A. I. F., Fesen, C., Jun. 1987. The Venus NO* Night Airglow: Model Calculations Using the Thermospheric General Circulation Model. In: Bulletin of the American Astronomical Society. Vol. 19 of Bulletin of the American Astronomical Society. p. 869.

Bougher, S. W., Rafkin, S., Drossart, P., Nov. 2006. Dynamics of the Venus upper atmosphere: Outstanding problems and new constraints expected from Venus Express. *Planet. Space Sci.* 54, 1371–1380.

Brecht, A. S., Bougher, S. W., Gérard, J.-C., Parkinson, C. D., Rafkin, S., Foster, B., Aug. 2011. Understanding the variability of nightside temperatures, NO UV and O_2 IR nightglow emissions in the Venus upper atmosphere. Journal of Geophysical Research (Planets) 116, 8004.

Cardesín Moinelo, A., 2010. Study and Implementation of the End-to-End Data Pipeline for the Virtis Imaging Spectrometer Onbaord Venus Express: "From Science Operations Planning to Data Archiving and Higher Lever Processing". Ph.D. thesis, ESA/INSA/INAF/UNIPD.

Carlson, R. W., Weissman, P. R., Smythe, W. D., Mahoney, J. C., May 1992. Near-Infrared Mapping Spectrometer experiment on Galileo. Space Science Reviews 60, 457–502.

Clancy, R. T., Muhleman, D. O., Nov. 1985. Diurnal CO variations in the Venus mesosphere from CO microwave spectra. *Icarus* 64, 157–182.

Clancy, R. T., Muhleman, D. O., 1990. Corrections regarding the lellouch et al. (1989) analysis of mars atmospheric 12co and 13co spectra. Icarus 85 (1), 120 – 128.

Clancy, R. T., Muhleman, D. O., Jan. 1991. Long-term (1979-1990) changes in the thermal, dynamical, and compositional structure of the Venus mesosphere as inferred from microwave spectral line observations of C-12O, C-13O, and CO-18. *Icarus* 89, 129–146.

Clancy, R. T., Sandor, B. J., Moriarty-Schieven, G., Feb. 2012. Thermal structure and CO distribution for the Venus mesosphere/lower thermosphere: 2001-2009 inferior conjunction sub-millimeter CO absorption line observations. *Icarus* 217, 779–793.

Clancy, R. T., Sandor, B. J., Moriarty-Schieven, G. H., Jan. 2003. Observational definition of the Venus mesopause: vertical structure, diurnal variation, and temporal instability. Icarus 161, 1–16.

Clancy, R. T., Sandor, B. J., Moriarty-Schieven, G. H., Aug. 2008. Venus upper atmospheric CO, temperature, and winds across the afternoon/evening terminator from June 2007 JCMT sub-millimeter line observations. *Planet. Space Sci.* 56, 1344–1354.

Crisp, D., Titov, D., 1997. The Thermal Balance of the Venus Atmosphere. In: S. W. Bougher, D. M. Hunten, & R. J. Phillips (Ed.), Venus II: Geology, Geophysics, Atmosphere, and Solar Wind Environment. p. 353.

Crovisier, J., Lellouch, E., de Bergh, C., Maillard, J., Lutz, B. L., Bézard, B., Nov. 2006. Carbon monoxide emissions at 4.7 μm from Venus' atmosphere. *Planet. Space Sci.* 54, 1398–1414.

Dickinson, R. E., 1972. Infrared radiative heating and cooling in the Venusian mesosphere. I. Global mean radiative equilibrium. Journal of Atmospheric Sciences 29, 1531–1556.

Drossart, P., Piccioni, G., Lopez-Valverde, M. A., Gilli, G., Coradini, A., Bibring, J. P., VIRTIS/Venus Express Team, VIRTIS/Rosetta Team, OMEGA/Mars Express Team, Oct. 2007. Carbon Dioxide Non-LTE Emission In The Telluric Upper Atmospheres. In: AAS/Division for Planetary Sciences Meeting Abstracts. Vol. 39 of AAS/Division for Planetary Sciences Meeting Abstracts. pp. 45.06–+.

Dudhia, A., 2000. Michelson Interferometer for Passive Atmospheric Sounding (MIPAS) Reference Forward Model (RFM) Software User's Manual. Oxford University, Oxford, UK.

Edwards, D. P., Lopez-Puertas, M., Lopez-Valverde, M. A., Aug. 1993. Non-local thermodynamic equilibrium studies of the 15-micron bands of CO2 for atmospheric remote sensing. *J. Geophys. Res.* 98, 14955.

Gilli, G., López-Valverde, M. A., Drossart, P., Piccioni, G., Erard, S., Cardesín Moinelo, A., Mar. 2009. Limb observations of CO_2 and CO non-LTE emissions in the Venus atmosphere by VIRTIS/Venus Express. Journal of Geophysical Research (Planets) 114, 0–+.

Gilli, G., López-Valverde, M. A., Funke, B., López-Puertas, M., Drossart, P., Piccioni, G., Formisano, V., Aug. 2011. Non-LTE CO limb emission at 4.7μm in the upper atmosphere of Venus, Mars and Earth: Observations and modeling. *Planet. Space Sci.* 59, 1010–1018.

Gurwell, M. A., Muhleman, D. O., Shah, K. P., Berge, G. L., Rudy, D. J., Grossman, A. W., May 1995. Observations of the CO bulge on Venus and implications for mesospheric winds. Icarus 115, 141–158.

Hanel, R. A., Conrath, B. J., Jennings, D. E., Samuelson, R. E., Apr. 2003. Exploration of the Solar System by Infrared Remote Sensing: Second Edition.

Hedin, A. E., Niemann, H. B., Kasprzak, W. T., Seiff, A., Jan. 1983. Global empirical model of the Venus thermosphere. *J. Geophys. Res.* 88, 73–83.

Huebner, W. F., Keady, J. J., Lyon, S. P., Sep. 1992. Solar photo rates for planetary atmospheres and atmospheric pollutants. *Astrophysics and Space Science*195, 1–289.

Irwin, P. G. J., de Kok, R., Negrão, A., Tsang, C. C. C., Wilson, C. F., Drossart, P., Piccioni, G., Grassi, D., Taylor, F. W., Jul. 2008. Spatial variability of carbon monoxide in Venus' mesosphere from Venus Express/Visible and Infrared Thermal Imaging Spectrometer measurements. Journal of Geophysical Research (Planets) 113, 0.

Kakar, R. K., Waters, J. W., Wilson, W. J., Jan. 1976. Venus - Microwave detection of carbon monoxide. Science 191, 379.

Keating, G. M., Bertaux, J. L., Bougher, S. W., Dickinson, R. E., Cravens, T. E., Hedin, A. E., 1985. Models of Venus neutral upper atmosphere - Structure and composition. Advances in Space Research 5, 117–171.

Lellouch, E., Clancy, T., Crisp, D., Kliore, A. J., Titov, D., Bougher, S. W., 1997. Monitoring of Mesospheric Structure and Dynamics. In: S. W. Bougher, D. M. Hunten, & R. J. Phillips (Ed.), Venus II: Geology, Geophysics, Atmosphere, and Solar Wind Environment. p. 295.

Lopez-Puertas, M., Taylor, F. W., 2001. Non-LTE radiative transfer in the atmosphere. World Scientific Pub., Singapore, Series on atmospheric oceanic and planetary physics, vol. 3 ISBN 9810245661.

López-Valverde, M. A., Drossart, P., Carlson, R., Mehlman, R., Roos-Serote, M., Oct. 2007. Non-LTE infrared observations at Venus: From NIMS/Galileo to VIRTIS/Venus Express. *Planet. Space Sci.* 55, 1757–1771.

López-Valverde, M. A., López-Puertas, M., Funke, B., Gilli, G., García-Comas, M., Drossart, P., Piccioni, G., Formisano, V., 2011. Modelling the Atmospheric Limb Emission of CO_2 at 4.3 μm in the Terrestrial Planets. Planet. Space Sci. 59, 988–998.

Mahieux, A., Vandaele, A. C., Neefs, E., Robert, S., Wilquet, V., Drummond, R., Federova, A., Bertaux, J. L., Dec. 2010. Densities and temperatures in the Venus mesosphere and lower thermosphere retrieved from SOIR on board Venus Express: Retrieval technique. Journal of Geophysical Research (Planets) 115, 12014–+.

Newman, M., Schubert, G., Kliore, A. J., Patel, I. R., Jun. 1984. Zonal winds in the middle atmosphere of Venus from Pioneer Venus radio occultation data. Journal of Atmospheric Sciences 41, 1901–1913.

Pätzold, M., Häusler, B., Bird, M. K., Tellmann, S., Mattei, R., Asmar, S. W., Dehant, V., Eidel, W., Imamura, T., Simpson, R. A., Tyler, G. L., Nov. 2007. The structure of Venus' middle atmosphere and ionosphere. *Nature* 450, 657–660.

Piccioni, G., VIRTIS/Venus Express Team, 2009. The visible and infrared thermal imaging spectrometer. in press ESA SP-1295, Eur. Space Agency Spec. Publ., ESA Publications Division, Noordwijk, The Netherlands,.

Rodgers, C. D., 2000. Inverse Methods for Atmospheric Sounding: Theory and Practice. Vol. 2 of Series on Atmospheric, Oceanic and Planetary Physics, F. W. Taylor, ed. World Scientific.

Roldán, C., López-Valverde, M. A., López-Puertas, M., Edwards, D. P., Sep. 2000. Non-LTE Infrared Emissions of CO_2 in the Atmosphere of Venus. Icarus 147, 11–25.

Seiff, A., 1983. Thermal structure of the atmosphere of Venus. pp. 215–279.

Seiff, A., Schofield, J. T., Kliore, A. J., Taylor, F. W., Limaye, S. S., 1985. Models of the structure of the atmosphere of Venus from the surface to 100 kilometers altitude. Advances in Space Research 5, 3–58.

Sonnabend, G., Kroetz, P., Sornig, M., Stupar, D., Jun. 2010. Direct observations of Venus upper mesospheric temperatures from ground based spectroscopy of CO_2. Geophys Res. Lett. 37, L11102.

Sonnabend, G., Krötz, P., Schmülling, F., Kostiuk, T., Goldstein, J., Sornig, M., Stupar, D., Livengood, T., Hewagama, T., Fast, K., Mahieux, A., Clancy, R. T., Oct. 2011. Thermospheric/mesospheric temperatures on Venus: comparison between ground-based high-resolution spectroscopy of CO2 and other techniques. In: EPSC-DPS Joint Meeting 2011, held 2-7 October 2011 in Nantes, France. p. 716.

Sonnabend, G., Sornig, M., Krötz, P., Stupar, D., Schieder, R., Apr. 2008. Ultra high spectral resolution observations of planetary atmospheres using the cologne tuneable heterodyne infrared spectrometer. J. Quant. Spectrosc. Radiat. Transfer 109, 1016–1029.

Sornig, M., Livengood, T., Sonnabend, G., Kroetz, P., Stupar, D., Kostiuk, T., Schieder, R., Aug. 2008. Venus upper atmosphere winds from ground-based heterodyne spectroscopy of CO_2 at 10μm wavelength. *Planet. Space Sci.* 56, 1399–1406.

Titov, D. V., Svedhem, H., Koschny, D., Hoofs, R., Barabash, S., Bertaux, J.-L., Drossart, P., Formisano, V., Häusler, B., Korablev, O., Markiewicz, W. J., Nevejans, D., Pätzold, M., Piccioni, G., Zhang, T. L., Merritt, D., Witasse, O., Zender, J., Accomazzo, A., Sweeney, M., Trillard, D., Janvier, M., Clochet, A., Nov. 2006. Venus Express science planning. *Planet. Space Sci.* 54, 1279–1297.

Titov, D. V., Taylor, F. W., Svedhem, H., Ignatiev, N. I., Markiewicz, W. J., Piccioni, G., Drossart, P., Dec. 2008. Atmospheric structure and dynamics as the cause of ultraviolet markings in the clouds of Venus. *Nature* 456, 620–623.

Vandaele, A. C., De Mazière, M., Drummond, R., Mahieux, A., Neefs, E., Wilquet, V., Korablev, O., Fedorova, A., Belyaev, D., Montmessin, F., Bertaux, J., Dec. 2008. Composition of the Venus mesosphere measured by Solar Occultation at Infrared on board Venus Express. Journal of Geophysical Research (Planets) 113, 0–+.

von Clarmann, T., Glatthor, N., Grabowski, U., Höpfner, M., Kellmann, S., Kiefer, M., Linden, A., Mengistu Tsidu, G., Milz, M., Steck, T., Stiller, G. P., Wang, D. Y., Fischer, H., Funke, B., Gil-López, S., López-Puertas, M., 2003. Retrieval of temperature and tangent altitude pointing from limb emission spectra recorded from space by the Michelson Interferometer for Passive Atmospheric Sounding (MIPAS). J. Geophys. Res. 108 (D23).

von Zahn, U., Kumar, S., Niemann, H., Prinn, R., 1983. Composition of the venus atmosphere. In: Hunten, D. M., Colin, L., Donahue, T. M., Moroz, V. I. (Eds.), Venus. Univ. of Arizona Press, Tucson, AZ, pp. 299–430.

Chapter 5

Conclusions and future work

This Thesis presents part of the efforts which I carried out during my PhD at the *Instituto de Astrofísica de Andalucia* (IAA-CSIC) for the investigation of the upper mesosphere/lower thermosphere of Venus (90-170 km altitude), using data from the satellite Venus Express (VEx). This is the first mission in more than 20 years to study the Venus atmosphere systematically from orbit. In this work we used data from VIRTIS, one of the six instruments on board VEx, which consists of two channels, the imaging spectrometer (VIRTIS-M) and the high resolution spectrograph (VIRTIS-H). Together with SPICAV/SOIR and VeRa on board VEx, VIRTIS offered a unique opportunity to sound the upper atmosphere of Venus, for the first time with high spectral and spatial resolution, in different spectral ranges. The scientific exploitation of these VIRTIS measurements is one of the goals pursued in this work. In particular, daytime limb measurements acquired by VIRTIS during 2006-2010 have been extensively analyzed in this Thesis, with focus on the IR windows between 4-5 μm, where the strongest non-local thermodynamic equilibrium (non-LTE) emissions, typical of the upper layers of planetary atmospheres, have been detected. The emissions observed around 4.3 μm and 2.7 μm are attributed to CO_2 fluorescence of solar radiation, while the emission at 4.7 μm is produced by a similar excitation in the ro-vibrational bands of CO. As previously shown in studies of the Earth's atmosphere, those data can be extremely valuable not only to validate theoretical tools, as non-LTE models, but also to derive atmospheric parameters in those highly unknown regions of the upper planetary atmosphere. This constitutes one of the objectives of this Thesis, regarding the atmosphere of Venus.

In this chapter the main results obtained in this work are summarized. They are divided into three topics, corresponding to the three chapters where they are presented: 1) Analysis of the VIRTIS/VEx limb measurements at 4.3 μm and 4.7 μm; 2) Validation of the Venus non-LTE model; 3) Retrieval of temperatures and CO abundances in the Venus upper atmosphere from VIRTIS measurements around 4.7 μm.
The last section of this chapter also includes a list of ideas for future work.

5.1 Analysis of the VIRTIS limb measurements at 4.3 μm and 4.7 μm

Since the beginning of the VEx scientific phase in June 2006 a considerable fraction of the work has been devoted to the analysis and the understanding of VIRTIS observations. The spectral region of our interest is between 4-5 μm where strong non-LTE emissions by CO_2 and CO are observed, as mentioned above.

Our initial study was focused on limb daytime observations from both channels, VIRTIS-H and VIRTIS-M, from periapsis and apoapsis, and was intended to understand the behavior of the two instruments, correlate their observations, describe the data quality and to identify possible systematic effects. This study resulted as essential to guide the selection of the most suitable data for the retrieval carried out in the latest phase of the Thesis. In fact, although VIRTIS-M was potentially better than VIRTIS-H at characterizing the spatial variability of those emissions, given its larger amount of spectra, unfortunately, most of the periapsis data contained a systematic instrumental bias, perhaps from some stray-light contamination, specially severe at $\lambda > 4.5$ μm. In addition to this, the limb spectra presented a systematic "odd-even" effect, which produces an oscillation in the spectral domain, plus an instrumental effect in spectra from the apoapsis, called "smiling effect". This last effect deforms the actual field of view in an amount similar to the projected size of one pixel, which can be as large as 20 km. It was detected thanks non-LTE predictions at 4.3 μm and a correction to reduce it was proposed in this work.
All these considerations led us to discard VIRTIS-M measurements for the rest of the work, and to devote the analysis to VIRTIS-H data. Moreover, the high spectral resolution of VIRTIS-H was more promising to derive atmospheric parameters, like temperature and CO abundance simultaneously, since it permitted a clear separation of the CO lines. A first qualitative comparison with the non-LTE model was also performed during the first phase of the data analysis.
The main conclusions of this work can be listed as follows:

- Strong emissions in the limb were clearly identified at 4.3 and 4.7 μmwith both VIRTIS-H and VIRTIS-M, and attributed to non-LTE daytime solar excitations of CO_2 and CO, respectively.

- The basic non-LTE features of the CO_2 and CO fluorescence predicted by the theoretical model, like the altitude and SZA variations, are clearly observed by VIRTIS in a global or averaged sense. No attempt to carry out a very detailed data-model was pursued since the actual atmospheric structure of of Venus was unknown at the precise time and location of each measurement.

- Individual spectra with good signal-to-noise ratio are detectable up to about 160 km and 120 km in the case of CO_2 and CO, respectively.

- The ro-vibrational double-branch structure of CO, typical of diatomic molecules, is clearly identified with the VIRTIS-H resolution. The CO(1-0), or fundamental band (FB) becomes optically thin above 130-140 km, with a moderate contribution to the observed spectra up to this altitude, while the CO(2-1) first hot (FH) band dominates the spectra up to about 125 km.

- From the first analysis of VIRTIS data, the possibility of performing retrievals and to improve our knowledge of these parameters in the upper atmosphere of Venus was very encouraging, and was a strong motivation for later phases of the Thesis.

5.2 Non-LTE model validation for Venus and studies of comparative aeronomy

Given the non-LTE nature of the previously mentioned emissions, a proper model is required for their analysis and interpretation. One of the objectivea of this thesis is the validation of a non-LTE model for the infrared emissions by CO_2 and CO in the Venus atmosphere developed at IAA-CSIC (Roldán et al., 2000; López-Valverde et al., 2007). The model is based on previous modeling efforts for the Martian atmosphere (Lopez-Valverde and Lopez-Puertas, 1994) and much earlier efforts for the Earth's atmosphere (Lopez-Puertas et al., 1986; López-Puertas et al., 2005). Those strong daytime CO_2 and CO emissions are typical of the upper atmospheric layers of the three terrestrial planets, and we performed here a common analysis to find similarities and differences between them, with the help of these similar non-LTE models. This analysis has been applied to a selection of recent daytime limb measurements of the upper atmosphere of Venus , Mars and the Earth taken by VIRTIS/Venus Express, PFS/Mars Express and MIPAS/Envisat, respectively.

Regarding the study on the 4.3 μm CO_2 emission we stress the following conclusions:

- In general, the non-LTE models can explain the main spectral features in the measurements from the three planets. However, the simulations for Mars and Venus predicted an incorrect ratio of the emission at two wavelengths, 4.4 and 4.32 μm. A solution which solved this discrepancy is to increase of quenching rate of the vibrational ν_3 quanta of the high energy CO_2 states by a factor in the bracket 2-4. This factor falls within the experimental uncertainty in these rates and it reduces the discrepancy by a factor 2 at least.

- The 4.3 μm emission for Mars is smaller than for Venus and the Earth. This is consistent with the larger distance of the "red" planet from the Sun, since those emissions depend strongly on the solar illumination.

- A number of theoretical tests showed that in both Mars and Venus the maximum sensitivity to temperature and to CO_2 density perturbations is around the peak of emission of CO_2 at 4.3 μm. Therefore, those atmospheric parameters could in principle be retrieved from VIRTIS and PFS data, being this study more promising for Venus due to the stronger excitation.

Regarding the analysis of CO non-LTE emission around 4.7 μm, the main results are the following:

- CO measurements around 4.7 μm from PFS and VIRTIS-H have been compared directly with non-LTE simulations for the first time. The agreement is satisfactory within the measurement uncertainties.

- The main contribution to the CO emission in the upper mesosphere of Venus comes from the FH band, while the FB dominates the emission in the lower thermosphere, where it becomes optically thinner. This is similar on Mars but different on the Earth, where the FB has a much larger contribution at all altitudes, which is consistent with the much smaller relative abundance of CO on the the terrestrial atmosphere.

- The maximum of the 4.7 μm emission is observed on Venus between 90 ad 110 km. This altitude peak is 68 km on Mars, which is an entirely equivalent pressure level. However, on Earth the peak emission occurs at a lower altitude (larger pressure), since the atmosphere is more transparent to the FB band.

- Sensitivity studies of the limb CO emission observed by VIRTIS-H, confirmed that these emissions should be exploited to derive atmospheric parameters such as CO density and temperature in the upper atmosphere of Venus.

5.3 Retrieval of CO and temperature in the upper atmosphere of Venus

In the last part of the thesis we focused on the non-LTE retrieval of temperature and CO abundances from those VIRTIS-H measurements. More than 9000 daytime limb spectra have been analyzed from 90 to 170 km tangent altitude from the whole mission, covering the period of about four years (June 2006 to November 2010). They have been used to validate the non-LTE model and to check for atmospheric variability. The data selected for the retrieval are a subset of VIRTIS-H measurements, with small FOV ($< 5km$) and from tangent altitudes between 100 and 150 km, to avoid strong scattering effect from the lower mesosphere and to discard the low S/N spectra from the upper thermosphere.
A special retrieval scheme was designed for the inversion of these measurements, which incorporates the non-LTE model as a key ingredient of the forward model. The scheme is very stable, and follows two steps. The first one is based on a χ^2 minimization of the simulation-data differences, using a set of pre-computed spectra for a variety of CO and temperature values. The second step is a linear inversion, with a proper treatment of the measurement errors following the Optimal Estimation Theory (Rodgers, 2000). A specific error analysis was performed to cover the most important uncertainties. The results of CO and temperature were compared with a few data available.
Our results can be summarized as follows:

- CO abundances and temperatures in the upper atmosphere of Venus, between 100 and 150 km tangent altitudes, have been retrieved simultaneously from limb VIRTIS-H limb measurements at 4.7 μm.

- VIRTIS data show [CO] latitudinal variations, with higher densities in the equatorial region during high solar illumination conditions. We also found a variation of about a factor 2 between noon and near-terminator measurements, at all altitudes, with the largest abundance in the sub-solar point. These variations are consistent with a strong source of CO from CO_2 photo-dissociation at the sub-solar point, plus a

sub-solar to anti-solar circulation which seems to control the transport of the CO in the lower thermosphere.

- The retrieval uncertainties are very large and dominated by the measurement noise, especially at the highest altitudes. The errors in temperature are specially large and require large averages of data before the retrieval can be applied meaningfully.

- The temperature retrieval was performed for large averages of data. Constrained by large error bars and vertical averaging, the results consist on three vertical profiles for the sub-solar region, and for noon and the morning hours at high northern latitudes. The most interesting result in the upper mesosphere is the presence of a clear mesopeak in the morning hours at high latitudes, and not present at noon at none of the two latitude bands. This last result collides with a mesopeak driven by radiative processes, unless a radiative enhancement is smaller than the VIRTIS error bars. It is not fully consistent either with the subsolar-to-antisolar mechanism obtained for the carbon monoxide distribution.

- VIRTIS measurements of CO and temperature are consistent, within the error bars and the different mapping, with SPICAV/Soir measurements below 120 km altitude. The agreement with ground-based measurements is doubtful, as the mesopeak obtained by Sonnabend et al. (2010) is more representative of the sub-solar point, while VIRTIS does not observe in such conditions.

5.4 Future work

Here a few recommendations for future extensions and applications of this work are proposed:

- The comparison of the obtained CO with independent data would be very beneficial, but it is very limited so far due to the lack of measurements during daytime above 100 km. Our results have been compared only with a couple of vertical profiles between 100-120 km from SPICAV/SOIR, published so far. In general, they seem to agree within error bars. However, the validation of these VIRTIS measurements would be more complete after a comparison with more a extended dataset from Venus Express. New profiles from SPICAV/SOIR are being processed currently (Mahieux, personal communication) and promise to be very useful in this direction. Other VEx instruments, like VeRa, are only providing temperatures below 90 km, so far.

- A comparison with theoretical 3-D global models has not been tackled yet. The Venus Thermospheric GCM, of Michigan State University, and the LMD-Venus GCM, this one still under development, may be specially suited to analyze the present results. For such purpose, averages of GCM simulations similar to those used in the data analysis should be considered. The different variations obtained for CO and temperature in the upper mesosphere from VIRTIS data seem to pose a special challenge for the models.

- Regarding the methodology developed for the analysis of these data, several applications are foreseen in a near future. One on-going project is the modification of this non-LTE scheme to study the observations by VIRTIS-H in the 4.3 μm spectral region both in nadir and in the limb. And a second application is the study of similar limb measurements by the instruments PFS and OMEGA on board Mars Express. The present inversion scheme offers a good chance to be exported to exploit the data successfully (non 1-D profiles, similar spectral resolution to VIRTIS, and 4.3 and 4.7 μm simultaneous measurements)

Bibliography

Alexander, M. J., Stewart, A. I. F., and Bougher, S. W. (1992). Local-time asymmetries in the Venus thermosphere. *LPI Contributions*, 789:1–2.

Allen, D. A. and Crawford, J. W. (1984). Cloud structure on the dark side of Venus. *Nature*, 307:222–224.

Atreya, S. K. and Gu, Z. G. (1994). Stability of the Martian atmosphere: Is heterogeneous catalysis essential? *J. Geophys. Res.*, 99:13133–13145.

Bailey, J., Meadows, V. S., Chamberlain, S., and Crisp, D. (2008). The temperature of the Venus mesosphere from O_2 ($a\Delta g1$) airglow observations. *Icarus*, 197:247–259.

Baines, K. H., Atreya, S., Carlson, R. W., Crisp, D., Drossart, P., Formisano, V., Limaye, S. S., Markiewicz, W. J., and Piccioni, G. (2006). To the depths of Venus: Exploring the deep atmosphere and surface of our sister world with Venus Express. *Planet. Space Sci.*, 54:1263–1278.

Barabash, S., Fedorov, A., Sauvaud, J. J., Lundin, R., Russell, C. T., Futaana, Y., Zhang, T. L., Andersson, H., Brinkfeldt, K., Grigoriev, A., Holmström, M., Yamauchi, M., Asamura, K., Baumjohann, W., Lammer, H., Coates, A. J., Kataria, D. O., Linder, D. R., Curtis, C. C., Hsieh, K. C., Sandel, B. R., Grande, M., Gunell, H., Koskinen, H. E. J., Kallio, E., Riihelä, P., Säles, T., Schmidt, W., Kozyra, J., Krupp, N., Fränz, M., Woch, J., Luhmann, J., McKenna-Lawlor, S., Mazelle, C., Thocaven, J.-J., Orsini, S., Cerulli-Irelli, R., Mura, M., Milillo, M., Maggi, M., Roelof, E., Brandt, P., Szego, K., Winningham, J. D., Frahm, R. A., Scherrer, J., Sharber, J. R., Wurz, P., and Bochsler, P. (2007a). The loss of ions from Venus through the plasma wake. *Nature*, 450:650–653.

Barabash, S., Sauvaud, J.-A., Gunell, H., Andersson, H., Grigoriev, A., Brinkfeldt, K., Holmström, M., Lundin, R., Yamauchi, M., Asamura, K., Baumjohann, W., Zhang, T. L., Coates, A. J., Linder, D. R., Kataria, D. O., Curtis, C. C., Hsieh, K. C., Sandel, B. R., Fedorov, A., Mazelle, C., Thocaven, J.-J., Grande, M., Koskinen, H. E. J., Kallio, E., Säles, T., Riihela, P., Kozyra, J., Krupp, N., Woch, J., Luhmann, J., McKenna-Lawlor, S., Orsini, S., Cerulli-Irelli, R., Mura, M., Milillo, M., Maggi, M., Roelof, E., Brandt, P., Russell, C. T., Szego, K., Winningham, J. D., Frahm, R. A., Scherrer, J., Sharber, J. R., Wurz, P., and Bochsler, P. (2007b). The Analyser of Space Plasmas and Energetic Atoms (ASPERA-4) for the Venus Express mission. *Planet. Space Sci.*, 55:1772–1792.

Bertaux, J.-L., Nevejans, D., Korablev, O., Villard, E., Quémerais, E., Neefs, E., Montmessin, F., Leblanc, F., Dubois, J. P., Dimarellis, E., Hauchecorne, A., Lefèvre, F., Rannou, P., Chaufray, J. Y., Cabane, M., Cernogora, G., Souchon, G., Semelin, F., Reberac, A., van Ransbeek, E., Berkenbosch, S., Clairquin, R., Muller, C., Forget, F., Hourdin, F., Talagrand, O., Rodin, A., Fedorova, A., Stepanov, A., Vinogradov, I., Kiselev, A., Kalinnikov, Y., Durry, G., Sandel, B., Stern, A., and Gérard, J. C. (2007a). SPICAV on Venus Express: Three spectrometers to study the global structure and composition of the Venus atmosphere. *Planet. Space Sci.*, 55:1673–1700.

Bertaux, J.-L., Vandaele, A.-C., Korablev, O., Villard, E., Fedorova, A., Fussen, D., Quémerais, E., Belyaev, D., Mahieux, A., Montmessin, F., Muller, C., Neefs, E., Nevejans, D., Wilquet, V., Dubois, J. P., Hauchecorne, A., Stepanov, A., Vinogradov, I., Rodin, A., Bertaux, J.-L., Nevejans, D., Korablev, O., Montmessin, F., Vandaele, A.-C., Fedorova, A., Cabane, M., Chassefière, E., Chaufray, J. Y., Dimarellis, E., Dubois, J. P., Hauchecorne, A., Leblanc, F., Lefèvre, F., Rannou, P., Quémerais, E., Villard, E., Fussen, D., Muller, C., Neefs, E., van Ransbeeck, E., Wilquet, V., Rodin, A., Stepanov, A., Vinogradov, I., Zasova, L., Forget, F., Lebonnois, S., Titov, D., Rafkin, S., Durry, G., Gérard, J. C., and Sandel, B. (2007b). A warm layer in Venus' cryosphere and high-altitude measurements of HF, HCl, H_2O and HDO. *Nature*, 450:646–649.

Bougher, S. W. (1995). Comparative thermospheres venus and mars. *Adv. Space Res.*, 15:21–.

Bougher, S. W., Alexander, M. J., and Mayr, H. G. (1997). Upper Atmosphere Dynamics: Global Circulation and Gravity Waves. In S. W. Bougher, D. M. Hunten, & R. J. Phillips, editor, *Venus II: Geology, Geophysics, Atmosphere, and Solar Wind Environment*, page 259.

Bougher, S. W., Dickinson, R. E., Ridley, E. C., Roble, R. G., Nagy, A. F., and Cravens, T. E. (1986). Venus mesosphere and thermosphere. II - Global circulation, temperature, and density variations. *Icarus*, 68:284–312.

Bougher, S. W., Gerard, J. C., Stewart, A. I. F., and Fesen, C. (1987). The Venus NO* Night Airglow: Model Calculations Using the Thermospheric General Circulation Model. In *Bulletin of the American Astronomical Society*, volume 19 of *Bulletin of the American Astronomical Society*, page 869.

Bougher, S. W., Rafkin, S., and Drossart, P. (2006). Dynamics of the Venus upper atmosphere: Outstanding problems and new constraints expected from Venus Express. *Planet. Space Sci.*, 54:1371–1380.

Brecht, A. S., Bougher, S. W., Gérard, J.-C., Parkinson, C. D., Rafkin, S., and Foster, B. (2011). Understanding the variability of nightside temperatures, NO UV and O_2 IR nightglow emissions in the Venus upper atmosphere. *Journal of Geophysical Research (Planets)*, 116:8004.

Brown, R. H., Baines, K. H., Bellucci, G., Bibring, J.-P., Buratti, B. J., Capaccioni, F., Cerroni, P., Clark, R. N., Coradini, A., Cruikshank, D. P., Drossart, P., Formisano,

V., Jaumann, R., Langevin, Y., Matson, D. L., McCord, T. B., Mennella, V., Miller, E., Nelson, R. M., Nicholson, P. D., Sicardy, B., and Sotin, C. (2004). The Cassini Visual And Infrared Mapping Spectrometer (Vims) Investigation. *Space Science Review*, 115:111–168.

Carlson, R. W., Weissman, P. R., Smythe, W. D., and Mahoney, J. C. (1992). Near-Infrared Mapping Spectrometer experiment on Galileo. *Space Science Reviews*, 60:457–502.

Clancy, R. T. and Muhleman, D. O. (1985). Diurnal CO variations in the Venus mesosphere from CO microwave spectra. *Icarus*, 64:157–182.

Clancy, R. T. and Muhleman, D. O. (1991). Long-term (1979-1990) changes in the thermal, dynamical, and compositional structure of the Venus mesosphere as inferred from microwave spectral line observations of C-12O, C-13O, and CO-18. *Icarus*, 89:129–146.

Clancy, R. T., Sandor, B. J., and Moriarty-Schieven, G. (2012). Thermal structure and CO distribution for the Venus mesosphere/lower thermosphere: 2001-2009 inferior conjunction sub-millimeter CO absorption line observations. *Icarus*, 217:779–793.

Clancy, R. T., Sandor, B. J., and Moriarty-Schieven, G. H. (2003). Observational definition of the Venus mesopause: vertical structure, diurnal variation, and temporal instability. *Icarus*, 161:1–16.

Clancy, R. T., Sandor, B. J., and Moriarty-Schieven, G. H. (2008). Venus upper atmospheric CO, temperature, and winds across the afternoon/evening terminator from June 2007 JCMT sub-millimeter line observations. *Planet. Space Sci.*, 56:1344–1354.

Collard, A. D., Taylor, F. W., Calcutt, S. B., Carlson, R. W., Kamp, L. W., Baines, K. H., Encrenaz, T., Drossart, P., Lellouch, E., and Bezard, B. (1993). Latitudinal distribution of carbon monoxide in the deep atmosphere of Venus. *Planet. Space Sci.*, 41:487–494.

Coradini, A., Capaccioni, F., Drossart, P., Semery, A., Arnold, G., and Benkhoff, J. (1999). VIRTIS: an Imaging Spectrometer for the ROSETTA mission. In *AAS/Division for Planetary Sciences Meeting Abstracts 31*, volume 31 of *AAS/Division for Planetary Sciences Meeting Abstracts*, page 29.07.

Cotton, D. V., Bailey, J., Crisp, D., and Meadows, V. S. (2012). The distribution of carbon monoxide in the lower atmosphere of Venus. *Icarus*, 217:570–584.

Crovisier, J., Lellouch, E., de Bergh, C., Maillard, J., Lutz, B. L., and Bézard, B. (2006). Carbon monoxide emissions at 4.7 μm from Venus' atmosphere. *Planet. Space Sci.*, 54:1398–1414.

d'Agostini, G. (2003). *Bayesian Reasoning in Data Analysis - A Critical Introduction*. World Scientific, Singapore.

de Bergh, C., Moroz, V. I., Taylor, F. W., Crisp, D., Bézard, B., and Zasova, L. V. (2006). The composition of the atmosphere of Venus below 100 km altitude: An overview. *Planet. Space Sci.*, 54:1389–1397.

de Kok, R., Irwin, P. G. J., Tsang, C. C. C., Piccioni, G., and Drossart, P. (2011). Scattering particles in nightside limb observations of Venus' upper atmosphere by Venus Express VIRTIS. *Icarus*, 211:51–57.

Dickinson, R. E. (1972). Infrared radiative heating and cooling in the Venusian mesosphere. I. Global mean radiative equilibrium. *Journal of Atmospheric Sciences*, 29:1531–1556.

Dickinson, R. E. (1973). Infrared radiative heating and cooling in the Venusian mesosphere. II. Day-to-night variation. *Journal of Atmospheric Sciences*, 30:296–301.

Dickinson, R. E. and Ridley, E. C. (1977). Venus mesosphere and thermosphere temperature structure. II - Day-night variations. *Icarus*, 30:163–178.

Drossart, P. (2005). Infrared spectroscopy of planetary atmospheres. *Comptes Rendus Physique*, 6:817–824.

Drossart, P., Piccioni, G., Adriani, A., Angrilli, F., Arnold, G., Baines, K. H., Bellucci, G., Benkhoff, J., Bézard, B., Bibring, J., Blanco, A., Blecka, M. I., Carlson, R. W., Coradini, A., di Lellis, A., Encrenaz, T., Erard, S., Fonti, S., Formisano, V., Fouchet, T., Garcia, R., Haus, R., Helbert, J., Ignatiev, N. I., Irwin, P. G. J., Langevin, Y., Lebonnois, S., Lopez-Valverde, M. A., Luz, D., Marinangeli, L., Orofino, V., Rodin, A. V., Roos-Serote, M. C., Saggin, B., Sanchez-Lavega, A., Stam, D. M., Taylor, F. W., Titov, D., Visconti, G., Zambelli, M., Hueso, R., Tsang, C. C. C., Wilson, C. F., and Afanasenko, T. Z. (2007a). Scientific goals for the observation of Venus by VIRTIS on ESA/Venus express mission. *Planet. Space Sci.*, 55:1653–1672.

Drossart, P., Piccioni, G., Gérard, J. C., Lopez-Valverde, M. A., Sanchez-Lavega, A., Zasova, L., Hueso, R., Taylor, F. W., Bézard, B., Adriani, A., Angrilli, F., Arnold, G., Baines, K. H., Bellucci, G., Benkhoff, J., Bibring, J. P., Blanco, A., Blecka, M. I., Carlson, R. W., Coradini, A., di Lellis, A., Encrenaz, T., Erard, S., Fonti, S., Formisano, V., Fouchet, T., Garcia, R., Haus, R., Helbert, J., Ignatiev, N. I., Irwin, P., Langevin, Y., Lebonnois, S., Luz, D., Marinangeli, L., Orofino, V., Rodin, A. V., Roos-Serote, M. C., Saggin, B., Stam, D. M., Titov, D., Visconti, G., Zambelli, M., Tsang, C., Ammannito, E., Barbis, A., Berlin, R., Bettanini, C., Boccaccini, A., Bonnello, G., Bouyé, M., Capaccioni, F., Cardesin, A., Carraro, F., Cherubini, G., Cosi, M., Dami, M., de Nino, M., Del Vento, D., di Giampietro, M., Donati, A., Dupuis, O., Espinasse, S., Fabbri, A., Fave, A., Ficai Veltroni, I., Filacchione, G., Garceran, K., Ghomchi, Y., Giustizi, M., Gondet, B., Hello, Y., Henry, F., Hofer, S., Huntzinger, G., Kachlicki, J., Knoll, R., Kouach, D., Mazzoni, A., Melchiorri, R., Mondello, G., Monti, F., Neumann, C., Nuccilli, F., Parisot, J., Pasqui, C., Perferi, S., Peter, G., Piacentino, A., Pompei, C., Réess, J.-M., Rivet, J.-P., Romano, A., Russ, N., Santoni, M., Scarpelli, A., Sémery, A., Soufflot, A., Stefanovitch, D., Suetta, E., Tarchi, F., Tonetti, N., Tosi, F., and Ulmer, B. (2007b). A dynamic upper atmosphere of Venus as revealed by VIRTIS on Venus Express. *Nature*, 450:641–645.

Drossart, P., Piccioni, G., Lopez-Valverde, M. A., Gilli, G., Coradini, A., Bibring, J. P., VIRTIS/Venus Express Team, VIRTIS/Rosetta Team, and OMEGA/Mars Express Team

(2007c). Carbon Dioxide Non-LTE Emission In The Telluric Upper Atmospheres. In *AAS/Division for Planetary Sciences Meeting Abstracts*, volume 39 of *AAS/Division for Planetary Sciences Meeting Abstracts*, pages 45.06–+.

Dudhia, A. (2000). *Michelson Interferometer for Passive Atmospheric Sounding (MIPAS) Reference Forward Model (RFM) Software User's Manual*. Oxford University, Oxford, UK.

Encrenaz, T. H., Lellouch, E., Cernicharo, J., Paubert, G., Gulkis, S., and Spilker, T. (1995). The thermal profile and water abundance in the Venus mesosphere from H_2O and HDO millimeter observations. *Icarus*, 117:162–172.

Esposito, L. W., Bertaux, J.-L., Krasnopolsky, V., Moroz, V. I., and Zasova, L. V. (1997). Chemistry of Lower Atmosphere and Clouds. In S. W. Bougher, D. M. Hunten, & R. J. Phillips, editor, *Venus II: Geology, Geophysics, Atmosphere, and Solar Wind Environment*, page 415.

Esposito, L. W., Knollenberg, R. G., Marov, M. I., Toon, O. B., and Turco, R. P. (1983). *The clouds are hazes of Venus*, pages 484–564. Univ. of Arizona Press, Tucson, AZ.

Faure, G. and Mensing, T. M. (2007). *Introduction to Planetary Science: The Geological Perspective*. Springer.

Fimmel, R. O., Colin, L., Burgess, E., Mark, H., and Guastaferro, A. (1983). *Pioneer Venus.*

Formisano, V., Angrilli, F., Arnold, G., Atreya, S., Bianchini, G., Biondi, D., Blanco, A., Blecka, M. I., Coradini, A., Colangeli, L., Ekonomov, A., Esposito, F., Fonti, S., Giuranna, M., Grassi, D., Gnedykh, V., Grigoriev, A., Hansen, G., Hirsh, H., Khatuntsev, I., Kiselev, A., Ignatiev, N., Jurewicz, A., Lellouch, E., Lopez Moreno, J., Marten, A., Mattana, A., Maturilli, A., Mencarelli, E., Michalska, M., Moroz, V., Moshkin, B., Nespoli, F., Nikolsky, Y., Orfei, R., Orleanski, P., Orofino, V., Palomba, E., Patsaev, D., Piccioni, G., Rataj, M., Rodrigo, R., Rodriguez, J., Rossi, M., Saggin, B., Titov, D., and Zasova, L. (2005). The Planetary Fourier Spectrometer (PFS) onboard the European Mars Express mission. *Planet. Space Sci.*, 53:963–974.

Funke, B., López-Puertas, M., García-Comas, M., Stiller, G. P., von Clarmann, T., Höpfner, M., Glatthor, N., Grabowski, U., Kellmann, S., and Linden, A. (2009). Carbon monoxide distributions from the upper troposphere to the mesosphere inferred from 4.7 Œºm non-local thermal equilibrium emissions measured by mipas on envisat. *Atmospheric Chemistry and Physics*, 9(7):2387–2411.

Gérard, J.-C., Hubert, B., Gustin, J., Shematovich, V. I., Bisikalo, D., Gladstone, G. R., and Esposito, L. W. (2011). EUV spectroscopy of the Venus dayglow with UVIS on Cassini. *Icarus*, 211:70–80.

Gierasch, P. J., Goody, R. M., Young, R. E., Crisp, D., Edwards, C., Kahn, R., Rider, D., del Genio, A., Greeley, R., Hou, A., Leovy, C. B., McCleese, D., and Newman, M. (1997).

The General Circulation of the Venus Atmosphere: an Assessment. In S. W. Bougher, D. M. Hunten, & R. J. Phillips, editor, *Venus II: Geology, Geophysics, Atmosphere, and Solar Wind Environment*, page 459.

Gilli, G., López-Valverde, M. A., Drossart, P., Piccioni, G., Erard, S., and Cardesín Moinelo, A. (2009). Limb observations of CO_2 and CO non-LTE emissions in the Venus atmosphere by VIRTIS/Venus Express. *Journal of Geophysical Research (Planets)*, 114:0–+.

Gilli, G., López-Valverde, M. A., Funke, B., López-Puertas, M., Drossart, P., Piccioni, G., and Formisano, V. (2011). Non-LTE CO limb emission at 4.7μm in the upper atmosphere of Venus, Mars and Earth: Observations and modeling. *Planet. Space Sci.*, 59:1010–1018.

Gladstone, G. R., Yelle, R. V., and Majeed, T. (2002). *Solar System Upper Atmospheres: Photochemistry, Energetics, and Dynamics*, pages 23–+.

Gurwell, M. A., Muhleman, D. O., Shah, K. P., Berge, G. L., Rudy, D. J., and Grossman, A. W. (1995). Observations of the CO bulge on Venus and implications for mesospheric winds. *Icarus*, 115:141–158.

Hanel, R. A., Conrath, B. J., Jennings, D. E., and Samuelson, R. E. (2003). *Exploration of the Solar System by Infrared Remote Sensing: Second Edition.*

Häusler, B., Pätzold, M., Tyler, G. L., Simpson, R. A., Bird, M. K., Dehant, V., Barriot, J.-P., Eidel, W., Mattei, R., Remus, S., Selle, J., Tellmann, S., and Imamura, T. (2006). Radio science investigations by VeRa onboard the Venus Express spacecraft. *Planet. Space Sci.*, 54:1315–1335.

Hedin, A. E., Niemann, H. B., Kasprzak, W. T., and Seiff, A. (1983). Global empirical model of the Venus thermosphere. *J. Geophys. Res.*, 88:73–83.

Hollenbach, D. J., Whitten, R. C., and Prasad, S. S. (1985). The thermal structure of the dayside upper atmosphere of Venus above 125 KM. *Icarus*, 64:205–220.

Huebner, W. F., Keady, J. J., and Lyon, S. P. (1992). Solar photo rates for planetary atmospheres and atmospheric pollutants. *Astrophysics and Space Science*, 195:1–289.

Ignatiev, N. i., Moroz, V. i., Zasova, L. V., and Khatuntsev, I. v. (1999). Water vapour in the middle atmosphere of Venus:An improved treatment of the Venera 15 ir spectra. *Planet. Space Sci.*, 47:1061–1075.

Irwin, P. G. J., de Kok, R., Negrão, A., Tsang, C. C. C., Wilson, C. F., Drossart, P., Piccioni, G., Grassi, D., and Taylor, F. W. (2008). Spatial variability of carbon monoxide in Venus' mesosphere from Venus Express/Visible and Infrared Thermal Imaging Spectrometer measurements. *Journal of Geophysical Research (Planets)*, 113:0.

Jenkins, J. M. (1998). Radio Occultation Studies of Venus' Atmosphere with Magellan. Technical report.

Jenkins, J. M. and Steffes, P. G. (1991). Comparison of Kalman and Wiener Filtering Techniques for Processing Pioneer Venus Radio Occultation Data. In *Bulletin of the American Astronomical Society*, volume 23 of *Bulletin of the American Astronomical Society*, page 1195.

Kakar, R. K., Waters, J. W., and Wilson, W. J. (1976). Venus - Microwave detection of carbon monoxide. *Science*, 191:379.

Keating, G. M., Bertaux, J. L., Bougher, S. W., Dickinson, R. E., Cravens, T. E., and Hedin, A. E. (1985). Models of Venus neutral upper atmosphere - Structure and composition. *Advances in Space Research*, 5:117–171.

Keating, G. M., Nicholson, J. Y., and Lake, L. R. (1980). Venus upper atmosphere structure. *J. Geophys. Res.*, 85:7941–7956.

Kliore, A. J. and Mullen, L. (1988). Changes in the Temperature of Venus Upper Atmosphere from Solar Maximum to Minimum. In *Bulletin of the American Astronomical Society*, volume 20 of *Bulletin of the American Astronomical Society*, page 832.

Krasnopolsky, V. A. (2006). Chemical composition of Venus atmosphere and clouds: Some unsolved problems. *Planet. Space Sci.*, 54:1352–1359.

Krasnopolsky, V. A. (2011). Atmospheric chemistry on Venus, Earth, and Mars: Main features and comparison. *Planet. Space Sci.*, 59:952–964.

Lee, Y. J., Titov, D. V., Tellmann, S., Piccialli, A., Ignatiev, N., Pätzold, M., Häusler, B., Piccioni, G., and Drossart, P. (2012). Vertical structure of the Venus cloud top from the VeRa and VIRTIS observations onboard Venus Express. *Icarus*, 217:599–609.

Lellouch, E., Clancy, T., Crisp, D., Kliore, A. J., Titov, D., and Bougher, S. W. (1997). Monitoring of Mesospheric Structure and Dynamics. In S. W. Bougher, D. M. Hunten, & R. J. Phillips, editor, *Venus II: Geology, Geophysics, Atmosphere, and Solar Wind Environment*, page 295.

Lellouch, E., Goldstein, J. J., Rosenqvist, J., Bougher, S. W., and Paubert, G. (1994). Global circulation, thermal structure, and carbon monoxide distribution in Venus' mesosphere in 1991. *Icarus*, 110:315–339.

Limaye, S. S. and Suomi, V. E. (1981). Cloud motions on Venus - Global structure and organization. *Journal of Atmospheric Sciences*, 38:1220–1235.

López-Puertas, M., Funke, B., Gil-López, S., López-Valverde, M. Á., von Clarmann, T., Fischer, H., Oelhaf, H., Stiller, G., Kaufmann, M., Koukouli, M. E., and Flaud, J.-M. (2005). Atmospheric non-local thermodynamic equilibrium emissions as observed by the Michelson Interferometer for Passive Atmospheric Sounding (MIPAS). *Comptes Rendus Physique*, 6:848–863.

Lopez-Puertas, M., Lopez-Valverde, M. A., and Taylor, F. W. (1992). Vibrational temperatures and radiative cooling of the CO2 15 micron bands in the middle atmosphere. *Quarterly Journal of the Royal Meteorological Society*, 118:499–532.

Lopez-Puertas, M., Molina, A., Rodrigo, R., and Taylor, F. W. (1986). A non-LTE radiative transfer model for infrared bands in the middle atmosphere. I - Theoretical basis and application to CO2 15 micron bands. *Journal of Atmospheric and Terrestrial Physics*, 48:729–748.

Lopez-Puertas, M. and Taylor, F. W. (2001). *Non-LTE radiative transfer in the atmosphere*. World Scientific Pub., Singapore, Series on atmospheric oceanic and planetary physics, vol. 3 ISBN 9810245661.

López-Valverde, M. A., Drossart, P., Carlson, R., Mehlman, R., and Roos-Serote, M. (2007). Non-LTE infrared observations at Venus: From NIMS/Galileo to VIRTIS/Venus Express. *Planet. Space Sci.*, 55:1757–1771.

López-Valverde, M. A., Gilli, G., García-Comas, M., González-Galindo, F., Drossart, P., and Piccioni, G. (2008). The upper atmosphere of Venus observed by Venus Express. *Lecture Notes and Essays in Astrophysics*, 3:13–32.

Lopez-Valverde, M. A. and Lopez-Puertas, M. (1994). A non-local thermodynamic equilibrium radiative transfer model for infrared emission in the atmosphere of Mars. 2: Daytime populations of vibrational levels. *J. Geophys. Res.*, 99:13117–13132.

López-Valverde, M. A., López-Puertas, M., Funke, B., Gilli, G., García-Comas, M., Drossart, P., Piccioni, G., and Formisano, V. (2011). Modelling the Atmospheric Limb Emission of CO_2 at 4.3 μm in the Terrestrial Planets. *Planet. Space Sci.*, 59:988–998.

Luz, D., Berry, D. L., Piccioni, G., Drossart, P., Politi, R., Wilson, C. F., Erard, S., and Nuccilli, F. (2011). Venus's Southern Polar Vortex Reveals Precessing Circulation. *Science*, 332:577–.

Mahieux, A., Vandaele, A. C., Neefs, E., Robert, S., Wilquet, V., Drummond, R., Federova, A., and Bertaux, J. L. (2010). Densities and temperatures in the Venus mesosphere and lower thermosphere retrieved from SOIR on board Venus Express: Retrieval technique. *Journal of Geophysical Research (Planets)*, 115:12014–+.

Marcq, E., Bertaux, J., Montmessin, F., Belyaev, D., Fedorova, A., Vandaele, A., and Neefs, E. (2010). SO_2 Above The Clouds Of Venus As Measured By SPICAV-UV In Nadir. In *AAS/Division for Planetary Sciences Meeting Abstracts 42*, volume 42 of *Bulletin of the American Astronomical Society*, page 974.

Marcq, E., Encrenaz, T., Bézard, B., and Birlan, M. (2006). Remote sensing of Venus' lower atmosphere from ground-based IR spectroscopy: Latitudinal and vertical distribution of minor species. *Planet. Space Sci.*, 54:1360–1370.

Markiewicz, W. J., Titov, D. V., Ignatiev, N., Keller, H. U., Crisp, D., Limaye, S. S., Jaumann, R., Moissl, R., Thomas, N., Esposito, L., Watanabe, S., Fiethe, B., Behnke, T., Szemerey, I., Michalik, H., Perplies, H., Wedemeier, M., Sebastian, I., Boogaerts, W., Hviid, S. F., Dierker, C., Osterloh, B., Böker, W., Koch, M., Michaelis, H., Belyaev, D., Dannenberg, A., Tschimmel, M., Russo, P., Roatsch, T., and Matz, K. D. (2007a). Venus Monitoring Camera for Venus Express. *Planet. Space Sci.*, 55:1701–1711.

Markiewicz, W. J., Titov, D. V., Limaye, S. S., Keller, H. U., Ignatiev, N., Jaumann, R., Thomas, N., Michalik, H., Moissl, R., and Russo, P. (2007b). Morphology and dynamics of the upper cloud layer of Venus. *Nature*, 450:633–636.

McMahon, S. K. (1996). Overview of the Planetary Data System. *Planetary and Space Science*, 44:3–12.

Mendillo, M., Nagy, A., and Waite, J. H. (2002). *Atmospheres in the solar system: comparative aeronomy.*

Mueller-Wodarg, I. C., Yelle, R. V., Mendillo, M., and Galand, M. (2006). Energetics of planetary upper atmospheres. *AGU Spring Meeting Abstracts*, page A1.

Niemann, H. B., Kasprzak, W. T., Hedin, A. E., Hunten, D. M., and Spencer, N. W. (1980). Mass spectrometric measurements of the neutral gas composition of the thermosphere and exosphere of Venus. *J. Geophys. Res.*, 85:7817–7827.

Ohtsuki, S., Iwagami, N., Sagawa, H., Ueno, M., Kasaba, Y., Imamura, T., Yanagisawa, K., and Nishihara, E. (2008). Distributions of the Venus 1.27-μm O_2 airglow and rotational temperature. *Planet. Space Sci.*, 56:1391–1398.

Payan, S., de La Noë, J., Hauchecorne, A., and Camy-Peyret, C. (2005). A review of remote sensing techniques and related spectroscopy problems. *Comptes Rendus Physique*, 6:825–835.

Piccialli, A., Tellmann, S., Titov, D. V., Limaye, S. S., Khatuntsev, I. V., Pätzold, M., and Häusler, B. (2012). Dynamical properties of the Venus mesosphere from the radio-occultation experiment VeRa onboard Venus Express. *Icarus*, 217:669–681.

Piccialli, A., Titov, D., Tellmann, S., Migliorini, A., Read, P., Grassi, D., Paetzold, M., Haeusler, B., Piccioni, G., and Drossart, P. (2010). Thermal zonal winds in the Venus mesosphere from the Venus Express temperature soundings. In *38th COSPAR Scientific Assembly*, volume 38, page 1357.

Piccioni, G., Drossart, P., Coradini, A., Arnold, G., Sémery, A., Peter, G., Cosi, M., Saggin, B., Erard, S., Lebonnois, S., and The Virtis Team (2006). First results from VIRTIS on Venus Express 1. Overview. In *36th COSPAR Scientific Assembly*, volume 36 of *COSPAR, Plenary Meeting*, pages 2263–+.

Piccioni, G., Drossart, P., Sanchez-Lavega, A., Hueso, R., Taylor, F. W., Wilson, C. F., Grassi, D., Zasova, L., Moriconi, M., Adriani, A., Lebonnois, S., Coradini, A., Bézard, B., Angrilli, F., Arnold, G., Baines, K. H., Bellucci, G., Benkhoff, J., Bibring, J. P., Blanco, A., Blecka, M. I., Carlson, R. W., di Lellis, A., Encrenaz, T., Erard, S., Fonti, S., Formisano, V., Fouchet, T., Garcia, R., Haus, R., Helbert, J., Ignatiev, N. I., Irwin, P. G. J., Langevin, Y., Lopez-Valverde, M. A., Luz, D., Marinangeli, L., Orofino, V., Rodin, A. V., Roos-Serote, M. C., Saggin, B., Stam, D. M., Titov, D., Visconti, G., Zambelli, M., Ammannito, E., Barbis, A., Berlin, R., Bettanini, C., Boccaccini, A., Bonnello, G., Bouye, M., Capaccioni, F., Cardesin Moinelo, A., Carraro, F., Cherubini,

G., Cosi, M., Dami, M., de Nino, M., Del Vento, D., di Giampietro, M., Donati, A., Dupuis, O., Espinasse, S., Fabbri, A., Fave, A., Veltroni, I. F., Filacchione, G., Garceran, K., Ghomchi, Y., Giustini, M., Gondet, B., Hello, Y., Henry, F., Hofer, S., Huntzinger, G., Kachlicki, J., Knoll, R., Driss, K., Mazzoni, A., Melchiorri, R., Mondello, G., Monti, F., Neumann, C., Nuccilli, F., Parisot, J., Pasqui, C., Perferi, S., Peter, G., Piacentino, A., Pompei, C., Reess, J.-M., Rivet, J.-P., Romano, A., Russ, N., Santoni, M., Scarpelli, A., Semery, A., Soufflot, A., Stefanovitch, D., Suetta, E., Tarchi, F., Tonetti, N., Tosi, F., and Ulmer, B. (2007). South-polar features on Venus similar to those near the north pole. *Nature*, 450:637–640.

Piccioni, G. and VIRTIS/Venus Express Team (2009). The visible and infrared thermal imaging spectrometer. in press ESA SP-1295, Eur. Space Agency Spec. Publ., ESA Publications Division, Noordwijk, The Netherlands,.

Plaut, J. J., Saunders, R. S., Stofan, E. R., Kirk, R. L., Schaber, G. G., Soderblom, L. A., Ford, P. G., Pettengill, G. H., Campbell, D. B., and Stacy, N. J. S. (1992). Anomalous scattering behavior of selected impact parabola features: Magellan cycle-to-cycle comparisons. *LPI Contributions*, 789:92–93.

Ramanathan, V. (1974). A simplified stratospheric radiative transfer model - Theoretical estimates of the thermal structure of the basic and perturbed stratosphere. In D. J. Wuebbles & J. S. Chang, editor, *2nd International Conference on the Environmental Impact of Aerospace Operations in the High Atmosphere*, pages 147–154.

Rengel, M., Hartogh, P., and Jarchow, C. (2008). Mesospheric vertical thermal structure and winds on Venus from HHSMT CO spectral-line observations. *Planet. Space Sci.*, 56:1368–1384.

Rodgers, C. D. (2000). *Inverse Methods for Atmospheric Sounding: Theory and Practice*, volume 2 of *Series on Atmospheric, Oceanic and Planetary Physics, F. W. Taylor, ed.* World Scientific.

Roldán, C., López-Valverde, M. A., López-Puertas, M., and Edwards, D. P. (2000). Non-LTE Infrared Emissions of CO_2 in the Atmosphere of Venus. *Icarus*, 147:11–25.

Rothman, L. S., Jacquemart, D., Barbe, A., Chris Benner, D., Birk, M., Brown, L. R., Carleer, M. R., Chackerian, C., Chance, K., Coudert, L. H., Dana, V., Devi, V. M., Flaud, J.-M., Gamache, R. R., Goldman, A., Hartmann, J.-M., Jucks, K. W., Maki, A. G., Mandin, J.-Y., Massie, S. T., Orphal, J., Perrin, A., Rinsland, C. P., Smith, M. A. H., Tennyson, J., Tolchenov, R. N., Toth, R. A., Vander Auwera, J., Varanasi, P., and Wagner, G. (2005). The HITRAN 2004 molecular spectroscopic database. *Journal of Quantitative Spectroscopy and Radiative Transfer*, 96:139–204.

Russell, C. T. (1992). The Pioneer Venus mission. *Washington DC American Geophysical Union Geophysical Monograph Series*, 66:225–236.

Russell, C. T., Luhmann, J. G., and Strangeway, R. J. (2006). The solar wind interaction with Venus through the eyes of the Pioneer Venus Orbiter. *Planet. Space Sci.*, 54:1482–1495.

Sagdeev, R. Z. (1986). An overview of the Soviet VEGA balloon experiment and studies of the atmosphere of Venus. *NASA STI/Recon Technical Report N*, 87:19321.

Sandor, B. J. and Clancy, R. T. (2005). Water vapor variations in the Venus mesosphere from microwave spectra. *Icarus*, 177:129–143.

Schloerb, F. P., Robinson, S. E., and Irvine, W. M. (1980). Observations of CO in the stratosphere of Venus via its J = 0 - 1 rotational transition. *Icarus*, 43:121–127.

Schubert, G., Covey, C., del Genio, A., Elson, L. S., Keating, G., Seiff, A., Young, R. E., Apt, J., Counselman, C. C., Kliore, A. J., Limaye, S. S., Revercomb, H. E., Sromovsky, L. A., Suomi, V. E., Taylor, F., Woo, R., and von Zahn, U. (1980). Structure and circulation of the Venus atmosphere. *J. Geophys. Res.*, 85:8007–8025.

Schubert, G. and Covey, C. C. (2007). Venus Atmosphere Dynamics Workshop. In *Planetary Atmospheres*, pages 105–106.

Seiff, A., Schofield, J. T., Kliore, A. J., Taylor, F. W., and Limaye, S. S. (1985). Models of the structure of the atmosphere of Venus from the surface to 100 kilometers altitude. *Advances in Space Research*, 5:3–58.

Sharma, R. D. and Wintersteiner, P. P. (1990). Role of carbon dioxide in cooling planetary thermospheres. *Geophys. Res. Lett.*, 17(12):2201–2204.

Smrekar, S. E., Stofan, E. R., Mueller, N., Treiman, A., Elkins-Tanton, L., Helbert, J., Piccioni, G., and Drossart, P. (2010). Recent Hotspot Volcanism on Venus from VIRTIS Emissivity Data. *Science*, 328:605–.

Sonnabend, G., Kroetz, P., Sornig, M., and Stupar, D. (2010). Direct observations of Venus upper mesospheric temperatures from ground based spectroscopy of CO_2. *Geophys Res. Lett.*, 37:L11102.

Sonnabend, G., Krötz, P., Schmülling, F., Kostiuk, T., Goldstein, J., Sornig, M., Stupar, D., Livengood, T., Hewagama, T., Fast, K., Mahieux, A., and Clancy, R. T. (2011). Thermospheric/mesospheric temperatures on Venus: comparison between ground-based high-resolution spectroscopy of CO2 and other techniques. In *EPSC-DPS Joint Meeting 2011, held 2-7 October 2011 in Nantes, France*, page 716.

Sonnabend, G., Sornig, M., Krötz, P., Stupar, D., and Schieder, R. (2008). Ultra high spectral resolution observations of planetary atmospheres using the cologne tuneable heterodyne infrared spectrometer. *J. Quant. Spectrosc. Radiat. Transfer*, 109:1016–1029.

Steffes, P. G., Jenkins, J. M., Austin, R. S., Tyler, G. L., and Seale, E. H. (1991). Radio Occultation Studies of the Venus Atmosphere with the Magellan Spacecraft. In *Bulletin of the American Astronomical Society*, volume 23 of *Bulletin of the American Astronomical Society*, page 1196.

Svedhem, H. and Titov, D. (2011). Venus Express - Status and major results. In *EPSC-DPS Joint Meeting 2011, held 2-7 October 2011 in Nantes, France.*, page 1618.

Svedhem, H., Titov, D., Taylor, F., and Witasse, O. (2009). Venus Express mission. *Journal of Geophysical Research (Planets)*, 114:0.

Svedhem, H., Titov, D. V., McCoy, D., Lebreton, J.-P., Barabash, S., Bertaux, J.-L., Drossart, P., Formisano, V., Häusler, B., Korablev, O., Markiewicz, W. J., Nevejans, D., Pätzold, M., Piccioni, G., Zhang, T. L., Taylor, F. W., Lellouch, E., Koschny, D., Witasse, O., Eggel, H., Warhaut, M., Accomazzo, A., Rodriguez-Canabal, J., Fabrega, J., Schirmann, T., Clochet, A., and Coradini, M. (2007). Venus Express: The first European mission to Venus. *Planet. Space Sci.*, 55:1636–1652.

Taylor, F. and Grinspoon, D. (2009). Climate evolution of Venus. *Journal of Geophysical Research (Planets)*, 114:0.

Taylor, F. W. (1995). Carbon monoxide in the deep atmospheres of Venus. *Advances in Space Research*, 16:81–.

Taylor, F. W. (2006). Venus before Venus Express. *Planet. Space Sci.*, 54:1249–1262.

Taylor, F. W., Crisp, D., and Bézard, B. (1997). Near-Infrared Sounding of the Lower Atmosphere of Venus. In S. W. Bougher, D. M. Hunten, & R. J. Phillips, editor, *Venus II: Geology, Geophysics, Atmosphere, and Solar Wind Environment*, page 325.

Taylor, F. W., McCleese, D. J., and Diner, D. J. (1979). Polar clearing in the Venus clouds observed from the Pioneer Orbiter. *Nature*, 279:613.

Taylor, F. W., Schofield, J. T., and Valdes, P. J. (1985). Temperature structure and dynamics of the middle atmosphere of Venus. *Advances in Space Research*, 5:5–23.

Tellmann, S., Pätzold, M., Häusler, B., Bird, M. K., and Tyler, G. L. (2009). Structure of the Venus neutral atmosphere as observed by the Radio Science experiment VeRa on Venus Express. *Journal of Geophysical Research (Planets)*, 114:E00B36.

Titov, D., Lebreton, J., Lellouch, E., and Taylor, F. (2002). *Venus Express: a proposed ESA mission to Venus in 2005.* 34th COSPAR Scientific Assembly, Houston, USA, 2002.

Titov, D. V., Markiewicz, W. J., Ignatiev, N. I., Song, L., Limaye, S. S., Sanchez-Lavega, A., Hesemann, J., Almeida, M., Roatsch, T., Matz, K.-D., Scholten, F., Crisp, D., Esposito, L. W., Hviid, S. F., Jaumann, R., Keller, H. U., and Moissl, R. (2012). Morphology of the cloud tops as observed by the Venus Express Monitoring Camera. *Icarus*, 217:682–701.

Titov, D. V., Svedhem, H., Koschny, D., Hoofs, R., Barabash, S., Bertaux, J.-L., Drossart, P., Formisano, V., Häusler, B., Korablev, O., Markiewicz, W. J., Nevejans, D., Pätzold, M., Piccioni, G., Zhang, T. L., Merritt, D., Witasse, O., Zender, J., Accomazzo, A., Sweeney, M., Trillard, D., Janvier, M., and Clochet, A. (2006). Venus Express science planning. *Planet. Space Sci.*, 54:1279–1297.

Titov, D. V., Svedhem, H., and Wilson, C. (2011). Venus Express: five years of atmospheric observations. In *EPSC-DPS Joint Meeting 2011, held 2-7 October 2011 in Nantes, France.*, page 1332.

Titov, D. V., Taylor, F. W., Svedhem, H., Ignatiev, N. I., Markiewicz, W. J., Piccioni, G., and Drossart, P. (2008). Atmospheric structure and dynamics as the cause of ultraviolet markings in the clouds of Venus. *Nature*, 456:620–623.

Vandaele, A. C., De Mazière, M., Drummond, R., Mahieux, A., Neefs, E., Wilquet, V., Korablev, O., Fedorova, A., Belyaev, D., Montmessin, F., and Bertaux, J. (2008). Composition of the Venus mesosphere measured by Solar Occultation at Infrared on board Venus Express. *Journal of Geophysical Research (Planets)*, 113:0–+.

von Zahn, U., Kumar, S., Niemann, H., and Prinn, R. (1983). Composition of the venus atmosphere. In Hunten, D. M., Colin, L., Donahue, T. M., and Moroz, V. I., editors, *Venus*, pages 299–430. Univ. of Arizona Press, Tucson, AZ.

Wilson, A. and Chicarro, A., editors (2004). *Mars express : the scientific payload*, volume 1240 of *ESA Special Publication*.

Wilson, W. J., Klein, M. J., Kahar, R. K., Gulkis, S., Olsen, E. T., and Ho, P. T. P. (1981). Venus. I - Carbon monoxide distribution and molecular-line searches. *Icarus*, 45:624–637.

Witasse, O. and Nagy, A. F. (2006). Outstanding aeronomy problems at Venus. *Planet. Space Sci.*, 54:1381–1388.

Yung, Y. L. and Demore, W. B. (1982). Photochemistry of the stratosphere of Venus - Implications for atmospheric evolution. *Icarus*, 51:199–247.

Zasova, L. V., Moroz, V. I., Esposito, L. W., and Na, C. Y. (1993). SO_2 in the Middle Atmosphere of Venus: IR Measurements from Venera-15 and Comparison to UV Data. *Icarus*, 105:92–109.

Zhang, T. L., Baumjohann, W., Delva, M., Auster, H.-U., Balogh, A., Russell, C. T., Barabash, S., Balikhin, M., Berghofer, G., Biernat, H. K., Lammer, H., Lichtenegger, H., Magnes, W., Nakamura, R., Penz, T., Schwingenschuh, K., Vörös, Z., Zambelli, W., Fornacon, K.-H., Glassmeier, K.-H., Richter, I., Carr, C., Kudela, K., Shi, J. K., Zhao, H., Motschmann, U., and Lebreton, J.-P. (2006). Magnetic field investigation of the Venus plasma environment: Expected new results from Venus Express. *Planet. Space Sci.*, 54:1336–1343.